ICACE 2024

# 4th INTERNATIONAL CONGRESS OF APPLIED CHEMISTRY & ENVIRONMENT




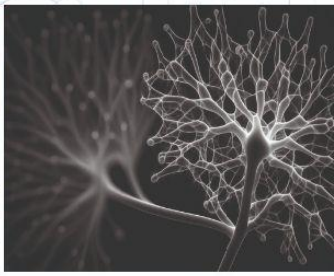

ICACE 2024

# BOOK OF ABSTRACTS

December 12th - 14th, 2024

Palm Beach Palace Tozeur

# Welcome Message

**Dear Partners,**
**Dear colleagues,**
**Dear students,**

It is with great pleasure and pride that I welcome you to the 4th edition of the International Congress of Applied Chemistry and Environment (ICACE-4), organized by the Environmental Chemistry and Clean Processes Research Laboratory (LCE2P) of the Faculty of Sciences, University of Monastir, in partnership with the Laboratory of Thermal and Thermodynamics of Industrial Processes (L2TPI) at the National Engineering School, University of Monastir. This congress will take place from December 12 to 14, 2024, in the beautiful city of Tozeur, Tunisia.

The Environmental Chemistry and Clean Processes research laboratory, which I have the honor to direct, is especially proud to host this event. The significance of this congress is heightened given that the previous edition was held remotely in a challenging health context. This year, we are delighted to return to in-person exchanges, bringing together researchers from diverse backgrounds to foster new collaborations. We also celebrate the opportunity to support young researchers at the beginning of their careers, allowing them to broaden their scientific and cultural horizons.

The choice of Tozeur as the venue is deliberate. Known for its vast palm groves and stunning sun-baked brick architecture, Tozeur is a jewel of southern Tunisia. The region's high solar irradiation also makes it an ideal location to highlight renewable energy, particularly solar power, as a key solution for clean processes aimed at combating climate change.

As scientists, we are not only observers and analysts of the environmental changes facing our world, but we are also committed to providing solutions. The themes explored at this congress—environment and climate change, clean processes and renewable energy, sustainable textiles and circular economy, green chemistry and natural substances, and biomaterials and nanotechnology—are vital in shaping the future of our planet.

We are honored to have esteemed scientists joining us, including Professors Marie-Odile SIMONNOT, Slah MSAHLI, Sabria BARKA, Heikki SEPPÄ, Estelle METAY, and Ahmed BELLAGI. Their participation will undoubtedly enrich our discussions.

This congress would not have been possible without the unwavering support of our long-time partner, the Laboratory of Thermal and Thermodynamics of Industrial Processes, as well as our sponsors: CHIMITEX Industry, the French Institute of Tunisia, and the ETC Group.

I would also like to thank Professor Kamel CHARRADA, President of the University of Monastir, for his encouragement of scientific initiatives, and Professor Hichem BEN JANNET, Dean of the Faculty of Sciences of Monastir, for his continuous support of our laboratory's scientific and cultural events.

Special thanks go to Dr. Ibtissem MOUSSA, President of the Organizing Committee, and Professor Nizar MEKSI, President of the Scientific Committee, for their leadership and dedication in ensuring the success of this event.

Finally, I extend my heartfelt thanks to all the delegates present here for sharing their research and passion for discussing such a crucial theme—our environment and its future.

I wish you all a productive and inspiring conference.

**Professor Hatem DHAOUADI**
**Chairman of the ICACE-4 congress**

## Organizers

Laboratoire de Chimie de l'Environnement et des Procédés Propres

ASSOCIATION TUNISIENNE DES TECHNOLOGIES DURABLES

## Partner

L.R. THERMIQUE THERMODYNAMIQUE DES PROCEDES INDUSTRIELS

## Sponsors

UNIVERSITE DE MONASTIR

FACULTE DES SCIENCES DE MONASTIR

CHIMIE TEX PLUS

ETC Group

INSTITUT FRANÇAIS Tunisie

# ORGANIZING COMMITTE

## CONFERENCE CHAIR

**Pr. Hatem DHAOUADI**, Professor, Faculty of Sciences of Monastir.

## PRESIDENT OF THE SCIENTIFIC COMMITTEE

**Pr. Nizar MEKSI**, Professor, National School of Engineering of Monastir.

## PRESIDENT OF THE ORGANIZING COMMITTEE

**Dr. Ing. Ibtissem MOUSSA**, Assistant Professor, Higher Institute of Technology Studies of Ksar Hellal.

## ORGANIZING COMMITTEE

**Pr. Sonia DRIDI**, Professor, Preparatory Institute of Engineering Studies of Monastir.

**Dr. Ing. Imene GHEZAL**, Assistant Professor, Higher Institute of Technology Studies of Ksar Hellal.

**Dr. Wafa GHEDIRA**, Faculty of Sciences of Monastir.

**Dr. Ing. Maha ABDELILEH**, National Engineering School of Monastir.

**Dr. Ing. Noureddine BAAKA**, Assistant Professor, Higher Institute of Fashion of Monastir.

**Dr. Siwar MAJDOUB**, Assistant Professor, Biotechnology Center of Sfax.

**Dr. Amira ZGOLLI**, Faculty of Sciences of Monastir.

**Dr. Ing. Monia CHAABANE**, Assistant Professor, National Engineering School of Monastir.

**Mr. Nizar KEREKNI**, Faculty of Sciences of Monastir.

**Mr. Maryi TEIEB**, Faculty of Sciences of Monastir.

**Dr. Ing. Ghazza MASMOUDI**, Assistant Professor, Faculty of Sciences of Monastir.

**Dr. Ing. Imen CHERMITI**, Assistant Professor, Faculty of Sciences of Monastir.

# SCIENTIFIC COMMITTEE

**Mohamed Farouk MHENNI**, Professor Emeritus, Faculty of Sciences of Monastir, Tunisia.

**Zine MIGHRI**, Professor Emeritus, Faculty of Sciences of Monastir, Tunisia.

**Chedly BOUDOKHANE,** Professor Emeritus, Faculty of Pharmacy of Monastir, Tunisia.

**Sonia DRIDI-DHAOUADI**, Professor, Preparatory Institute of Engineering Studies of Monastir, Tunisia.

**Saoussem HAMMAMI**, Professor, Faculty of Sciences of Monastir, Tunisia.

**Rafik GHARBI**, Professor, Faculty of Sciences of Monastir, Tunisia.

**Marie-ODILE SIMONNOT**, Professor, University of Lorraine, France.

**Heikki SEPPÄ**, Professor, University of Helsinki, Finland.

**Salah AKKAL**, Professor, University of Mentouri Constantine 1, Algeria.

**Aminoddine HAJJI**, Professor, Yazd University, Iran.

**Ahmed BELLAGI**, Professor Emeritus, National School of Engineers of Monastir, Tunisia.

**Hatem MHIRI,** Professor, National School of Engineers of Monastir, Tunisia.

**Mustapha MAJDOUB**, Professor, Faculty of Sciences of Monastir, Tunisia.

**Hatem MAJDOUB**, Professor, Faculty of Sciences of Monastir, Tunisia.

**Houcine BARHOUMI**, Professor, Faculty of Sciences of Monastir, Tunisia.

**Ayoub HAJ SAID**, Professor, Microelectronics and Nanotechnology Research Center of Sousse, Tunisia.

**Latifa BERGAOUI**, Professor, National Institute of Applied Sciences and Technology, Tunisia.

**Sabria BARKA**, Professor, Higher Institute of Biotechnology of Monastir, Tunisia.

**Néji LADHAARI**, Professor, Higher Institute of Fashion of Monastir, Tunisia.

**Faouzi SAKLY**, Professor, Higher Institute of Technological Studies of Ksar-Hellal, Tunisia.

**Mohamed BEN HASSEN**, Professor, Higher Institute of Technological Studies of Ksar-Hellal, Tunisia.

**Amel BABAY**, Professor, Higher Institute of Technological Studies of Ksar-Hellal, Tunisia.

**Mohamed Hassen V BAOUAB**, Professor, Preparatory Institute for Engineering Studies in Monastir, Tunisia.

**Mohamed HAMDAOUI**, Professor, National School of Engineering of Monastir, Tunisia.

**Adel GHITH**, Professor, National School of Engineering of Monastir, Tunisia.

**Faten FAYALA GUITH**, Professor, National School of Engineering of Monastir, Tunisia.

**Taoufik HARIZI**, Professor, Higher Institute of Fashion of Monastir, Tunisia.

**Saber BEN ABDESSALEM**, Professor, National School of Engineering of Monastir, Tunisia.

**Khaled BOUGHZALA**, Professor, Higher Institute of Technological Studies of Ksar-Hellal, Tunisia.

**Boubaker JAOUACHI**, Professor, National School of Engineering of Monastir, Tunisia.

# Conference Abstracts

# From polyols to amphiphiles

**Estelle METAY**
Equipe CAtalyse SYnthèse et ENvironnement (CASYEN)
Institut de Chimie et Biochimie Moléculaires et Supramoléculaires (ICBMS), UMR-CNRS 5246
Université Claude Bernard Lyon1, campus LyonTech-la Doua
43 bd du 11 novembre 1918, 69622, Villeurbanne, France.

*E-mail address:* : estelle.metay@univ-lyon1.fr

## ABSTRACT

Surfactants, solvents and other useful molecules are widely used in a variety of industries such as paints, coatings, pharmaceuticals, food, cosmetics, polymers and household detergents. The most widely used compounds are derived from non-renewable raw materials and many of them need to be substituted. As a result, the synthesis of environmentally friendly products using renewable resources and environmentally friendly processes remains a challenge. In this area, we have developed a benign, environmentally friendly process for the synthesis of glycerol monoethers by catalytic reductive alkylation using palladium on carbon and an acidic ion exchange resin as a recyclable co-catalyst. The physicochemical properties of such glycerol monoethers were evaluated and some structural modifications were considered to obtain salt-resistant hydrotropes. In parallel, we are developing methods for the preparation of polyols to provide a wide range of biosourced raw materials.

## REFERENCES

- "Synthesis of Dipentaerythritol from Pentaerythritol under Acidic Conditions" Org. Process Res. Dev. 2020, 24, 2591-2603.
- "Solvent-Free Approaches for Preparing Dipentaerythritol from Pentaerythritol and 3,3-Bis(hydroxymethyl)oxetane" Org. Process Res. Dev. 2021, 25(11), 2490-2501.
- "Selective catalytic oxidation of diglycerol" Green Chem. 2021, 23, 1154-1159.
- "Eco-conception of Highly Salt-Tolerant AlkylEther Carboxylate Hydrotropes with a Glyceryl Spacer" Chemistry a European journal doi.org/10.1002/chem.202200274.

# Thermal and acoustic performance of natural fiber-based materials

**Slah Msahli[a], Melek Ayadi[a,b,c], Riadh Zouari[a], César Segovia[b], Ayda Baffoun[d], Nicolas Dauchez[c,*], Nicolas Brosse[e]**

[a] Laboratoire de Génie Textile, Université de Monastir, Monastir, Tunisie.
[b] Université de Lorraine, Centre d'Essais Textile Lorrain CETELOR, Epinal, France.
[c] Université de technologie de Compiègne, Alliance Sorbonne Université, Laboratoire Roberval, Centre de recherche Royallieu, CS 60319, 60203 Compiègne Cedex, France.
[d] Textile Materials and Process Research Unit, University of Monastir, Monastir, Tunisia.
[e] Université de Lorraine, Laboratoire d'Etude et de Recherche sur le Matériau Bois, Nancy, France.
*E-mail address:* slah.msahli@gmail.com

## ABSTRACT

There is currently an increasing interest in substituting synthetic building materials by more sustainable ecofriendly products. The aim of this study is to valorize biosourced fibers to develop new building insulation panels which contribute to reduce negative environmental impact of conventional synthetic and mineral products. First, raw fibers extracted from Posidonia Océanica and Stipa Tenacissima are characterized from a chemical, physical and hygrothermal point of view with the aim to settle their intrinsic properties. Then, panels made from extracted natural fibers mixed with bicomponent fibers were produced using a textile airlaid technology. This technology offers the feature to develop isotropic non-woven structures by orienting randomly the fibers on the fabric surface. The prepared panels are then analyzed for their hygrothermal properties. It was found that the developed panels have thermal conductivity value of 0.0356- 0.0392 W/m.K and of 0.0365-0.0397 W/m.K for Posidonia and Alfa, respectively, which is considered in the same range of those of commonly used thermal insulation materials for buildings. The second part of this work aimed to investigate the sound absorption coefficient of the airlaid panels for different densities. The results showed that increasing the density resulted in an enhancement of the sound absorbing performance of the panels due to increased airflow resistivity. Finally, the resistance of the panels to five common mold types in buildings was investigated and the results showed that panels based on Posidonia and Alfa mixed with 10% PET bicomponent fibers presented no proliferation of the tested micro-organisms after 28 days of incubation, revealing their natural resistance to the five mold strains. Thus, the developed panels may effectively contribute to reducing energy needs in buildings, while ensuring high hygrothermal and acoustic comfort for occupants.

# Green Hydrogen: Power to X.

**Ahmed BELLAGI**

*Laboratory of Thermal and Thermodynamic of Industrial Processes, National School of Engineers of Monastir, road of Ouardanine, 5000 Monastir, Tunisia*
*E-mail address: ahmedbellagi@yahoo.fr*

## ABSTRACT

Power-to-X (P2X) refers to a suite of innovative technologies that convert renewable electricity, such as solar or wind energy, into versatile chemical energy carriers. These carriers, including green hydrogen, can be stored, transported, or utilized as raw materials across a variety of industries, from chemical manufacturing to clean fuel production. The core of this process lies in the production of green hydrogen through water electrolysis, a method powered exclusively by renewable electricity, making it a key enabler of sustainable energy systems. Green hydrogen plays a foundational role in the P2X ecosystem. It can be used directly as a clean and efficient fuel, or it can be transformed into a range of other valuable products, such as methane, ammonia, and synthetic hydrocarbons. These compounds are essential for decarbonizing sectors where direct electrification remains challenging, such as aviation, maritime transport, and heavy industrial processes.

Beyond its industrial applications, the adoption of P2X technologies addresses critical issues in renewable energy integration. They enable the efficient storage and management of electricity surpluses, particularly during periods of high renewable energy production. This contributes to the stability and reliability of power grids while also ensuring that renewable resources are fully utilized. Furthermore, by converting renewable electricity into storable chemical forms, P2X creates pathways for energy export, offering countries with abundant renewable resources a new avenue for economic growth..

# Reconstructing past climatic changes in the North African-Mediterranean region over multimillenial timescales

**Heikki SEPPÄ**

*Department of Geosciences and Geography, University of Helsinki, Finland*
*E-mail address:* heikki.seppa@helsinki.fi

## ABSTRACT

The climate in the North African and Mediterranean regions is strongly influenced by the main atmospheric and oceanic circulation patterns related to the dynamics in atmospheric pressure gradients and in ocean temperature and salinity. To investigate the past changes in the climate of these regions, and by inference in the circulation patterns driving these changes, geological proxy data can be obtained for example from sedimentary sequences from the bottoms of the lakes and ocean, from the geological features associated with former water basins, and from the deposits preserved in the numerous caves. Such geological records can span timescales from hundreds to hundreds of thousands of years, providing thus valuable opportunities to investigate the climate history in the regions. In this presentation, I will go through the main types of geological records of past climate, and their potential strengths and weaknesses in climate history studies. I will focus on biological, chemical and physical records obtained from lake and marine sediments, which are mostly available in the Mediterranean region and mostly reflect changes in the precipitation and moisture availability. I will also present evidence from former lakes, which existed in Sahara during more humid climatic periods, and from records which are based on investigating the caves which exist in Tunisia and elsewhere in North Africa. I will show that the climate history in the region includes both long-term trends, which are associated with the slowly changing amount of solar insolation in the region, and more sudden shifts between higher and lower precipitation. The most dramatic climatic anomalies characterized by extreme aridity can be observed during the glacial period especially in the records from the western Mediterranean and West African regions, and they are likely linked with so-called Heinrich stadials, abrupt dry and cold events, which are documented also in Europe and the North Atlantic region. I will discuss the methods to detect such sudden anomalies in geological records of past climates, and the potential atmospheric and oceanic processes, which may have caused them.

# Processes for recovering critical metals: focus on recycling and agromining

**Marie-Odile SIMONNOT, Baptiste LAUBIE, Rémi DEMOL**

Laboratory of Reactions and Process Engineering, UMR 7274, University of Lorraine – CNRS, Nancy, France.

Contact : marie-odile.simonnot@univ-lorraine.fr

## ABSTRACT

The rapidly growing demand for digital technologies and electric vehicles is leading to a drastic increase in metal consumption. But metals, like fossil fuels, are in short supply around the world. Europe has drawn up a list of critical or strategic raw materials (CRMs), considered essential and subject to supply risks. This list, revised every three years, currently includes 34 CRMs.

It has therefore become essential to exploit metals found in secondary resources and to recycle those found in objects at the end of their life, such as mobile phones or batteries. More generally, the term 'urban mine' is now used to describe waste deposits that are potentially rich in metals.

However, recycling or exploiting secondary resources such as metal-rich soils or mining waste, require the use of chemical reagents and energy, and generate waste, gas and effluents. This is all the more true given that the target metals are usually found at low concentrations in solid matrices of complex composition.

This presentation focuses on the separation processes used in hydrometallurgy, as part of the recycling and exploitation of secondary resources. After the physical separation stages (e.g. dismantling, crushing, etc.), the hydrometallurgy stages involve leaching, which is the transfer of the metals of interest into solution, followed by recovery and purification. These stages involve unitary separation operations that are standard in chemical engineering (precipitation, liquid-liquid extraction, adsorption/ion exchange and, more recently, membrane processes). A focus will be on agromining, which involves growing hyperaccumulator plants to extract metals from soils and then recovering them from the plant biomass. Finally, the environmental impact of recycling processes will be discussed, with a particular focus on the multi-criteria, multi-stage life cycle analysis approach.

# Chemistry, so close...so far; so good...so bad

**Sabria BARKA**

*Environmental and Marine Toxicology Research Unit, UR 09-03, IPEIS, Sfax University, Sfax, Tunisia.*
*E-mail address:* sabriabarka2@yahoo.fr

## ABSTRACT

Chemistry is the most intimate science to Man since it plays a vital role in the advanced understanding of our world and the improvement of life's quality and comfort, which shapes and defines modernity. But Chemistry is dual as it puts on a darker face, which evokes evils and words which rhyme with "pollution", "toxicity" and "death". The current observation of the state of environmental degradation has forced global awareness and Chemistry is positioning itself as part of the solution by further innovating and creating Green Chemistry.

This conference offers a perspective on the importance of Chemistry in everyday life, the impact it can have on our environment, the threat that potentially compromises the physical integrity of all living beings as well as a questioning of the relevance and safety of the restorative solutions that it can provide.

# Oral Communications

# Environment and Climate Changes

# Carbon and Water Footprint of jeans - a Life Cycle Assessment Approach

**Mouna Hadj Nasr[a], Hassen Hedfi[b] and Ayda Baffoun[a]**

*(a) Textile Materials and Processes Research Unit MPTex, National Engineering School of Monastir, University of Monastir, Monastir 5019, Tunisia*

*(b) Mechanical Engineering Laboratory LGM, National Engineering School of Monastir, University of Monastir, Monastir 5019, Tunisia*

**ABSTRACT**

The jeans sector is renowned for its significant environmental footprint due to high consumption of water and energy consumption. Life Cycle Assessment (LCA) is the most widely used method for calculating the environmental impact of products. This study adopts a cradle-to-gate approach to evaluate the environmental impacts of a pair of jeans, focusing on two major impact categories: global warming and water consumption. Results reveal that a single pair of jeans emits 12.6 kg of $CO_2$ eq, primarily attributable to the fabric manufacturing phase, which accounts for 47% of total emissions. Additionally, water consumption per pair of jeans amounts to 60.6 x $10^{-2}$ $m^3$, with the cotton growing phase responsible for 82% of the total consumption.

**KEYWORDS :** life cycle assessment, jeans sector, environmental footprint, SimaPro®.

## 1. INTRODUCTION

The clothing industry, one of the largest globally, is widely known for its environmental damage throughout the entire life cycle of a garment [1]. Jeans manufacturing is recognized as one of the most environmentally impactful sectors in the textile industry [2]. The rapid expansion of jeans production is intensifying this environmental impact [3]. Various studies estimate that producing a single pair of jeans requires between 5,700 to 15,000 liters of water [2] ], with other sources citing a range of 9,000 to 11,000 liters [3]. Another report indicates a total water consumption of 3,781 liters throughout the jeans' entire lifecycle [4]. Regarding climate change impact, a study found that jeans manufacturing generates approximately 96 million tons of CO2 eq annually [2]. Carbon footprint assessments also show that emissions range from 33.4 kg [4] to 90.37 of CO2 eq [5] over the lifetime of a pair of jeans. The jeans industry needs to adopt sustainable measures covering the entire product lifecycle to reduce its environmental impact. This requires a comprehensive assessment of each stage in the supply chain, from raw material extraction to jeans disposal. Life Cycle Assessment (LCA) is designed to ensure product sustainability and support environmental decision-making [3]. This study analyzes the life cycle of a single pair of jeans, chosen as a benchmark given their widespread popularity - jeans are worn by nearly half of the world's population [6].

Few LCA studies cover jeans specifically [2,4,7–10]. This research aims to address this gap by integrating robust and recent (2024) primary data from a Tunisian manufacturer for jeans manufacturing processes, including cutting, sewing, washing, and finishing. More specifically, this study aims to analyze the carbon and water footprints of a pair of jeans while identifying the main factors contributing to these impacts.

This study is structured as follows: Section 2 covers methodology, detailing the research scope and the data collection process. Section 3 provides life cycle impact assessment (LCIA) results, focusing on carbon and water footprints and discussing the primary impact sources. Finally, Section 4 presents the conclusions.

## 2. MATERIAL AND METHODS

For this study, we employed the LCA approach in compliance with ISO 14040 and ISO 14044 standards [11,12]. LCA is a systematic method for assessing the environmental impacts of a product throughout its lifespan, involving four key stages: Goal and scope definition, Life Cycle Inventory (LCI), life cycle impact assessment (LCIA), and interpretation [13].

### 2.1. Goal and scope

The primary goal of this LCA study was to assess the carbon and water footprints of a single pair of jeans. The chosen functional unit is "the production of men's size 32/32 jeans that weighs 0.6 kg". This analysis is conducted within the "cradle-to-gate" system boundaries (**Fig. 1**), covering raw materials production, denim

fabric production, transportation, and the manufacturing processes (i.e. cutting, sewing, washing, and finishing) of the jeans. Therefore, the study excludes the use and end-of-life phases, as well as the production of infrastructure and machinery.

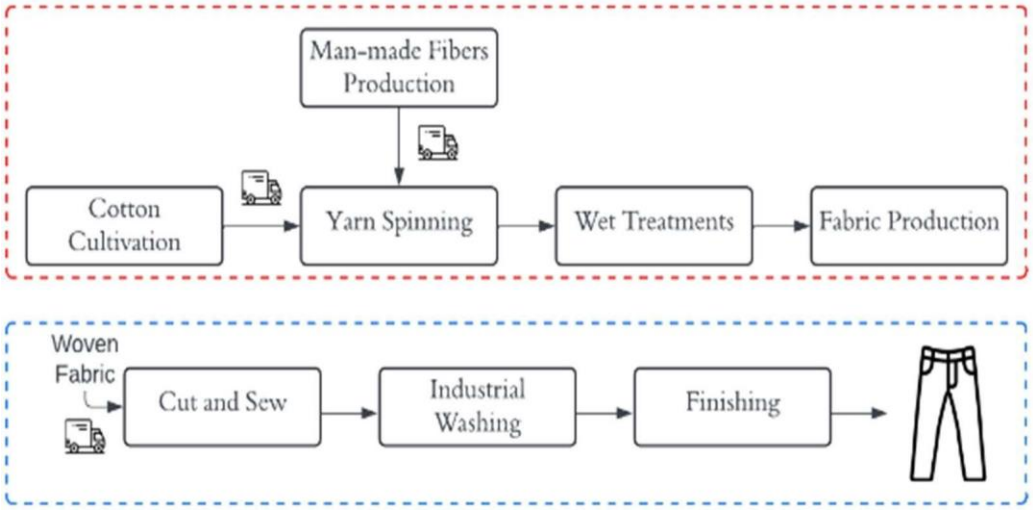


**Fig. 1** System boundaries of the analyzed jeans under the cradle-to-gate approach

### 2.2. Data collection

The inventory was developed using primary data, consisting of site-specific information gathered from a Tunisian jeans mill in 2024, specifically for the processes within the blue-outlined study boundaries. When primary data were unavailable, secondary data were sourced from the Ecoinvent v9.3.1 database and previous reports (for processes within the red-outlined boundaries). Therefore, data for stages such as raw materials and denim fabric production are mainly based on hypothetical scenarios and assumptions. It is also essential to note that transport between various stages has been considered, except when processes occur within the same facility or when facilities are close to each other. A summary of the data used in this study is provided in Table 1.

**Table 1.** Data sources

| Data | Sources | Note |
|---|---|---|
| Cotton cultivation and ginning | Ecoinvent v9.3.1 | Data based on Cotton Inc. (2016) |
| Man-made fibers production | [8] | Country specific, China |
| Yarn Spinning | [8] | We substituted the used Electricity Mix with 'Electricity, low voltage {EG}' |
| Wet treatments (dyeing and bleaching) | [8] | - |
| Fabric production (92% cotton, 6% PES, 2% Elastane) | [8] | - |
| Cut and sew | Site-specific data | Jeans mill based in Tunisia, 2024 |
| Industrial Washing | Site-specific data | Jeans mill based in Tunisia, 2024 |
| Finishing (i.e. sundries application and packaging) | Site-specific data | Jeans mill based in Tunisia, 2024 |
| Ship Transportation | Ecoinvent v9.3.1 | Transport, freight, sea, container ship {GLO} |
| Road Transportation | Ecoinvent v9.3.1 | Transport, freight, lorry 16-32 metric ton, EURO3 {RoW} |

## 3. Results and discussion

### 3.1. Life cycle impact assessment

The third phase of the LCA, per ISO 14044, is the LCIA. During this phase, the LCI inputs and outputs are assessed to determine their impacts on human health and the environment [2]. This study examined two impact categories: global warming and water consumption, using the ReCiPe 2016 v1.1, midpoint, Hierarchist (H) method in SimaPro® 9.5 software. The priority given to these two impact categories stems from two main considerations. Firstly, to respond to society's growing concern about global warming, which is consistently highlighted in all LCA studies and is the most evaluated impact category. Furthermore, the substantial use of water in jeans production is particularly critical in the context of Tunisia's persistent water shortage crisis. Table 2 presents the LCA results for producing one pair of jeans (0.6 kg).

**Table 2.** Characterized LCA results of jeans production

| Impact Category | Unit | Value |
|---|---|---|
| Global Warming | Kg $CO_2$ eq | 12.6 |
| Water Consumption | $m^3$ | 0.606 |

### 3.2. Contribution analysis by life cycle phase

A contribution analysis was carried out to pinpoint the primary causes of the environmental impact throughout the jeans' production processes, as shown in **Fig. 2**. Regarding the global warming indicator, the fabric manufacture phase is responsible for 47% of the total impact. This significant contribution is mainly due to the resource-intensive processes involved, such as spinning, wet treatments (including warp yarn dyeing and weft yarn bleaching), drying and weaving, all of which require substantial electricity and heat. The jeans production phase is the second-largest contributor to global warming, accounting for 38%, primarily due to fossil fuel use for electricity and heating, particularly during industrial washing, drying, cutting, and sewing. Meanwhile, the cotton-growing phase has the lowest global warming impact, accounting for just 15%. This is mainly explained by the energy consumption involved in preparing the soil, harvesting the cotton, and shipping it to the factories [3].

The analysis revealed that water consumption is highest in the cotton-growing phase, responsible for 82% of the impact. This is mainly due to the high-water demand of cotton [3,14]. Jeans production phase (including cutting, sewing, washing, and finishing) causes a far smaller impact, yet still represents the second largest contributor to water usage, with 12% of the total impact. This result is consistent with expectations, considering the well-known water-intensive process of industrial jeans washing [14,15]. Despite being water-intensive, fabric manufacturing has the lowest water consumption impact in this study, possibly due to using generic data; site-specific data might yield more accurate results.

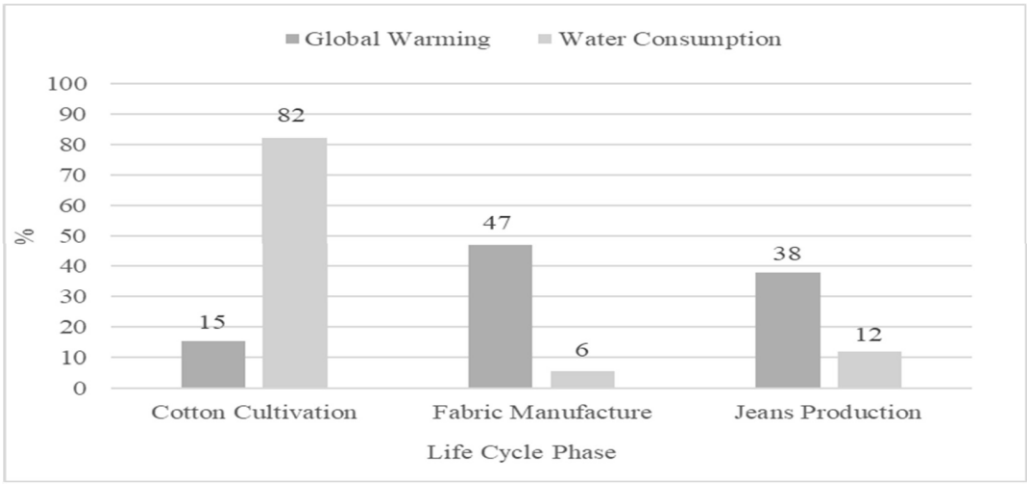


**Fig. 2** Contribution of the three life cycle stages: cotton cultivation, fabric manufacture, and jeans production to the environmental impact of jeans.

## 4. CONCLUSION

This study examined the carbon and water footprints of a single pair of jeans using a cradle-to-gate approach with recent and reliable data. It highlighted that the fabric manufacturing phase is the primary contributor to global warming impact. The jeans production phase followed closely as the second significant contributor, while the cotton-growing phase had the least impact on global warming. On the other hand, the cotton growing phase is the biggest contributor to water consumption, followed by the jeans production phase and the fabric manufacturing phase. By analyzing these environmental indicators, we gain insight into the jeans industry's ecological footprint at various stages, helping identify critical areas for implementing effective sustainable strategies to reduce environmental impact and drive forward an eco-friendlier jeans industry.

## REFERENCES

1. MAJA NELLSTRÖM, M.S. A Comparative Life Cycle Assessment of Nudie Jeans' Repair and Reuse Concept MAJA NELLSTRÖM, MATE SARIC. **2019**.
2. Åslund Hedman, E. Comparative Life Cycle Assessment of Jeans: A Case Study Performed at Nudie Jeans 2018.
3. Muthu, S.S. *Sustainability in Denim*; 2017; ISBN 9780081020432.
4. Levi Strauss & Co. The Life Cycle Of A Jean. Understanding the Environmental Impact of a Pair of Levi's 501 Jeans. *Levi Strauss & Co.* **2015**, 16–50.
5. Luo, Y.; Wu, X.; Ding, X. Carbon and Water Footprints Assessment of Cotton Jeans Using the Method Based on Modularity : A Full Life Cycle Perspective. *Journal of Cleaner Production* **2022**, *332*, 130042, doi:10.1016/j.jclepro.2021.130042.
6. Athey, S.N.; Adams, J.K.; Erdle, L.M.; Jantunen, L.M.; Helm, P.A.; Finkelstein, S.A.; Diamond, M.L. The Widespread Environmental Footprint of Indigo Denim Microfibers from Blue Jeans. *Environmental Science \& Technology Letters* **2020**, *7*, 840–847.
7. Arvidsson, E. Environmental Comparison of Jeans Made from Organic Cotton and Conventional Cotton Using LCA A Case Study at J . Lindeberg. **2019**.
8. Sandin, G.; Roos, S.; Spak, B.; Zamani, B.; Peters, G. Environmental Assessment of Swedish Clothing Consumption—Six Garments, Sustainable Futures. *Gothenburg, Sweden* **2019**, 167.
9. Morita, A.M.; Moore, C.C.S.; Nogueira, A.R.; Kulay, L.; Ravagnani, M.A. da S.S. Assessment of Potential Alternatives for Improving Environmental Trouser Jeans Manufacturing Performance in Brazil. *Journal of Cleaner Production* **2019**, *247*, doi:10.1016/j.jclepro.2019.119156.
10. Bongiovanni, R.; Tuninetti, L. Life Cycle Analysis of a Jean Produced in Argentina. **2018**.
11. ISO 14040:2006 - Management Environnemental — Analyse Du Cycle de Vie — Principes et Cadre Available online: https://www.iso.org/fr/standard/37456.html (accessed on 20 May 2024).
12. ISO 14044:2006 - Management Environnemental — Analyse Du Cycle de Vie — Exigences et Lignes Directrices Available online: https://www.iso.org/fr/standard/38498.html (accessed on 20 May 2024).
13. Fidan, F.; Aydoğan, E.K.; Uzal, N. An Integrated Life Cycle Assessment Approach for Denim Fabric Production Using Recycled Cotton Fibers and Combined Heat and Power Plant. *Journal of Cleaner Production* **2020**, *287*, doi:10.1016/j.jclepro.2020.125439.
14. Zhao, M.; Zhou, Y.; Meng, J.; Zheng, H.; Cai, Y.; Shan, Y.; Guan, D.; Yang, Z. Virtual Carbon and Water Flows Embodied in Global Fashion Trade-a Case Study of Denim Products. *Journal of Cleaner Production* **2021**, *303*, 127080.
15. Sülar, V.; Soy, B.; Yağci, K. A Case Study for Water Footprint Assessment of a Denim Product. *TEXTEH Proceedings* **2021**, *2021*, 142–147, doi:10.35530/tt.2021.55.

# Sustainable Composite Materials Based on Southwest Tunisian Clay for Energy Efficiency in Buildings

**Najah Majouri [a,b], Jalila Sghaier [a], Mohamed El mankibi [b]**
**(a)***LRTTPI, National Engineering School of Monastir (ENIM), University of Monastir, Tunisia*
*(b)LTDS, National School of State Public Works (ENTPE), University of Lyon, France E-mail: najahmajouri78@gmail.com*

**ABSTRACT**

This research explores the development and analysis of composite materials made from clay found in southwest Tunisia, aimed at improving the thermal and mechanical properties of construction materials. The study utilizes locally sourced, sustainable clays to create materials with enhanced insulation capabilities, which could help lower the energy demands of buildings. The process involved blending two different clay types to maximize performance, followed by detailed assessments of thermal conductivity and compressive strength. The findings reveal a reduction in thermal conductivity by up to 38% and a mechanical strength increase to 2000 kN, indicating the potential of these composites for use in energy-efficient construction. This work contributes to the advancement of cost-effective building materials that could play a role in reducing both energy consumption and carbon emissions.

**KEYWORDS:** Composite materials, Southwest Tunisia clay, Thermal properties, Mechanical properties, Sustainable building materials.

## 1. INTRODUCTION

Extensive research highlights the advantages of natural materials in construction, such as reducing indoor temperatures by up to 25%, which significantly lowers energy consumption (hanna et al., 2022). Additionally, natural materials help cut greenhouse gas emissions over a building's lifespan (Bernardo-Arugay et al., 2023). Clay, widely used in hot, arid regions for millennia (Muntari and Windapo, 2021), remains essential in construction and is highly valued for its durability, insulating properties, and structural stability (Singh, 2022). In southwestern Tunisia, the tradition of using clay bricks has persisted due to their environmental benefits and performance (Majouri et al., 2024). Clay is a sustainable, eco-friendly material known for properties like humidity regulation and infrared radiation emission(Ihekweme et al., 2020). It is a key component in various industrial applications, including ceramics(Semiz, 2017), composed primarily of silicon, aluminum, and oxygen (Wang et al., 2021). While unfired clay is more sustainable, fired clay bricks offer superior mechanical properties, making them suitable for modern construction (Boukili et al., 2021). Few studies have examined the potential of Tunisian clay for ceramics, but research shows that clays from areas like Gabes, Douiret, and the Cap Bon Basin demonstrate high plasticity and minimal shrinkage, meeting international standards (Mahmoudi et al., 2017), (Mahmoudi et al., 2016), (Chalouati et al., 2021). In southwest Tunisia's El Djerid region, large clay deposits are underutilized. This study seeks to evaluate these clays' potential in construction, with a focus on improving energy efficiency. The research analyzes the thermal, mechanical, and physical properties of fired clay samples, assessing their suitability for durable, energy-efficient building materials.

## 2. MATERIAL AND METHODS

The fired clay was prepared from two distinct clay types by mixing them with 30% water and molding the mixture into standardized specimens. After air-drying and oven-drying at 105°C, the bricks were fired at 700°C and cooled slowly to prevent cracking. Various tests were conducted to assess the bricks properties, including compressive strength, thermal conductivity, microstructure (optical microscopy), water absorption, and density, confirming their suitability for construction.

## 3. RESULTS AND DISCUSSIONS

This study effectively demonstrates the potential of composite materials derived from locally sourced clays in southwest Tunisia, showing notable enhancements in both thermal and mechanical properties critical for construction applications.

### 3.1. Thermal Conductivity

The integration of two different clay types resulted in a notable reduction in thermal conductivity, achieving a decrease of up to 38%. This enhancement is crucial for improving the insulation effectiveness of building materials, which can lead to reduced energy consumption for heating and cooling. The results indicate that these composite materials have the potential to sustain comfortable indoor temperatures, thereby enhancing energy efficiency in buildings.

### 3.2. Compressive Strength

The mechanical performance of the composite materials also demonstrated substantial gains, achieving a compressive strength of 2000 kN. This increase indicates strong structural integrity, allowing the materials to withstand various construction stresses, including loads and impacts. The blending of different clay types likely resulted in a more uniform material with fewer imperfections, enhancing its overall strength and durability.

### 3.3. Future Research Directions

While the results are encouraging, further research is necessary to evaluate the long-term durability and performance of these composites across diverse environmental conditions. Subsequent studies should explore the effects of varying firing temperatures and durations on both mechanical and thermal characteristics, as well as the materials' responses to fluctuations in humidity and temperature. Exploring the incorporation of recycled materials into these composites could further enhance their sustainability and help minimize construction waste.

## 4. CONCLUSION

In summary, this research validates the potential for developing composite materials using locally sourced clays from southwest Tunisia to improve the thermal and mechanical characteristics of construction materials. The effective blending of two distinct clay types resulted in a reduction of thermal conductivity by up to 38% and an increase in mechanical strength to 2000 kN. These findings underscore the potential of these composites for energy-efficient construction, contributing to the development of sustainable, cost-effective building materials that reduce energy consumption and carbon emissions. Future research should focus on assessing the long-term durability and environmental impact of these materials to further validate their application in modern construction.

## REFERENCES

1. Cartwright, J., *Big stars have weather too*. 2007, IOP Publishing PhysicsWeb.
2. Bernardo-Arugay, I., Echavez, F., Lumasag, L., Cahigao, J., Aligno, E., Dispo, R.V., Dionio, S.K., Saladaga, C.J., Looc, B., Simplicio, A.M., V.Rivera Virtudazo, R., 2023. Evaluation of Linamon Red Clay, Salvador Black Cinder and Kapatagan Diatomaceous Earth of the Southern Philippines. Minerals 13, 252. https://doi.org/10.3390/min13020252
3. Boukili, G.E., Lechheb, M., Ouakarrouch, M., Dekayir, A., Kifani-Sahban, F., Khaldoun, A., 2021. Mineralogical, physico-chemical and technological characterization of clay from Bensmim (Morocco): Suitability for building application. Construction and Building Materials 280, 122300. https://doi.org/10.1016/j.conbuildmat.2021.122300
4. Chalouati, Y., Bennour, A., Mannai, F., Srasra, E., 2021. Characterization, thermal behavior and firing properties of clay materials from Cap Bon Basin, North East of Tunisia, for ceramic applications. Clay Minerals 55, 1–29. https://doi.org/10.1180/clm.2021.4
5. hanna, C., Aly, A., shebl, sayed, Abdallah, A., 2022. An empirical study on the thermal behavior of rice husk in eco-friendly brick for external walls of buildings. JES. Journal of Engineering Sciences 50, 248–262. https://doi.org/10.21608/jesaun.2022.141836.1144
6. Ihekweme, G.O., Shondo, J.N., Orisekeh, K.I., Kalu-Uka, G.M., Nwuzor, I.C., Onwualu, A.P., 2020. Characterization of certain Nigerian clay minerals for water purification and other industrial applications. Heliyon 6, e03783. https://doi.org/10.1016/j.heliyon.2020.e03783
7. Mahmoudi, S., Bennour, A., Meguebli, A., Srasra, E., Zargouni, F., 2016. Characterization and traditional ceramic application of clays from the Douiret region in South Tunisia. Applied Clay Science 127–128, 78–87. https://doi.org/10.1016/j.clay.2016.04.010

8. Mahmoudi, S., Bennour, A., Srasra, E., Zargouni, F., 2017. Characterization, firing behavior and ceramic application of clays from the Gabes region in South Tunisia. Applied Clay Science 135, 215–225. https://doi.org/10.1016/j.clay.2016.09.023
9. Majouri, N., mankibi, M., Sghaier, J., 2024. Characterization and Evaluation of Southwest Tunisian Clays for the Development of New Clay-Based Building Materials. pp. 343–353. https://doi.org/10.1007/978-981-99-8501-2_31
10. Muntari, M., Windapo, A., 2021. Clay as Sustainable Building Material and its Benefits for Protection in the Built Environment. IOP Conference Series: Materials Science and Engineering 1144, 012044. https://doi.org/10.1088/1757-899X/1144/1/012044
11. Semiz, B., 2017. Characteristics of clay-rich raw materials for ceramic applications in Denizli region (Western Anatolia). Applied Clay Science 137. https://doi.org/10.1016/j.clay.2016.12.014
12. Singh, N., 2022. Clays and Clay Minerals in the Construction Industry. Minerals 12, 301. https://doi.org/10.3390/min12030301

# Improvement of Dark blue reactive dye Degradation via Heterogeneous Catalysis of Fenton Reaction

**Sahar Mazgar, Ghazza Massmoudi, Hatem Dhaouadi**
*Laboratory of Research Environmental Chemistry and clean process, Faculty of Sciences of Monastir, University of Monastir, Tunisia*

*E-mail : Saharmazgar316@gmail.com*

**ABSTRACT**

Heterogeneous Fenton using solid catalysts has emerged as a robust advanced oxidation process for wastewater treatment, offering advantages such as minimal iron sludge production and a wide operational pH range. In this investigation, we employed natural kaolinite clay from Tunisia containing ferrous ions as a solid catalyst for degrading a model synthetic textile dye wastewater based on Dark Blue azo dye in the presence of $H_2O_2$.

To study the heterogeneous Fenton reaction, we measured the release of $Fe^{2+}$ by the clay at various pH levels to optimize the required clay quantity. Adjusting the pH parameter proved crucial in the Fenton process, with optimization showing maximum dye removal at a pH of 4. Furthermore, under identical optimal conditions, we conducted a comparative analysis between heterogeneous Fenton and reactions classical Fenton, while also considering the effect of adsorption. During the heterogeneous Fenton reaction, adsorption may occur due to interactions between the liquid and solid phases. Therefore, we conducted a comprehensive analysis covering adsorption isotherms, kinetics, and thermodynamics. Our findings showed that adsorption only contributed 8% to the removal of the Dark Blue dye. Moreover, an additional study was carried out to assess the impact of ultrasound application on the heterogeneous Fenton reaction.

The comparison of different methods reveals that heterogeneous Fenton is not only more effective than the classical Fenton reaction for wastewater treatment but also more environmentally friendly. This study provides crucial information for developing sustainable water treatment technologies for reactive textile dyes.

**KEYWORDS:** Heterogeneous Catalysis, Fenton Reaction, Wastewater Treatment, Kaolinite Clay, Dark Blue Dye

## 1. INTRODUCTION

In recent years, Advanced Oxidation Processes (AOPs) have gained attention for their effectiveness in removing non-biodegradable contaminants from industrial wastewater. Among them, the Fenton process is particularly promising due to its high efficiency, low cost, and simplicity. It operates in an acidic pH with hydrogen peroxide (H2O2) and Fe2+ salts as catalysts, generating OH radicals that break down various organic compounds (Equation 1):

$$Fe^{2+} + H_2O_2 \rightarrow Fe^{3+} + OH^- + OH^{\bullet} \qquad (1)$$

Despite its effectiveness, the classical Fenton reaction faces challenges such as sludge generation with high iron content and the need for very acidic conditions (pH=3). To address these issues, research is focusing on using supports for iron ions, such as zeolite, silica, clay, and activated carbon, to develop novel heterogeneous Fenton catalysts.

Critical factors for heterogeneous solid phases include density, pore volume, porosity, and surface area. Kaolinite, a clay mineral with a layered silicate structure, has low cation exchange capacity and porosity, affecting its adsorption and catalytic properties.

Synthetic dyes, major pollutants due to their unique properties and simple synthesis, result in significant effluent loss during processing. This study uses kaolinite clay as a catalyst in the Fenton process to treat wastewater contaminated with Dark Blue (DB) dye from the textile industry. This method is cost-effective and environmentally friendly, potentially guiding future research on new catalysts for treating industrial dye wastewater.

## 2. MATERIAL AND METHODS

### 2.1. Materials and products using

This study employed a UV-Visible Spectrophotometer (Jenway 6705 UV/vis) to measure light transmittance and absorbance accurately. Additionally, an Ultrasonicator (Hielscher UIP1000hdT) was used to improve reaction rates and efficiencies in sono-Fenton processes. Key materials include Dark Blue dye, known for its intense color on cotton and acrylic fabrics, and clay sourced from Moknine, Tunisia. The clay was chosen based on specific particle size and optimized physicochemical properties to meet the study's experimental requirements.

### 2.2. The pH-Dependent Release of $Fe^{2+}$ from Clay

In this section, the objective was to investigate the relationship between clay quantities and the release of iron over a pH range of 3 to 7. Increasing amounts of clay were introduced into buffered solutions at specific pH levels and agitated for one hour, mirroring the typical duration of the Fenton process. Subsequently, solid and liquid phases were separated through centrifugation at 150 rpm. The concentration of iron in the supernatants was determined using a $Fe^{2+}$ calibration curve protocol.

### 2.3. Adsorption of Dark Blue dye on Kaolinite clay

During this study, kaolinite was used as the adsorbent and Dark Blue (DB) dye as the adsorbate to analyze adsorption modeling, kinetics, and thermodynamics. We followed a standardized procedure: DB dye solutions ranging from 10 to 80 mg/L were mixed with 0.012 g of adsorbent at pH 4, stirred for 80 minutes at 150 rpm, and then centrifuged for 25 minutes at 3000 rpm. The absorbance of the supernatant was measured using spectrophotometry at the dye's maximum wavelength [3].

### 2.4. Removal of the DB dye by heterogeneous Fenton catalysis

#### 2.4.1. pH Optimization of the Reaction

The efficient removal of dye DB by the heterogeneous Fenton reaction is significantly influenced by the pH of the solution. In this study, we used buffer solutions with pH values ranging from 3 to 7, maintaining continuous agitation for 60 minutes.

#### 2.4.2. Homogeneous Fenton reaction

The study examined the removal of azo dye DB using a molar ratio of 1:3.9:50 for the concentrations of [dye]:[$Fe^{2+}$]:[$H_2O_2$], with clay as the catalyst for the source of [$Fe^{2+}$] concentrations. This optimal ratio was determined for the removal of azo dye DB through the classical Fenton process [4].

This section presents the optimization of the pH for the Fenton reaction. All these experiments were conducted using a dye concentration of 30 mg/L, corresponding to a concentration of 4.8 mg/L of $Fe^{2+}$ and 25% $H_2O_2$.

To enhance DB dye degradation efficiency, we compared the heterogeneous Fenton process with ultrasound treatment. During Sono-Fenton, the solution was stirred and exposed to ultrasound at 75% amplitude at room temperature, with samples collected after 15 minutes.

## 3. RESULTS AND DISCUSSIONS

### 3.1. The pH-Dependent Release of $Fe^{2+}$ from Clay

This study aims to optimize the quantities of clay required as catalysts for Fenton reactions at various pH levels, while maintaining a constant $Fe^{2+}$ concentration of 4.8 mg/L (which represents the optimal [$Fe^{2+}$] concentration for the Fenton reaction studied in this work). Figure 1 illustrates the relationship between the concentration of ferrous ions ($Fe^{2+}$) and the amount of clay across different pH levels (3, 4, 5, 6, and 7).

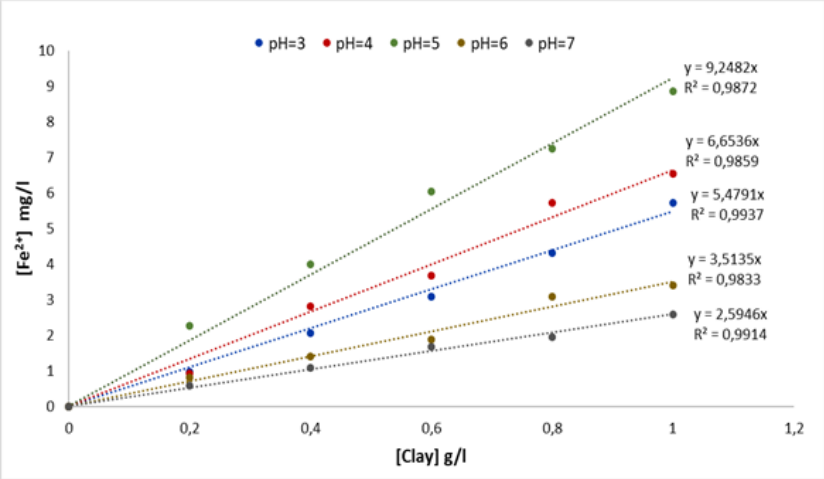


**Fig.1**: Quantification of $Fe^{2+}$ released by clay at pH levels 3, 4, 5, 6, and 7.

### 3.2. Adsorption of Dark Blue dye on Kaolinite clay

The study explored DB dye adsorption on kaolinite using Langmuir, Freundlich, and Dubinin-Radushkevich (DR) isotherms. The DR model fit best ($R^2 = 0.9836$). Kinetic models (pseudo-first-order, pseudo-second-order, and intra-particle diffusion) were compared, with pseudo-first and pseudo-second-order models showing better fit. Thermodynamic analysis indicated a non-spontaneous process with positive $\Delta G°$ values at all temperatures for Dark blue adsorption on natural kaolin. Physisorption dominated, with $\Delta H° < 40$ kJ/mol, and a negative $\Delta S°$ indicating reduced disorder at the solid/solution interface due to adsorbed molecule dimensions (Table 1).

**Table 1:** Thermodynamic parameters of DB dye adsorption by Kaolinite.

| T°(k) | ΔG° (K J/mol) | ΔH (K J/mol) | ΔS (J/mol K) |
|---|---|---|---|
| 308,15 | 2,934 | 9,073 | 19,887 |
| 318,15 | 2,753 | | |
| 328,15 | 2,572 | | |
| 338,15 | 2,329 | | |

### 3.3. Removal of the DB dye by heterogeneous Fenton catalysis

#### 3.2.1. pH Optimization of the Reaction

The results show that pH significantly affects how well DB dye is degraded using heterogeneous Fenton catalysis. The best efficiency, achieving about 31% dye removal within an hour, occurs at pH 4 (Figure 2). At higher pH levels, ferrous ions become unstable and turn into ferric ions, while the ability of hydrogen peroxide to oxidize decreases as it breaks down into oxygen and water.

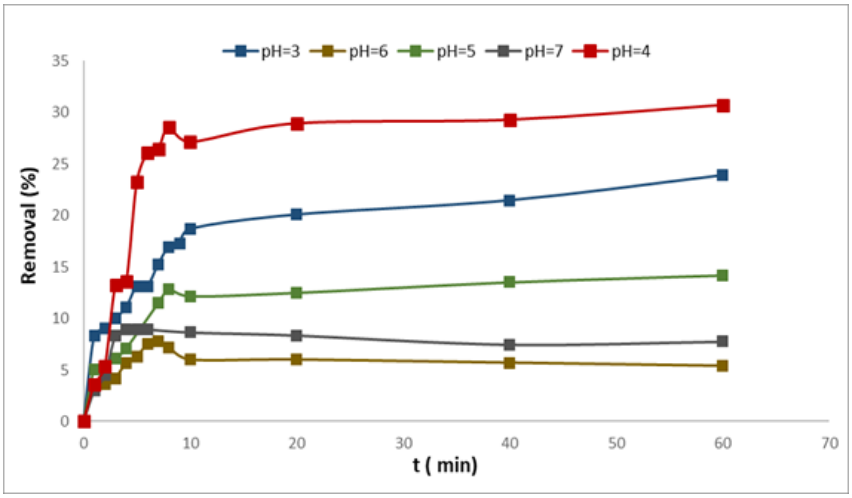


**Fig.2**: Optimization of the heterogeneous Fenton Reaction pH

### 3.2.2. Homogeneous Fenton reaction

Figure 3 demonstrates that in the classical Fenton process (without clay), maximum DB dye removal reaches about 17% after 5 minutes but decreases afterward. In contrast, the heterogeneous catalytic Fenton (with clay) process achieves approximately 31% dye reduction after 1 hour. This difference is mainly due to clay's role in suspending the iron catalyst, allowing for better access to hydrogen peroxide molecules and thus enhancing reaction efficiency.

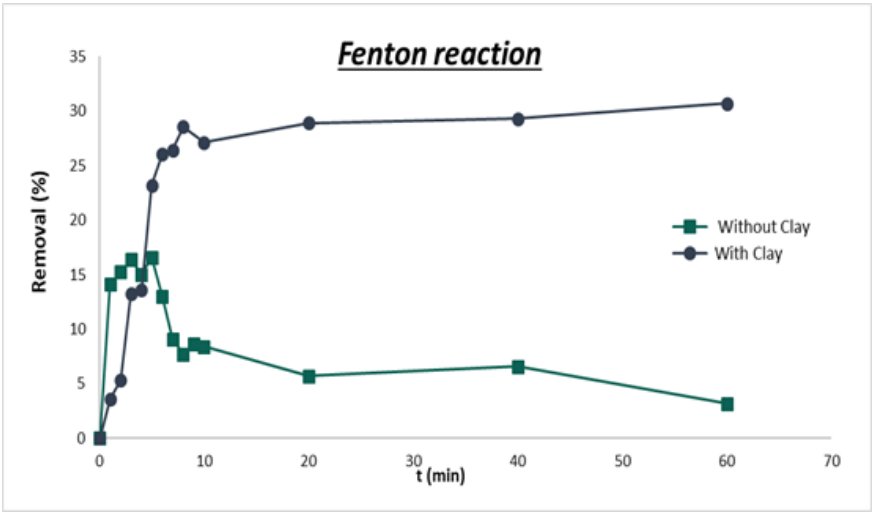


**Fig.3**: Results between homogeneous Fenton process and heterogeneous catalytic Fenton process.

Furthermore, the combination of heterogeneous Fenton reaction and ultrasound shows promise for dye degradation. This method proved highly effective by enhancing the release of ferrous ions from the clay through ultrasound. In this study, the heterogeneous Sono-Fenton process achieved approximately 75% efficiency in removing DB dye within just 15 minutes.

## 4. CONCLUSION

This study explored eco-friendly methods to improve pollutant degradation, focusing on the heterogeneous Fenton reaction using azo dye DB as a model pollutant and raw kaolinite as a catalyst. The results showed that the homogeneous Fenton reaction at pH 4 was not effective in removing DB, with a reduction similar to adsorption. Although adsorption occurred alongside the heterogeneous Fenton reaction, the colour reduction was

limited to 8%. This low efficiency was confirmed by the clay characteristics and adsorption analysis results. However, combining the heterogeneous Fenton reaction with ultrasound achieved the best results, with a 75% reduction of the Dark Blue dye using kaolinite as a catalyst.

## REFERENCES

1. M. Manna et S. Sen, « Advanced oxidation process: a sustainable technology for treating refractory organic compounds present in industrial wastewater », *Environ. Sci. Pollut. Res.*, vol. 30, p. 1-29, mars 2022, doi: 10.1007/s11356-022-19435-0.
2. N. Thomas, D. D. Dionysiou, et S. C. Pillai, « Heterogeneous Fenton catalysts: A review of recent advances », *J. Hazard. Mater.*, vol. 404, p. 124082, févr. 2021, doi: 10.1016/j.jhazmat.2020.124082.
3. M. Musah, Y. Azeh, J. Mathew, M. Umar, Z. Abdulhamid, et A. Muhammad, « Adsorption Kinetics and Isotherm Models: A Review », *Caliphate J. Sci. Technol.*, vol. 4, nº 1, p. 20-26, févr. 2022, doi: 10.4314/cajost.v4i1.3.
4. N. E. H. Slama, G. Masmoudi, M. Fizer, R. Mariychuk, et H. Dhaouadi, « Optimization of Dark Blue reactive dye degradation with Fenton reaction based on experimental design methodology and DFT calculations », *Chem. Pap.*, vol. 77, nº 8, p. 4425-4437, août 2023, doi: 10.1007/s11696-023-02792-6.

# Experimental and DFT study on the removal of Azithromycin by activated carbon prepared from grape seeds

**Mabrouk Sirine, Dhaouadi Hatem**

*Laboratory of Environmental and Clean Process Chemistry, Faculty of Sciences of Monastir, University of Monastir; Monastir, Tunisia*

sirinemabrouk53@gmail.com

**ABSTRACT**

This study examines the synthesis of activated carbon from grape seeds, with ($H_3PO_4$) as an adsorbent for the elimination of azithromycin (AZT). The activated carbon obtained has a porous structure and a specific surface area of 543 $m^2.g^{-1}$, with a pH charge point of 2.5. The adsorption isotherm follows the Langmuir model, while the kinetics is described by the pseudo-first order model. DFT analyses show that the adsorption of AZT is favorable and that the COOH group interacts more strongly than other functional groups. The results show that this waste-derived activated carbon is an effective adsorbent for treating wastewater containing pharmaceutical compounds.

**Keywords:** Grape seeds, Activated carbon, Adsorption, Azithromycin, Density functional theory (DFT).

## INTRODUCTION

Antibiotics are drugs frequently used to treat and prevent human and animal diseases. With their rapid increase in global use, these substances are often found in urban wastewater, surface water and groundwater. Azithromycin, an antibiotic of the macrolide class, is commonly used to treat bacterial infections in humans and to prevent them in aquaculture and livestock animals. It has been detected at high concentrations in sewage treatment plants, underlining the critical importance of its removal from aquatic environments. Several methods have been proposed to eliminate antibiotics such as advanced oxidation (AOP) [1], adsorption and biological processes [2] were reported. Among these, adsorption is one of the most effective methods for removing contaminants from water because of its cost-effectiveness, high efficiency and durability [3]. Activated carbon (CA) is commonly used as an adsorbent because of its large surface area, porous structure, high efficiency, simplicity of design, its simplicity of design and cost-effectiveness, as well as its ability to separate various chemical compounds [4]. Activated carbon production is relatively expensive, which has led to growing interest in developing it from accessible and affordable biomass feedstocks [5]. Several studies have shown the relevance of this approach, such as using coffee grounds to remove phenol and methylene blue [6].

The present study aims to investigate and use grape seeds as a precursor for CA synthesis and its application for AZT elimination. Various analytical methods have been applied to characterize the prepared adsorbent. The isotherm and kinetics of the AZT adsorption process on activated carbon were also evaluated. In addition, analyses based on the functional density theory (DFT) were carried out to better understand the mechanism of adsorption of AZT on activated carbon. DFT studies also provide information on the influence of functional groups such as –OH, –CHO and –COOH present at the carbon surface on the adsorption process.

## MATERIALS AND METHODS

### 1. Preparation of activated carbon

Grape seeds, supplied by AGRILAND ® in Kairouan, Tunisia, were used for the production of activated carbon by chemical activation with $H_3PO_4$. 200 g of the precursor was mixed with $H_3PO_4$ (85% vol.) for 24 hours, then subjected to a thermal treatment at 800°C for 3 hours. The AC obtained was rinsed with hot distilled water until a neutral pH was reached.

### 2. Characterization of activated carbon

The textural properties of the prepared activated carbon (AC) were tested by adsorption/desorption of $N_2$ at -196°C; using the Brunauer-Emmett-Teller (BET) method to determine the specific surface and the Barret-Joyner-Halenda (BJH) method for pore size distribution. The morphology of the surface was examined by scanning electron microscopy (SEM). The surface chemistry was assessed by determining pH at zero charge point ($pH_{PZC}$). Surface functions were also measured by acid-base titration according to the Boehm 1966 method.

### 3. Adsorption experiments

The prepared AC was tested as an adsorbent for liquid phase AZT. Batch adsorption studies were performed at room temperature by mixing 0.2 g CA with 20 mL of AZT solutions at concentrations ranging from 20 to 300 mg. $L^{-1}$. All tests were performed under agitation with measurements taken at different time intervals (from 2 to 240 min) until equilibrium was reached. The AZT concentrations at equilibrium were analyzed at 210 nm by high-performance chromatography (HPLC). The amount of AZT adsorption on AC was calculated as a function of the equilibrium (Eq. 1) and at any time (Eq. 2) adsorption capacity.

$$q_e(\text{mg g}^{-1}) = \frac{(C_0 - C_{e,})}{m} V \quad (1)$$

$$q_t(\text{mg g}^{-1}) = \frac{(C_0 - C_{t,})}{m} V \quad (2)$$

Where $C_0$, $C_e$ and $C_t$ are the concentrations of AZT in solution (mg. $L^{-1}$) at start, at any time t and at equilibrium, respectively; V (L) is the volume of solution and m (g) is the mass of AC.

Langmuir and Freundlich models were applied to adjust the equilibrium isothermal data. Pseudo-first order (PFO), pseudo-second order (PSO) and intra-particle diffusion models were used to analyze the experimental kinetic data.

### 4. Theoretical study

A theoretical study was conducted to elucidate the mechanism of adsorption of AZT on active sites present at the surface of the developed activated carbon. Geometric optimization calculations and vibrational frequency analyses were performed using the (DFT/B3LYP) approach with the 6-311G (d, p) base set, integrating dispersion interactions via the Grimme correction with Becke - Johnson dumping. The effects of water solvent were included in the calculations using the polarizable continuum model (CPCM). All calculations reported here were performed using the GaussView molecular visualization software, from the Gaussian 09 package, used for design, optimization and theoretical calculation respectively. The adsorption energy ($E_{ads}$) of azithromycin (AZT) on the surface of the AC was determined using equation (3).

$$E_{ads} = E_{AC+AZT} - (E_{AC} + E_{AZT}) \quad (3)$$

Where $E_{AC}$, $E_{AZT}$ and $E_{AC+AZT}$ represent the total energies of the free AC and Azithromycin molecules and the « AC-AZT » complex, respectively.

## RESULTS AND DISCUSSIONS

### 1. Characterization of activated carbon

The BET specific surface of the prepared AC is 543 $m^2$. $g^{-1}$ with a total pore volume of 0.218 $cm^3$. $g^{-1}$ and an average pore size of 3.08 nm. Figure 1 shows a SEM image of the AC, showing an uneven and rough surface with cavities. These characteristics could promote the adsorption process.

The $pH_{pzc}$ of the developed AC was about 2.5, indicating that its net surface charge becomes positive below this pH and negative above, suggesting a predominance of acidic functional groups.

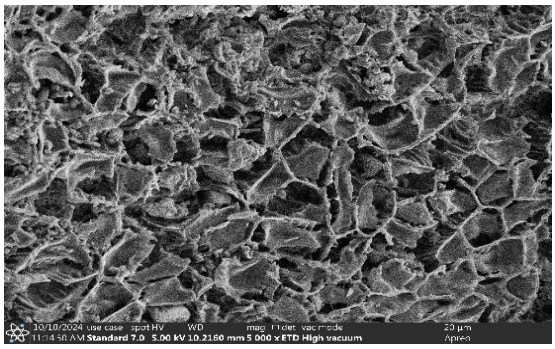

**Fig 1.** SEM image of prepared AC

The results of the Boehm titration, summarized in Table 1, confirm the acidity of the AC surface by the presence of carboxylic, phenolic and lactonic groups.

**Table 1.** Acid and basic sites on the surface of prepared CA

| Acid functions | (méq. $g^{-1}$) | Percentage (%) |
|---|---|---|
| **Carboxylic** | 0.95 | 32 |
| **Lactonic** | 0.55 | 18 |
| **Phenolic** | 1.49 | 50 |
| **Total acidity** | 2,99 (± 0,02) | |
| **Total basicity** | 2,37 (± 0,03) | |

## 2. Batch adsorption studies

### 2.1 Adsorption kinetics studies

The kinetic study of PCT adsorption on AC shown in Figure 2 shows a rapid adsorption during the first 15 minutes, due to the large number of vacant sites available on the surface of the AC. The adsorption has then reached equilibrium after 30 min, indicating saturation of the sites on the coal.

The pseudo-first order model represents a better fit of experimental data, with higher correlation coefficients ($R^2$ = 0.99) than the PSO and intra-particle diffusion models.

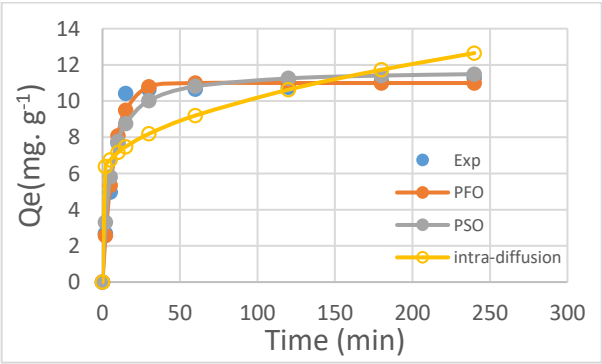


**Fig 2.** Kinetic study of AZT adsorption on CA

### 2.2 Adsorption isotherms studies

Experimental equilibrium data were adjusted using the isothermal models of Langmuir and Freundlich (Figure 3). The Langmuir model is better at describing the adsorption behaviour of AZT, with a higher correlation coefficient ($R^2$ = 99%) than the Freundlich model. This model suggests a single-layer adsorption on a homogeneous surface of the AC with maximum adsorption capcity $q_{max}$ was 54.45 mg. $g^{-1}$. The results revealed that the AC prepared in this work could be an alternative adsorbent for removing pharmaceutical compounds from wastewater.

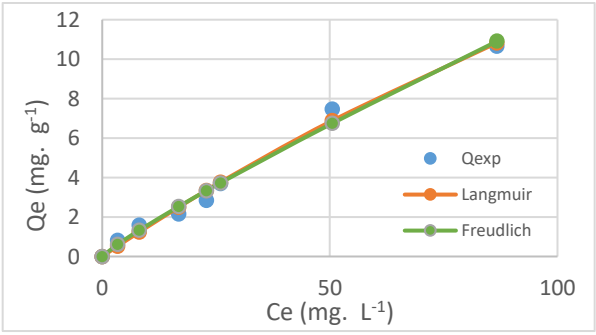


**Fig 3.** AZT on AC adsorption isotherms

## 3. Computational studies

### 3.1. Activated carbon model

In this study, the pristine was used to model the surface of the AC. To study the influence of a functional group, groups –OH, –CHO and –COOH were introduced into active sites, selected according to the results of the Boehm assay.

### 3.2. Theoretical modeling

The highest occupied molecular orbital (HOMO) and the lowest unoccupied molecular orbital (LUMO) identify areas of the molecule that can share electrons. Figure 4 shows that the LUMO orbital of the AZT molecule is mainly located on carbonyl groups (C=O) and protons on oxygen atoms, while the HOMO is associated with amine groups ($NH_2$). The HOMO-LUMO gap reflects the hardness or softness of a molecule, with soft molecules having a smaller energy gap, which promotes their adsorption. In this context, AZT with a deviation of ΔE = - 4.642 eV shows an easier adsorption on the carbon surface (Fig. 4).

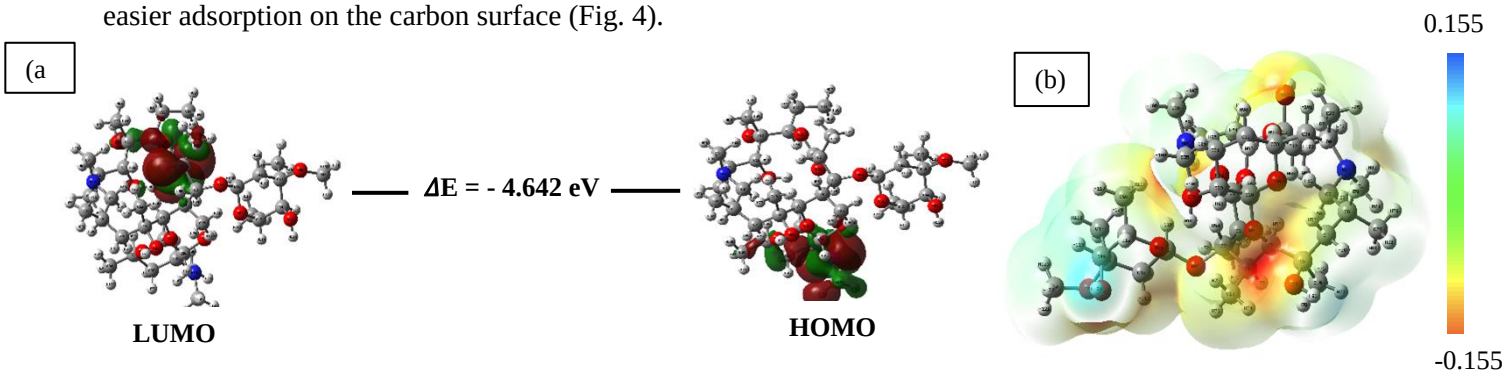


**Fig 4.** Highest HOMO occupied molecular orbital density, lowest LUMO (a) unoccupied molecular orbital density and MEP ($e/au^3$ scale) mapping of AZT (b) by DFT at B3LYP/6–311G (d, p)

Quantum chemistry descriptors were studied to better understand the characteristics of AZT. The values of these descriptors for AZT are presented in Table 2.

**Table 2. Quantum chemical descriptors values for AZT**

| Quantum chemical parameters | HOMO Energy ($E_H$, eV) | LUMO Energy ($E_L$, eV) | Energy gap (□E = $E_H$-$E_L$, eV) | Chemical potential ($\mu = \frac{-(E_H+E_L)}{2}$, eV) | Global chemical hardness ($\eta = \frac{(-E_H+E_L)}{2}$, eV) | Electrophilicity index ($\omega = \frac{\mu^2}{2\eta}$, eV) |
|---|---|---|---|---|---|---|
| **AZT** | -8.230 | -3.588 | -4.642 | 5.909 | 2.321 | 7.521 |

The molecular electrostatic potential (MEP) surface has been generated and illustrated in Figure 4. The different colors on this surface indicate the values of the electrostatic potential. The analysis shows that negative potentials (Red) focus on carbonyl groups (C=O) and hydroxyl (-OH), suggesting electrophilic attack sites, while positive areas (Blue) are is found on the hydrogen atom of hydroxyl groups and amines.

To evaluate the best interactions for AZT adsorption on activated carbon, the adsorption energies of different optimized configurations of AZT were analyzed. The results, shown in Figure 5, show that COOH groups significantly improve adsorption compared to CHO and OH groups. The order of stability of configurations is AC_COOH_AZT > AC_CHO_AZT > AC_OH_AZT. The optimized structure of activated carbon including the functional groups OH, CHO and COOH(AC) as well as its interaction with AZT is illustrated in Fig. 5d. The adsorption energy ($E_{ads}$) was found to be 4.94 kcal. $mol^{-1}$, which is lower than that of the interactions between AZT and each of the functional groups COOH and CHO taken separately. This suggests that the presence of multiple functional groups may lead to less favorable interactions, thus decreasing the overall efficiency of adsorption.

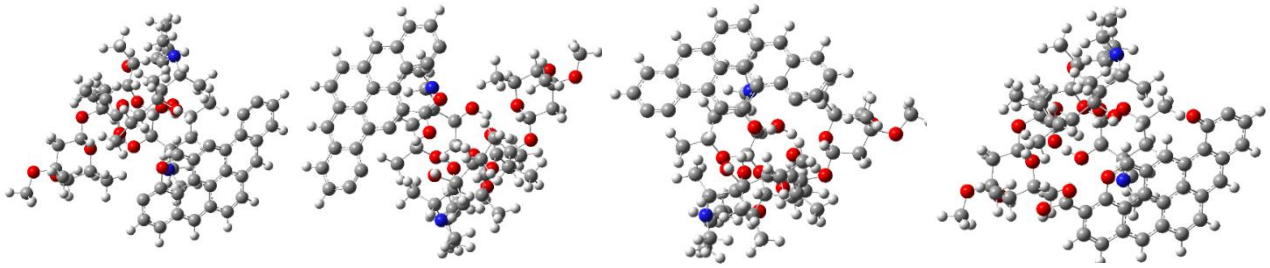

(a) **$Ea_{ds}$ = 5.98 kcal. $mol^{-1}$**

(b) **$E_{ads}$ = 6.21 kcal. $mol^{-1}$**

(c) **$E_{ads}$ = 1.63 kcal. $mol^{-1}$**

(d) **$E_{ads}$ = 4.94 kcal. $mol^{-1}$**

**Fig 5.** Structures optimisées des interactions entre AC et AZT : a) AC_CHO_AZT, b) AC_COOH_AZT, c) AC_OH_AZT, et d) AC_CHO_COOH_OH_AZT

## CONCLUSION

This study presents the synthesis of a new activated carbon prepared from grape seeds, an effective adsorbent for AZT removal. The developed material has a well-developed porous structure and a specific surface area of 543 $m^2.g^{-1}$. Adsorption experiments indicated that the PPO and Langmuir models presented the best fit to experimental kinetic and equilibrium data, respectively. The maximum adsorption capacity obtained was 54.45 mg. $g^{-1}$. DFT simulation studies have shown that the COOH group interacts with AZT more strongly than other functional groups. Overall, the results indicated that AC is an effective adsorbent that can be used to remove azithromycin from aqueous solutions.

## REFERENCES

1. Yang W, Hong P, Yang D et al (2021) Enhanced Fenton-like degradation of sulfadiazine by single atom iron materials fxed on nitrogen-doped porous carbon. J Colloid Interface Sci 597:56–65.
2. Tran NH, Chen H, Reinhard M, et al (2016) Occurrence and removal of multiple classes of antibiotics and antimicrobial agents in biological wastewater treatment processes. Water Res 104.
3. Supong A, Bhomick PC, Baruah M, et al (2019) Adsorptive removal of bisphenol A by biomass activated carbon and insights into the adsorption mechanism through density functional theory calculations. Sustain Chem Pharm 13.
4. Djilani C, Zaghdoudi R, Djazi F et al (2015) Adsorption of dyes on activated carbon prepared from apricot stones and commercial activated carbon. J Taiwan Inst Chem Eng 53:112–121.
5. Martins AC, Pezoti O, Cazetta AL, et al (2015) Removal of tetracycline by NaOH-activated carbon produced from macadamia nut shells: kinetic and equilibrium studies. Chem Eng J 260.
6. Laksaci H, Khelif A, Trari M, Addoun A (2017) Synthesis and characterization of microporous activated carbon from cofee grounds using potassium hydroxides. J Clean Prod 147.

# Response surface modeling of Amoxicillin removal from aqueous solution: Box–Behnken experimental design and batch adsorption

**Maryi Teieb [a], Hatem Dhaouadi [a], Sonia Dridi-Dhaouadi [a,b]**

*(a) Research Laboratory of Environmental Chemistry and Clean Processes, Faculty of Sciences, University of Monastir, Monastir, Tunisia*

*(b) Preparatory Institute for Engineering Studies, University of Monastir, Tunisia;*
*E-mail : meryiteyeib@gmail.com*

**ABSTRACT**

Water pollution, particularly the contamination of surface water resulting from the discharge of industrial and medical waste, has become a major concern in environmental studies. Various methodologies and strategies are employed to treat these contaminated waters, with adsorption on activated carbon being identified as a promising method for water purification. This research focuses on the removal of amoxicillin using activated carbon derived from Prickly Pear Seeds extracted under supercritical carbon dioxide (SC-PPSAC). Response surface methodology (RSM) was employed to determine the optimal conditions for removing amoxicillin (AMX) using SC-PPSAC. The effects of experimental factors (initial AMX concentration, adsorbent dose, time contact, and pH) on adsorption capacity were investigated, with the optimal parameters being an initial AMX concentration of 140 mg/L, a dosage of 0.1 g of SC-PPSAC, a solution pH of 3, and a time of 120 minutes. The adsorption kinetics followed the pseudo-second-order model and showed that equilibrium was reached within 120 minutes. The maximum adsorption capacity of AMX onto SC-PPSAC was calculated to be 17.8 mg/g.

**KEYWORDS:** Amoxicillin, Adsorption, Response surface, Optimization.

## 1. INTRODUCTION

A multitude of harmful substances, such as pharmaceuticals, including antibiotics, anti-inflammatory drugs, and analgesics, exert adverse effects on organisms and ecosystems. Even at low concentrations, these micropollutants can be detected in various water sources, including wastewater, surface water, groundwater, and drinking water.[1]

The rise of pharmaceutical contamination in wastewater due to trace drug residues has shown a notable increase in recent years, attributed to rising flu cases and the use of pharmaceutical additives. Amoxicillin, a β-lactam antibiotic from the aminopenicillin family, is extensively used to treat susceptible bacterial infections. It is the most commonly prescribed antibiotic worldwide, especially in pediatric cases, due to its high absorption rate and cost-effectiveness. A significant portion of these antibiotics is excreted by the human body in unmetabolized forms, leading to their accumulation [2].

Adsorption is one of the most important methods for removing pollutants from water and is the basis for commercially available filters. The widespread adoption of this technique is due to its simplicity and the use of readily available materials [3].

Response Surface Methodology (RSM) evaluates the relationships–between the response(s) and the independent variables, providing insight into the effects of the independent variables, either individually or collectively, in the various processes. This approach offers numerous benefits such as cost-effectiveness, reduced experimentation, the ability to examine parameter interactions on the response, prediction of outcomes, method validation, and time efficiency.[4] This technique employs low-order polynomial equations within a specified range of independent variables, which are then analyzed to determine the optimal values of the independent variables for achieving the optimal responses. RSM has gained particular significance in the study of heavy metal ion adsorption.[5]

This study primarily focuses on providing valuable insights and advancing sustainable water treatment methods, specifically targeting the removal of antibiotic contaminants from aqueous environments, using phosphoric acid activated carbon (SC-PPSAC). Additionally, an analysis has been conducted on the effect of different variables, such as pH, antibiotic concentration, contact time, and adsorbent mass, on the adsorption process.

## MATERIAL AND METHODS

### 2.1. Batch adsorption experiments

Batch adsorption experiments were performed to investigate the removal of AMX by SC-PPSAC in 30 mL glass flasks. An amount of 20–400 mg of SC-PPSAC was added to 20 mL of AMX solution with concentrations ranging from 50 to 800 mg/L ($C_0$). The pH of the solution was adjusted using 0.1 M HCl and 0.1 M NaOH. The glass flasks were sealed with plastic paraffin film and placed on a shaker at a constant temperature 30 ± 2 °C, agitated at 150 rpm for 180 minutes. After equilibrium was reached and the sorbent was separated from the solution, the remaining AMX concentration was determined using a spectrophotometer (CECIL-CE 2021). The adsorption capacity of AMX on SC-PPSAC ($Q_e$) was then calculated using the following equation:

$$Q_e = \frac{(C_0 - C_e)V}{m} \qquad (1)$$

Where $Q_e$: the amoxicillin uptake (mg AMX/g of sorbent), $C_0$ and $C_e$: the initial and final concentrations of AMX in the solution (mg/L), respectively, V: the total volume of the solution (mL), and m: the amount of the sorbent used (mg).

### 2.2. Response surface methodology (RSM)

The traditional approach involves the alteration of one variable at time while keeping all other parameters constant. Conducting experiments using this conventional technique, as well as examining parameter interactions, is both time-consuming and inefficient. Response Surface Methodology (RSM) serves as a key component of experimental design, enabling the evaluation of multiple factors and their interaction on the system response. This method integrates mathematical and statistical approaches and is particularly useful in situations where numerous variables influence the outcome. RSM involves three essential stages: experimental design, response surface modeling, and optimization. In this study, the Box-Behnken Design (BBD) was chosen and implemented using Minitab 19 statistical software.

## 2. RESULTS AND DISCUSSIONS

### 2.1. Effect of adsorbent dose

The investigation into the effect of adsorbent dose covered a range of SC-PPSAC masses, from 20 to 400 mg, in 20 mL of amoxicillin solution with an initial concentration ($C_0$) of 50 mg/L. The results are illustrated in Figure 1. As the mass of SC-PPSAC increased from 20 mg to 400mg, the adsorbed amount of amoxicillin decreased, ultimately reaching 2.4 mg /g with a removal efficiency of 95.31%. An increase in the adsorbent's mass leads to an increasing of the active sites suitable. This, in turn, enhances the number of accessible sites on the surface of adsorbent, resulting in a greater quantity of AMX being adsorbed. However, as the amount of adsorbent rises, the amount of AMX absorbed per gram of SC-PPSAC diminishes. This reduction is due to the accumulation of particles, which lowers the specific surface area and, consequently, decreases the overall adsorption capacity. Once the mass exceeds 0.1 g, further increases do not significantly impact the removal of AMX. Therefore, a mass of 0.1 g is identified as the optimal amount.[6]

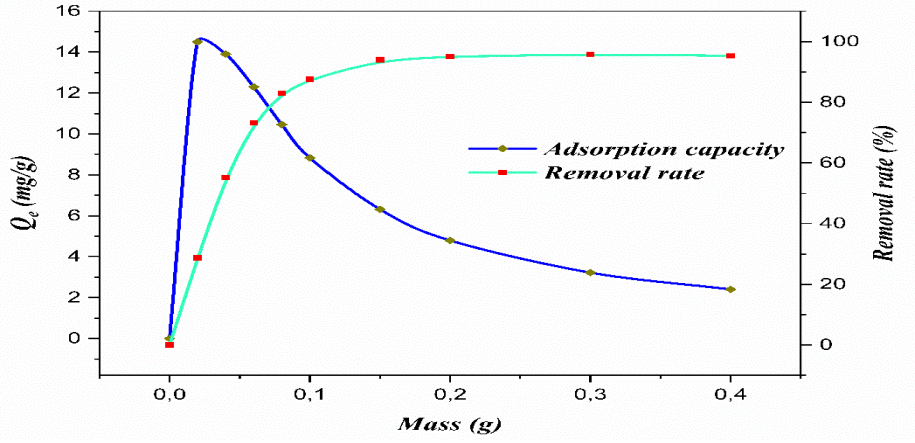


*Fig. 1.The effect of adsorbent dose on AMX adsorption capacity and removal rate*

### 2.2. Effect of contact time

Contact time is a crucial factor affecting the adsorption capacity. Figure 8 depicts the change in AMX adsorption capacity over time. The adsorption of AMX on SC-PPSAC was rapid within the first 20 minutes, followed by a gradual decrease in the adsorption rate-between 20 and 90 minutes, until equilibrium was reached at 120 minutes. Thus, 120 minutes was identified as equilibrium time.

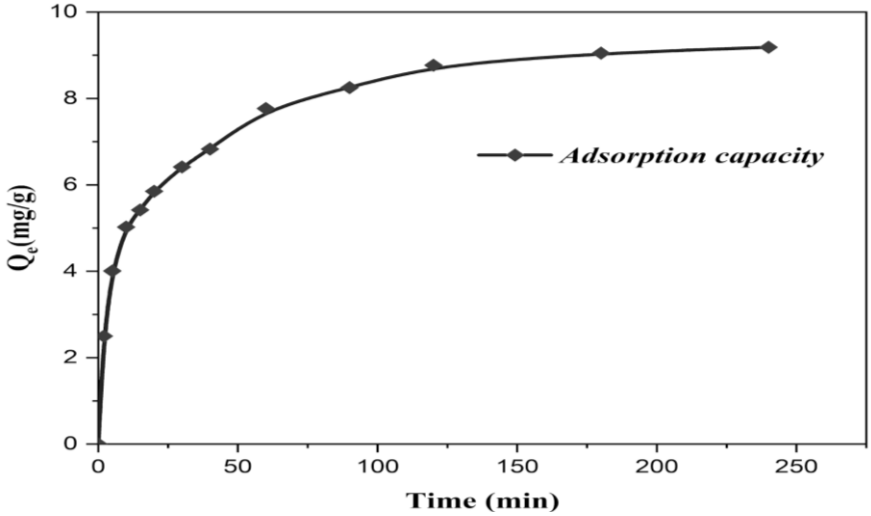


*Fig. 2. The effect of contact time on AMX adsorption capacity*

### 2.3. The design of experiments for conducting studies on adsorption

The selection of initial AMX concentration, time, pH, and adsorbent dose as independent variables was based on prior experiments. The adsorption capacity of AMX ($Q_e$) was designated as the response variable for these experiments. The experimental runs were carried out in a random order across three levels. A total of twenty-seven runs were established for the experimental design. To account for pure error, the central point was replicated three times. An analysis of the response was conducted to assess the AMX adsorption performance. The variables were coded at low (-1), middle (0), and high (+1) levels as reported in Table 1, along with the experimental design determining the factors.

Table 1. Variables and their Levels

| Levels | Mass (g) | $C_0$ (mg/L) | Time (min) | pH |
|---|---|---|---|---|
| -1 | 0.05 | 50 | 20 | 3 |
| 0 | 0.1 | 100 | 70 | 7 |
| +1 | 0.15 | 150 | 120 | 11 |

To gain a better understanding of the AMX adsorption process, three-dimensional response surface plots were analyzed. In each plot, the effects of two factors on AMX adsorption capacity were investigated while keeping the other factors at their optimal values. Figure 3 shows the simultaneous effects of time and pH on AMX adsorption capacity. While the contact time increase and pH decrease principally leads to an increase in adsorption capacity. This response surface plot indicated that the best conditions of interaction between pH and contact time were found at pH 3 with a reaction time of 120 min. In This case, the adsorption capacity reaches 17 mg/g.

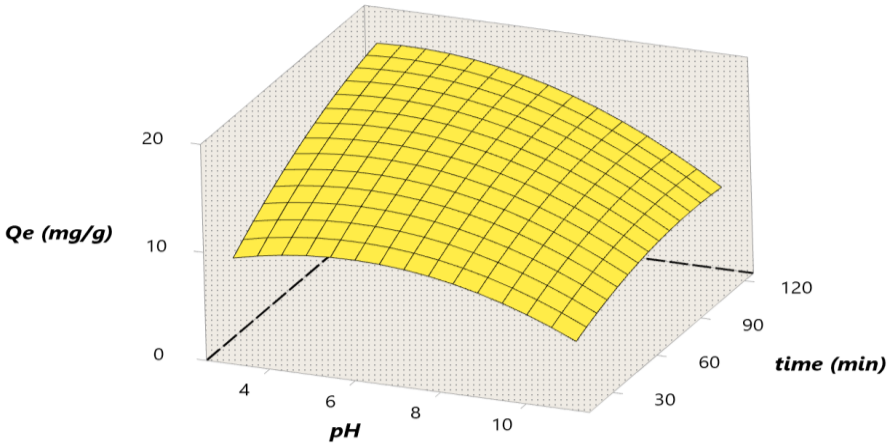


***Fig. 3.*** *Simultaneous effect of pH and contact time on AMX adsorption capacity*

## 3. CONCLUSION

The study focuses on the use of Box-Behnken experimental design approach to optimize process parameters for the removal of AMX from aqueous solutions using SC-PPSAC. The batch experimental data revealed that the maximum adsorption capacity of SC-PPSAC, approximately 17 mg/g, was achieved under these optimal conditions : m=0.1 g, $C_0$=140 mg/L, t=120 min, and pH=3.

## REFERENCES

1. El Farissi, H., Beraich, A., Lamsayah, M., Talhaoui, A., El Bachiri, A.: The efficiency of carbon modified by phosphoric acid (H3PO4) used in the removal of two antibiotics amoxicillin and metronidazole from polluted water: Experimental and theoretical investigation. Journal of Molecular Liquids. 391, 123237 (2023).
2. Touijer, A., Yahia, E.H., Saidi, M., Taouil, H., Allaoui, M., Ahmed, S.I.: Removal of Amoxicillin from an Aqueous Solution by Activated Carbon Prepared from Biomass. J. Ecol. Eng. 24, 63–79 (2023).
3. Moussavi, G., Alahabadi, A., Yaghmaeian, K., Eskandari, M.: Preparation, characterization and adsorption potential of the NH4Cl-induced activated carbon for the removal of amoxicillin antibiotic from water. Chemical Engineering Journal. 217, 119–128 (2013).
4. Yetilmezsoy, K., Demirel, S., Vanderbei, R.J.: Response surface modeling of Pb(II) removal from aqueous solution by Pistacia vera L.: Box–Behnken experimental design. Journal of Hazardous Materials. 171, 551–562 (2009).
5. Shojaeimehr, T., Rahimpour, F., Khadivi, M.A., Sadeghi, M.: A modeling study by response surface methodology (RSM) and artificial neural network (ANN) on Cu2+ adsorption optimization using light expended clay aggregate (LECA). Journal of Industrial and Engineering Chemistry. 20, 870–880 (2014).
6. Gemici, B.T., Ozel, H.U., Ozel, H.B.: Removal of methylene blue onto forest wastes: Adsorption isotherms, kinetics and thermodynamic analysis. Environmental Technology & Innovation. 22, 101501 (2021).

# Contamination and Ecological Quality Status of the Southern Tunisian coasts

**Nawfel Mosbahi[a], Lassad Neifar[a], Jean-Claude Dauvin[b]**

*(c) Laboratoire de Biodiversité Marine et Environnement, Faculté des Sciences de Sfax, Université de Sfax, BP 1171, 3038 Sfax, Tunisie*
*(d) Université de Caen Normandie, UNICAEN, Laboratoire Morphodynamique Continentale et Côtière, CNRS, UMR 6143 M2C, 24 rue des Tilleuls, 14000 Caen, France*
*Email: nawfel.mosbahi.etud@fss.usf.tn*

**ABSTRACT**

The Gulf of Gabès, located in the central Mediterranean Sea, is now undergoing a high stress caused by intensive anthropogenic pressures due to trawling practices, while pollution (e.g phosphogypsum inputs, industrial waste) and shipping activity are causing more serious environmental problems. These anthropogenic activities impacting marine systems, causing a deterioration of seagrass beds, notably the *Posidonia oceanica* meadows, a decline in fisheries, and changing the structure functioning of benthic communities. To assess the impact of the increasing pollution, several methods and indices have been established. Macrobenthic communities are largely used as an environmental bioindicators, especially in the polluted environment where their sensitivity to pollutants may be expressed by a modification in the benthic assemblages. The present study reports the response of benthic macrofauna sampled during ten years' survey) to multiple anthropogenic pressures and to improve our knowledge of the impact of metallic contamination on structure of macrobenthic communities, as well as the Ecological Quality Status (EcoQS) in Southern Tunisian coasts. Based on the quantitative and qualitative analysis of 420 surface sediment samples collected in Southern Tunisian coasts by specific sampling methodologies depending on the sediment type and depth for each studied zone. The sampling was carried out from January 2013 to April 2023, identifying 282 macrobenthic taxa. Among them, polychaetes (34%) and crustaceans (32%) are the most dominant groups. Three macrobenthic assemblages were identified according to their environmental characteristics such as sediment type, organic matter content and heavy metal contamination. The benthic and biotic indices (AMBI, BENTIX and BO2A) are applied to assess the ecological status of Southern Tunisian coasts, which varies from poor to good status. The EcoQS of the southern Tunisian coasts was significantly influenced by the environmental conditions for each studied site (e.g. organic matter, heavy metals contamination). The present study could be considered as providing important baseline data for the implementation of environmental policies and management plans in the future.

**KEYWORDS:** Heavily metal contamination, Macrobenthic fauna, Southern Tunisian coasts, Benthic assemblages, Environmental impact.

## 1. INTRODUCTION

The Gulf of Gabes, located in the Southeast of Tunisia, owns one of the largest continental shelves in the Eastern Mediterranean Basin. Despite its importance to the economy and for wildlife conservation, the marine ecosystems of the Gulf of Gabès is subject to the loss and degradation of biodiversity caused by bottom-trawling fishing [1] and pollution due to various anthropogenic activities linked to the maritime discharges rendering the harbour environment hostile for native species and opening a window for the proliferation of native and exotic opportunistic species [2, 3, 4] and essentially to the phosphate industry [5]. It is exposed, since 1988, to large quantities of phosphogypsum from the phosphoric acid and chemical products industry of Sfax, Skhira and Gabès are released into the Gulf of Gabes [6]. Phosphogypsum contains several pollutants like heavy metals, fluorine, phosphorus and even radionuclides generating radioactivity [6, 7]. In 2010, Tunisia was a leading country of phosphate production (8 million tons) being the fifth phosphate producer worldwide with around 13 million tons of phosphate ore extracted. This chemical pollution had negative impacts on biodiversity and had trig gered the disappearance or at least the reduction, of seagrass cover in the Gulf, *Posidonia oceanica* meadows in particular and decline in fishing [3, 7].

Due to the limitations of physico-chemical approaches available to measure the impact of disturbances on marine ecosystems [8], Ecological studies relying only on these approaches to assess the impact of pollution on marine communities can be confusing. Ecologists note the importance of benthic communities to establish the ecological status of communities [8,9] and assess biological integrity of marine systems [9]. Furthermore, benthic macrofauna is a powerful tool to detect even slight environment changes [9]. It may locally detect the level of stress and integrate the recent history of stress, constituting a sort of memory for the system. The composition and structure of benthic macrofauna is one of the indicated biological quality elements to be used for marine ecological status assessment [9, 10]. like the rest of the Mediterranean, the Gulf of Gabès, the marine ecosystems are subject to the loss and degradation of biodiversity caused by bottom trawling fishing [1] and pollution due to various anthropogenic

activities linked to the phosphate industry [5,6], as well as maritime discharges rendering the harbor environment hostile for native species and opening a window for the proliferation of native and exotic opportunistic species [3]. The present study aims to improve our knowledge of the heavy metals' distribution, the structure and diversity of macrobenthic communities, as well as the EcoQS in the Southern Tunisian coasts. The correlations between the benthic ecological quality and heavily metal contamination are evaluated.

## 2. MATERIAL AND METHODS

### 2.1 Study area

The Gulf of Gabès (GG) is located in the central part of the Mediterranean Sea, delimited by the south-eastern coast of Tunisia (Fig. 1). Its climate is dry (average annual precipitation: 210 mm year-1) and sunny with strong easterly winds. The tide is semidiurnal, with a maximum range of about 2.3 m near the coast around the Kneiss Islands [11]. The GG supports one of the most productive ecosystems in the Mediterranean Sea, not only associated with significant economic importance (contributing about 65% of the national fish production in Tunisia). In spite of its importance for fisheries and high natural heritage value, the GG is considered as one of the most heavily polluted Mediterranean areas owing to the presence of well-developed coastal cities generating various sources of industrial, agricultural and domestic contaminants [3, 4, 7].

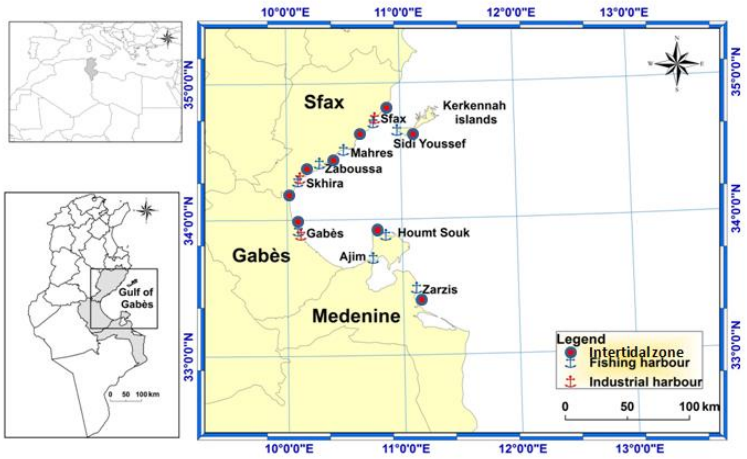


**Fig. 1** Map of the study area indicating the studied areas in Southern coasts of Tunisia.

### 2.2 Sampling design and sample treatments

The sampling was carried out from January 2013 to April 2023 in nine sites including harbors and intertidal ecosystems (Fig. 1). For each site, three stations were sampled. At each station, five replicate samples were taken with a Van Veen grab covering a unit surface of 0.05 $m^2$: i.e., four samples for biological analyses representing a total surface of 0.2 $m^2$, and the last replicate for sediment analyses (sediment type, organic matter content, and chemical contamination analyses). Each biological sample was sieved on a 1 mm mesh and the retained fractions were conserved in 5% formaldehyde saline solution. Some collected samples contained a hard fraction including pebbles and shells, which were preserved and considered for further studies. In the laboratory, after staining with Rose Bengal, samples were sorted; the individuals were identified to the lowest possible taxonomic level and then counted. In addition, the physiochemical parameters were measured during each sampling campaign.

### 2.3 Data Analysis

#### 2.3.1 Benthic indices

Collected data were used to calculate the species abundance (A, number of individuals estimated per $m^2$) to determine the most commonly used biodiversity indices for each station i.e.: the taxonomic richness (S, number of taxa), the Shannon-Weaver diversity index (H′) in $\log_2$ (and Pielou's evenness (J). Data analysis was carried out using version 6 of the PRIMER® (Plymouth Routines in Multivariate Ecological Research) software package. For the assessment of environmental quality, we make use of three biotic indices: AMBI (AZTI Marine Biotic Index), BENTIX and BO2A.

#### 2.3.2 Spatial patterns of the macrofauna assemblages

The spatial distribution of the macrofauna community of the southern Tunisian was analysed by group-average sorting classification. This was followed by a cluster analysis and Non-metric Multidimensional Scaling (n-MDS) ordination of stations or groups of stations, based on the Bray-Curtis similarity measure and calculated from square-

root transformed data. SIMilarity PERcentages (SIMPER) tests were performed to determine which species contributed most to within-group similarity. The significance of differences between the groups of samples so obtained was assessed by an Analysis of similarities (ANOSIM). The BIOENV procedure was used to identify which combination of environmental variables best explains the differences in macrofauna distribution. These multivariate analyses were applied by PRIMER®-v6 software.

## 3. RESULTS AND DISCUSSION

### 3.1 Benthic diversity

A total of 18,202 individuals were identified, belonging 282 macrozoobenthic taxa, 109 families and eight zoological groups unequally distributed among the sampling sites. Among them, polychaetes (34%) and crustaceans (32%) are the most dominant groups in the southern Tunisian coasts. The most abundant benthic species are *Cirratulus cirratus* (420 ind.m$^2$), *Cerithium scabridium* (310 ind.m$^2$), *Cymadusa filosa* (280 ind.m$^2$), and *Euclymene lombricoides* (280 ind.m$^2$). The dominance of these species was correlated by environnemental features of the studied sites. The three intertidal zones: Sfax, Skhira, and Gabès characterised by mud and fine sediment and high level of heavily metals contamination are dominated by pollution-tolerant species and opportunistic polychaetes species indicative of stressed environments, such as *Capitella capitata, Hediste diversicolor, Cirratulus cirratus, Heteromastus filiformis, Hediste diversicolor* and *Paracerceis sculpta.* These species are almost the same dominant species in others polluted [2,3,4,12]. These opportunistic benthic species are indeed adapted to occupying highly stressful or unstable habitats, which are also perturbed and/or denuded [12].

### 3.2 Linking macrobenthic fauna distribution and environmental variables

On the southern Tunisian coasts, three distinct benthic invertebrate assemblages are identified. These assemblages are correlated with dissimilarities of environmental variables during the sampling campaigns. The first assemblage (GA) corresponds to stations sampled in polluted zones (Sfax, Skhira, and Gabès) and commercial harbors characterized by muddy sediment with enrichment in organic matter and high concentrations of heavy metals. The second assemblage (GC) corresponds to stations sampled in fishing harbors and intertidal zones characterized by fine sediment. The last assemblage (GB) formed by stations sampled in Kneiss and Kerkennah islands composed of medium to coarse sand covered by *Posidonia oceanica* and *Zostera noltei* beds, characterized by high diversity indices with relatively low organic matter and heavy metal contents.

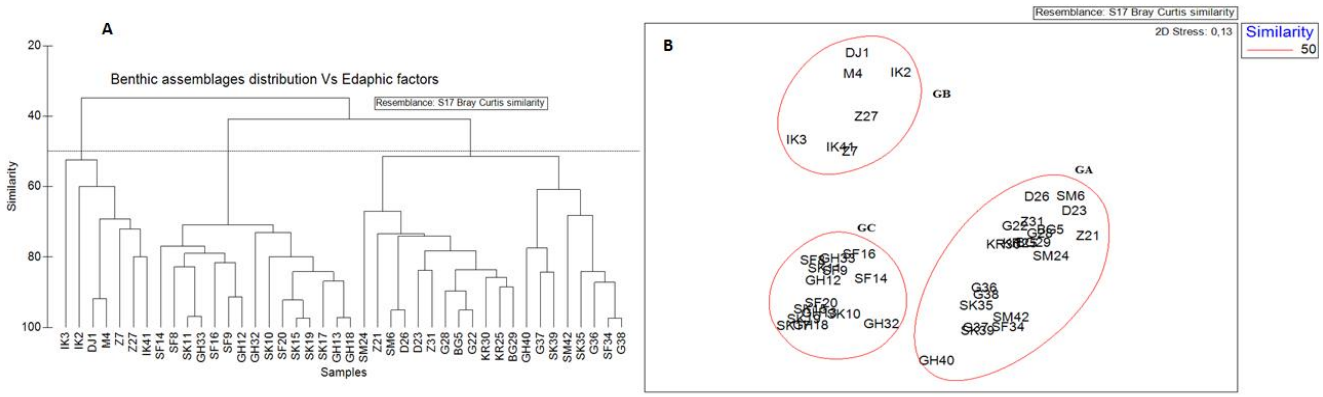


**Fig. 2.** (**A**) Cluster and (**B**) non-metric multidimensional scaling (n-MDS) of stations sampled in 12 Southern Tunisian coasts based on Bray-Curtis similarity matrix after square root-transformation of abundance data. Three groups of stations are identified by Cluster Analysis at a 50% similarity level.

These results are consistent with several previous studies showing that diversity and biotic indices and macrobenthic fauna distribution are generally influenced by edaphic factors like sediment type and heavy metal pollution [3,13, 14].

### 3.3 Ecological status of the southern Tunisian coasts

The ecological status ECoQS of the southern Tunisian coasts is assessed here using biotic indices, i.e. H', J', AMBI and BO2A, which show significant differences between stations. The low values are recorded in the polluted zones and in commercial harbors indicating moderate ecological status. Contrwaise, higher values of biotic indices are

enregistred in Kneiss and Kerkennah islands showing a good EcoQS. The results indices show a significant correlation with organic matter and heavy metal contamination in the southern Tunisian coasts.

## 4. CONCLUSION

The use of benthic macrofauna and biotic indices to determine the EcoQS of the southern Tunisian coasts reveals a spatial pattern with loss of diversity at stations in the commercial harbors and industrial zones in the GG. These stations are also strongly affected by chemical contaminants and appear to have poor to moderate ecological status compared to stations located in Marine protected areas of Kneiss islands and Kerkennah islands that yield a stable status and good Ecological Status.

## REFERENCES

1. Hattab, T., Ben Rais Lasram, F., Albouy, C., Sammari, C., Romdhane, M.S., Cury, P., Leprieur, F., Le Loc'h, F.: The use of a predictive habitat model and a fuzzy logic approach for marine management and planning. PLoSONE. 8, 76430.( 2013)
2. Boudaya, L., Mosbahi, N., Dauvin, J.C., Neifar, L.: Trophic and functional organization of the benthic macrofauna of an anthropogenic influenced area: the Skhira Bay (Gulf of Gabès, central Mediterranean Sea). Env. Sci. Poll. Res (2019) https://doi.org/10.1007/s11356-019-04809-8.
3. Mosbahi, N., Serbaji, M.N., Pezy, J.P., Neifar, L., Dauvin, J.C.: Response of benthic macrofauna to multiple anthropogenic pressures in the shallow coastal zone south of Sfax (Tunisia, central Mediterranean Sea). Env.Pollut. 253, 474 – 487(2019)
4. Mosbahi, N., Pezy, J.P., Neifar, L.,Dauvin, J.C.: Ecological status assessment and non-indigenous Species in industrial and fishing harbours from the Gulf of Gabès (central Mediterranean Sea).Env.Sci. Poll. Rese (2021) https://doi.org/10.1007/s11356-021-14729-1
5. Béjaoui, B., Rais, S., Koutitonsky, V. : Modélisation de la dispersion du phosphogypse dans le golfe de Gabès. Bull. Inst. Nat. Sci. Techn. Mer, Salammbô, Tunisia 31, 113-119 (2004)
6. Zaghden, H., Kallel, M., Louati, A., Elleuch, B., Oudot, J., Saliot, A.: Hydrocarbons in surface sediments from the Sfax coastal zone, (Tunisia) Mediterranean Sea. Mar. Poll. Bull. 50, 1287–1294 (2005)
7. Ayadi, N., Zghal, I., Aloulou, F., Bouzid, J.: Impacts of several pollutants on the distribution of recent benthic foraminifera: the southern coast of Gulf of Gabes, Tunisia. Env. Sci. Poll. Res. Int. 23, 6414–29 (2015)
8. Afli, A., Ayari, R., Zaabia, S.: Ecological quality of some Tunisian coast and Lagoon locations, by using benthic community parameters and biotic indices. Estuar. Coast. Shelf. Sci. 80, 269–280 (2008)
9. Blanchet, H., Lavesque, N., Ruellet, T., Dauvin, J.C., Sauriau, P.G., Desroy, N., Desclaux, C. et al.: Use of biotic indices in semi-enclosed coastal ecosystems and transitional waters habitats-implications for the implementation of the European Water Framework Directive. Ecol. Ind. 8, 360-372 (2008)
10.Dauvin, J.C.: Le benthos: témoin des variations de l'environnement. Océanis 19, 25–53 (1993)
11.Sammari, C., Koutitonsky, V.G., Moussa, M.: Sea level variability and tidal resonance in the Gulf of Gabès, Tunisia. Cont. Shelf Res. 26, 338-350 (2006)
12.Dauvin, J.C., Bakalem, A., Baffreau, A., Grimes, S.: Benthic ecological status of Algerian harbours. Mar. Poll. Bull. 125, 378-388 (2017)
13.Ruy, J., Khim, J.S., Kang, S.G., Kang, D., Lee, Ch.L., Koh, Ch.h.: The impact of heavy metal pollution gradients in sediments on benthic macrofauna at population and community levels. Env. Poll. 159. 2622-2629 (2011)
14.Tweedly, J.R., Warwick, R.M., Potter, I.C.: Can biotic indicators distinguish between natural and anthropogenic environmental stress in estuaries?. J. Sea. Rech. 102,10-21(2015)

# Evaluation of iron contamination and human health risk assessment in Groundwater of Catchment Area Water in Nakatt from Kiffa (Mauritania)

**Aichetou Brahim Boutebib[a], Abdoulaye Demba N'diaye[a] , Sid'Ahmed Baba Elhoumed[b] , Bocar Kalidou M'Baye[c] , Bakari Mohamed Semega[a]**

*(e) Unité de Recherche, Eau Pollution et Environnement, Département de Chimie, Faculté des Sciences et Techniques, Université de Nouakchott, Nouakchott, Mauritanie*
*(f) Service Laboratoire, Cellule Management Qualité, Société Nationale d'Eau (SNDE), Nouakchott, Mauritanie.*
*(g) Laboratoire de Chimie, Institut National de Recherches en Santé Publique, Nouakchott, Mauritanie*
*E-mail: aichetou.brahim3@gmail.com*

**ABSTRACT**

This study investigates the occurrence of iron (Fe) and its associated human health risks in the catchment area water in Nakatt from Kiffa in Mauritania. The study area was monitored during January and August. The occurrence of Fe in the groundwater showed significant spatial and temporal variations. The relationship between Fe and some physicochemical parameters was also analyzed statistically using Pearson's correlation matrix. Firstly, the results suggested that the concentration of Fe was influenced by the dissolution of Fe minerals. Secondly, the results show that the pH value was an important factor that influenced the Fe concentrations in the groundwater. The Water Quality Index (WQI) and Comprehensive Pollution Index (CPI) methods were used to evaluate the suitability for human consumption. The results show that WQI and CPI are strongly influenced by Fe indicating that Fe removal would contribute to excellent well water. In addition, CPI also shows that the pH is a parameter to be optimized for possible potabilization. The result of the health risk assessment revealed that the Hazard Quotient (HQ) values of Fe were larger than one (HQ > 1) in January for all sampling sites, indicating that all groups (adults, children, and infants) have a significant level of health risk from drinking this groundwater. However The result of the health risk assessment showed that HQ values for Fe were less than one (HQ < 1) in August for infants, children, and adults, suggesting that the Fe could pose no or lower level of toxic impacts on these groups (adults, children, and infants). From the results of the present study, it is highly recommended that different treatment techniques should be employed to purify groundwater of Catchment Area Water in Nakatt from Kiffa before consumption.

**KEYWORDS:** GROUNDWATER, IRON, KIFFA, MAURITANIA.

## 1. INTRODUCTION

Groundwater is one of the primary freshwater sources for drinking, irrigation, and industrial uses in most communities worldwide [1]. However, the quality of global water has rapidly declined for decades due to the impact of both natural and anthropogenic factors [2]. Some chemicals might produce immediate impacts on human health because of the nature of the hazardous chemicals [3]. Severe human health implications are associated with heavy metal exposure. Among the heavy metals, Fe is a fairly abundant element in rocks and is found in the form of silicates, oxides as well as hydroxides, carbonates and sulfides [4]. Drink of water containing Fe at concentrations 3 mg/L or higher for a long time causes hemochromatosis and other effects [5]. At the same time, the oxidation of Fe makes water turbid and odorous, and excessive Fe content in groundwater also causes pipeline rust and blockage of wells [6]. Encouraging results obtained by assessment of Fe contamination in groundwater of catchment area water from Derwiche in Mauritania [7] have incited us to search new routes to study the catchment area water from Nakatt in Mauritania. The present study aims to investigate the contamination levels of Fe in the groundwater in catchment area water in Nakatt from Kiffa in Mauritania and to evaluate the non-carcinogenic risk to the health of the population (adults, children, and infants) due to Fe contamination water. It is important to note that assessing water quality is an important strategy for food safety and human health.

## 2. MATERIALS AND METHODS

### 2.1. Description of the study area

Assaba is the third region in the administrative classification of Mauritania. The Wilaya of Assaba is located in south-central Mauritania and occupies an area of 36,600 km². Its capital is Kiffa (Fig 1), the second largest Mauritanian city in population. Assaba is an agropastoral zone par excellence. The boreholes are located in the Kiffa city watershed at the level of the pumping station (Nakatt). The selected boreholes were F2, F14Bis, and F15. These

boreholes are located at about 30 km from Kiffa. It is important to note that there is no industrial production and no agricultural activities in the study area.

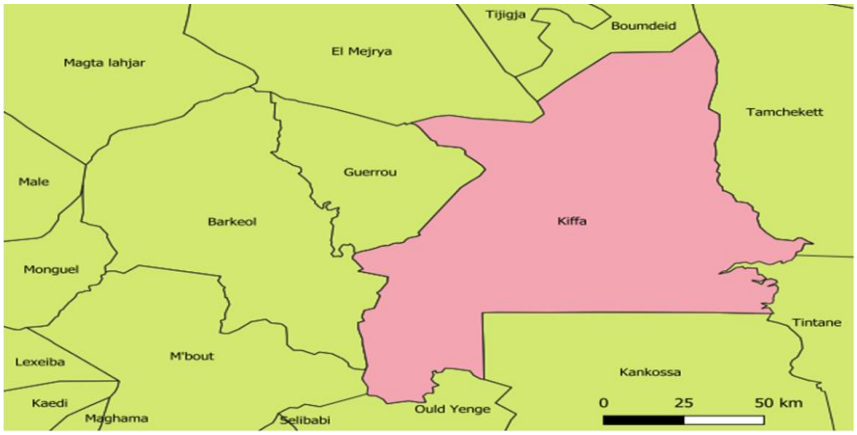


**Fig. 1.** Kiffa localisation

### 2.2. Sampling procedures and physicochemical parameters

Water samples were collected from three sampling sites (Boreholes) scattered along the catchment area in Nakatt from Kiffa. The samples were collected two times: the first sampling was done in January and the last in August corresponding to the rainy period. The sampling for the analysis of physico-chemical parameters was carried out at the selected site, using a 1.5 L polyethylene bottle. The collected samples were stored at 4°C in insulated boxes and transported to the laboratory. The physicochemical parameters such as temperature, pH, Electrical Conductivity (EC), Total Dissolved Solids (TDS), Total Hardness (TH), Calcium ($Ca^{2+}$), Magnesium ($Mg^{2+}$), Chlorides ($Cl^-$), Nitrates ($NO_3^-$), Phosphates ($PO_4^{3-}$), Organics Matters (OM), and Iron (Fe) are listed in Table 1.

**Table 1.** Water quality parameters and measurement methods

| **Parameter** | Unit | **Measuring equipment and method analysis** |
|---|---|---|
| Temperature | ° C | pH meter |
| pH | … | pH meter HI 991001 |
| EC | µS/cm | conductimeter HI98192 |
| TDS | mg/L | conductimeter HI98192 |
| TH | ° F | Titrimetry, Complexometry with EDTA black of eriochrome. |
| $Ca^{2+}$ | mg/L | Titrimetry, complexometry with EDTA |
| $Mg^{2+}$ | mg/L | Titrimetry, complexometry with EDTA |
| $Cl^-$ | mg/L | Volumetric dosage with Silver nitrate |
| $NO_3^-$ | mg/L | Photometer Wagtech 7100 |
| $PO_4^{3-}$ | mg/L | Photometer Wagtech 7100 |
| OM | mg/L | Hot oxidation in an acid medium by potassium permanganate |
| Fe | mg/L | Photometer Wagtech 7100 |

### 2.3. Calculation of Water Quality Index (WQI)

The determined WQI values are classified into five classes as mentioned by Ramakrishnaiah et al. (2009) [8]. In this study the WQI for drinking purposes is considered and permissible WQI for the drinking water is taken as:

Overall

$$WQI = \frac{\sum_{i=1}^{n} q_i w_i}{\sum_{i=1}^{n} w_i}$$

### 2.4. Comprehensive pollution index (CPI)

The CPI is classified into five categories as mentioned by Son et al, (2020) [9]. The formula to calculate CPI is presented as follows:

$$CPI = \frac{1}{n}\sum_{i=1}^{n} PI_i$$

Where CPI= Comprehensive Polluted Index; n= number of monitoring parameters; PIi =the pollution index number i. PIi is calculated according to the following equation:

$$PI = \frac{C_i}{S_i}$$

Where $C_i$ = measured concentration of parameter number in water; $S_i$= permitted limitation of parameter number according to environmental standard.

### 2.5. Hazard Quotient

HQ is used to measure the non-carcinogenic due to the exposure of non-carcinogenic contaminants. Based on the USEPA toxicants division, Fe is considered non-carcinogenic contaminants. HQ is calculated by using the following equation

$$HI = \frac{CDI}{RfD}$$

RfD (mg/kg/day) refers to the reference dose (0.7 mg/kg/day for Fe). CDI is the chronic daily intake (mg/kg/day) and is calculated by

$$CDI = \frac{C \times IR \times EF \times ED}{BW \times AT}$$

Where C is the concentration of Fe (mg/L); IR is the drinking water ingestion rate in L/day (3.53 L/day for adults, 1.0 L/day for children, and 0.25 L/day for infants; ED is the exposure duration in years (70 years for adults and 6 years for children and 1 year for infants; EF is the exposure frequency in days/year (365 days for adults, children, and infants; BW is the average body weight in kg (50 kg for adults, 15 kg for children, and 6.9 kg for infant; and AT is the averaging time (AT=365 ED(d)).

## 3. RESULTS AND DISCUSSIONS

### 3.1. Physicochemical parameters

The physicochemical parameters such as Temperature, pH, EC, TDS, TH, $Ca^{2+}$, $Mg^{2+}$, $Cl^-$, $NO_3^-$ , $PO_4^{3-}$, and OM studied in the catchment area water in Nakatt during January and August were represented in Table 2. The Temperature, pH, EC, TDS, TH, $Ca^{2+}$, $Mg^{2+}$, $Cl^-$, $NO_3^-$ , $PO_4^{3-}$, and OM contents of water samples are within WHO for drinking water [10].

**Table 2.** Statistical summary of the physicochemical parameters of the catchment area water in Nakatt

| | January | | | August | | |
|---|---|---|---|---|---|---|
| Parameters | Maximum | Minimum | Mean | Maximum | Minimum | Mean |
| **T (°C)** | 28 | 27.2 | 27.56 | 29 | 28.4 | 28.63 |
| **pH** | 7.32 | 6.86 | 7.12 | 7.66 | 7.01 | 7.27 |
| **EC (µS/cm)** | 109 | 79 | 91 | 182.5 | 122.5 | 143.13 |
| **TDS (mg/L)** | 54 | 40 | 45.33 | 70.2 | 48.6 | 56.7 |
| **TH (°F)** | 3.4 | 3.2 | 3.2 | 4.8 | 3.4 | 4.06 |
| **$Ca^{2+}$ (mg/L)** | 6.41 | 4 | 5.47 | 9.61 | 4 | 6.70 |
| **$Mg^{2+}$ (mg/L)** | 27.59 | 26 | 26.53 | 38.41 | 27.55 | 33.99 |
| **$Cl^-$ (mg/L)** | 21.3 | 17.75 | 20.11 | 28.4 | 21.3 | 24.85 |
| **$NO_3^-$(mg/L)** | 15.5 | 2.4 | 6.86 | 1.3 | 1.1 | 1.2 |
| **$PO_4^{3-}$(mg/L)** | 1.5 | 0.16 | 0.72 | 1.4 | 0.16 | 0.65 |
| **MO (mg/L)** | 1.28 | 0.64 | 0.96 | 1.98 | 1.2 | 1.53 |

### 3.2. Spatio- Temporal Variation of Fe

Fe values vary within a range of 15.7-38.4 mg/L in January and 9-10 mg/L in August (**Fig. 2**). It is observed that the Fe contents show very high values in January. The decrease in Fe in August probably due to the dilution effect of rain water. The limiting Fe concentration is set at 0.3 mg/L [10].

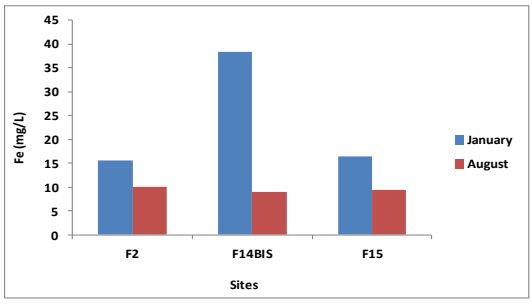


**Fig. 2.** Spatio-temporal variation of Fe

The strong and positive correlation was found between Fe–TDS (r=0.918) and Fe – EC (r=0.880) during August, suggesting that the concentration of Fe was influenced by dissolution minerals in groundwater. However this dissolution is favourized by the pH. The strong and negative correlation obtained between Fe – pH confirms this hypothese. According to Harvey and Fuller (1998) [11], a decrease in pH will accelerate the dissolution of carbonates and hydroxides.

However, it is important to note that negative and significant correlations between Fe andTDS (r=-0.410) and Fe and EC (r=-0.357) were obtained during January. These results showed that the catchment area water in Nakatt well was influenced by dissolved minerals in groundwater during the rainy period. The higher Fe concentrations obtained in catchment area water in Nakatt during January might have been the results of interaction of underground oxidized iron minerals with OM present. In addition, the observed slightly acidic pH values recorded in January can accelerate the dissolution of $Fe_2CO_3$ present in rocks. Similar observations are reported by Mondal et al. (2010) [12].

### 3.3. Assessment of the water quality using WQI

When Fe studies are included in the calculation of the WQI for the catchment area water in Nakatt from Kiffa (Table 3), all values of WQI are higher than 300 which means that the water is unsuitable for drinking. However, without including Fe **(**Table 4), all values are lower than 50 which mean that the water is excellent for drinking.

**Table 3.** WQI values for all parameters

| Sites | January | Quality | August | Quality |
|---|---|---|---|---|
| **F2** | 4742.97 | Unsuitable for drinking | 3023.63 | Unsuitable for drinking |
| **F14Bis** | 3150.53 | Unsuitable for drinking | 2721.15 | Unsuitable for drinking |
| **F15** | 4985.20 | Unsuitable for drinking | 2872.26 | Unsuitable for drinking |

**Table 4.** WQI values without including Fe

| Sites | January | Quality | August | Quality |
|---|---|---|---|---|
| **F2** | 36.70 | Excellent water | 49.24 | Excellent water |
| **F14Bis** | 40.51 | Excellent water | 44.91 | Excellent water |
| **F15** | 44.45 | Excellent water | 46.66 | Excellent water |

### 3.4. Assessment of the water quality using CPI

When Fe studies are included (Table 5) in the calculation of the CPI for the catchment area water in Nakatt from Kiffa all values of CPI are higher than 2.01 which means that the water is heavily polluted. Without including Fe **(**Table 6), all values of CPI are between 0.21 and 0.40 which means that the water is sub clean. However, without including Fe and pH (Table 7), all values of CPI are between 0.21 and 0.40 which means that the water is clean.

**Table 5.** CPI values for all parameters

| Sites | June | Quality | August | Quality |
|---|---|---|---|---|
| **F2** | 7.70 | Heavily polluted | 4.99 | Heavily polluted |
| **F14Bis** | 18.50 | Heavily polluted | 4.51 | Heavily polluted |
| **F15** | 8.06 | Heavily polluted | 4.74 | Heavily polluted |

**Table 6.** CPI values  without including Fe

| Sites | June | Quality | August | Quality |
|---|---|---|---|---|
| **F2** | 0.26 | Sub clean | 0.26 | Sub clean |
| **F14Bis** | 0.25 | Sub clean | 0.26 | Sub clean |
| **F15** | 0.23 | Sub clean | 0.25 | Sub clean |

**Table 7.** CPI values without including Fe and pH

| Sites | June | Quality | August | Quality |
|---|---|---|---|---|
| **F2** | 0.15 | Sub clean | 0.15 | Clean |
| **F14Bis** | 0.13 | Sub clean | 0.13 | Clean |
| **F15** | 0.11 | Sub clean | 0.13 | Clean |

### 3.5. Human health risk assessment

Human chronic health risk of groundwater of Catchment Area Water in Nakatt from Kiffa through the exposure of oral  routes for adults, children and infants in January and August are presented in **Figures 3-4,** respectively.

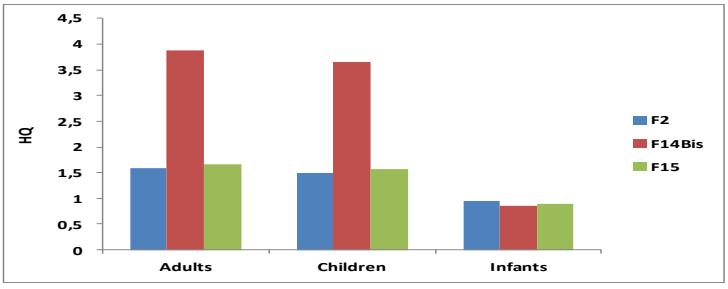


**Figure 3.** Spatial variation of HQ values for adults, children and infants  in January

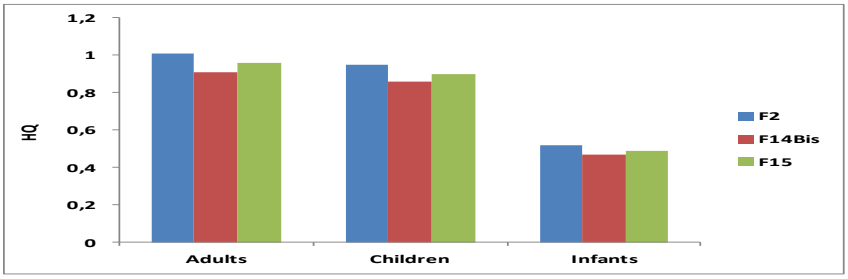


**Figure 4.** Spatial variation of HQ values for adults, children and infants in August

The result of the health risk assessment revealed that the HQ values of Fe were larger than one (HQ > 1) in January for all sampling sites, indicating that all groups (adults, children, and infants) have a significant level of health risk from drinking this source of water over a lifetime.
However This study showed that HQ values for Fe were less than one (HQ < 1) for adults, children, and infants, suggesting that the Fe could pose no or lower level of toxic impacts on these groups (infants, children, and adults) over a long period of exposure.

## 4. CONCLUSION

This study investigates the occurrence of Fe in the catchment area water in Nakatt from Kiffa city in Mauritania. The occurrence of Fe in the groundwater showed significant spatial and temporal variations. The relationship between Fe and some physicochemical parameters was also analysed statistically using Pearson's correlation matrix. Firstly, the results suggested that the concentration of Fe was influenced by dissolution of iron minerals. Secondly, the results show that the pH value was an important factor that influenced the Fe concentrations in the groundwater. The WQI and CPI are used to identify the influence of the Fe contamination. These results indicate that Fe removal would contribute to excellent well water. However, PCI also shows that the pH is a parameter to be optimized for possible potabilization. This study showed that the HQ values of Fe were larger than one (HQ > 1) in January at all sampling sites, indicating that all groups (adults, children, and infants) have a significant level of health risk from drinking this source of water over a lifetime. However This study showed that HQ values for Fe were less than one (HQ < 1) for infants, children, and adults, suggesting that the Fe could pose no or lower level of toxic impacts on these groups (adults, children, and infants) over a long period of exposure. From the result of the present study, it is highly recommended that different treatment techniques should be employed to purify groundwater before consumption.

## REFERENCES

1. Marghade, D., Malpe, D.B., Subba Rao, N. Applications of geochemical and multivariate statistical approaches for the evaluation of groundwater quality and human health risks in a semi-arid region of eastern Maharashtra, India. Environ Geochem Health. 43:683-703 (2021)
2. Vadde, K.K., Jianjun, W., Long, C., Tianma, Y., Alan, J. Raju, S. Assessment of water quality and identification of pollution risk locations in Tiaoxi river (Taihu watershed), China. Water 10, 183 (2018)
3. Alemu, Z.A., Teklu, K.T., Alemayehu, T.A., Balcha, K.H., Mengesha, S.D. Physicochemical quality of drinking water sources in Ethiopia and its health impact: a retrospective study. Environ Syst Res.;4:22 (2015)
4. Zhang, Z., Xiao, C., Adeyeye, O., Yang, W., Liang, X Source and Mobilization Mechanism of Iron, Manganese and Arsenic in Groundwater of Shuangliao City. Northeast China Water 12 (2):534 (2020)
5. Weng H, Qin Y, Chen X Elevated iron and manganese concentrations in groundwater derived from the Holocene transgression in the Hang-Jia-Hu Plain. China Hydrogeol J 15:715–726 (2007)
6. Ye, X., Cui, R., Wang, L., Du, X. The influence of riverbank filtration on regional water resources: A case study in the second Songhua River Catchment, China. Water Sci. Tech. Water Supply 20, 1425–1438 (2020)
7. Boutebib, A. B., N'diaye, A. D., Elhoumed, S. B., M'Baye, B. K., El Hadj Ali, Y. A., Hammouti, B., Semega, B.M. Assessment of Iron Contamination in Groundwater of Catchment Area Water. Indonesian Journal of Science & Technology 8 (3), 429-438 (2023)
8. Ramakrishnaiah CR, Sadashivaiah C, Ranganna G Assessment of water quality index for the groundwater in Tumkur Taluk, Karnataka tate, India, E-Journal of Chemistry, 6 (2), 523-530 (2009)
9. Son, C.T., Giang, N. T.H., Thao, T. P. , Nui, N. H., Lam, N. T. , Cong, V. H. Assessment of Cau River water quality assessment using a combination of water quality and pollution indices. Journal of Water Supply: Research and Technology—AQUA, 69-2 (2020)

10. WHO (World Health Organisation) Guidelines for drinking water quality (4th edition), Geneva, Switzerland (2011)
11. Harvey, J., Fuller, C. Effect of enhanced manganese oxidation in the hyporheic zone on basin-scale geochemical mass balance. Water Res. Res. 34, 623–636 (1998)
12. Mondal, N.C., Singh, V.S., Puranik, S.C., Singh, V.P. Trace element concentration in groundwater of pesarlanka island, krishna delta India. Environ. Monit. Assess. 163, 215–227 (2010)

# Climate change-induced drought impacts on water resources in Tunisia: on the urgent need for adaptation

**Haykel Sellami**[a]

*(a) Laboratory, Géoressources, CERTE Borj Cedria, Soliman*
*E-mail: haysellami@yahoo.fr*

**ABSTRACT**

This work sheds light on the effects of climate change-induced drought over Tunisia by examining historical data, climate change projections while emphasizing the urgent need for adaptation strategies to mitigate its impacts. Based on a large ensemble of climate models, we investigated the spatiotemporal propagation of meteorological droughts using multi-drought indices (SPI, SPEI and PDSI) and projected change in drought frequency, duration and severity over Tunisia. We also assessed the mutual interactions between the three drought indices using Information Theory. Drought frequencies and duration are likely to increase in the future with increasing gradient with SN direction. The northern Tunisia is found to be prone to future droughts and is identified as an urgent area for implementing adaptation actions. We propose a framework for dynamic adaptation of water resources to drought impacts within the ADAPTEAU-C project. The project is committed to provide a state-of-the-art risk assessment on climate change induced drought impacts on water resources and provide adaptation scenarios based on comprehensive updated and consolidated scientific knowledge. It presents an integrated and dynamic adaptation framework putting the hydrological system into the core of its approach.

**KEYWORDS** Climate change; Droughts; Water resources; Tunisia

## 1. INTRODUCTION

There is a consensus that changes in climate during the past century will amplify in the future and the Mediterranean will be prone to warmer and drier climate conditions, leading to an increased drought frequencies and duration (Essa et al., 2023). While drought impacts have been keenly expressed on water resources availability resulting on detrimental impacts on various components of environmental systems and economic sectors at global and regional scale, there is a limited knowledge how climate change will impact drought characteristics and its spatiotemporal evolution at the country scale which is needed for implementing adaptation action. Tunisia is one of these Mediterranean countries identified as hot spot for climate change (Sellami et al., 2016). Yet with limited water resources, the country has a long history of recurrent severe droughts. Recent studies (e.g. Tanarhte et al., 2024) showed that frequency, intensity and geospatial coverage of droughts have significantly increased in Tunisia since 1900 and a shift towards dry conditions over the region in the recent decades. These findings are supported by the observed prolonged meteorological droughts resulted in significant water crises with critical impacts on the socioeconomic sectors in Tunisia since 2016. Droughts either meteorological, hydrological and agricultural are usually evaluated indirectly using indices. The Standard Precipitation Index (SPI; Mckee et al., 1993), the Standardized Precipitation Evapotranspiration Index (SPEI; Vicente-Serrano et al., (2010), and the Palmer Drought Severity Index (PDSI; Palmer, 1965) are among the most popular indices used for monitoring drought with different spatiotemporal scales and over various environmental and climatic conditions. However, assessment of drought based on single index is still not informative due to the complex interaction in space and time of droughts. For instance, meteorological drought is the onset for the others drought types can propagate in a complex cascade leading to soil moisture deficit (agricultural drought) and extended water balance deficit (hydrological drought). In addition, drought types do not manifest at the same temporal and spatial scales due to the lag time, environmental settings, socioeconomic settings. Furthermore, a single drought event can lead to different drought types and impacts. For example, meteorological drought takes short time to be expressed into soil moisture deficit, while the operational management of water reservoirs, aquifers, etc. can extend the lag time between meteorological drought onset and hydrological impacts. Climate change will make the analysis of drought more complex as it will impact drought drivers (precipitation, temperature, evapotranspiration, etc.) and hydrological processes which may result in further shortage of water resources in Tunisia. Therefore, the need for adaptation is urgent for securing water resources against drought impacts. However, developing adaptation/mitigation actions requires comprehensive studies on the projected effects of climate change on drought characteristics and spatiotemporal propagation which are unfortunately still missing in Tunisia.

## 2. MATERIALS AND METHODS

Here we propose an approach to bridge this gap by coupling an ensemble of climate change projection models with multi-drought indices over Tunisia and propose a modelling-based framework for dynamic adaptation of water resources to drought impacts.

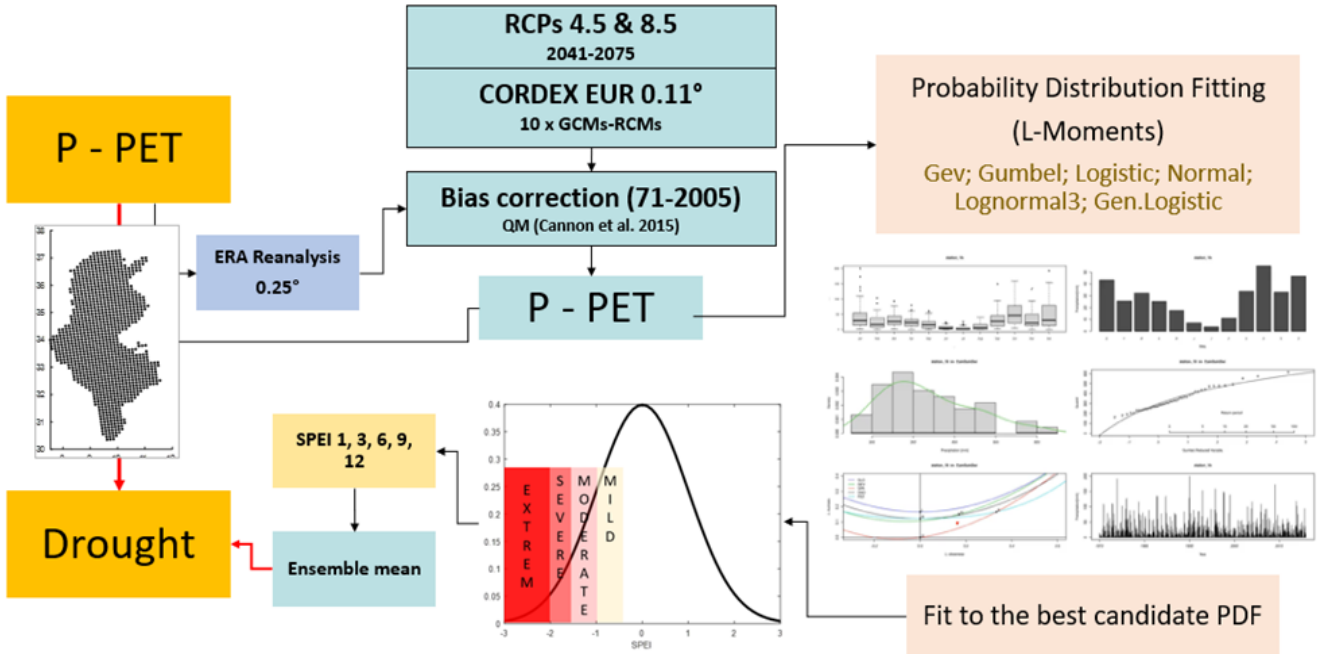


**Fig. 1** Flowchart taking SPEI as an example for drought analysis

We followed the methodology described in Fig. 1 to calculate SPI, SPEI and PDSI drought indices. At first stage, we fitted the precipitation data for SPI and the climatic water balance (P-PET) to probability distribution model (PDF) by testing several distributions. Then, the PDFs parameters were estimated using the L-Moments method. In the next step, the fitted PDF is converted into standard normal distribution giving either SPI or SPEI. For the PDSI, the approach developed by [*M Ma et al.*, 2014]), is used in this study. It is based on water balance model that accounts for water supply (i.e., precipitation), evaporative demand, runoff and recharge in a two-layer model but with a moisture anomaly probabilistic approach at different timescale, for accurate calculation and comparison over temporal and spatial hydrometeorological conditions.

By comparing drought characteristics (frequency, severity, duration and spatial extent) in the reference period (1971-2005) to these projected for 2040-2100 period as derived from the ensemble of the climate model projection (ECM), we investigated the effects of climate change on spatiotemporal trends of droughts.

## 3. RESULTS AND DISCUSSIONS

The results revealed a significant increase in all drought characteristics over Tunisia in the future as compared to the baseline period. All drought indices are expected to increase in Duration, frequency and spatial extent with a positive upward trend making dry and warm areas drier and warmer. Aridity is expected also to move up from the south to the north of Tunisia. Severity is also projected to increase both in magnitude and spatial coverage. Areas that are project to face extended droughts are corroborated with these prone to warmer and drier climate condition (meaning with reduced precipitation and increased temperature). These results are observed for both selected timesteps (3- and 12 month) and under both RCPs scenarios with higher magnitude of change under RCP 8.5 than 4.5.

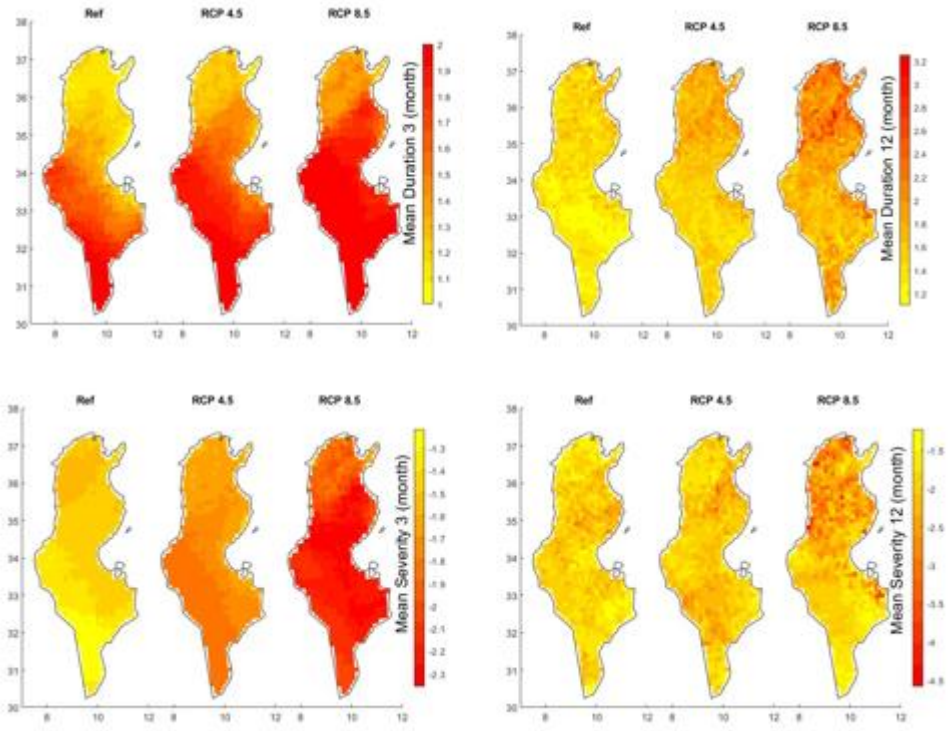


**Fig. 2** Changes in SPEI characteristics for 3- and 12- month between reference and future period under RCP4.5 and RCP8.5

Based on the projected changes in drought characteristics, we identified areas that are most likely to experience more sever drought and that require urgent need for adaptation. Therefore, we propose a framework for dynamic adaptation of water resources to drought impacts in these areas by providing a state-of-the-art risk assessment on climate change induced drought impacts on water resources and adaptation scenarios based on comprehensive updated and consolidated drought analysis and projection. Figure 3 presents the developed dynamic adaptation where the hydrological system is in the core of its approach.

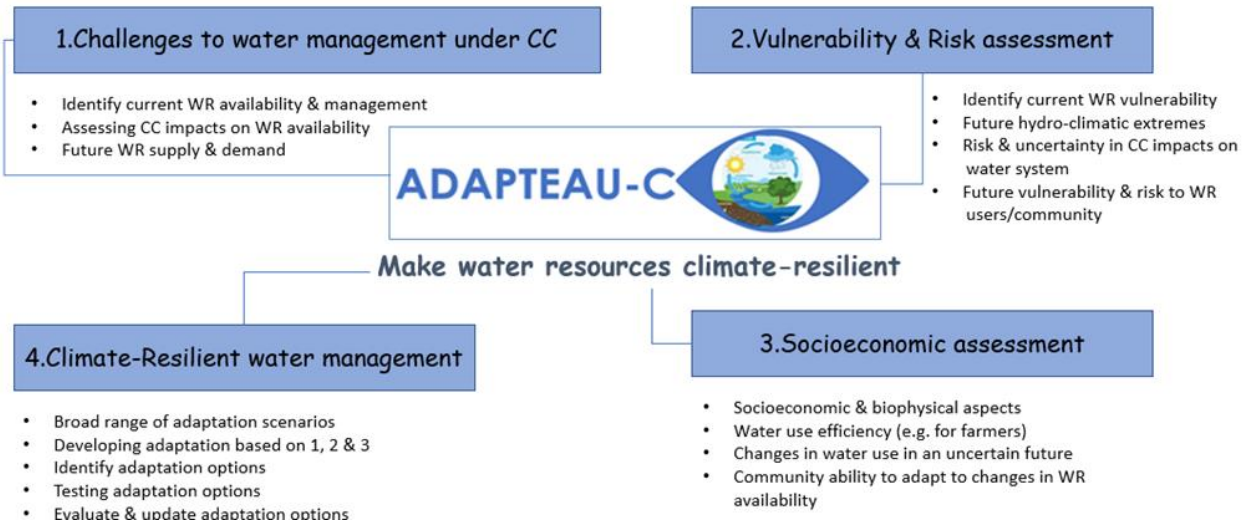


**Fig. 3** Dynamic water resources adaptation approach to drought impacts under climate change as developed within the ADAPTEAU-C project1[1]

[1] ADAPTEAU-C is a projected funded by the Ministry of Higher Education and Research for 2023-2026, domiciliated in the Laboratoire de Géoressources, CERTE. It gathers over 18 researchers from over 8 academic and research national and international institutions ESIM, ENIS, FST, FSB, INAT / BE, US, FR, IT and 8 socioeconomic partners (DGRE, CRDAs, ONGs)

## 4. CONCLUSION

We showed that climate change will increase droughts frequency, duration, severity and spatial coverage over Tunisia in the future. The impacts of droughts are likely to reduce water resources availability, yet limited, highlighting the urgent need for adaptation. To increase water resources resilience to these projected impacts we come up with a dynamic adaptation framework to be implemented in the areas prone to severe drought impacts.

## REFERENCES

1. Essa, Y. H., M. Hirschi, W. Thiery, A. M. El-Kenawy, and C. Yang (2023), Drought characteristics in Mediterranean under future climate change, *npj Climate and Atmospheric Science*, *6*(1), 133, doi:10.1038/s41612-023-00458-4.
2. Ma, M., L. Ren, F. Yuan, S. Jiang, Y. Liu, H. Kong, and L. Gong (2014), A new standardized Palmer drought index for hydro-meteorological use, Hydrological Processes, 28(23), 5645-5661, doi:https://doi.org/10.1002/hyp.10063.
3. Mckee, T. B., N. J. Doesken, and J. Kleist (1993), The relationship of drought frequency and duration to time scales, In: Eighth conference on applied climatology, American meteorological society, Anaheim, CA.
4. Palmer, W. C. (1965), Meteorological droughts, U.S. Department of Commerce, Weather Bureau Research Paper, 45-58.
5. Sellami, H., S. Benabdallah, I. La Jeunesse, and M. Vanclooster (2016), Quantifying hydrological responses of small Mediterranean catchments under climate change projections, Science of The Total Environment, 543, 924-936, doi:https://doi.org/10.1016/j.scitotenv.2015.07.006.
6. Tanarhte, M., A. J. De Vries, G. Zittis, and T. Chfadi (2024), Severe droughts in North Africa: A review of drivers, impacts and management, Earth-Science Reviews, 250, 104701, doi:https://doi.org/10.1016/j.earscirev.2024.104701.
7. Vicente-Serrano, S. M., F. Domínguez-Castro, T. R. McVicar, M. Tomas-Burguera, M. Peña-Gallardo, I. Noguera, J. I. López-Moreno, D. Peña, and A. El Kenawy (2020), Global characterization of hydrological and meteorological droughts under future climate change: The importance of timescales, vegetation-CO2 feedbacks and changes to distribution functions, International Journal of Climatology, 40(5), 2557-2567, doi:https://doi.org/10.1002/joc.6350.

# Clean Processes and Renewable Energy

# Thermodynamic analysis of sustainable H2-rich syngas recovery and ammonia synthesis possibility through SCWG of Tunisian agricultural waste biomass

**Raoudha Garma[a], Doniazed Sioud[b], Housam Binous[c], Ahmed bellagi[b]**

*(a) Physics Department, Higher School of Science and Technology of Hammam Sousse, University of Sousse, Sousse, Tunisia*
*(b) Energy Engineering Department, National Engineering School of Monastir, University of Monastir, Monastir, Tunisia*
*(c) Chemical Engineering Department, National Institute of Applied Sciences & Technology, University of Carthage, Tunis, Tunisia*
*E-mail: raoudhagarma83@gmail.com*

**ABSTRACT**

The production of hydrogen represents a promising source for research on the energy transition towards sustainable and renewable energies. In this context, hydrogen-rich syngas productionfor ammoniasynthesisvia super-critical water gasification process of Tunisian date palm residue (DPR) is stimulated and discussed using AspenOne software. It is found that gasification temperature and biomass feedstock concentration considerably affect the hydrogen concentration in the producer gases. The ammonia production decreases sharply for a reaction temperature above 450K, so it is useless to increase temperature as the ammonia synthesis is favored by high pressures and low temperatures.

**KEYWORDS:** Tunisian agricultural wastes, Hydrogen, Aspen Plus, Biomass SCW gasification, Ammonia synthesis

## 1. INTRODUCTION

The waste generated by agricultural and agro-industrial activities is considerable and poses a definite threat to the environment and a waste of precious organic matter. Numerous studies have shown that these organic-rich waste materials constitute new raw materials for many industries.Moreover, their valorization represents an optimal solution as it contributes to the elimination of the pollution affecting the environment and allows the production of high-value-added substances[1].

Since the Tunisian economy is based on agricultural activities and mainly on date production (around 389,000 tons for the 2023-2024 season [2]), the Date Palm Residues (DPR) is retrieved as one of the most abounded biomasses.Consequently, this abundant availability of Date palm wastes attracted a specific attention to be a source of renewable energy. Supercritical water gasification, SCWG, (T > 374°C, $P > 22.1P > 22.1$MPa) is a thermochemical process which converts biomass into an energy-rich gaseous mixture (mainly composed of CO, CO2, H2 and CH4) using an oxidizing agent and is considered as one of the efficient way of harnessing the energy embedded in biomass[3, 4].In this paper, we propose a thermodynamic study of the supercritical water gasification of Tunisian date palm residues (fruit stalks pruning) using Aspen Plus software. A numerical simulation model is developed for the hydrogen purification and the ammonia synthesis process. The effect of the different operating parameters is presented and analyzed.

## 2. MATERIAL AND METHODS

**Fig. 1** represents a simplified Aspen Plus® model of gasification, syngas purification and ammonia synthesis process of the Tunisian DPR. Feedstock (DATEPALM) is introduced in a decomposition reactor (DECOMP, RYIELD block). Proximate and ultimate analyses of the non-conventional biomass, **table 1**, are used to determine the components with the Soave–Redlich–Kwong (SRK) Eos. Supercritical water (SCW) and the DECOMP reactor outputs feed together the gasifier (GASIF, RGibbs reactor). The producer gases are then purified. CO2 is transformed to CaCo3 (CO2CAP)by adding CaO and then eliminated in the solid separator (SEPSOLID). Vapor is the condensed (COOLER) and liquid water is removed (H2OFLASH). Finally hydrogen is slipped (H2SLIPT) and introduced together with nitrogen (N2) to the (NH3PROD) reactor for ammonia production (NH3).

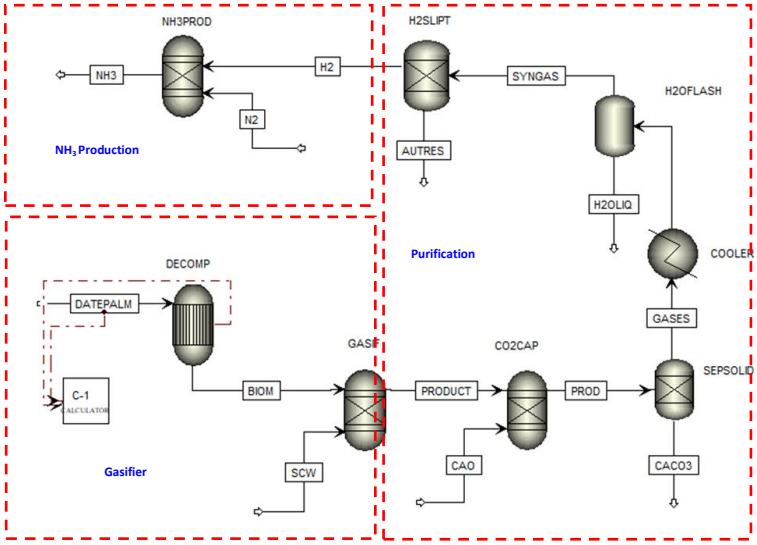


**Fig. 1**PDR SCW Gasification and ammonia synthesis model in Aspen Plus

**Table 1.**Ultimate and proximate analysis of Tunisian DPR [5].

| **Proximate analysis (% mass)** | |
|---|---|
| Moisture | **5.80** |
| FC | **8.20** |
| Ash | **5.4** |
| VM | **80.60** |
| **Ultimate analysis (% mass)** | |
| C | **41.55** |
| H | **7.27** |
| O | **51.08** |
| **N** | **0.106** |

## 2. RESULTS AND DISCUSSIONS

### 3.1. Gasifier model validation

The present model results were compared with published experimental data [6] and literature model predictions [7 ]to validate the predicted PRODUCT gas composition. **Fig. 2** depicts our model results with those of [7] and the experimental data in [6] for steam to biomass ratios between 0.5 and 1 at 700°C gasification temperature. One can note that the present model predicts fairly well the molar fraction of CO and CO2, underestimates CH4 concentrations and shows higher H2 concentrations than their bibliographical counterparts. Pala [7] made similar remarks when comparing his model results with Fremaux experimental data [6].

### 3.2. Operating parameters effect on the SCWG producer gases

**Fig.3** depicts the effect of temperature, **fig.3 (a)**, feedstock concentration*B/S*, **fig.3 (b),** on the producer gases molar fraction.Referring to **fig.3 (a)** one can note that, for fixed pressure,H2 molar fraction increases sharply with temperature to reach its maximum value around 67% at 1100K, then it decreases slightly as the temperature increases further. Thus, one can concludes that increasing the temperature beyond this limit only increases losses without improving performance.Discussing **fig.3 (b)**, one can realize that, for fixed pressure and temperature, H2 molar fraction is considerably decreasing from 65% to 22% as biomass to steam (*B/S*) concentration is increasing from 5wt.% to 50 wt.%. Accordingly, one can deduce that the gasification of a small amount of biomass (small B/S) is rather recommended for the production of hydrogen-rich syngas. **Rq.**: The reactor pressure does not have a significant effect on DPR equilibrium (not presented here); it has a minimal effect on the product gases over the pressure studied range (240-340 bars) ; the same behavior was already observed in previous work[8].

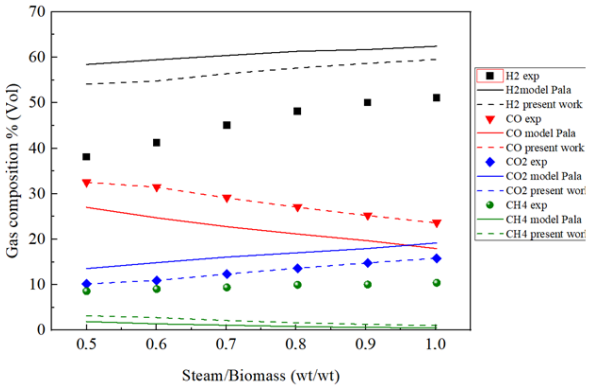


**Fig. 2** SCW gasification model validation: model results vs. experimental data [6] and model results of [7]

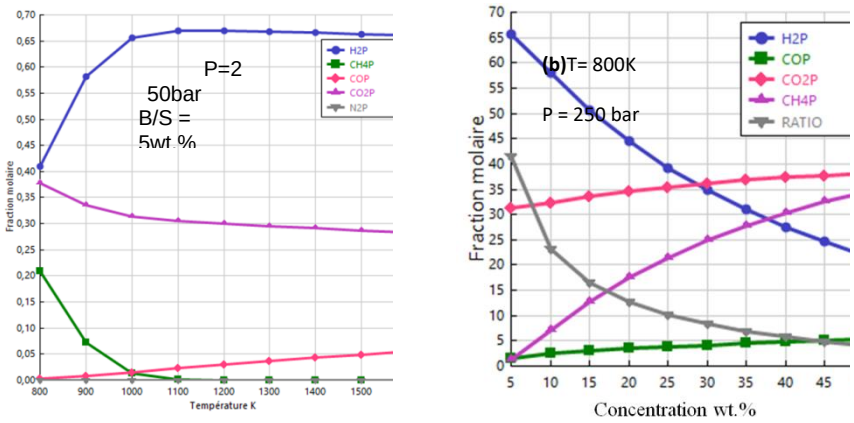


**Fig. 3** operating parameters effect on the producer gases: (a) gasifier temperature effect, (b) pressure effect

### 3.3. Ammonia synthesis

Ammonia is an essential compound to all biological processes because nitrogen is present in all proteins and related biological molecules. It is also of strategic importance as it is used as refrigerant in cold producing machines and to produce fertilizers and explosives [9].Therefore, we propose in the present paper a thermodynamic model developed withAspen Plus To simulate the possibility of ammonia synthesis through SCW gasification of Tunisian date palm residues (DPR).

**Fig. 4 (a)** shows the evolution of NH3, N2, and H2 at the outlet of the ammonia synthesis reactor as a function of the N2 feeding the reactor inlet.Initially, the hydrogen flow was around 0.12kmol/h. As the N2 increases, the H2 decreases and consequently NH3 forms according to the reaction in **Eq. 1** and it increases it progressively. From almost 0.04kmol/h of N2 feed, the production of ammonia stabilizes at 0.03 kmol/h the H2 steadies at 0.08 04 kmol/h and the N2 flow increases sharply (N2 Feed does not react anymore). In fact, the hydrogen becomes insufficient and the reaction does not take place.

The effect of the reactor (NH3PROD) temperature (300K to 800K) on the produced amount of ammonia is illustrated in **fig. 4(b).** It is observed that maximum ammonia production is favored for temperature in the range [300K-450K]. Beyond 450 K, the production of ammonia decreases dramatically as the temperature increases.

$$N_2 + 3H_2 \rightarrow 2NH_3 \quad \Delta H^{\circ}_{298} = -92kJ \qquad \textbf{(1)}$$

Thus, it is useless to increase temperature above this limit since the production of ammonia is favored by high pressures and low temperatures.

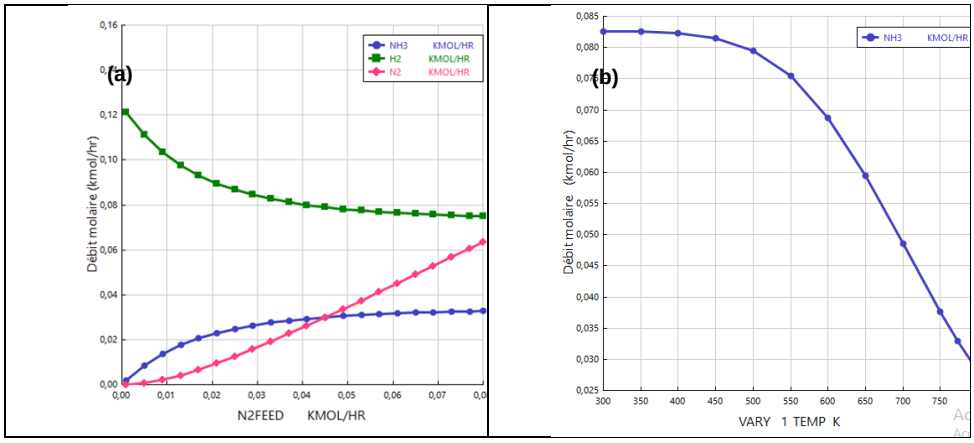


**Fig. 4** Ammonia synthesis behavior vs. N2 feed (a) and Reactor temperature (b)

## 4. CONCLUSION

In this paper, numerical simulation of SCWG process of the non-conventional Tunisian biomass DPR is presented and discussed with Aspen Plus. The sensitivity analysis study of the operating parameters showed that the maximum hydrogen production is achieved at around 1100K for 250 bars and 5 wt.% feed concentration. Further, H2 molar ratio is hindered by increasing the concentration of biomass feedstock. Pressure was retrieved with not significant effect on DPR equilibrium. The proposed model proves the possibility of producing ammonia through DPR SCWG process. the model confirms that ammonia synthesis is promoted by high pressures and low temperatures.

## REFERENCES

1. Kaidi, F., Touzi, A.: Production de Bioalcool à Partir des Déchets de Dattes.Rev. Energ. Ren. : Production et Valorisation – Biomasse. 75–78(2001)
2. https://www.webmanagercenter.com/2023/09/14/513687/agriculture-production-de-389-mille-tonnes-de-dattes-pour-la-saison-2023-2024/
3. Arnavat, M.P., Bruno, J.C., Coronas, A.: Review and analysis of biomass gasification models. Renewable and Sustainable Energy Reviews.14, 2841–2851 (2010)
4. Tushara, M. S. H. K., Duttaa, A., Xu, C. (Ch.).:Simulation of Supercritical Water Gasification of Biomass by Aspen plus, 2014 ASABE and CSBE/SCGAB Annual International Meeting, Montreal, Quebec Canada July 13 – 16 (2014)
5. Ben Sidhom, G., Hassen-Trabelsi, A.B., Sghairoun, M., Alper, K., Trabelsi, I. Pyrolysis of Tunisian Date Palm Residues for the Production and Characterization of Bio-Oil, Bio-Char and Syngas. In: Kallel, A., Ksibi, M., Ben Dhia, H., Khélifi, N. (eds) Recent Advances in Environmental Science from the Euro-Mediterranean and Surrounding Regions. EMCEI 2017.Advances in Science, Technology & Innovation. Springer, Cham. 1561–1563 (2018).
6. Fremaux, S.,Beheshti,S.M., Ghassemi, H.,Markadeh, R.S.: An experimental study on hydrogen-rich gas production via steam gasification of biomass in a research-scale fluidized bed, Energy Conversion and Management.9, 427–432 (2015)
7. Pala, L. P. R.,Wang, Q.,Kolb, G.,Hessel, V.:Steam gasification of biomass with subsequent syngas adjustment using shift reaction for syngas production: An Aspen Plus model. Renewable Energy. 101, 484-492 (2017)
8. Garma, R., Binous, H., Bellagi,A.: Supercritical Water Gasification of Tunisian Agricultural Waste for Energy Recovery: Comparative thermodynamic study of sustainable H2 rich syngas production using Aspen Plus. The 13th International Renewable Energy Congress. 978-1-6654-8897-6/22/$31.00 ©2022 IEEE(2022) DOI: 10.1109/IREC56325.2022.10001962
9. Binous, H., Bellagi, A.: Calculations of complex chemical reaction equilibria using stoichiometric and non-stoichiometric approaches in combination with arc-length continuation. Engineering Reports, Wiley: https://doi.org/10.1002/eng2.12506 (2022).

# Technical Study of a Solar Powered Ejector Absorption Cooling System Under Tunisian Climatic Conditions

**Doniazed Sioud, Ismail Boukholda and Ahmed Bellagi**

*Departement of energy, National School of engineers of Monastir, ENIM, University of Monastir, 5030 Tunisia*

*E-mail: siouddoniazed@gmail.com*

**ABSTRACT**

In this paper, a solar absorption cooling system is theoretically investigated. A Linear Fresnel Solar Concentrator drives a combined ejector single effect absorption cycle. High performance is comparable to double effect absorption cycle in the combined ejector single effect absorption, which require driven temperatures higher than single-effect ones. A mathematical model of the collector concentrator is represented to analyze its optical performance. Simulations are conducted to examine the performance of the combined absorption cycle $COP_{cycle}$, instead of studying the entire machine performance $COP_{system}$. Simulations are carried out for a generator driving temperature and pressure of 180 to 230 and 198 to 270 kPa, respectively. A case study in the cooling season, during summer typical Tunisian day, showing how cycle and system performance are affected by sun radiation and surrounding temperature, are investigated. Simulation results show that collector efficiency is between 0.54 and 0.78 and that $COP_{system}$ and $COP_{cycle}$ reach minimum values at 14:00, about 0.7 and 0.45 respectively.

**KEYWORDS:** Solar cooling combined absorption system, linear Fresnel collector, simulation.

## 1. INTRODUCTION

All over the world there is a high energy demand, especially in hot weather regions such as Mediterranean cities because of the important demand of cooling and air conditioning particularly in the spring and summer periods, for buildings and industrial processes in both small and high scale. Thus this holds a significant part of energy consumption in buildings which necessitates, due to the actual energy emergency, quick steps must be taken to lower energy expenses and their negative environmental effects. Governments and researchers deal with the use of solar cooling technologies as an attractive solution. A 250 kW thermal prototype utilizing a Fresnel concentrator [1] was studied both theoretically and experimentally. Results demonstrated that thermal effectiveness per day was greater than 40%.Tests of a solar/gas cooling plant at Seville in Spain were done during 2008–2009 [2]. The technology of Fresnel concentrator, in another industrial process, was studied like an integrated multi-effect device and solar building concentrated power station [3]. Five Algerian coastline locations were analyzed using a dynamic model, using TRNSYS 17 software However the main disadvantages are vast regions of collectors if the double effect absorption cycle is used, and limited efficiency of solar powered devices once single-effect absorption chillers are adopted. Some modified configurations, such as ejector single effect cycle [4,5], which requires a high temperature heat source and has a double effect cycle efficiency due to the integration of an ejector between before the condenser. In this paper, a solar combined single effect system is studied. So a Linear Fresnel collector is used to produce high temperature flow able to produce steam in high temperature to drive the generator. The effect of driving chilled water and inlet cooling water temperatures on the overall system and on the ejector absorption cycle performance's, respectively $COP_{system}$ and $COP_{cycle}$ are performed. Additionally, a study of a specific case of an ordinary summer day is studied.

## 2. SYSTEM DESCRIPTION

A linear Fresnel collector connected to an ejector single effect system using liBr-H2O represents the solar cooling system under study, presented in Fig. 1. While the adopted Linear concentrating Fresnel collector (IS-LF11) [6] has a surface of 136m$^2$. In the objective of producing driving steam at higher temperature ranging from 180 °C to 230°C to drive the generator of the cooling machine, to drive one unit of the combined liBr-H2O absorption chiller to produce cooling temperatures in the range of 12°C to 4°C were simulated.

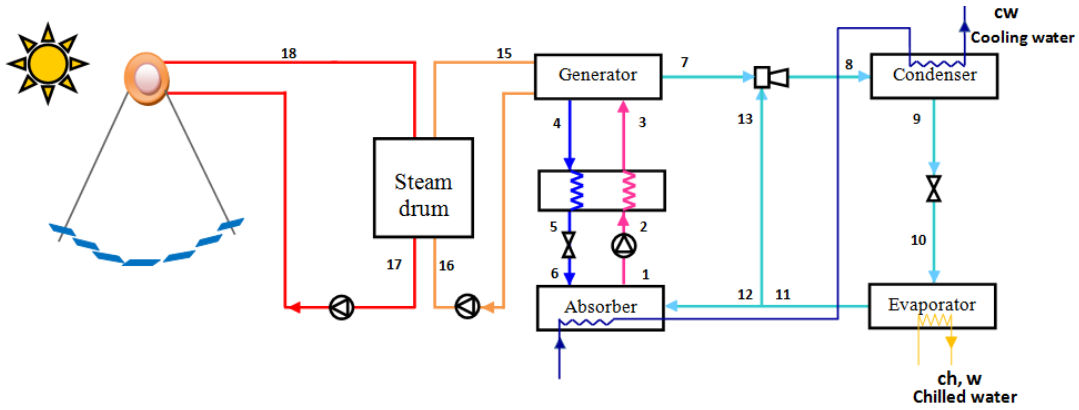


**Fig. 1.** Solar ejector absorption single effect system

## 3. MATHEMATICAL MODEL

### 3.1. Model of Linear Fresnel collector

Optic performance is characterized via a correction factor defined as (IAM) which is the incidence angle modifier, taken in account to determine the Optical performance for different angle of incidence, which should be multiplied with η0. With $\Delta T$ is the difference between surrounding air and heat transfer flow HTF, temperatures:

$$\Delta T = T_{HTF} - T_{amb}\, T^2 \qquad (1)$$

In second order, the primary reflector's thermal losses per square meter is as follows:

$$\dot{q}_{loss} = u_0 A_{aperture} \Delta T + u_1 A_{aperture} \Delta T^2 \qquad (2)$$

The collector's useful heat source depends on both thermal loss and optical performance, calculated as below:

$$\dot{q} = \eta_{optical}\,(\alpha,\theta)_\delta G.A - \dot{q}_{loss}(\Delta T) \approx \eta_0\, IAM_l(\theta_{l,\delta}).IAM_t(\theta_{t,\delta}).A.G - u_1.A.\Delta T^2 \qquad (3)$$

Using the approximation of the optical performances (efficiency) which is represented by the factored bidirectional IAM projected transversely and longitudinally on zenith angles, respectively $\theta_t$ and $\theta_l$.

The ratio of useable thermal energy to the solar irradiation gathered $G.A$ is provided by the collector's thermal efficiency, or η.

$$\eta \approx \eta_0\, IAM_l(\theta_{l,\delta}).IAM_t(\theta_{t,\delta}) - u_1.A.\frac{\Delta T^2}{G} \qquad (4)$$

When the sun is at its zenith, $IAM_t$ and $IAM_l$ both equal 1.

### 3.2. Combined ejector single effect absorption cycle model

For the purposes of simulating the performance of this particular absorption system, the principles of mass and energy conservation are used. This absorption system $COP$ is defined as:

$$COP_{cycle} = \frac{\dot{Q}_e}{\dot{Q}_{steam,g} + \sum \quad \dot{W}_P} \qquad (5)$$

## 4. RESULTS AND DISCUSSIONS

The combined ejector single effect absorption refrigeration cycle coupled with the linear Fresnel collector was thermodynamically analyzed using a computer model built with the Engineering Equation Solver (EES) software [7]. The total coefficient of performance is a crucial metric for characterizing the whole system performance $COP_{system}$of a solar ejector-absorption refrigerator. The collector efficiency (η) multiplied by the combined refrigeration cycle coefficient of performance$COP_{cycle}$, yields the total $COP_{system}$ of the solar absorption system, which is defined as follows [8]: $COP_{system} = \eta.COP_{cycle}$ (6)

### 4.1. Chilled water temperature effects on system and cycle efficiencies

For different inlet chilled water temperature $T_{ch,w}$, driving temperature impacts in the overall cycle $COP_{system}$ and on the performances of the combined absorption machine $COP_{cycle}$ is represented in Fig. 2, if the cooling fluid is at 32° C. So first, the $COP$ increases when the driving temperature rises and decreases with the increase of the chilled water temperature.

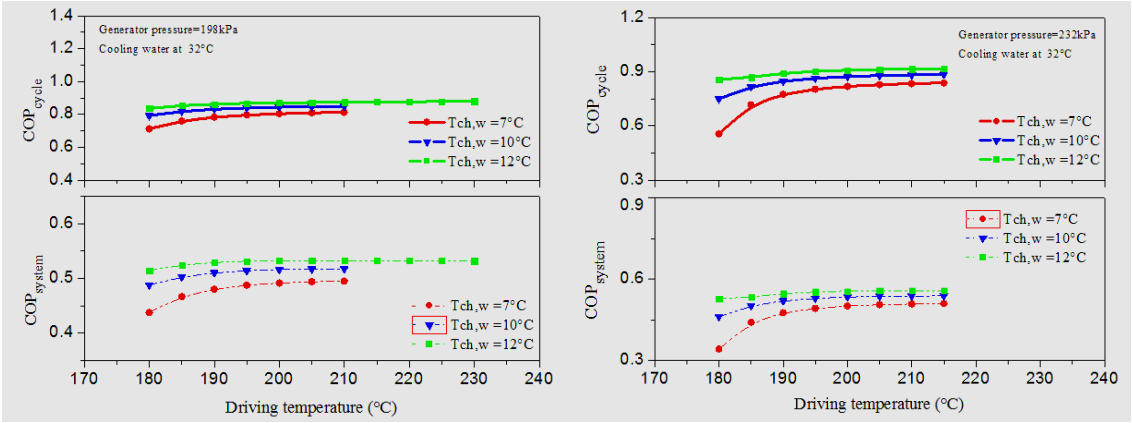


(a) (b)

**Fig. 2.** Effect of driving and chilled water temperature on the COP vs, generator pressure set at (a) 198kPa and (b) 232kPa

### 4.2. Case study according to Hourly local data

In July 2008, [9] conducted a thermal check of weather and solar conditions. An example of (16 July 2008) day in the northern Tunisian capital, which has a Maritime environment defined by abundant sun energy, is depicted in Fig. 3(a). The tested region is situated at latitude 36° and longitude 10°. With 350 clear days annually. The temperature of the surrounding air therefore ranges from 27°C to 39°C, and the solar radiation is at least 250W/m2 and exceeds 900W/m2. At 12:00, the maximum sun radiation is 958 W/m$^2$. At 14:00, however, the highest recorded ambient temperature was 37 °C. The Linear Collector employed in the simulations had an average efficiency of around 0.6 for normal summer days (Fig. 3 (a)) and a highest value of 0.62 (Fig. 3 (b)). The efficiency of the collector as explained above (model collector) and Eq (5) relies on the temperature differential among the surrounding temperature and the heat transfer flow, which is quadratic. Therefore, rather than the irradiation G, the efficiency of the collector is influenced by the working values of $T_{HTF}$. Thus, when the heat transfer flow temperature is less, collector efficiency is higher, as shown in Fig. 4. Also as illustrated in Fig. 3(a), because of the varying patterns of solar radiation and the surrounding temperature between 11:00 and 15:00, the collector efficiency is specifically higher at this period than the rest of the day, as represented in Fig.4.

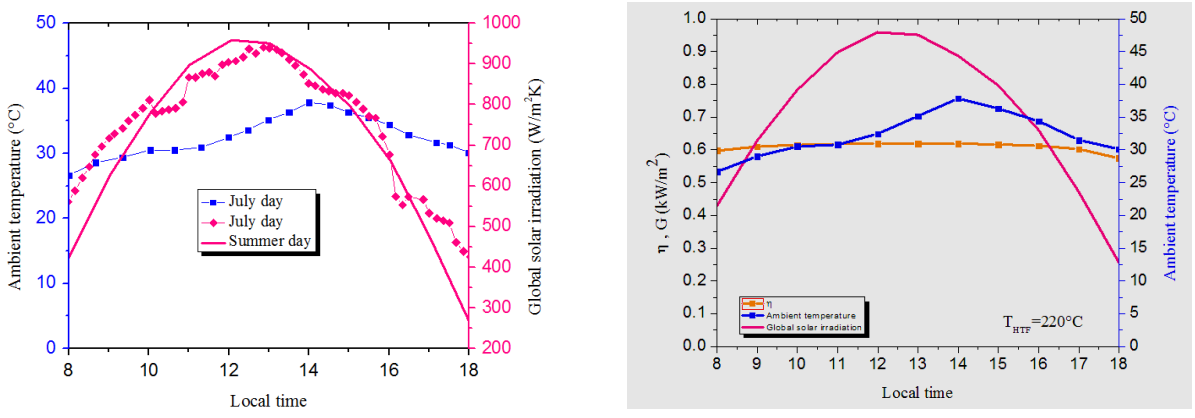


(a) (b)

**Fig. 3.(a)** Evolutions of the solar irradiation and the surrounding temperature in a July typical summer day, in Tunisia, ref [9], **(b),** and Linear Fresnel efficiency of the collector vs, solar irradiation and surrounding temperature as heat transfer flow temperature is fixe

Fig. 5 Shows the evolution $COP_{system}$ and $COP_{cycle}$ along the operating period of the local time, reach levels greater than 0.7 at all frequently. Both $COP$ variation decreases with increasing the ambient temperature, that is

why the curves have the reciprocate trend of the ambient temperature curve. Therefore, they reach a minimum when the ambient temperature is at the highest point at hour 14:00.

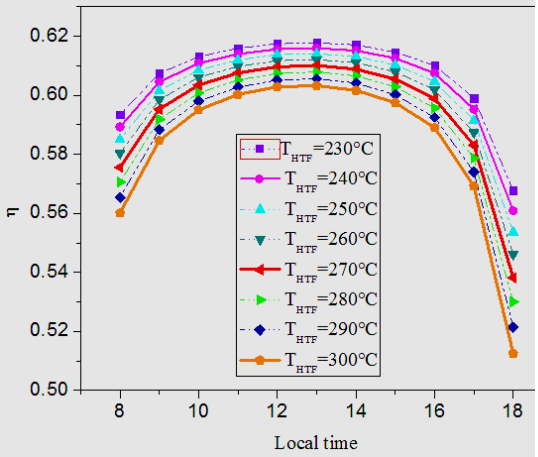


**Fig. 4.** Collector efficiency during one day for different HTF temperatures

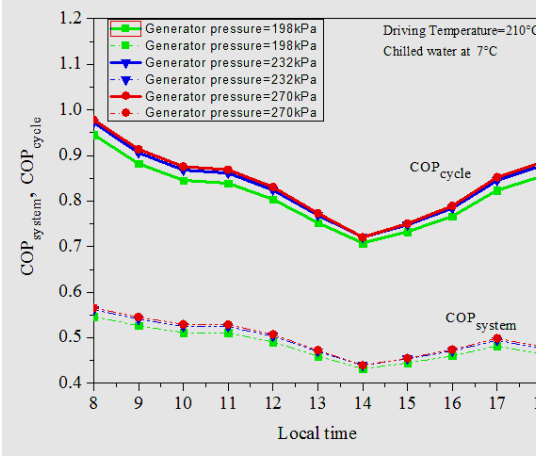


**Fig. 5**. $COP_{system}$ and $COP_{cycle}$ at local time for different pressure in the generator

## 5. CONCLUSION

A solar cooling combined ejector single effect absorption system is proposed and investigated. Steam condensation ranges from 180°C to 230°C power the refrigerator studied, via heat from the pressured water from Linear Fresnel Collector that coupled the combined single effect cycle. A case study of a typical summer day is studied. According to the analysis, the Linear Collector employed in the simulations had an average efficiency of around 0.6 and a maximum efficiency of 0.62. Also it is found that the collector efficiency depends on the temperature differential between the ambient temperature and the heat transfer flow that is quadratic. So both temperature of the working values of $T_{HTF}$ and the irradiation G affects the collector efficiency. When the temperature of the heat transfer flow is less, the collector efficiency is higher. The evolution $COP_{system}$ and $COP_{cycle}$ along the operating period of the local time, reach levels greater than 0.7. Both performance variations decrease with increasing the surrounding temperature.

## REFERENCES

1. Hani B., Djaffar S., Christophe L., Noureddine S.: Theoretical and experimental performance analysis of a Fresnel type solar concentrator. Renewable Energy. 101, 782-793 (2017).
2. Pablo B., Francisco J. P. , Felipe R., “Solar absorption cooling plant in Seville. Solar Energy. 84, 1503–1512 (2010).
3. Mohammed L., Driss N., Djamel O. :Analysis of the feasibility of combining concentrating solar power with multi effect desalination for the Algerian coast. International Journal of Renewable Energy Research. 782–793 (2017).
4. Sun D.W., Eames I. W., Aphornratana S.: Analysis of a Solar Operated Ejector Absorption Refrigeration System. International Journal of Refrigeration. 19, No. 3, pp. 172-180, 1996.
5. Aphornratana S., Eames I. W., Experimental investigation of a combined ejector-absorption refrigerator”, International Journal of Energy Research. 22, 195-2 07 (1998).
6. Industrual Fresnel web
7. Christine W., Michael B., Florian M., Alexander H., Tomas N.: Solar cooling with water-ammonia absorption chillers and concentrating solar collector-operational experience. International Journal of refrigeration.39, 57-76 (2014).
8. Klein S.A., Alvarado F., Engineering equation solver. Middleton, WI: F–chart software, 2003.
9. Balghouthi M., Chahbanib M.H.: Investigation of a solar cooling installation in Tunisia Author links open overlay panel. Applied Energy . 98, 138-148 (2012).

# Oxidation of methylene blue in aqueous solution by the modified sono-Fenton process

**Abdessalem Omri[a,b], Sourour Salhi[a], Mourad Benzina[a]**

*(a) Laboratory of Water-Energy-Environment (LR3E), code: AD-10-02, National School of Engineers of Sfax, University of Sfax, BP W, 3038 Sfax, Tunisia.*
*(b) Faculty of Sciences of Gafsa, University of Gafsa, 2112 Gafsa, Tunisia.*
*Email: omri.abdesslem.taieb@gmail.com*

## ABSTRACT

Natural hematite was used as a catalyst for activating persulfate (PS) to oxidize methylene blue (MB) under ultrasonic irradiation (US). The pretreated hematite was characterized by different physicochemical techniques. X-ray difraction analysis showed that the hematite catalyst mainly consists of $Fe_2O_3$ and $SiO_2$ crystallites. BET analysis shows that the prepared catalyst has a specific surface area of 7.83 $m^2/g$ and a pore volume of 0.049 $cm^3/g$. FTIR spectrums indicated the presence of (Fe-O-Si) groups. The results of the MB oxidation study showed that the percentage of discoloration depends on the initial concentration, acoustic power, pH and concentration of the oxidizing solution. The percentage of MB degradation reaches 97% after 45 min. The hematite/US/PS system also proved to be an effective method for removing MB.

## KEYWORDS

Methylene blue, oxidation, persulfate, modified sono-Fenton.

## 1. INTRODUCTION

Pollution of water resources is an acute problem today. It is the result of the massive use of organic and mineral emissions of agricultural, urban and industrial origin. These pollutants include: synthetic dyes used in the textile industry [1]. Today, there are several processes for treating polluted water wastewater, including advanced oxidation processes, which appear as a promising alternative approach in the wastewater field [2,3]. The main objective of our work is the establishment of a sono-chemical treatment process for the oxidation of methylene blue dye using a natural iron oxide (hematite) and persulfate ions activated by ultrasound. This adopted process is often referred to as modified sono-Fenton.

## 2. MATERIAL AND METHODS

The natural hematite samples used in our work were collected from Djebel Djerissa, located in northern Tunisia, 54 km south of Kef Governorate. After pretreatment (crushing, drying, grinding and acid activation), the hematite powder was used as a catalyst. Various techniques were used to study the structural, textural and chemical properties of the prepared catalyst. Degradation experiments were carried out in a 250 mL Erlenmeyer, which was placed in an ultrasonic bath.

## 3. RESULTS AND DISCUSSIONS

A physicochemical characterization by the B.E.T method showed that the catalyst (hematite) has an internal porosity of 21% and a specific surface area of around 7.83 $m^2/g$. Mineralogical analysis of the crystal structure of natural hematite (Fig. 1) proves that this material is mainly composed of hematite (H) and quartz (Q).

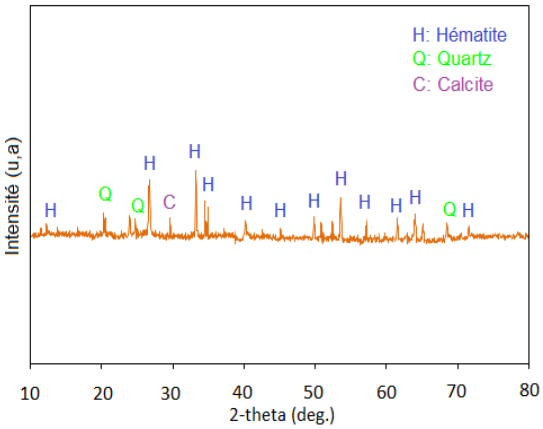


**Fig.1** Diffractogram of natural hematite

The results obtained show that the catalyst based on natural iron oxide is more efficient in the degradation of MB by the modified sono-Fenton process (Fig. 2). We obtain a degradation of 97% of MB after 45 min of reaction which denotes the synergistic effect in the presence of iron species and oxidant (persulfate) used in the modified Fenton process and ultrasonic irradiation (US) used in sonolysis.

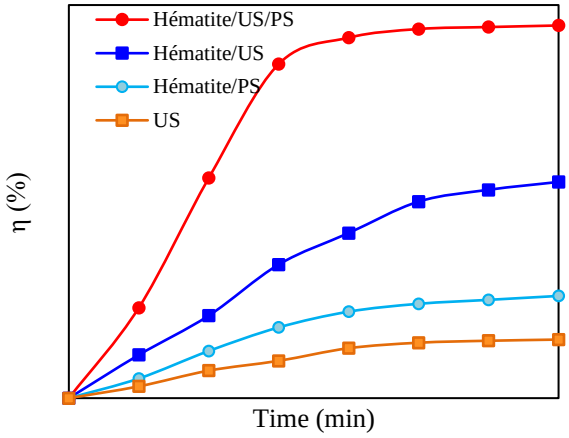


**Fig.2** Effect of different systems on MB Discoloration.

## 4. CONCLUSION

Physico-chemical analysis of natural iron oxide has confirmed that this ore is characterized by a hematite content equal to 47% and a pore diameter of around 13.58 nm. A degradation percentage of 97% of MB was obtained after 45 min. The Hematite/US/PS system also proved to be an effective process for eliminating MB.

## REFERENCES

1. Oladoye, P.O., Ajiboye, T.O., Omotola, E.O., Oyewola, O.J.: Methylene blue dye: Toxicity and potential elimination technology from wastewater. Resul. Eng. 16, 100678 (2022)
2. Serna-Galvis, E.A., Porras, J., Torres-Palma, R.A.: A critical review on the sonochemical degradation of organic pollutants in urine, seawater, and mineral water. Ultrason. Sonochem. 82, 105861 (2022)
3. Omri, A., Benzina. M.: Degradation of Alizarin Red S by Heterogeneous Fenton-Like Oxidation Over Copper-Containing Sand Catalysts. Catal Surv Asia 25, 76-92 (2021)

# Comparison of two cylindrical receivers with spiral tube

**Hiba Cherif, Jalila Sghaier, and Hatem Mhiri**

*Laboratory of Thermal and Thermodynamics in Industrial Processes, National Engineering School of Monastir, Monastir 5000, Tunisia*

*E-mail: hiba.cherif@yahoo.fr*

**ABSTRACT**

This study explores different receiver configurations to enhance the thermal efficiency of a parabolic solar concentrator. By maintaining a constant residence time for the working fluid, while adjusting the flow rate and the cross-section of the spiral tube, a comparison of two 19-turn spiral receivers was performed. The results indicate that the solar collector with 19-turn spiral tube of 5 mm diameter provides the highest system performance.

**KEYWORDS:** Parabolic dish, Spiral receiver, Thermal performance, Outlet temperature

## 1. INTRODUCTION

A parabolic dish is designed to concentrate sunlight onto a focal point where the receiver is located. The receiver's role is to absorb the concentrated sunlight and convert it into heat. By focusing on material properties, geometric alignment, receiver design and continuous optimization, significant improvements in thermal efficiency and overall system performance can be achieved. Bellos et al. [1] numerically studied five different cavity receiver shapes using SolidWorks software under various operating temperature levels to determine the design that maximizes the thermal efficiency of the solar collector. The shapes examined were cylindrical, rectangular, spherical, conical, and cylindro-conical. Their findings indicate that the cylindro-conical shape provides the best design, achieving a thermal efficiency of 67.95%, an exergy efficiency of 35.73%, and an optical efficiency of 85.42% at an operating temperature of 300°C. Conversely, the rectangular shape was found to be the least effective design. K. Ravi Kumar et al. [2] numerically studied a parabolic trough solar concentrator with a porous disc receiver. A three-dimensional (3D) simulation of the porous disc receiver was carried out using Fluent 6.3 CFD software. The effects of geometric parameters of the porous disc and fluid parameters on the heat transfer enhancement of the receiver were also studied. The numerical simulation results showed that the porous disc receiver experiences a smaller pressure drop compared to the solid disc receiver due to less obstruction. Correlations for the Nusselt number and friction factor were proposed for the porous disc receiver to calculate the heat transfer characteristics.

In this study, two spiral absorber configurations are studied while keeping the same residence time of the working fluid by varying the fluid flow rate and the section of the spiral tube, in order to determine the best configuration that ensures the optimum performance of the system.

## 2. MATERIAL AND METHODS

This study was conducted using Ansys Fluent, the geometry of the parabolic dish is modeled in GAMBIT 2.3. The first receiver configuration is a 19-turn spiral tube of 5 mm diameter. For the second configuration, the same fluid residence time is kept by varying the argon flow rate and the diameter of the spiral tube in order to study their effect on the thermo-fluid behavior inside the receiver, the receiver configuration is a 19-turn cylinder of 7.07 mm diameter. In addition, it is important to specify that the fluid enters the spiral tube through its periphery and exits from the central spiral. Table 1 shows the properties of the different configurations studied.

**Table 1.** Geometric properties of the different configuration

| | **Config.1** | **Config.2** |
|---|---|---|
| | Cylindrical absorber with spiral tube | Cylindrical absorber with spiral tube |
| **Diameter** | 0.4 m | 0.4 m |
| **Height** | 0.008 m | 0.008 m |
| | 19 turn | 19 turn |
| | ( 5 mm of diameter) | (7.07 mm of diameter) |

The different receiver configurations studied, created in GAMBIT, are given in figure 1.

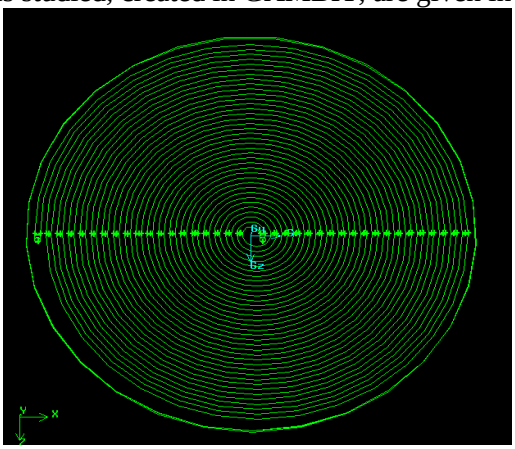

Config.1

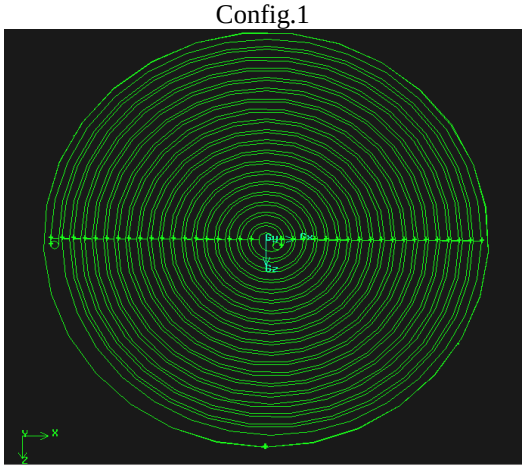

Config.2

**Fig. 1** The different receiver's configurations

## 3. RESULTS AND DISCUSSIONS

Figure 2 illustrates the temperature distribution of the working fluid inside the different receiver configurations and its outlet temperature. It can be seen that the outlet temperature of the fluid from the 19-turn 5 mm spiral tube is the highest (see Fig. 2.b.Config.1). As an example, the average outlet temperature of the fluid from the 19-turn 5 mm spiral tube cylindrical absorber is equal to 1256 K, while for the 19-turn 7.07 mm absorber (see Fig.2.b.Config.2), its average outlet temperature is about 1231 K and this is clearly shown in Fig. 3 which shows the average outlet temperature of the fluid from each configuration. Keeping the same residence time of the working fluid and the same distribution of the solar flux, by comparing the temperature profiles for the different configurations, it is confirmed that the fluid from configuration 1 has the highest temperature. In fact, for the second configuration, the argon flow rate and the section of the spiral tube are doubled, while keeping the same fluid residence time, and subsequently its fluid temperature decreases due to the increase in flow rate.

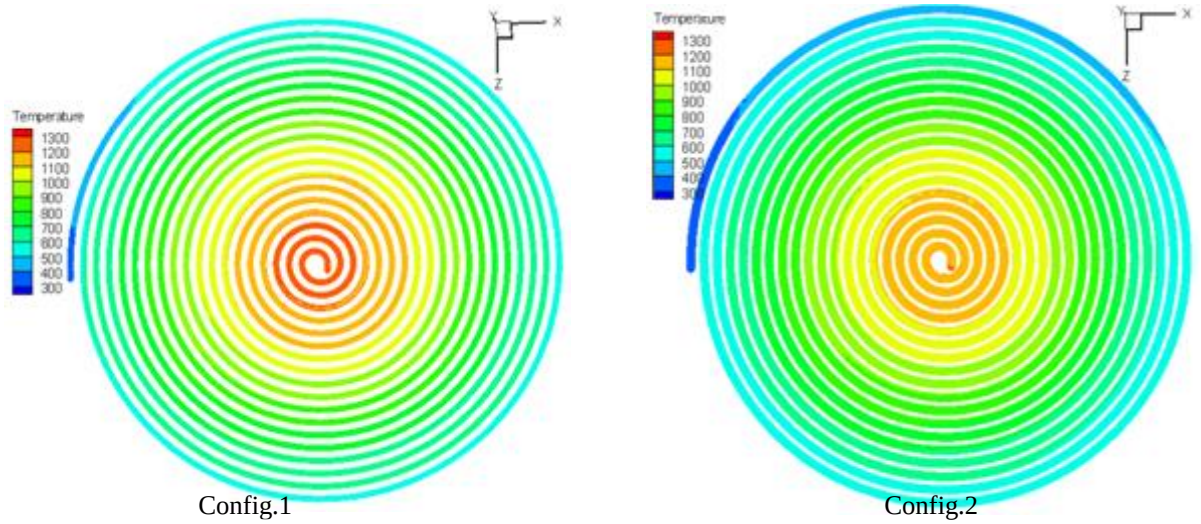


Config.1 Config.2

Fluid temperature distribution

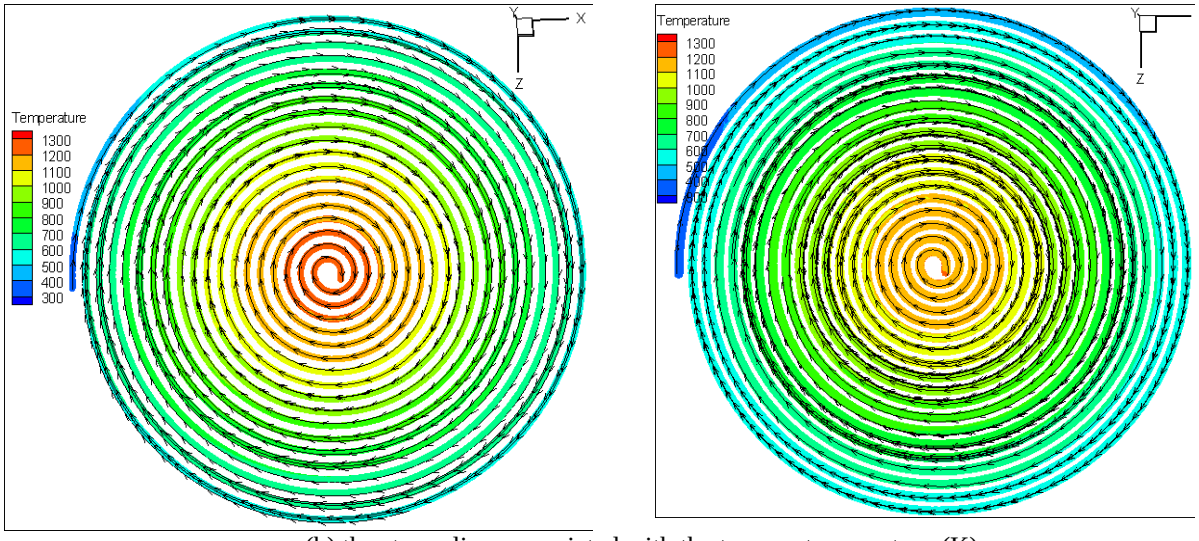


Config.1 Config.2

(b) the streamlines associated with the temperature contour (K)

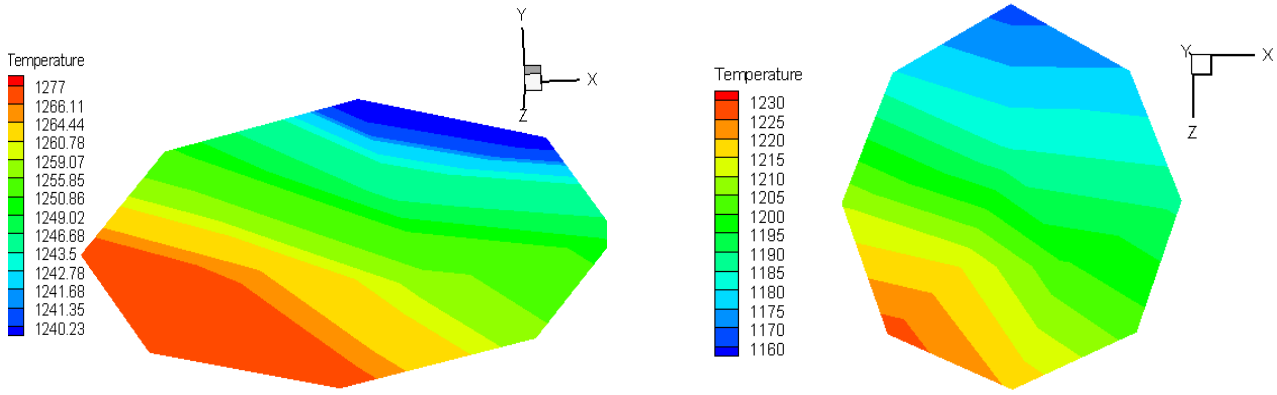


Config .1 Config .2

(c) The Outlet temperature distribution (K)

**Fig. 2** Temperature distribution for different configurations

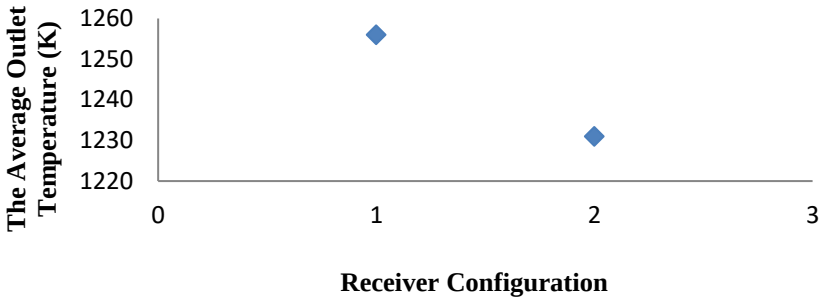


**Fig. 3** Average outlet temperature for different receiver configurations

To evaluate the thermal performance of the system, the thermal efficiencies for the different system configurations are presented. The total thermal efficiency of the entire system is defined as follows **[3]**:

$$\eta_{th} = \frac{\dot{Q}_{gain}}{\dot{Q}_{rad}} = \frac{\dot{m} C_p (T_{out} - T_{in})}{I_b A_c}$$

Where $\dot{Q}_{gain}$ is the useful power obtained by the heat transfer fluid passing through the receiver, $\dot{Q}_{rad}$ is the solar power absorbed by the entire system, $I_b$ is the normal direct solar radiation and $A_c$ is the opening surface of the solar collector.
Table 2 shows the total thermal efficiencies of different tested configurations.

**Table 2**. Thermal efficiency of the system

| Configuration | Thermal efficiency of the system $\eta_{th}$ (%) |
|---|---|
| **Config.1 : D $_{tube\ spiral}$ =5 mm** | 22.8 |
| **Config.2 : D $_{tube\ spiral}$ = 7.07 mm** | 22.2 |

From Table 2, comparing the thermal efficiency of the different configurations, we see that the thermal efficiency of the 5 mm diameter spiral absorber Config.1 is higher than that of the 7.07 mm diameter receiver Config.2.

## 4. CONCLUSION

In order to optimize the thermal performance of the parabolic solar concentrator, different receiver configurations are studied in this study. By maintaining the same residence time of the working fluid in the receiver, varying the fluid flow rate and the section of the spiral tube, comparing the two 19-turn spiral receivers, the results of this study clearly showed that the solar collector with the 19-turn spiral wound tube of 5 mm diameter is the best configuration ensuring the best performance of the solar system.

## REFERENCES

1. Evangelos Bellos , Erion Bousi, Christos Tzivanidis , Sasa Pavlovic. Optical and thermal analysis of different cavity receiver designs for solar dish concentrators. Energy Conversion and Management, Volume 2, April 2019, 100013
2. K. Ravi Kumar, K. S. Reddy. Effect of porous disc receiver configurations on performance of solar parabolic trough concentrator. Heat Mass Transfer (2012) 48:555–571 DOI 10.1007/s00231-011-0903-8
3. Cherif. Hiba, Anissa Ghomrassi , Jalila Sghaier , Hatem Mhiri , Philippe Bournot . A receiver geometrical details effect on a solar parabolic dish collector performance. Energy Reports 5 (2019) 882–897

# Numerical Analysis of Influence of Blade Geometry on Wind Capture Systems

**Marwa Ezzine[a, c], Hiba cherif [a, c] Zied Guidara[b ,c], Jalila Sghaier[a]**

*(a) Laboratory of Thermal research and Thermodynamics of Industrial Processes (LTTPI), National School of Engineers of Monastir (ENIM), University of Monastir,Road ibn El Jazzar 5019 Monastir, TUNISIA*
*(b) Laboratory of Electro-Mechanic Systems (LASEM), National School of Engineers of Sfax (ENIS), University of Sfax , B.P. 1173, Road Soukra km 3.5, 3038 Sfax, TUNISIA*
*(c) Department of Mechanical Engineering, ISSAT, University of Kairouan, Tunisia*

*Email: marwaezzine26@gmail.com*

## ABSTRACT

Wind energy is a renewable energy source that harnesses natural airflows to generate electricity. This paper presents a comprehensive numerical study aimed at optimizing the efficiency of wind capture systems, particularly those equipped with fins of various shapes. The primary objective is to analyze the influence of fin geometry on system performance, with a specific focus on maximizing wind speed within the cylindrical section of the system. We begin by simulating different fins configurations to assess their impact on the system's wind capture capacity. Then, we establish the relationship between this capacity and the amplification coefficient, which quantifies the increase in wind speed through the system. By comparing the results, we will identify the optimal blade shape to maximize both wind capture efficiency and wind speed amplification, relative to a baseline system. This study enables the optimization of system design for enhanced performance under various wind conditions, paving the way for more efficient and cost-effective solutions in wind energy utilization.

**KEYWORDS:** Wind energy, numerical study, wind capture system, performance optimization.

## 1. INTRODUCTION

For centuries, wind catcher systems have played an important role in natural cooling and ventilation, particularly in the Middle East, where they function as effective passive cooling solutions in architecture. These systems optimize airflow to improve ventilation, and recent innovations have adapted wind catchers to improve the efficiency of wind turbines. Research shows that variations in wind catcher geometry have a significant impact on wind turbine performance, affecting wind speed, flow dynamics, and energy production. Sadeghi et al. (2020) reviewed the historical use of passive cooling in Middle Eastern architecture, highlighting the role of wind catchers in natural ventilation. Building on this, Ahmad et al. (2021) provided a modeling framework for wind catcher systems, highlighting their potential in modern ventilation. Calautit and Hughes (2019) reviewed the integration of wind sensors into thermal systems, focusing on operational efficiency, while Alavi and Gholizadeh (2023) explored their applicability in renewable energy. Finally, Zare et al. (2024) presented an innovative wind sensor design to optimize wind speed for energy applications, thereby improving aerodynamic performance.. An exemplary innovation in this field is the wind rotor integrated with a wind catcher system, introduced by Ezzine et al. (2023). As illustrated in Figure 1, this design diverges from traditional double wind turbine (DWT) models by isolating the wind rotor from the intake, utilizing a wind catcher to capture airflow from multiple directions and heights. This paper conducts a parametric analysis of four geometric configurations. Using computational fluid dynamics (CFD) simulations, we assess their effects on airflow properties. Findings indicate that model 1 configuration can enhance airflow within the system's cylindrical section, supporting the optimal design of wind catchers.

### 2. Description of the system

The system, shown in Figure 1, comprises five key components: wind collector, wind booster, wind accelerator with cones, cylindrical section, and diffuser. Its main function is to capture airflow exceeding 1m/s, increasing the mass flow rate and energy until the cylindrical part.

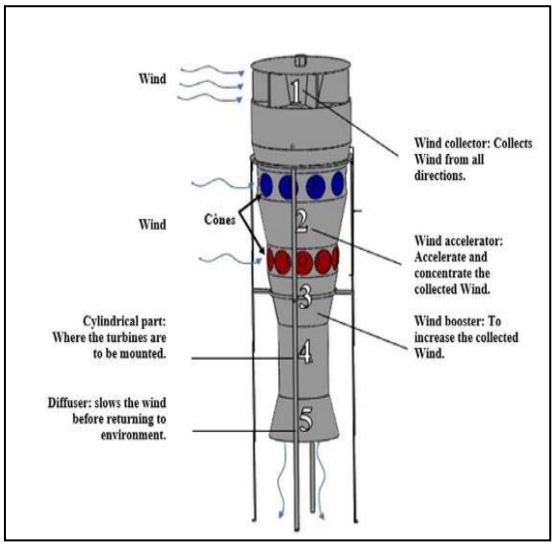


**Fig. 1** Wind Catcher System Components: (1) Wind Collector, (2) Wind Accelerator, (3) Wind Booster, (4) Cylindrical Section, (5) Diffuser (Ezzine et al., 2023)

## 3. Impact of collector fin geometry

This section provided a numerical analysis of the impact of the collector fin geometry on system performance, focusing on optimizing flow within the cylindrical part. The study began by simulating various fin geometries and examining how these configurations affected the system's wind capture capacity. It then explored the relationship between this air capture capacity and the amplification coefficient, quantifying the increase in air speed within the system. The study aimed to determine the optimal fin shape to maximize wind capture efficiency and speed amplification compared to the base system, thereby optimizing system design for peak performance in various wind conditions. Figure 2 shows the three configurations examined.

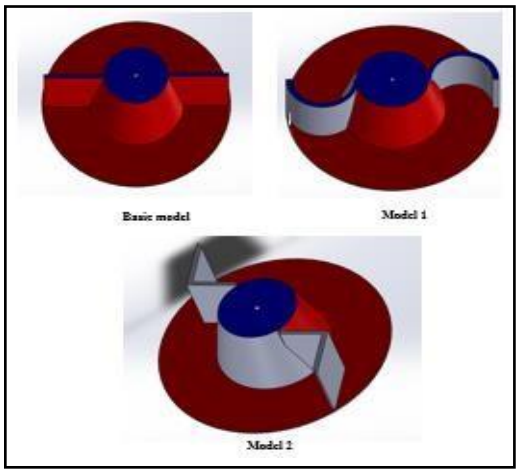


**Fig 2.** Three configuration Numerical Simulation

In this paper, we aim to perform a numerical simulation of our wind catcher system using ANSYS Fluent and Gambit. The system includes a front collector with various geometric shapes, as shown in Figure 2, to study its influence on wind speed amplification. The turbulence model used is the realizable k-ε model, validated in the study by Ezzine et al. (2023). We consider an incoming wind speed range of 2 m/s to 5 m/s to evaluate the impact of the system on the outlet wind speed.

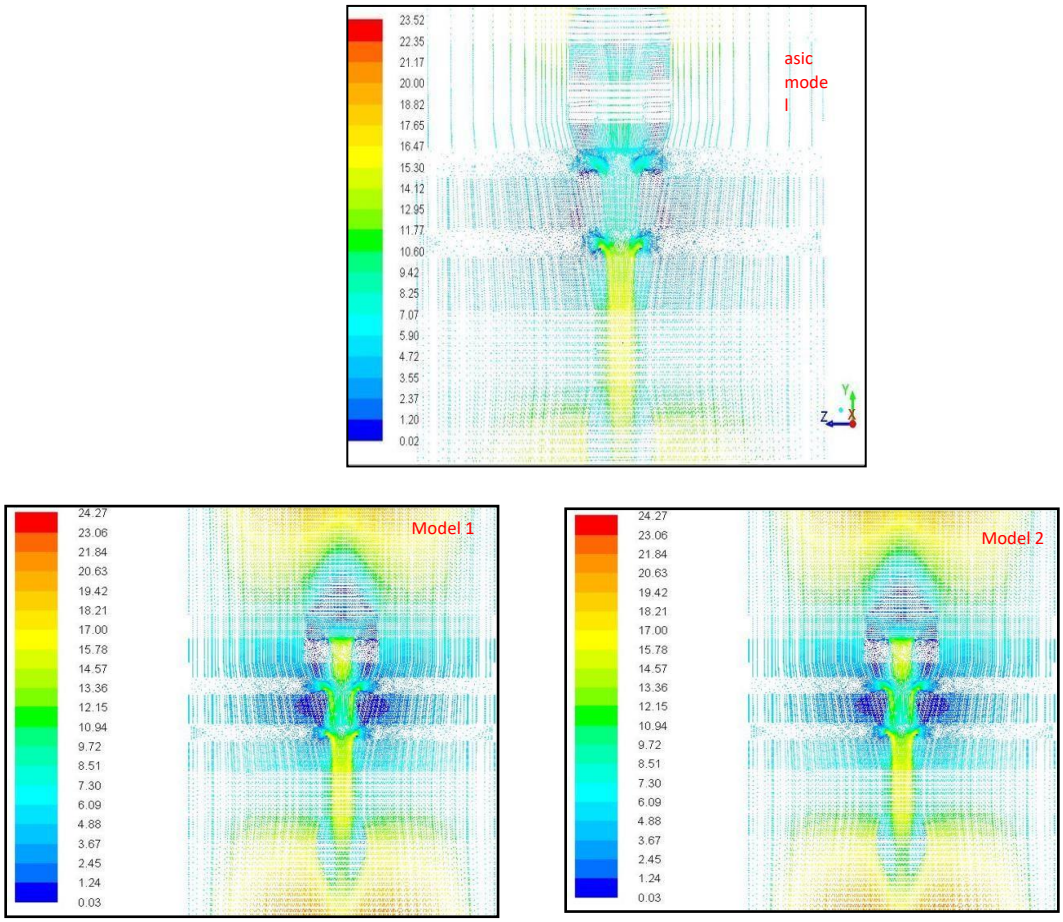


**Fig.3** Numerical simulation of three configurations

**Table 1.** Numerical Data on the Influence of fin geometry on Exit Wind Speed

| Incoming Wind velocity (m/s) | Collector with two fins Basic system | Model 1 | Model 2 |
|---|---|---|---|
| **2** | **5.92** | **6** | **5.46** |
| **3** | **8.93** | **9.1** | **8.23** |
| **4** | **11.96** | **12.03** | **11.23** |
| **5** | **15.29** | **15.34** | **14.12** |

**Table 2.** Influence of the Fin geometry on the Amplification Coefficient

| | Collector with two fins Basic system | Model 1 | Model 2 |
|---|---|---|---|
| **Wind velocity** | 15.29 | 15.34 | 14.12 |
| **Amplification coefficient** | 3.004 | 3.068 | 2.82 |

From the results obtained from different geometric configurations of collector fins, it is observed that the wind speed increases in the middle of the cylindrical section as the fin structure becomes arc-shaped (model 1), as

shown in Tables 1 and 2. Table 2 indicates that the amplification coefficient is improved with arc-shaped fin model 1.

## 4. Conclusion

This study highlights the importance of fine geometry in the design of efficient wind collector systems. A streamlined fin shape facilitates higher wind speeds and greater efficiency by minimizing the obstacles to the airflow. Therefore, the arc model 1 geometry gives optimal results, tripling the wind speed in the central cylindrical part of the system to 3.068. This insight is essential for optimizing wind collector designs to maximize performance in various applications.

## References

1.Sadeghi, H., Hashemi, M., & Fathi, M. (2020). "Historical utilization of passive cooling strategies in Middle Eastern architecture: A review of wind catchers in natural ventilation." Journal of Architectural Heritage, 14(3), 205-220

2.Ahmad, M., Mahmood, A., & Ali, M. (2021). "Dynamic modeling of wind catcher systems for natural ventilation in modern buildings." Renewable Energy and Environment, 19(4), 450-465.

3. Calautit, J. K., & Hughes, B. R. (2019). "The integration of wind sensors and thermal management systems in wind catchers for enhanced operational efficiency." Building Services Engineering Research and Technology, 40(2), 215-230.

4. Alavi, S. & Gholizadeh, R. (2023). "Applicability of wind catchers in renewable energy contexts: A focus on energy generation capabilities." Journal of Sustainable Architecture and Energy, 15(1), 118-132.

5. Zare, H., Rezaei, N., & Shakeri, S. (2024). "Innovative wind catcher design for optimized wind speed in energy applications: Advances in aerodynamic performance." Energy Conversion and Management, 212, 112345.

6. Ezzine, M., et al. (2023). Numerical and experimental investigation of a wind rotor equipped with a catcher system' International Journal of Low-Carbon Technologies 2023, 18, 1140–1153

# Sustainable Textiles and Circular Economy

# Valorisation of Tunisian tannery wool for thermal insulation

**Rihab Harizi [a], Taoufik Harizi [a], Ikram Zbali [b]**

*(a) LGTEX Laboratory*
*(b) University of Monastir, ISMM*
*E-mail: Hrizirihab52@gmail.com*

**ABSTRACT**

Waste wool fibers can be used for thermal applications due to their natural properties. The objective of this work is to use Tunisian tannery wool to produce needle-punched nonwoven fabric as eco-insulation material. The thermal conductivity, as well as other physical properties, is analyzed to assess the suitability of these materials for thermal insulation applications. Additionally, the influence of three fabrication parameters, such as surface mass input card (MSEC), number of folds (NP), and needle density (DA), are examined on each result to optimize the thermal conductivity. The results show that the combination of (1,1,2) yields the best thermal conductivity values, achieved with a value of 0.031 W.m/K.These findings demonstrate that Tunisian tannery wool is a potential source for sustainable thermal insulation in the field of eco-building. It offers comparable performance to tannery wool-based insulation in Iran, as well as its recyclablity, cost-effectively, and sustainability.

**KEYWORDS:** waste wool, tannery wool, eco-insulation, thermal property, sustainability.

## 1. INTRODUCTION

The tannery wool is often regarded as waste. In Tunisia; it is usually used on the artisanal or thrown [1].
However, sheep wool has interesting physical and chemical properties to be exploited in the field of civil engineering, particularly as thermal insulation to address the issue of high energy consumption used for heating homes [2]. Additionally, its commercialization in the industry is limited due to its high cost [1]. Thus, researchers have explored other alternatives, such as the use of waste wool, to benefit from its economic and environmental advantages [2]. They have replaced virgin wool fibers with its waste.
In this study, Tunisian waste wool was collected from crossbred sheep. Then, these short fibers needling to produce a nonwoven. Also, the physical and thermal insulation properties were investigated. Finally, the effect of surface mass input card (MSEC), number of folds (NP), and needle density (DA) on physical property and thermal insulation behavior of the woolen fabrics were studied.

## 2. MATERIALS AND METHODS

### 2.1. Manufacturing process

Tunisian tannery wool used have a diameter of 28.4 µm, length of 45 mm, tensile strength of 9 cN/tex, and elongation at break of 27.04%[3]. The manufacturer of nonwoven fabric was done with needling process. In the initial stage, the row material was weighed and manually fed into the mini carding machine to achieve an acceptable homogeneity of the web. It is worth noting that to increase the overall surface mass input, the cotton carding machine must be equipped with a cylinder to receive the web at its start. Subsequently, the layering of fibers into web layers was carried out in the lapping stage. The consolidation of the web was achieved mechanically using needle punching, which is both an environmentally friendly process and feasible due to the availability of needle punching equipment in our LGTEX laboratory. Moreover, this technique is most suitable for webs obtained from the carding machine, providing sufficient cohesion for a nonwoven fabric. The needle-punching machine in our laboratory is equipped with 1000 needles of gauge 36. For the available samples, two passes were required to achieve consolidation on both sides.
Experience design: A Taguchi plan (L9) was employed for our study. A main effects plot was utilized to observe the impact of each studied parameter on the surface mass, thickness, air permeability, and thermal conductivity of the fabric. Subsequently, optimization was performed using overlaid contour diagrams.

### 2.2. Physical Property of fabric

Morphology of structure: M50 was used in the process.
Mass per unit area was measured following the ISO 9073-1:1989 standard. A sample measuring 125x2000 mm is cut using scissors and a ruler, then weighed using a precision balance ($10^{-4}$ g).
The test is repeated five times under atmospheric conditions of T=22°C ±3 and H=61% ± 3%.

Thickness was according to the ISO 9073-1:1989 standard. The method involves applying a constant pressure of 0.2 kPa normal to the surface of the fabric, the section area of the circular presser foot 2500 $mm^2$ capable of vertical movement and a horizontal reference plate.

Bulk density ($g/m^3$) defined by this equation:

$$(kg/m^3) = Ms/e \quad \textbf{(1)}$$

$\rho$: bulk density of nonwoven fabric
$Ms$: Mass per unit area
$e$: thickness

Air permeability measurement is carried out according to ISO 9073-15: 2007.
The machine used is the TEXTEST Fx3300 Air Permeability III.
The area of the sample is 20 $cm^2$, and the test was repeated 10 times with 3 different pressure drops: 100, 125, and 200 Pa.
The porosity of the fabric (%) is calculated using the following formula:

$$\text{Porosity (\%)} = (1 - \rho F / \rho f) * 100 \quad (2)$$

ρF : Bulk density of the fabric

ρf: Density of sheep wool fiber = 1.314 $g/cm^3$

### 2.3. Thermal property

Thermal conductivity is measured using the steady-state box method; a device commonly used to measure thermal properties and frequently employed in characterizing construction materials. Also, we propose using the Maxwell-Eucken model equation to calculate conductivity for the remainder.

$$\lambda = \lambda_s * (1 - \varphi) + \lambda_f * \varphi \quad \textbf{(3)}$$

This equation takes into account the porosity of the material (φ) as well as the thermal conductivity of the solid ($\lambda s$=0.097) and the fluid ($\lambda_f$ = 0.026 W/mK).

## 3. RESULTS AND DISCUSSIONS

### 3.1. Physical property

**Table 1.** Results of structural morphology

| | Reference | B114 | B126 | B138 | B518 | B526 | B534 | B216 | B224 | B238 |
|---|---|---|---|---|---|---|---|---|---|---|
| image | 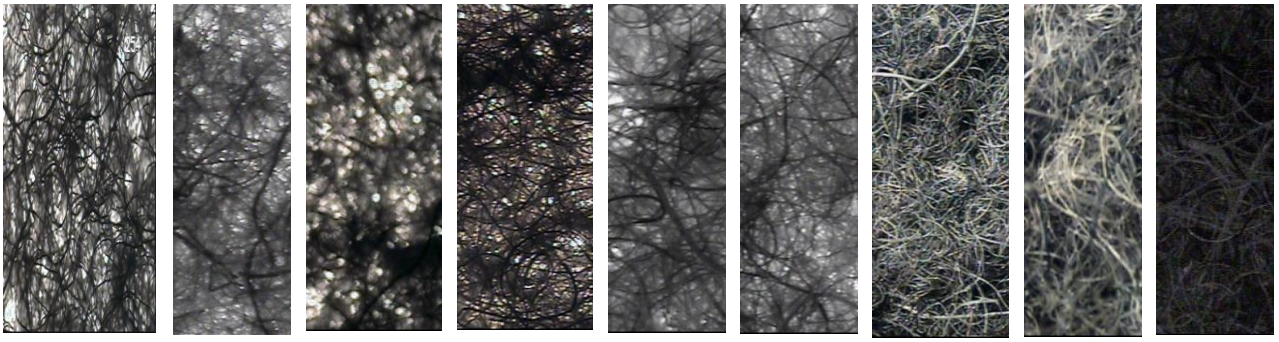 | | | | | | | | | |

**Morphology of Structure**

The images obtained by the M50 microscope are presented in Table 1. It shows that nonwovens fabric made from sheep wool waste have a uniform fibrous structure, ideal for insulation in the construction field.

It consists of a network of fibers arranged in a more or less random and overlapping manner to form overlapping layers, creating a porous network. This porosity affects the thermal and acoustic properties of our final product. It should be noted that the fibers vary in diameter and length, as we are dealing with waste from natural fiber.

**Mass per unit area**

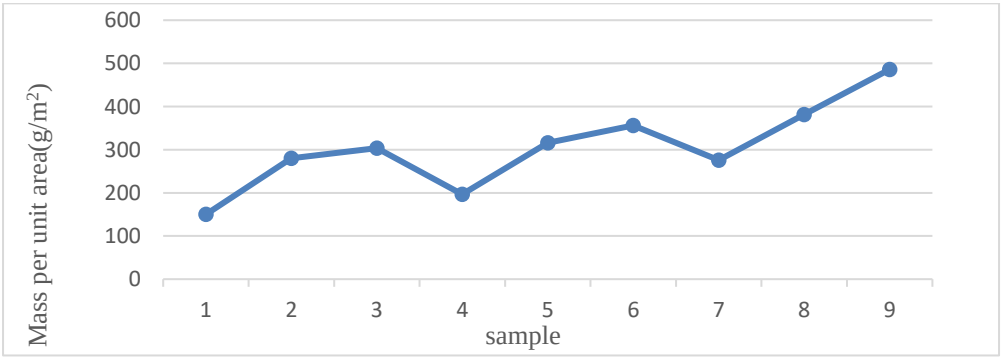


**Fig.1.** Variation of Mass per unit area

**Thickness**

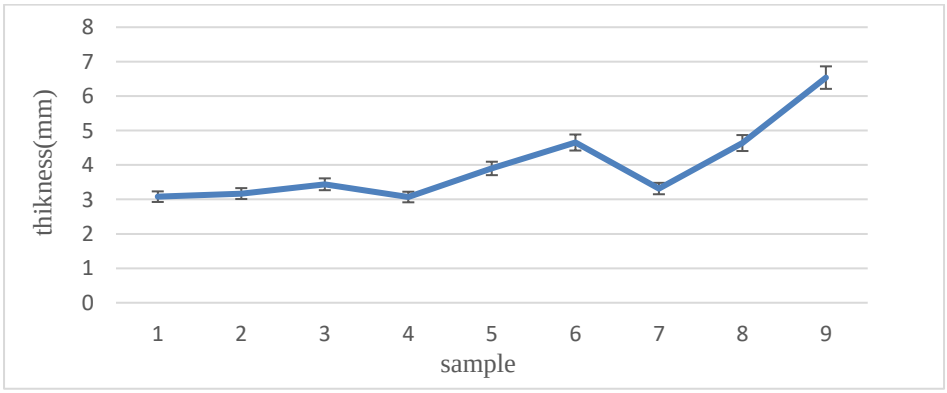


**Fig. 2.** Variation of thickness

**Bulk density**

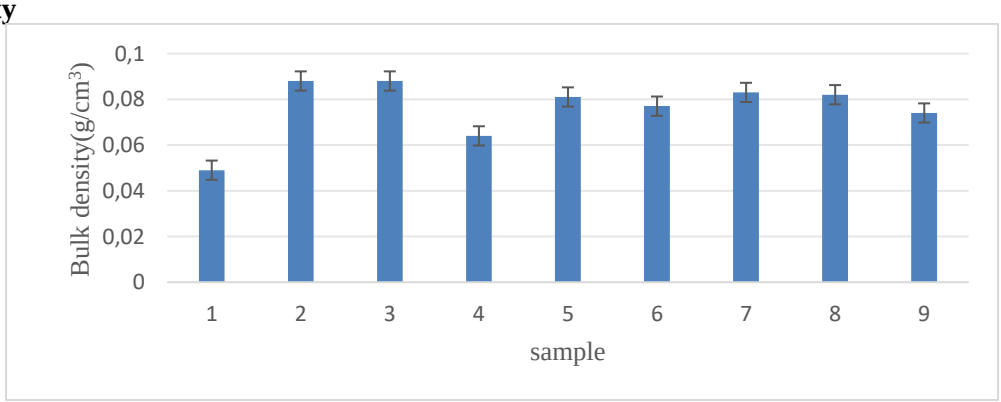


**Fig.3.** Variation of bulk density

**The air permeability**

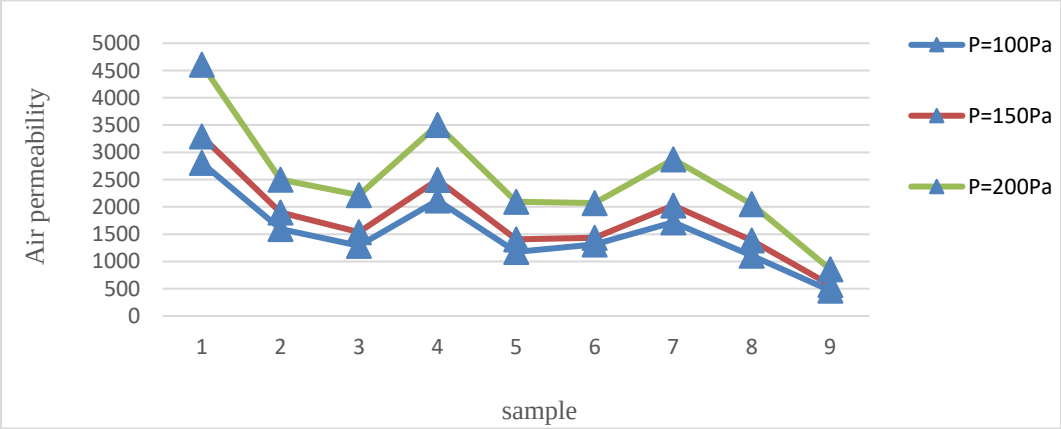


**Fig. 4**. Variation of air permeability

**Porosity**

The porosity of the fabric is 94%

This rate is considered high and close to the porosity rate of needle-punched nonwoven made from palm leaf, which is equal to 93.97%.

### 3.2. Thermal propriety

**Table 2.** Results of thermal resistance and thermal conductivity

| | **B516** | **B528** |
|---|---|---|
| **Thermal resistance ($m^2kw^{-1}$)** | 0.179 | 0.089 |
| **Thermal conductivity (W/mK)** | 0.033 | 0.067 |

**Table 3.** Results of thermal conductivity

| **Sample** | **B114** | **B126** | **B138** | **B516** | **B528** | **B534** | **B218** | **B224** | **B236** |
|---|---|---|---|---|---|---|---|---|---|
| **Thermal conductivity (W/mK)** | 0.0309 | 0.0351 | 0.0351 | 0.033 | 0.0344 | 0.0344 | 0.0351 | 0.0351 | 0.0379 |

The analysis of results from various measurements has allowed us to highlight a set of relatively important characteristics compared to other types of nonwovens:

Surface mass and thickness ranging between 140g/$m^2$ and 488 g/$m^2$, and from 3 to 7 mm respectively, resulting in an apparent density of 0.044g/$cm^3$ to 0.091 g/$cm^3$.

Pronounced porous structure justified by porosity and air permeability (200Pa drop) with values ranging from 83% to 93% and from 858 L.$m^{-2}$.$s^{-1}$ to 4722 L.$m^{-2}$.$s^{-1}$ respectively.

Thermal resistance ranging from 0.03 to 0.033W/m.K.

The use of the "superimposed contour graph" method led to the deduction that combinations (1,1,2)

## 4. CONCLUSION

This study has confirmed that this waste wool can be effectively transformed into needle-punched nonwovens, which are promising materials for thermal insulation. These nonwovens fabric offer good thermal resistance and can be used in a variety of applications, such as insulating walls, floors, and ceilings.

Surface mass and thickness ranging between 140g/$m^2$ and 488g/$m^2$, and from 3 to 7 mm respectively, resulting in an apparent density of 0.044g/$cm^3$ to 0.091g/$cm^3$.
Pronounced porous structure justified by porosity and air permeability (200Pa drop) with values 93% to 96% and from 858 L.$m^{-2}$.$s^{-1}$ to 4722 L.$m^{-2}$.$s^{-1}$ respectively. Waste wool have interesting thermal propriety and acoustic or in this study is limited in thermal proprety. Therefore, the acoustic proprety of Tunisian tannery wool will be studied.

**REFERENCES**

1. Bakatovich, A., Gaspar,F.: Composite material for thermal insulation based on moss raw material. Construct Build Mater. (2019). https://doi.org/10.1016/j.conbuildmat.2019.116699

2. Nassef,M., Elbasyoni,A.M., A Bar,A., Alnahrawy,A., H Hassanin, A.: Manufacturing and utilization of novel sustainable composites using pulled wool fibers waste from leather tanneries: Mechanical, physical, and dynamic characterization. J . Ind. Text. (2022). https://doi.org/10.1177/15280837211073358

3. Harizi,T., Abidi,F., Hamdaoui,R., Ben Ameur,Y.: Variation in Fleece Characteristics of Tunisian Sheep. Int. J. Text. Sci. (2015). https://doi.org/10.5923/j.textile.20150405.01

# Contribution of DFT to Understanding the Dyeing Mechanism of Natural and Synthetic Fibers

**Syrine Boussadia [a], Maha Abdelileh [a,b], Hatem Dhaouadi [a], Sonia Dridi-Dhaouadi[a,c]**

*(a) Laboratory of the Environment Chemistry &Clean Processes,Faculty of Sciences of Monastir, University of Monastir,Monastir,Tunisia*
*(b) Textile Engineering Department, National Engineering School of Monastir, Monastir, Tunisia*
*(c) Preparatory Institute for Engineering Studies of Monastir, 5019 Monastir, Tunisia*

*E-mail: sirineboussadia919@gmail.com*

**ABSTRACT**

Density functional theory (DFT) plays an important role in understanding and optimizing dyeing processes by analyzing the interactions between dye molecules and fibers. In this research paper, the interaction energies of the dye-fiber dimers, calculated using the B3LYP functional with a 6-311G (d,p) basis set, are correlated with color strength deviations (ΔK/S) and color differences (ΔE). The results demonstrate that the theoretical findings closely align with the experimental data, indicating that DFT is a reliable method for investigating molecular interactions during dyeing processes.

**KEYWORDS:** Density Functional theory (DFT), molecular interaction, theoretical results, experimental findings.

## 1. INTRODUCTION

Density Functional Theory (DFT) represents a significant advancement in the field of physics and quantum chemistry. As a computational method, DFT is grounded in the Hohenberg-Kohn theorems, which state that the total energy of a quantum system can be expressed as a functional of the electron density. This means that, instead of relying on wave functions, DFT allows for the calculation of electronic properties based on the distribution of electrons, significantly simplifying calculations for systems with many electrons. This approach allows for detailed studies of the electronic properties of quantum systems [1]. DFT is used to calculate the band structures of solids, revealing the distribution of electronic energy levels within a material [2]. This information is crucial for understanding the material's electrical, optical, and magnetic properties. Over the years, DFT has found applications across various scientific domains, including the textile industry, specifically in dyeing processes. It plays a crucial role in understanding and optimizing coloration processes [3].

In the field of textile dyeing, quantum modeling provides a precise theoretical framework for examining the mechanisms governing the interaction between dye molecules and textile fibers. It enables a thorough analysis of the electronic structures of dye molecules, predicts their light absorption properties, and clarifies their molecular interactions with textile substrates. The dyeing effectiveness of specific azo disperse dyes with pyrazole groups was assessed by calculating chemical descriptor parameters for their protonated tautomeric forms. The findings indicated that the dyes' absorption values, determined using the B3LYP/6-31G(d,p) basis set, were in close agreement with experimental results [3]. Furthermore, DFT facilitates the optimization of dye molecular structures to enhance their dyeing efficiency, chemical stability, and colorimetric properties.

This study proposes using the DFT approach to investigate the dyeing process of various textile fibers with an acid dye. The efficiency of this method in explaining dyeing results was evaluated by comparing the predicted interaction energy values with the observed colorimetric deviations and differences in color strength.

## 2. MATERIAL AND METHODS

### 2.1. Chemicals and Materials:

Acid Orange 67 ($C_{26}H_{21}N_4NaO_8S_2$) was used for dyeing textile fibers. Sodium sulfate ($Na_2SO_4$) and ammonium acetate served as dyeing auxiliaries in the experiments. A multi-fiber strip containing six types of fibers diacetate, cotton, polyamide, polyester, acrylic, and wool was utilized for the dyeing experiments (VIBRATECH DW ISO 105-F10).

### 2.2. Dyeing Process

The dyeing of a multi-fiber strip was conducted using Acid Orange 67 at a 1% shade, at a temperature of 100°C in a laboratory dyeing machine (AHIBA). The dyeing bath contained 2% ammonium acetate and 15% sodium sulfate. To ensure color reproducibility, each dyeing was performed twice. The dyeing process is illustrated in Figure 1.

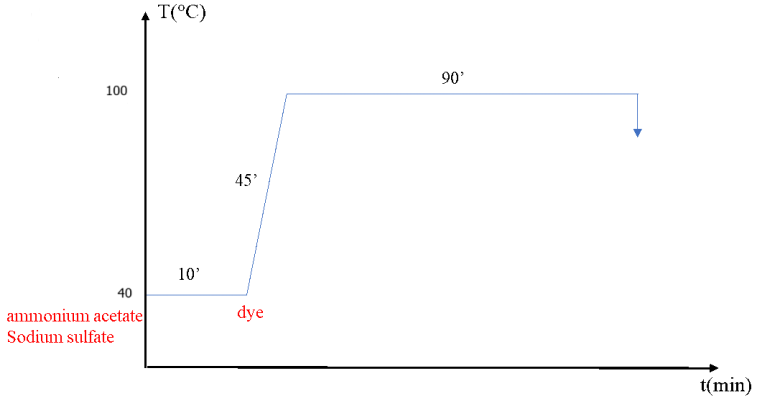


**Fig. 1**. Dyeing process of textile fibers with the acid orange 67 dye.

### 2.3. Color strength evaluation:

A SpectraFlash SF300 spectrophotometer (illuminant D65/observer 10°), equipped with Data Master 2.3 software (Datacolor International, USA), was used to measure the color strength (K/S) values of the dyed samples using the Kubelka-Munk formula [5]

$$\frac{K}{S} = \frac{(1-R)^2}{2R} - \frac{(1-R_0)^2}{2R_0} \qquad \textbf{(1)}$$

### 2.4. Evaluation of Color Difference (ΔE)* :

The color difference (ΔE) before and after washing was measured using the following formula:

$$\Delta E = \sqrt{\Delta L^{*2} + \Delta a^{*2} + \Delta b^{*2}} = \sqrt{(L_2^* - L_1^*)^2 + (a_2^* - a_1^*)^2 + (b_2^* - b_1^*)^2} \qquad \textbf{(2)}$$

Where ΔL* is the difference in lightness, Δa* is the difference in green/red hues and Δb* is the difference in blue/yellow hues, ($L1^*$, $a1^*$, $b1^*$) are the coordinates of the dyed sample before washing test and ($L2^*$, $a2^*$, $b2^*$) are the coordinates of the dyed sample after washing test.

### 2.5. Computational details

The DFT calculations were carried out using Gaussian program package 09, while Gauss View 5 was used for visualization of the structure and simulation of the vibrational spectra. In this study, the B3LYP 6-311 G basis set was employed to obtain the optimized structures of the acid orange 67 dye and the fibers.

## 3. RESULTS AND DISCUSSIONS

### 3.1. Evaluation of dyeing performances :

Dyeing experiments were conducted on various textile fibers using Acid Orange 67, as described in Section 2.2. To investigate the correlation between the interaction energy obtained via the DFT method and the experimental data, the deviations in dyeing strength and colorimetric coordinates before and after washing were measured. The results are presented in Table 1. This table indicates that diacetate (DA) has the lowest deviation in color strength, demonstrating the best dye fixation, followed by polyamide, wool, polyester (PE), acrylic, and finally cotton.

**Table 1.** Color strengths and colorimetric coordinates deviations of the dyed fibers

| Fiber | K/S | | Δ K/S (%) | CIELAB (L*a*b*) | | | | | | ΔE* |
|---|---|---|---|---|---|---|---|---|---|---|
| | | | | Dyed fabric | | | After washing | | | |
| | Dyed fabric | After washing | | L* | a* | b* | L* | a* | b* | |
| **Wool** | 15.18 | 8.64 | 43.08 | 48.29 | 39.47 | 49.13 | 50.94 | 35.98 | 40.69 | 9.51 |
| **Acrylic** | 0.79 | 0.45 | 43.03 | 82.07 | 6.13 | 31.73 | 84.80 | 1.86 | 23.48 | 9.68 |
| **Polyester** | 0.64 | 0.31 | 51.56 | 83.06 | 4.94 | 28.46 | 86.52 | -0.29 | 17.83 | 12.34 |
| **Polyamide** | 23.39 | 22.32 | 4.57 | 56.70 | 42.64 | 68.79 | 56.34 | 42.52 | 69.52 | 0.82 |
| **Cotton** | 1.75 | 0.64 | 63.00 | 77.23 | 12.19 | 42.68 | 82.48 | 5.64 | 25.86 | 18.8 |
| **Diacétate** | 8.33 | 8.20 | 1.56 | 72.46 | 22.37 | 73.41 | 72.15 | 23.67 | 72.52 | 1.61 |

### 3.2. Study of interaction energies:

The interaction energy values obtained by the DFT method using the B3LYP/6-311G (d,p) basis set provide insights into molecular bond strengths and stability. The interaction energy was determined using the following equation:

$$E\ (\text{interactions}) = E\ (\text{dimer}) - [E\ (\text{dye})_{\text{dimer}} + E(\text{fiber})_{\text{dimer}}] \quad \textbf{(3)}$$

Based on Table 2, the interaction energies can be ranked in descending order as follows:
E (AO67-DA)> E (AO67-PA)>E (AO67-Cys)>E (AO67-PE)>E (AO67-AN)>E (AO67-CNF)

The AO67-DA dimer has the highest interaction energy, suggesting stronger, more stable interactions between the dye molecules and the diacetate fiber. This can be explained by the fact that Van der Waals forces, resulting from the interaction of electric dipoles induced in the molecules, can strengthen the bond between orange acid 67 and diacetate. Conversely, the AO67-CNF dimer shows the lowest interaction energy, indicating relatively weaker interactions.

**Table 2.** Optimized dimer interaction energies

| Dimer | E (interaction) (kcal/mol) |
|---|---|
| **AO67-PE** | -7.79 |
| **AO67_AN** | 5.31 |
| **AO67-CNF** | -3.77 |
| **AO67_DA** | -15.55 |
| **AO67-PA66** | -14.22 |
| **AO67_CYS** | -13.11 |

Based on the results presented, we obtained the following orders for the interaction energy.

(ΔE): DA > PA > CYS > PE > AN > CNF, and for the color strength variation (ΔK/S): DA > PA > CYS > AN > PE > CNF. The results for interaction energy and color strength variation show a high degree of consistency, following almost the same order.
In contrast, the order of color difference (ΔE) is as follows: PA > DA > CYS > AN > PE > CNF. This order reveals a pattern where two synthetic fibers (PA and DA) are followed by one natural fiber (CYS), then two synthetic fibers (AN and PE), and finally another natural fiber (CNF).

## 4. CONCLUSION

In this study, we examined the interactions between an acid dye and various commonly used textile fibers, focusing on chemical reactivity and color fastness. The interaction energies of AO67 dimers with different fibers showed the following order: AO67-DA > AO67-PA > AO67-Cys > AO67-PE > AO67-AN > AO67-CNF, reflecting the dye's fixation ability and its impact on color strength. Our findings indicate that DFT analysis of interaction energies demonstrated a strong correlation with the experimental color strength deviation (ΔK/S) results, validating its predictive accuracy for dye performance.

## RREFERENCES

1. Ferhani, N. E. H.: Etude computationnelle des effets des substituant sur les propriétés moléculaires et la réactivité chimique des dérivés de pyridine-3- carbonitrile , Université Mohamed Khider de Biskra.
2. Marzari, N., Ferretti, A., Wolverton,C.: Electronic-structure methods for materials design. Nat.Mater . 20,736-749(2021).
3. Z. Omar, A., G. Mohamed,M., A. Hamed, E., A. El-atawy, M., Characterization, DFT calculations and dyeing performance on polyester fabrics of some azo disperse dyes containing pyrazole ring, J. Saudi Chem. Soc.27,101594 (2023).
4. Kubelka, P., New contributions to the optics of intensely light-scattering materials. Part I Opt. Soc. J. Am. 38, 448-457 (1948).

# Optimization of plasma treatment variables to improve dyeing process of COT/PET fabrics

**Ben Brahem Rahma, Abd Jelil Radhia, and Ladhari Neji**

*LGTex Laboratory, Higher institute of Technological Studies of Ksar Hellal, Tunisia*

*E-mail : rahmabrahem45@gmail.com*

**ABSTRACT**

This study explores the use of atmospheric pressure plasma as an environmentally friendly technology to improve the textile properties of COT/PET. We focused on optimizing the different effects of APPJ plasma parameters on COT/PET blends fabric to improve the dyeing process. Box–Behnken design was used for the optimization of plasma treatment process and to evaluate the effects and interactions.

We used the distance between the nozzle and the fabric, the time as the parameters of machine and humidity of the sample as a new parameters. The objective was to study the impact of these parameters on the capillarity and dyeing of the fabric studied.

The results revealed that the treatment time and distance have a negative effect for capillarity. The humidity of the fabric has a positive effect.

The optimum values of treatment were time 5m/min, the distance of 5cm were determined and the humidity of fabric was 56%. Moreover, the results of the analyzes showed that plasma treatment significantly improved capillarity fabric. The improvement in this capillarity has also led to an improvement in the dyeing properties of the fabric, particularly with regard to coloring strength and fastness to washing.

Several analytical techniques were used to evaluate the impact of plasma treatment on tissue properties: Attenuated Total Reflection Fourier transform infrared spectroscopy (ATR-FTIR), scanning electron microscopy (SEM), CIELAB system, and the parameter K/S.

**KEYWORDS:** Atmospheric pressure plasma, Capillarity, Box–Behnken design, COT/PET blends fabric

## 1. INTRODUCTION

Plasma treatment is considered as an ecofriendly technology in textile industry, because it can be a dry process using minimum amount of chemicals for functionalization of textile materials in times relatively shorter than the conventional wet treatments. The potential of plasma technology has been explored extensively for imparting the hydrophilic and adhesive properties to the natural and synthetic textile materials. Plasma treatment can induce changes in textile surface properties in terms of capillarity. Low-pressure plasma techniques have been effectively used for surface modification of textiles. Plasma can bring surface modification of textiles in variety of ways, like etching, cleaning, activation, and polymerization. The present study has been carried out COT/PET fabric to improve dyeing process with the use of APPJ plasma treatment. The parameters in plasma treatment were: humidity of fabric as a new parameter, distance between the nozzle and the fabric and duration of treatment.

## 2. MATERIALS AND METHODS

### 2.1. Materials

**Textile materials:** The used fabric weave: 75% cotton/25% polyester blend 195 g/m$^2$ weight per unit area (conditioned 65% HR; 21°C).

**Chemicals:** for the dyeing process, we employed Disperse dye (Red Setapers D), Direct dye (Red Tubuntin BWS), Sodium sulfate, Acetic acid and Dispersing agent DISPEX.

**Equipment:** the equipment used for fabric treatment and analysis included plasma treatment, scanning electron microscopy (SEM)**,** Attenuated Total Reflectance of Fourier Transform Infrared (ATR- FTIR) and CIELAB system and K/S measurement.

## 2.2. Methods

**Plasma treatment:** A plasma jet system from Plasmatreat was used for the pretreatment The jet was operated with ambient air. In this work, APPJ atmospheric-pressure plasma jet treatment was done on the fabric by varying its treatment time, distance between the nozzle and subtract and humidity fabric (Condition: power 280V).

**Box–Behnken design:** In this study, we used Box–Behnken as a spherical, revolving design.

**Table 1.** the input parameters and experimental design levels used in the present work

| Variables | Levels | | |
|---|---|---|---|
| Coded levels | -1 | 0 | +1 |
| Time (V) (min/m) | 5 | 10 | 15 |
| Distance (D) (cm) | 220 | 280 | 320 |
| Humidity (H) (%) | 6 | 24 | 56 |

**Capillarity of fabrics:** For measuring the capillarity fabric, capillary method was used. the specimens were cut with 13×5 cm dimension. To detect the position of the water line, a dye was added to water. The measured height of the rise in a given time (2min) was taken as a direct indication of capillarity of the tested fabrics.
The capillarity is calculated according to formule:

$$Cap\% = \frac{m_m - m_s}{m_s} \times 100 \quad (1)$$

where (Cap) is the capillarity , ($m_m$) is the final mass of the fabric after water absorption (2 min) and ($m_s$) the dry mass of the sample

**Dyeing procedure:** The conditions of dyeing was Mass of the sample equal to 1.5g, Bath ratio 1/10 and pH equal to 5.5
Figure 1. summarizes the steps of this process.

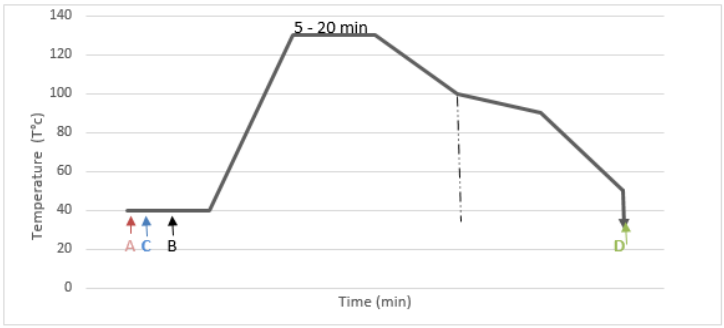


A: 1g/L dispersant + 5 -20 g/L sodium sulfate and pH=5-5.5
B: disperse dye + direct dye (red Setapers1et red tubutin BWS)
C: sodium sulfate
D : Wash, rinsing

**Fig. 1** Steps of dyeing process

**Colour measurements:** The colour yield of samples was evaluated by light reflectance measurements using SF 300 spectrophotometer. Relative colour strengths (K/S values).

**Colour fastness testing:** The dyed samples were tested for fastness properties according to standard methods, the specific tests were for colour fastness to washing ISO 105-C02:1989

# 3. RESULTS AND DISCUSSIONS

## 2.1. Characterization of treated and untreated fabrics with SEM

SEM micrograph of untreated fabrics is shown in Figure 2. The SEM image of the untreated fabric reveals that the surface of material has two types of fibers (cylindrical and smooth for polyester and other spiral fibers for cotton fibers).

The SEM micrograph of treated fabric in figure 3 showed some swelling at the end of the fibers, that means the high energy electrons in the atmospheric air plasma could affect the fabric surface and caused melting of some polyester fibers

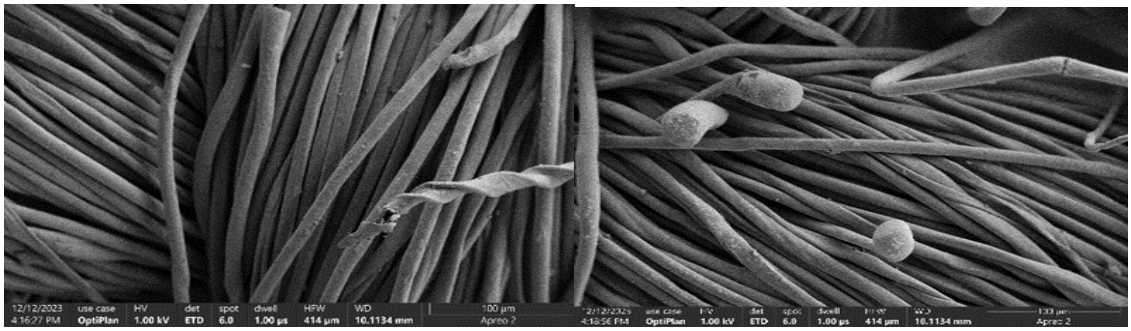

**Fig. 2** SEM micrographs of (a) untreated fabric (b) treated fabric

## 2.2.Analysis of treated fabric with ATR-FTIR

The bands appearing at 3431 and 1014 $cm^{-1}$ are assigned to intermolecular O–H bonded to C=O groups and O–H out-of-plane bending in terminal carboxylic groups in polyester chains. The band at 1711 $cm^{-1}$ can be assigned to stretching vibration of C=O group in ester.On the other hand, the fabric has transmission band corresponding to the elongation vibrations of the OH group and another band of elongation vibration of CH group with a transmittance of 96.38% coming from cellulose which confirms the presence of cotton in the fabric studied. According to the spectra of untreated and treated fabric (figure 4), the two samples (treated and untreated) have the same molecular structures, which allows us to conclude that the treatment does not profoundly modify the fabric, it keeps the basic structure of the material. On the other hand, after plasma treatment, the intensity of the 3430 cm-1 band and vibrations near this region was increased which represents an increase in functionality of hydroxyl groups and illustrates that the fabric is more hydrophilic after plasma treatment. Moreover, the spectrum corresponds to the treated sample shows the increase in C=O groups compared to the untreated sample, which means that it is a modification at the surface of fabric. It is found that the ATR-FTIR spectra of untreated and plasma treated samples do not indicate any significant difference in the surface chemical composition.

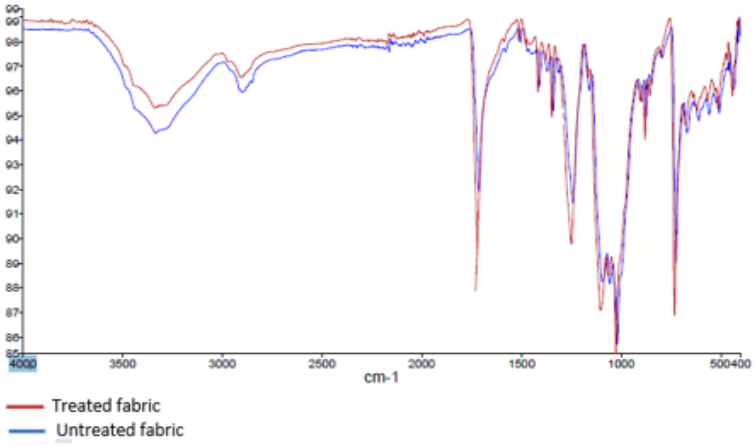


**Fig. 4** ATR-FTIR spectra of COT/PET fabric (treated and untreated)

### 2.3. Optimization of process parameters

RSM was applied to the experimental data using MINITAB. the experimental Box–Behnken design under RSM has been followed.

**Table2.** Box–Behnken design along with values of responses

| Std order | Run order | Time V | DistanceD | Humidity of fabric H | capillarity(%) |
|---|---|---|---|---|---|
| 1 | 11 | 5 | 3 | 24 | 73 |
| 2 | 12 | 15 | 3 | 24 | 68 |
| 3 | 13 | 5 | 8 | 24 | 62 |
| 4 | 5 | 15 | 8 | 24 | 54 |
| 5 | 14 | 5 | 5 | 6 | 63 |
| 6 | 8 | 15 | 5 | 6 | 55 |
| 7 | 1 | 5 | 5 | 56 | 76 |
| 8 | 15 | 15 | 5 | 56 | 58 |
| 9 | 2 | 10 | 3 | 6 | 52 |
| 10 | 7 | 10 | 8 | 6 | 49 |
| 11 | 6 | 10 | 3 | 56 | 66 |
| 12 | 9 | 10 | 8 | 56 | 56 |
| 13 | 10 | 10 | 5 | 24 | 62 |
| 14 | 4 | 10 | 5 | 24 | 61 |
| 15 | 3 | 10 | 5 | 24 | 63 |

**Model building and statistical analysis for capillarity**

The empirical relationships for capillarity(*Y*), and the tested variables as determined by MINITAB, is shown in the Equation below

$$\text{Capillarity}(Y) = 64{,}00 - 5{,}25V - 8{,}75D + 4{,}75H - 2{,}25V*V - 1{,}25D*D - 2{,}25H*H \quad \textbf{(2)}$$

The effect of time (V) is negative, as indicated by its coefficient which is equal to -5.25 in the model equation.

In this case, high speed values can lead to less satisfactory results in terms of capillarity.

The effect of distance (D) is also negative, as indicated by its coefficient which is equal to -8.75 in the model equation. This means that an increase in the distance between the nozzle and the sample leads to a decrease in the percentage of capillarity. Furthermore, the effect of distance (−8.75) is greater in absolute value than that of duration treatment (−5.25). This indicates that although increasing speed has a negative effect on capillarity, it is less pronounced than that of speed. on the other hand, the effect of fabric humidity (H) is positive, as indicated by its coefficient which is equal to 4.75 in the model equation. This means that an increase in humidity of fabric results in an increase in capillarity percentage. This observation suggests that the moisture in the fabric has a beneficial effect of capillarity.

It is important to note that this positive effect of humidity of fabric contrasts with the negative effects observed on time and distance.

The diagram of capillarity (Figure5) supports the conclusion that V, D, H had highly significant effects on capillarity.

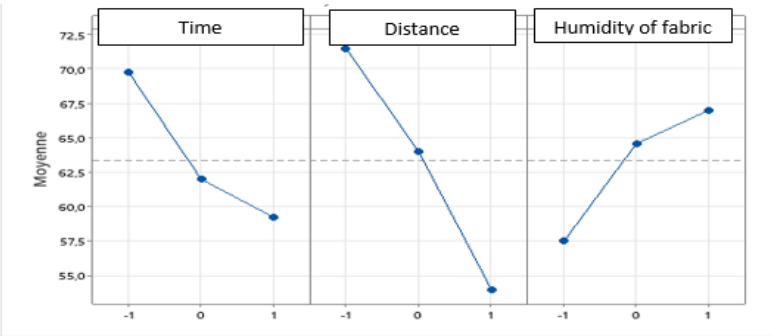


**Fig. 5** diagram of the effects of parameters

**Analysis of variance**

The statistical model was checked by the ANOVA results for the response surface are summarized in Tables 4 for capillarity.
Values of Prob >F less than 0.0500 indicate model terms are significant. In this case, V, D and H are significant model terms.
The lack-of-fit measured the failure of the model to represent the data in the experimental domain at points which were not included in the regression. The F-value for the lack- of-fit was not significant (p> 0.05), confirming the validity of the model. The value F of lack -of-fit 14.08 implies that the lack-of-fit is not significant (p> 0.05) relative to the pure error, confirming the validity of the model. There is a 6.7% chance that such a large lack-of-fit value could occur.
According to Table 3, V, D, H are significant model terms.
The goodness of the model can be checked by the determination coefficients $R^2$ and the adjusted $R^2$ (multiple correlation coefficient R).

**Table 3.** ANOVA for response surface of capillarity

| Source | Sum of squares | df | Mean squar value | *F*-value | P-value |
|---|---|---|---|---|---|
| Model | 752,15 | 9 | 83,572 | 9,44 | 0,0012 |
| V-Time | 190,12 | 1 | 190,12 | 21,4 | 0,0006 |
| D-Distance | 180,50 | 1 | 180,50 | 20,40 | 0,0006 |
| H-Humidity | 171,12 | 1 | 171,12 | 19,34 | 0,0007 |
| VD | 83,30 | 1 | 83,308 | 9,41 | 0,0028 |
| VH | 23,07 | 1 | 23,077 | 2,61 | 0,1670 |
| DH | 51,92 | 1 | 51,923 | 5,87 | 0,0600 |
| $V^2$ | 2,25 | 1 | 2.250 | 0,25 | 0,6360 |
| $D^2$ | 25,00 | 1 | 25,000 | 2,82 | 0,1540 |
| $H^2$ | 12,25 | 1 | 12,250 | 1,38 | 0,2920 |
| Residual | 44,25 | 5 | 8,850 | | |
| Lack-of-fit | 42.25 | 3 | 14,083 | 14.08 | 0.0670 |
| Pure error | 2,00 | 2 | 1,000 | | |
| Corrected total | 796,40 | 14 | | | |

Note $R^2$ –.94.44, Adj$R^2$ –.84.44, Pred$R^2$ – 14.55

Finally, the optimum values of treatment time 5m/min, the distance between the nozzle and the sample of 5cm

were determined and the humidity of fabric is 56%.

**Table 4.** Optimum and confirmative values of the process parameters for maximum capillarity

| Process parameters | Optimized parameter (predicted value) | Confirmation experiment (actual value) |
|---|---|---|
| Capillarity (%) | 75 | 76 |
| Time (m/min) | 5 | 5 |
| Humidity of fabric(%) | 56 | 56 |
| Distance (cm) | 5 | 5 |

### 3.2. Dyeing

In order to investigate the effect of plasma treatment on COT/PET fabric, untreated and treated samples were dyed.

K/S value of untreated and treated samples after dyeing is shown that plasma treated COT/PET fabric exhibits a higher color absorption compared with untreated fabric. Color absorption for 30 min plasma treatment of COT/PET fabric is about 9.25%. That is higher than untreated fabric (5%).

According to the results of K/S value, the plasma treatment increases the color absorption in the fabric COT/PET. Before wash, K/S value of untreated sample was 8.5 and after wash, it was 7.75. the result show that the K/S of treated sample was higher than the results of untreated sample (9.5 before wash and 9 after wash) which can be explained by the effect of plasma treatment on fabric dye fastness.

Furthermore, the results show that ΔE of untreated sample (1.7) is higher than ΔE of treated sample (1.1). This means that plasma treatment causes increasing the color absorption in the fabric COT/PET.

## CONCLUSION

The present study showed that the humidity of fabric has a positive capillarity effect. The application of plasma treatment in the dyeing of cotton/polyester fabric shows better results, a marked enhancement was registered in the colour shade; the enhanced of K/S was more than conventional dyeing. Moreover, dyeing with plasma pretreatment can be a more ecological alternative than the old process from a technical point of view since it increases the fixation rate of the dye. Therefore, through this type of APPJ plasma, we can reduce the consumption of chemicals and the amount of dye in wastewater, which makes it easier to treat dyeing wastewater.

## REFERENCES

1.Judd, D. B., Wysezcki, G.: Color in Business, Science and Industry, New York (2000)

2. Karthik,T., Murugan, R., Vijayan,M.: Optimization of plasma treatment variables to improve the hydrophilicity of polylinen® fabrics. J.Text.Inst. (2013) https://www.tandfonline.com/doi/abs/10.1080/00405000.2012.743647

3. Hashemizad, S. H., Mireshghi, S. S.: Environmentally friendly plasma pretreatment for preparation of self-cleaning polyester fabric with enhanced deposition of TiO2 nanoparticles. Biodivers.Environ. Sci(2014)
https://www.academia.edu/download/67758983/Environmentally_friendly_plasma_pretreat20210626-2108-1d09jcl.pdf

# Optimization of microwave-assisted aqueous extraction of colorants from date palm fiber fibrillium using multilevel factor design

**Rawdha Znegui[a,b]. Noureddine Baaka[a,b]. Nizar Meksi[a,c]. Hatem Dhaouadi[a]**

*(a) Laboratory of Environmental Chemistry and Clean Process (LCE2P-LR21ES04). Faculty of Sciences of Monastir. University of Monastir. Monastir 5019. Tunisia*
*(b) Department of Textile and Fashion Management. Higher Institute of Fashion of Monastir. Monastir 5000. Tunisia*
*(c)Department of Textile. National Engineering School of Monastir. University of Monastir. 5000 Monastir. Tunisia*

**ABSTRACT**

The increased demand for natural dyes has prompted scientists to look for fresh dyes. cutting-edge methods for drawing natural pigments from minerals. plants. and animals. The process of extracting natural colors from plants using the microwave-assisted extraction (MAE) approach has grown a lot in popularity in recent years. In this work. The household microwave oven was used to extract pigments from the fibrillium of date palm fiber. The parameters of extraction duration. microwave power and pH extraction were investigated in order to design this extraction technology. Total condensed tannins. total phenolic content. and total favonoids content were assessed in each instance. The extraction procedure was optimized by the use of a multilevel three-factor design. The suggested model has a high coefficient of determination. showing great edictability and good approximation.

**KEYWORDS:** Date Palm fibrillium, Natural dyes, Waste valorization, Optimization.

## 1. INTRODUCTION

The colors used for dyeing textiles can be classified into two main categories: natural colors and synthetic colors. Currently. interest in natural dyes is increasing due to global awareness of the environmental impact of the production and massive use of synthetic dyes. as well as the adverse health effects of some of them. Natural dyes. also called natural pigments. come mainly from plant roots. stems. leaves. flowers. fruits. animals or minerals of natural color (Faidi et al.. 2024; Gharred et al.. 2024).

For some time now. plants have been recognized as a sustainable and renewable source of high-value products. Therefore, the development of these active substances from plants presents considerable economic potential.

The *Phoenix dactylifera* L.. also called date palm. is a tree found in the desert regions of the world. where the climate is warm and dry. It is spicy. because it produces basal waste that meets the mechanism of total repetition. This date residue has been used for the manufacture of biochar. bioethanol or for water treatment. according to some studies. Several researches have been conducted on the use of date fibers as reinforcements in composite materials (AbouZeid et al.. 2024).

Our study focuses on the extraction of the natural dye from the waste of this tree. namely fibrillium. According to our bibliographic research. There is no research in this area.

There are different methods to extract the natural active ingredients. These approaches can be classic or innovative. Traditional methods employ organic solvents (such as ethanol. hexane. methanol. acetone. etc.) or water and are carried out at atmospheric pressure. These techniques are commonly used to extract natural compounds from aromatic and medicinal plants. However, the search for more environmentally-friendly methods is becoming a major concern for many industries. Indeed, regulatory security economics, social and environmental issues involve improved technology and the development of more efficient extraction methods in terms of efficiency, time and cost, while reducing the consumption of solvents.

With an emphasis on the extraction of natural dyes from this by-product. our research attempts to investigate the potential of date palm fiber fibrillium for textile dyeing. Wool textiles served as the test material for the evaluation of the dyeing performance. The effects of important experimental parameters like pH. extraction time. and power were investigated in relation to the dyeing outcomes. In order to improve the overall performance of the dyed wool fabrics as well as the dyeing efficiency. modeling and optimization of these extraction conditions were also carried out.

## 2. MATERIAL AND METHODS

### 2.1. Raw Materials

In March 2024. the waste of palm trees will not be exploitable. The fibrillium material was specially harvested in the Monastir region. The samples were cleaned. cut into small pieces and dried at 80°C for 45 minutes. Eventually. They are finely grated to be transformed into powder.

**Fig.1** The stages of preparation of plant material in this study.

### 2.2. Extraction of Coloring Components

The technique of extraction of the dyeing material is aqueous extraction. It consists of dissolving 3g of the plant material in 500 ml of water. The set was placed in a reflux mounting in an assisted microwave with a power of 500W for 3 minutes. Once the extraction was completed. the remaining mixture was passed through a filtering system and the colored aquatic extract was recovered. ready to be used as a dye bath for textile fibers later.

**Fig. 2** The process of extracting dye by assisted microwave

### 2.3. Phytochemical Study

The aqueous extracts were used to perform a preliminary phytochemical screening. a qualitative analysis based on color and/or precipitation reactions to detect some chemical elements present in our biomass. This analysis was carried out using the already standardized methods.

## 3. RESULTS AND DISCUSSIONS

### 3.2. Phytochemical Study of the dyeing material

Phytochemical tests were performed to detect the presence of various secondary chemical species in the aquatic palm tree fibrillium extract.

The results of these tests are shown in the following table and figure:

**Table 1.** Results of phytochemical analyses of the color solution of: fibrillium

| ***Secondary metabolites*** | ***Infusion**** |
|---|---|
| Flavonoïdes | + |
| Tanins | + |
| Composés terpéniques | + |
| Saponines | + |

* +: Presence of compounds /- No compound

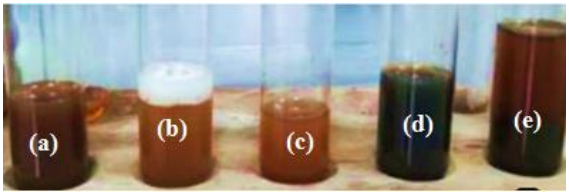


**Fig. 3** Phytochemical analysis results: *(a) aqueous extract (test). (b) saponin test. (c) flavonoid testing. (d) phenol and tannin testing. and (e) terpenic compounds test*

These results show the richness of this plant in terms of flavonoids. tannins. terpenic compounds and saponins:

- The saponins were identified by producing stable foam after intense stirring of 2 ml of date palm fibrillium aquatic extract.
- The presence of tannins and phenols in the aqueous fibrillium extract was observed by the formation of a blue-black color with the addition of 2 mL of 2% iron chloride (III) solution and 2 ml of the extract itself.
- The presence of flavonoids was identified by the formation of a red hue when zinc dust was present in the aquatic extract of fibrillium from date palm. then by the drop-by-drop addition of chlorhydric acid concentrated.

### 3.3. Optimization of the extraction process

#### *3.3.1. Experimental design*

Experimental designs provide a structured approach for simultaneously examining the effects of multiple input variables. known as factors. on an output variable. or response. These designs consist of a series of carefully controlled experiments or tests. during which the input variables are systematically manipulated. At each stage. data are collected to capture the effect of these changes. enabling researchers to analyze the relationships between the factors and the response. This approach helps identify the specific conditions within processes. as well as the key components of products. that significantly impacts quality.

Through the application of experimental designs. it becomes possible to determine the factor settings that yield optimal results. allowing for more precise control over production processes. These methodologies are critical for optimizing both performance and quality in various fields of science and industry. By investigating the design of experiments. the interaction between input variables and the response can be elucidated. facilitating the development of a robust statistical model. In the context of process optimization. such models are often expressed through regression equations that describe the behavior of the system. offering valuable insights into how each factor contributes to the outcome. As outlined by Ben Ticha et al. [1.2]. These models are essential for enhancing process efficiency and ensuring product consistency. leading to improved decision-making in experimental research and industrial applications.

- **TFC** = 19.624 + 2.977 P(W) + 0.593 pH + 0.706 t(min) + 0.13993 P(W)*pH - 0.694 P(W)* t(min) - 1.123 pH* t(min). **$R^2$ = 99.52%. $R^2_{adj}$=97.34%**

- **TPC** = 31.728 + 4.887 P(W) + 1.025 pH + 1.207 t(min) - 0.177 P(W)*pH - 1.188 P(W)*t(min) - 1.883 pH*t(min). **$R^2$ = 99.59%. $R^2_{adj}$=97.75%**

- **CT** = 8.7467+ 2.0567 p(W) + 0.3758 pH + 0.9433 t(min) - 0.1142 P(W)*pH - 0.9400 P(W)*t(min) - 0.6158 pH*t(min). **$R^2$ = 99.86%. $R^2_{adj}$=99.22%**

The $R^2$ coefficient is a key indicator of the accuracy of a model's predictions. An $R^2$ value of 100% indicates a perfect fit. where the model accounts for all variability in the data. while a value of 0% suggests that the model fails to predict the outcome reliably.

In the current study. the correlation coefficients ($R^2$) for the model were found to be. respectively. 99.52%. 99.59%. and 99.86% for the total flavonoid content. the total phenolic content and the condensed tannin

content. These high $R^2$ values indicate a strong correlation between the predicted and observed values. demonstrating that the proposed models exhibit a high degree of predictability.

This suggests that the models are effective in capturing the relationship between the variables and the response. providing reliable insights into the behavior of the system. The robustness of these models is further supported by the fact that they maintain predictive power across multiple types of responses. reinforcing their potential utility in optimizing processes such as dyeing and chemical extractions

### 3.3.2. *Study of interactions diagram*

An interaction diagram provides a visual representation of the extent to which different input parameters interact with one another and how these interactions influence the output responses. This type of analysis is crucial for understanding whether the effect of one factor depends on the level of another. thus revealing complex relationships that might not be evident through individual factor analysis.

Figure 4 illustrates the interaction diagrams for various responses. including condensed tannins content (a). flavonoids content (b). and phenolic content (c). These diagrams help to identify synergistic or antagonistic interactions between input parameters. allowing for a more nuanced optimization of the process. By studying these interactions. researchers can determine how combinations of factors contribute to the overall outcome and adjust parameters to enhance the quality and efficiency of the results.

According to this fgure. it can be noted:

– A strong interaction between microwave duration and pH of the extraction.

– A weak interaction between duration and power of extraction

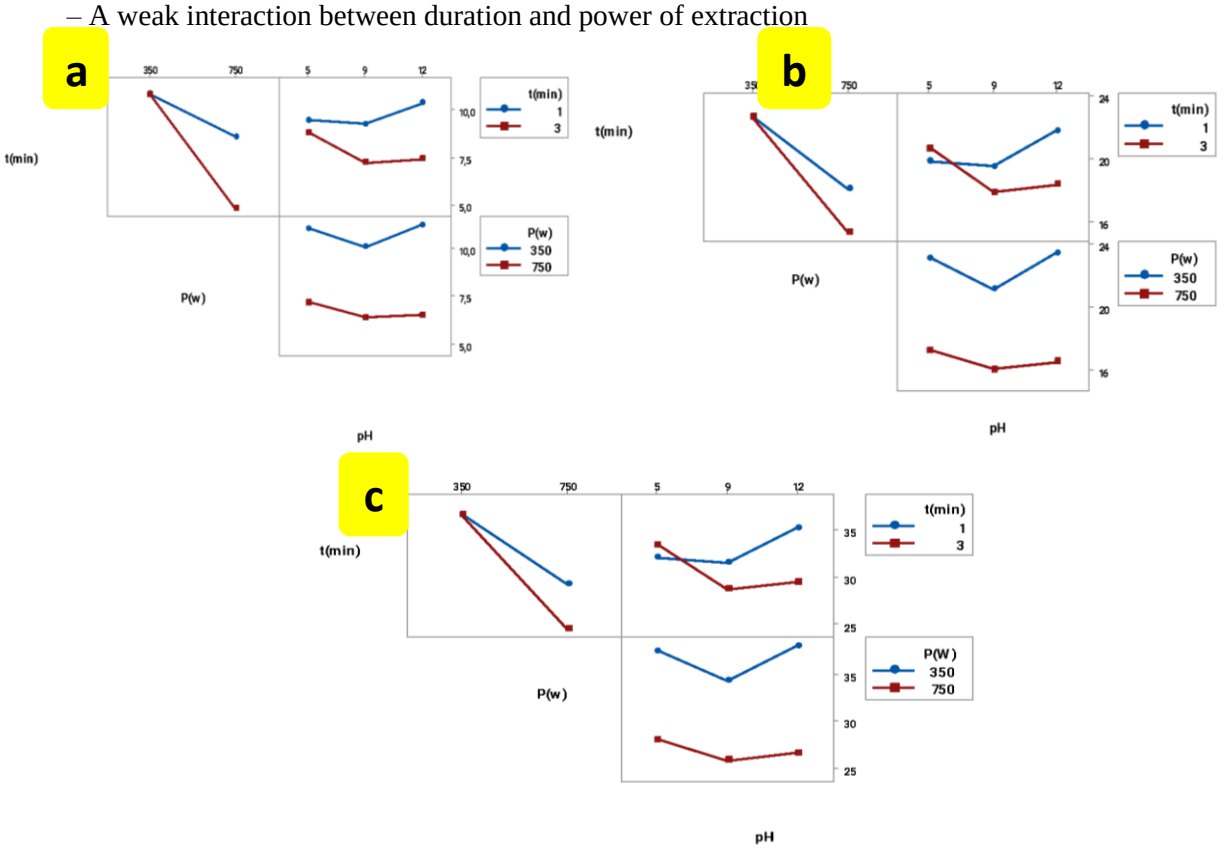


**Fig.4** Interaction diagrams for condensed tannins (a). flavonoids (b). color phenols (c)

### 3.3.3. *Analysis of variance (ANOVA)*

Analysis of variance (ANOVA) is a statistical technique used to examine the differences between group means and the variability within groups. aiming to understand how different factors influence a response variable. ANOVA is closely related to regression analysis. as both methods investigate the relationship between a response variable and one or more independent variables. However. while regression focuses

more on predicting the outcome. ANOVA primarily tests whether the means of different groups significantly differ from one another.

In this study. ANOVA is employed to examine the effects of various extraction parameters on the response's variables. The analysis assesses the statistical significance of the model. identifying whether individual factors and their interactions significantly contribute to variability in the outcome. The results of the ANOVA analysis were presented in Table 1.

**Table 1.** Variance analysis for the flavonoïdes content, phenolic content and tannins content

| **Analysis of variance of flavonoïdes** | | | | | |
|---|---|---|---|---|---|
| **Source** | **DF** | **Adj SS** | **Adj MS** | **F-value** | **p-value** |
| **Regression** | 4 | 118.258 | 29.564 | 11.93 | 0.003 |
| **Linear** | 4 | 118.258 | 29.564 | 11.93 | 0.003 |
| **Power** | 1 | 106.386 | 106.386 | 42.91 | 0.000 |
| **Duration** | 1 | 5.978 | 5.978 | 2.41 | 0.164 |
| **pH** | 2 | 5.894 | 2.947 | 1.19 | 0.359 |
| **Error** | 7 | 17.353 | 2.479 | | |
| **Total** | 11 | 135.611 | | | |
| **Analysis of variance of phenolic content** | | | | | |
| **Source** | **DF** | **Adj SS** | **Adj MS** | **F-value** | **p-value** |
| **Modèle** | 4 | 320.28 | 80.069 | 11.53 | 0.003 |
| **Linéaires** | 4 | 320.28 | 80.069 | 11.53 | 0.003 |
| **Puissance** | 1 | 286.58 | 286.580 | 41.27 | 0.000 |
| **Durée** | 1 | 17.48 | 17.476 | 2.52 | 0.157 |
| **pH** | 2 | 16.22 | 8.111 | 1.17 | 0.365 |
| **Error** | 7 | 48.60 | 6.943 | | |
| **Total** | 11 | 368.88 | | | |
| **Analysis of variance of tannins** | | | | | |
| **Source** | **DF** | **Adj SS** | **Adj MS** | **F-value** | **p-value** |
| **Modèle** | 4 | 320.28 | 80.069 | 11.53 | 0.003 |
| **Linéaires** | 4 | 320.28 | 80.069 | 11.53 | 0.003 |
| **Puissance** | 1 | 286.58 | 286.580 | 41.27 | 0.000 |
| **Durée** | 1 | 17.48 | 17.476 | 2.52 | 0.157 |
| **pH** | 2 | 16.22 | 8.111 | 1.17 | 0.365 |
| **Error** | 7 | 48.60 | 6.943 | | |
| **Total** | 11 | 368.88 | | | |

## 4. CONCLUSION

Environmental concerns and the growing awareness among consumers of the harmful effects of synthetic dyes have driven manufacturers to adopt more sustainable alternatives. such as natural dyes. In this study. The microwave extraction technique applied to date palm fiber fibrillium proved to be a promising method for producing a natural textile dye. A three-factor. multilevel experimental design was utilized. demonstrating both effectiveness and reliability in determining the optimal conditions for the extraction process. Furthermore. applying the resulting dye extract to wool using microwaves achieved high dye absorption. yielding brown hues with excellent color fastness.

## REFERENCES

1. Faidi, K., Haddar,W., Ben ticha, M., Baaka, N., Mokni, R.E., Mighri, Z., Dhaouadi, H.: Optimization of Conventional Extraction for Luteolin Dye from Asphodelus tenuifolius Cav Applied to Wool Fabrics. *Chemistry Africa*. *7*, 3677-3689 (2024).
2. Gharred, N., Baaka,N., Dhaouadi,H., Dridi-Dhaouadi, S.: Eco-friendly Dyeing Process on Wool Fabric Using Wastewater from the Essential Oil Extraction of Inula graveolens. *Chemistry Africa*. *7*, 1323-1336 (2024).
3. AbouZeid, E. M., Afifi, A. H., Hussei, R. A., Salama, A. A., Youssef, F. S., El-Ahmady, S. H., Ammar, N. M.: Phoenix dactylifera L.: an overview of phytochemical constituents and impact on women's health. *Chemistry & Biodiversity*. *21*, e202400456 (2024).
4. Ben Ticha, M., Meksi, N., Drira, N., Kechida, M., Mhenni, M.F.: A promising route to dye cotton by indigo with an ecological exhaustion process : a dyeing process optimization based on a response surface methodology. Ind. Crops Prod. 46.350–358 (2013).
5. Ben Ticha. M., Meksi, N.,Kechida,M., Mhenni, M.F.: Green process for indigo dyeing: efect and modeling of physico-chemical parameters using statistical analysis. Int J Environ Res. 7:697–708 (2013).

# Advanced Modeling and Optimization of Acrylic Fibers Cationization Using Combined Response Surface Methodology (RSM) and Artificial Neural Networks (ANN)

**Maha Abdelileh[a,b], Manel Ben Ticha [c] , Nizar Meksi[a,b] · Hatem Dhaouadi [a]**

*(a) Faculty of Sciences of Monastir, Research Laboratory of Environmental Chemistry and Clean Processes, University of Monastir, 5000 Monastir, Tunisia*
*(b) Department of Textile, National Engineering School of Monastir, University of Monastir, 5000 Monastir, Tunisia*
*(c) Department of Early Childhood, University College of Turabah, Taif University, P.O. Box 11099, Taif 21944, Saudi Arabia*

**ABSTRACT**

In this study, the non-polarity and low affinity of acrylic fibers for indigo carmine were investigated. To achieve satisfactory dyeing quality, a cationic agent was used to treat the acrylic fibers. The effects of key cationization process parameters namely, the percentage of the cationizing agent, cationization temperature, duration, and cationization bath pH on the dyeing performance of acrylic fibers with indigo carmine were evaluated. Dyeing results were assessed by measuring color strength (K/S) and dye bath exhaustion (E%). The acrylic cationization process was modeled and optimized using a combined approach of artificial neural networks (ANN) and response surface methodology (RSM). The ANN model demonstrated a strong correlation between experimental and predicted color strength values. Optimization using RSM revealed that the optimal conditions for cationization were: 90% cationic agent, pH 4, 75 minutes of cationization time, and a temperature of 90°C, resulting in the best dyeing quality. Cationization of acrylic fibers has proven to be an effective method for enhancing their affinity for indigo carmine.

**KEYWORDS:** acrylic fibers, cationization, neural network, response surface methodology.

## 1. INTRODUCTION

Acrylic fibers are characterized by their low affinity to most textile dyes, low recovery rate and high glass transition temperature. To improve the dyeing performance of acrylic fibers, a number of research projects have been undertaken. The modification of acrylic via the conversion of certain nitrile groups present in the fiber to amino groups has been explored in order to dye acrylic fibers with natural dyes without solvents and under atmospheric pressure. This method makes the fiber more hydrophilic and less crystalline. It also increases the affinity of acrylic for anionic dyes at acidic pH [1-2]. Pre-treatment of acrylic fibers with a cationic agent to improve dyeability has also been reported [3]. It has been shown that increasing the number of quaternary ammonium groups in acrylic fibers increases the rate of absorption of natural dyes by acrylic.
In recent years, the textile industry has explored the application of artificial neural networks (ANN) combined with response surface methodology (RSM) in various processes, such as dyeing cotton with reactive dyes [4], and extracting natural dyes [5]. ANN is a statistical method conceptually inspired by the function of biological neurons. However, its biological accuracy is now of little relevance, instead its success lies in its ability to model complex and nonlinear relationships effectively. The most commonly used ANN model is the multilayer perceptron (MLP), which delivers strong practical results. MLP is typically trained using the gradient backpropagation algorithm, a method widely employed for solving nonlinear problems.

This study aims to address the challenges associated with dyeing acrylic fibers with the acid dye indigo carmine. To improve the dyeability of acrylic fabrics, we propose the development of a cationization process. Rewin OS was selected as the cationic agent for modifying the acrylic fibers. Additionally, the impact of various process variables on the pretreatment efficiency was investigated. The dyeing process was then modeled using artificial neural networks (ANN), and response surface methodology (RSM) was employed alongside ANN to determine the optimal experimental conditions.

## 2. MATERIALS AND METHODS

### 2.1. Chemicals and Materials

The chemicals used in this study were of analytical grade: sodium hydroxide (NaOH, CDM, Tunisia) and acetic acid ($CH_3COOH$, Parachimic, Tunisia). Rewin OS (Bezema AG, Switzerland), an ammonium-based preparation, was employed as the cationic agent. Indigo carmine powder ($C_{16}H_8N_2Na_2S_2O_8$, LOBA Chemie, Germany) was used for dyeing the acrylic fabric.

A 100% acrylic fabric was selected for dyeing, with the following specifications: plain weave, mass per area of 230 g/m², warp count of 11 yarns/cm, and weft density of 20 yarns/cm**.**

### 2.2. Cationization of Acrylic Fabric

The acrylic fabrics were treated with the cationic agent Rewin OS before dyeing with indigo carmine under the following conditions: 90% cationic agent, pH 4.5-5, temperature of 50°C, and a treatment duration of 60 minutes. The percentage of the cationic agent was selected based on preliminary studies. This pretreatment was performed in a laboratory dyeing machine (Ahiba, DataColor International, USA). After treatment, the acrylic samples were dried at room temperature.

### 2.3. Dyeing of Acrylic Fabric

The pretreated acrylic samples were dyed in a dye bath containing 5% indigo carmine at a pH of 7, using a liquor ratio of 1:50. The dyeing process was conducted in a laboratory autoclave (Ahiba, Datacolor International, USA) at 100°C, with a heating rate of 4°C/min, for 60 minutes. After dyeing, the samples were rinsed with cold water and dried at room temperature.

### 2.4. Color strength measurements

After dyeing, the color strength (K/S) of the acrylic samples was measured using a Datacolor Spectraflash 600+ spectrophotometer (USA). The color strength (K/S) in the visible region of the spectrum (400-700 nm) was calculated based on the Kubelka-Munk equation[15]:

$$\frac{K}{S} = \frac{(1-R)^2}{2R} - \frac{(1-R_0)^2}{2R_0} \quad \textbf{(1)}$$

### 2.5. Dyeing bath exhaustion measurements

The absorbance of the indigo carmine solution was measured before and after dyeing using a UV-visible spectrophotometer (Shimadzu, Japan) at a wavelength of 620 nm. The dye bath exhaustion (E%) was then calculated using the following equation:

$$E(\%) = \frac{(A_0 - A_r)}{A_0} \times 100 \quad \textbf{(2)}$$

Where $A_0$ and $A_r$ are, respectively, the absorbances of the indigo carmine solution before and after dyeing.

### 2.6. Structure of the Artificial Neural Network (ANN)

In this study, an optimal neural network with a single hidden layer, 8 hidden neurons, 4 input parameters, and color strength as output parameter was used to model the cationization process. The ANN model was designed using MATLAB with its neural network toolbox, based on experimental data. The network was trained using the back-propagation learning algorithm, specifically the gradient descent method with momentum and an adaptive learning rate (traingdx). The model's performance was evaluated by determining the correlation coefficient ($R^2$) and the mean square error (MSE).

### 2.7. Design of Experiments

Response surface methodology (RSM) was applied to determine the optimum conditions for the acrylic cationization process. The selected input parameters are the percentage of cationic agent, pH, cationization temperature, and cationization time and the studied response was the color strength (K/S) of the dyed samples. The response surface was generated by Minitab 14 software. According to this design, a total of 27 experiments were performed.

## 3. RESULTS AND DISCUSSIONS

### 3.1. Study of the effect of the cationization process

After several tests, it was observed that acrylic fabric exhibits no affinity for indigo carmine, with dyeing experiments showing very low color yield and minimal dye exhaustion. This outcome can be attributed to the presence of anionic carboxylic groups in the structure of acrylic fibers, which repel the negatively charged dye anions during the dyeing process. To enhance its affinity, the acrylic fabric was treated with Rewin OS cationic agent before dyeing. In this section, the influence of the percentage of the cationic agent, pH, cationization time, and cationization temperature on the evolution of color strength and bath exhaustion is shown in Figure 1.

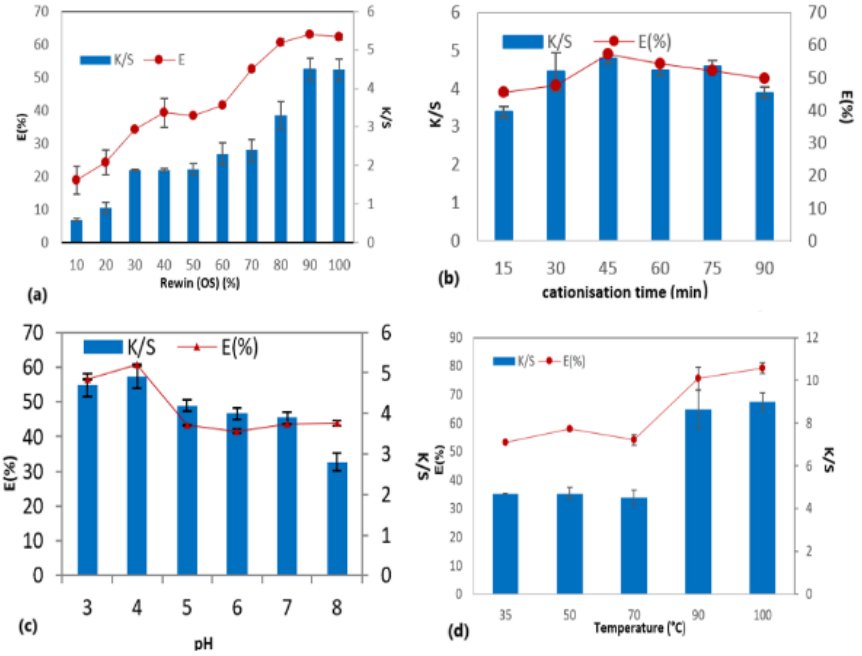


**Fig. 1** Evolution of color strength (K/S) and bath exhaustion E(%) as a function of (a): cationizing agent percentage, (b): cationisation time, (c): pH, and (d): cationisation temperature

Figure 1(a) shows an increase in bath exhaustion and color strength as the concentration of the cationizing agent increased from 10% to 90%. This improvement in dyeing performance can be attributed to the growing number of cationic sites in the acrylic fiber with the increasing concentration of the cationizing agent in the bath, which enhanced the fiber's affinity for the anionic dye indigo carmine. Regarding the effect of cationization time, we observe an increase in both color strength and bath exhaustion up to 45 minutes, likely due to the higher number of cationic sites attracting more dye. Beyond 45 minutes, both curves plateau, indicating that the fiber has reached saturation with the cationizing agent. Figure 1(c) demonstrates that optimal dyeing quality was achieved at a pH of 4. Beyond this pH, dyeing parameters progressively declined, confirming that the best dyeing results for acrylic fibers are obtained under acidic conditions. In terms of temperature (Figure 1(d)), the dyeing parameters remain nearly unchanged up to 70°C. This can be explained by the inefficiency of the acrylic cationization process at temperatures below the glass transition temperature (Tg) of the polymer. Above 70°C, a rapid improvement in both dyeing parameters is observed. This enhancement is due to the increased free volume within the polymer chains above Tg, allowing the cationizing agent to penetrate more easily into the fiber.

### 3.2. Artificial Neural Network (ANN) Modeling of the Acrylic Cationization Process

To develop the neural network, the data were split, with 80% used for training and 20% for testing. During training, all samples were simultaneously processed through the learning algorithm before the weights were updated. The correlation coefficient (R) values for training, validation, testing, and the overall model are presented in Figure 2. The model's goodness of fit was evaluated using the correlation coefficient, with a result of R = 89%. This indicates that 89% of the sample variation was statistically explained by the model, leaving only 11% of the total variance unexplained.

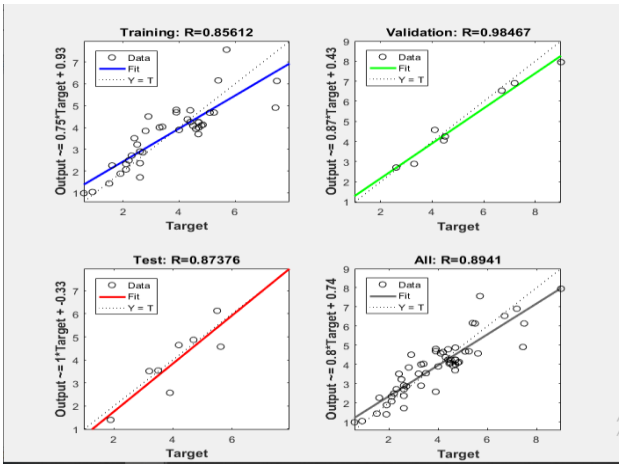


**Fig. 2** Regression values for learning, validation, testing, and overall mode

### 3.3. Optimization of the acrylic cationization process using the response surface method

The optimization of the cationization process leads to the following optimum conditions: a cationic agent percentage of 90%, a cationization bath pH of 4, a cationization time of 75 min, and a cationization temperature of 90°C (Table 1). In this case, this table indicates a predicted color strength of 8.06. Dyeing tests were carried out under these optimum conditions. An average color strength of 7.8 was obtained, indicating the validity of these conditions.

**Table 1.** Optimum conditions for the cationization process

| Optimal conditions | Cat(%) | Time (min) | pH | T (C°) | K/S |
|---|---|---|---|---|---|
| Values | 90 | 75 | 4 | 90 | 8 |

## 4. CONCLUSION

This research aims to enhance the dyeability of acrylic fabrics dyed with indigo carmine. The application of the cationizing agent Rewin OS to acrylic fabrics before dyeing introduces a novel approach. The influence of different process factors (cationizing agent concentration, pH, cationisation duration, cationisation temperature) on the dyeing quality of acrylic fabric were studied. The ANN model exhibited a good correlation between the experimental and predicted data. Besides, RSM was successfully used to obtain the optimal experimental parameters namely a cationic agent percentage of 90%, a pH of 4, a cationization time of 75 min and a cationization temperature of 90°C.

## REFERENCES

1. Burkinshaw, S.M., Gotsopoulos, A.: The pre-treatment of cotton to enhance its dyeability—I. Sulphur dyes. Dyes Pigm. 32, 209-228 (1996).
2. El- Shishtawy, R.M., Ahmed, N.S.E.: Anionic coloration of acrylic fibre. Part 1: Efficient pretreatment and dyeing with acid dyes. Colour.Technol. 121, 139-146 (2005).
3. Baaka,N., BenTicha, M., Haddar, W., Mhenni,M.F.: A Challenging Approach to Improve the Low Affinity of Acrylic Fibres to Be Successfully Dyed with a Bio-Colorant Extracted from Grape Marc. J. Renew. Mater. 7, 289–300 (2019).
4. Rosa, J.M., Guerhardt, F., Ribeiro, S.E.R., Belan, P.A., Lima, G.A., Santana, J.C.C., Berssaneti, F.T., Tambourgi, E.B., Vanale, R.M., de Araujo, S.A.: Modeling and optimization of reactive cotton dyeing using response surface methodology combined with artificial neural network and particle swarm techniques. Clean Technol. Environ Policy. 23, 2357 (2021).
5. Vedaraman, N., Sandhya, K.V., Charukesh, N.R.B., Venkatakrishnan, B., Haribabu,K., Sridharan, M.R., Nagarajan, R. : Ultrasonic extraction of natural dye from Rubia Cordifolia, optimisation using response surface methodology (RSM) & comparison with artificial neural network (ANN) model and its dyeing properties on different substrates. Chem. Eng. Process. 114, 46 (2017).

# Spent Coffee Grounds as a Promising Source of Natural Textile Dyes: Optimization of the Extraction Process

**Ines Khemissi[1,2], Noureddine Baaka[1,3], Faouzi Khedher[1,2],Boubaker Jaouachi[2,4]**

[1]Higher Institute of Fashion of Monastir, Department of Textile Management, Arab Golf AV Monastir, Tunisia
[2]Textile Engineering Laboratory of the Higher Institute of Technological Studies of Ksar Hellal, University of Monastir-Tunisia, Monastir, Tunisia
3University of Monastir, Faculty of Sciences of Monastir, Research laboratory - Environmental Chemistry and Clean Processes (LR21ES04), 5000 Monastir, Tunisia
[4]National School of Engineers of Monastir, University of Monastir-Tunisia, Monastir, Tunisia

**ABSTRACT**

Spent coffee grounds (SCG) represent an abundant and underutilised biomass with great potential as a source of natural dyes for the textile industry. This study investigates the optimisation of the extraction process to maximise dye yield from SCG. Various extraction parameters, including temperature, extraction time, extraction pH, and solid-to-liquid ratio, were systematically examined to identify the most effective conditions for dye recovery. The combined effects of these extraction conditions on the total phenolic content (TPC) and colour yield (K/S) were studied using a three-level four-factor Box-Behnken design. The optimum conditions for dye extraction were found to be 11, 105min, 70°C, and 80 g/l for extraction pH, extraction time and temperature, and mass of the powder respectively.

**KEYWORDS:** Spent coffee grounds; optimization, extraction, dyeing, wool

## 1. INTRODUCTION

The textile industry's increasing need for sustainable practices has accelerated the hunt for environmentally appropriate substitutes for synthetic dyes, which are frequently linked to health risks and environmental contamination. Natural dyes are a viable way to lessen the environmental impact of textile dyeing since they are made from renewable resources. Among potential sources, spent coffee grounds (SCG) have emerged as a valuable biomass due to their high availability and rich content of natural pigments.

Coffee is one of the most valuable commodity crops in the world trade. It contributes largely to the economies of more than 50 countries in Asia, Latin America, and Africa. (M. Ridder, 2023)

Coffee stands next to Petroleum in the international trade. In many producing countries, besides its tremendous contribution to foreign exchange, it serves as a means of livelihood for millions of people. It plays a vital role in their socio-economic values.

According to the International Coffee Organization (ICO), global coffee consumption has been steadily increasing over the years, with total coffee consumption reaching over 166 million bags (60 kilograms each) in recent years.

Some of the largest consumers of coffee include the United States, Brazil, Europe (particularly Scandinavian countries like Finland, Sweden, and Norway), and Asian countries like Japan and South Korea (Anshool Deshmukh, 2019)

Millions of tons of coffee grounds are thrown away as garbage annually throughout the world, which adds to en vironmental problems like methane emissions and landfill overflow.
Repurposing SCG as a natural dye source not only solves waste management issues but also fits with the circula r economy's tenets.
However, to get high dye production and colourfastness, the extraction procedure needs to be refined to fully realize the potential of SCG for textile dyeing.

Optimizing the SCG extraction procedure to create natural textile colours is the main goal of this work. This research attempts to enhance dye recovery while upholding environmentally friendly standards by methodically analyzing important processing parameters, such as solvent type, temperature, extraction duration, and solid-to- liquid ratio. The findings of this research may present a viable and economical substitute for synthetic dyes, rendering SCG a desirable choice for industrial and environmental uses.

In this research, we aim to explore the potential of SCG for textile dyeing, focusing on the extraction of natural dyes from this by-product. The dyeing performance was assessed using wool fabrics as a test material. Key experimental factors such as pH, the amount of SCG, extraction duration, and temperature were examined for their impact on the dyeing results. Furthermore, modelling and optimization of these extraction conditions were conducted to enhance the dyeing efficiency and overall performance of the dyed wool fabrics.

## 2. MATERIALS AND METHODS

### 2.1. Sample material and chemicals

A locally sourced plain-woven wool was used for dyeing. Spent coffee grounds were supplied from a local coffeehouse as well as personal residences in Monastir, Tunisia. Sodium hydroxide, sodium hydrosulphite and acetic acid glacial were used.

### 2.2. Extraction process

The hot steeping method was used for extracting the dyeing solution from the SCGs. This method involves submerging a quantity of SCGs in water, with constant stirring using heat to accelerate the extraction process. The solution is then filtered twice using a mesh at first and then a filtering paper to get rid of the rest of the SCGs.

## 3. RESULTS AND DISCUSSIONS

### 3.1. Factors affecting the extraction process

The solid-liquid extraction of colourants is influenced by several operational parameters that can have either a positive or negative impact. These parameters include time, temperature, pH, liquid/solid ratio, and particle size, among others. Our focus will be on developing an extraction process specifically for colourants from spent coffee grounds (SCGs) by closely studying the effect of these experimental factors.

We will evaluate the quality of the extraction by monitoring the polyphenol content and measuring the colour strength (K/S) on wool samples dyed with each extract. For the dyeing process, we will adhere to standard conditions, which include a pH of 5, a temperature of 80°C, a duration of 45 minutes, and a dye concentration of 40g/L.

This approach will allow us to optimize the extraction process and ensure consistent, high-quality results in the dyeing of wool.

#### 3.1.1. Effect of pH extraction

Figure 1 presents the colour yield (K/S) and total phenolic content (TPC) of aqueous extracts obtained at varying pH levels. As shown, both the colour yield and TPC increase progressively as the pH rises, reaching their peak at pH 9. This effect is likely due to the acidic nature of the colouring components,

which are more efficiently extracted under mildly basic conditions. However, beyond pH 9, the total phenolic content (TPC) decreases as the pH rises. This decline can be explained by the behaviour of phenolic groups, including polyphenols and flavonoids, present in the colouring components. These groups react with the base, forming water-soluble salts that reduce the phenolic concentration.

Similarly, the colour yield decreases above pH 9 due to the increasing concentration of sodium hydroxide. At higher pH levels, the colouring components, particularly flavonoids and polyphenolics, undergo decomposition as they become less stable in highly alkaline environments over prolonged periods. This instability leads to a reduction in colour strength as the structural integrity of the pigments is compromised.

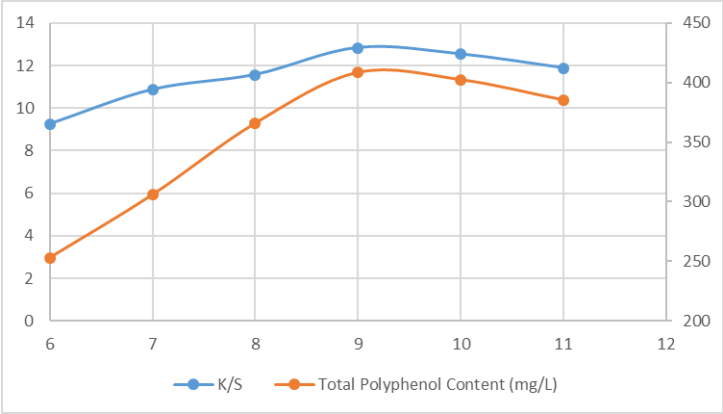


**Fig.1** Evolution of the TPC and k/s as a function of pH for hot extraction

### 3.1.2. Effect of temperature

The extraction temperature was varied throughout the experiment to evaluate its effect on phenolic yield and colour yield (K/S). Specifically, the temperature was adjusted to 30°C, 45°C, 60°C, 75°C, 90°C, and 100°C, allowing us to assess how different heat levels influence the extraction of phenolic compounds and the resulting colour yield of fabrics dyed with SCG extracts. Figure 2 presents the effect of these temperature variations on total phenolic content (TPC) and the relative colour yield (K/S) of the dyed fabrics.

As illustrated in the figure, both the phenolic yield and colour yield (K/S) increased progressively with temperature, peaking at 75°C. Beyond this point, from 75°C to 100°C, the yields stabilized, indicating that the optimal extraction temperature for both colour and phenolic content had been reached at 75°C. The rise in temperature from 30°C to 75°C enhances dye dissolution from the SCG, likely due to the improved solubility of colour components at elevated temperatures.

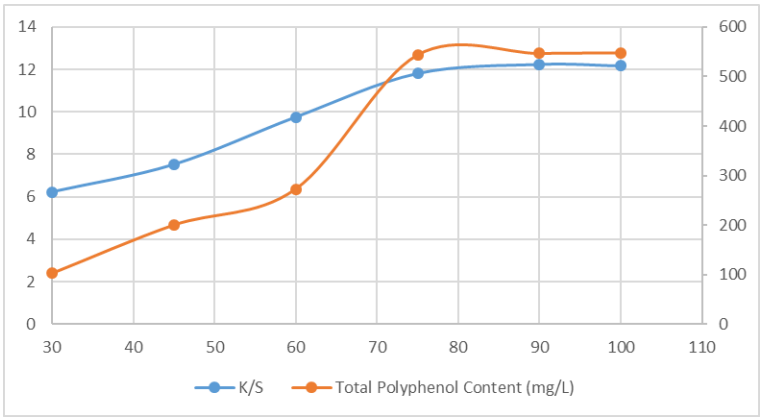


**Fig. 2** Evolution of the TPC and k/s as a function of temperature for hot extraction

### 3.1.3. Effect of time

Figure 3 illustrates the effect of extraction time on colour yield (K/S) and total phenolic content (TCP). Initially, the colour yield increases with extraction time, reaching its peak at 60 minutes. However, extending the extraction time beyond this point results in a decline in colour yield (K/S). This can be attributed to the prolonged contact between the solvent and the SCG, which extracts more colouring components, but further increases in time may lead to their decomposition at higher temperatures.

The maximum concentration of phenolic compounds is achieved at 60 minutes of extraction. Beyond this duration, the phenolic content begins to decrease, likely due to increased oxygen exposure, which promotes the oxidation of phenolic compounds.

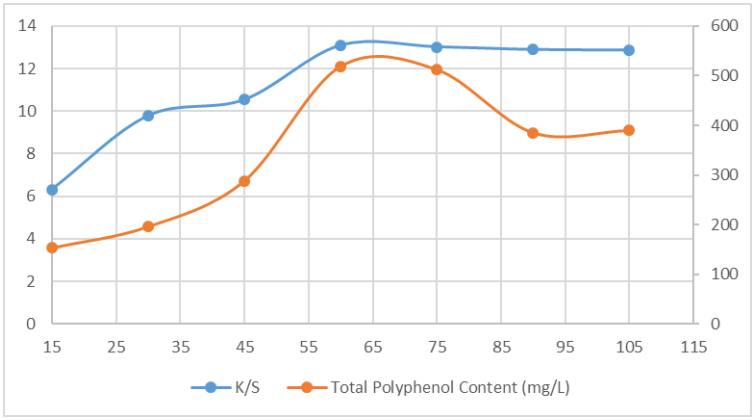


**Fig. 3** Evolution of the TPC and K/S as a function of time for hot extraction

### 3.1.4. Effect of SCGs concentration

The quantity of material used during extraction is a critical factor influencing the efficiency of the process. Figure 4 illustrates the effect of sample weight on both the colour yield (K/S) and the total phenolic content (TPC). The data indicate that the extraction performance improves as the mass of SCG increases, reaching an optimal value at a concentration of 60 g/L.
The stabilization of colour yield beyond 60 g/L can be attributed to the overcrowding of colouring components in the solution. At this stage, the excess pigments begin to interact with each other rather than binding effectively to the fabric, thus limiting the improvement in dyeing performance. A similar trend is observed with the phenolic

content, where further increases in sample mass fail to enhance the extraction of phenolic compounds, likely due to saturation effects where the solvent's capacity to dissolve additional phenolics becomes limited.

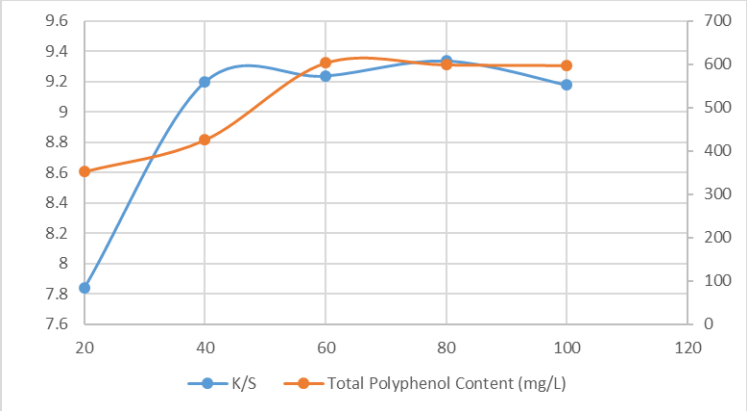


**Fig. 4** Evolution of the TPC and k/s as a function of SCG concentration for hot extraction

### 3.2. Optimization of the extraction process

#### 3.2.1. Model establishment

Through multiple regression analysis of the experimental data, a correlation between the studied properties and the input parameters was established, expressed by the following second-order polynomial equations (in coded values):

$$K/S= -53.1+5.65X_1+0.493X_2-0.046X_3+0.329X_4-0.294X_1^2-0.00401X_2^2-0.00151X_3^2-0.000433X_4^2+0.007X_1X_2+0.01962X_1X_3-0.0149X_1X_4+0.00195X_2X_3-0.000765X_2X_4-0.000635X_3X_4. \quad (1)$$

With $R^2$ =0.941

$$TPC=-5858+483X_1+63.1X_2+15.7X_3+27.2X_4-20.02X_1^2-0.04745X_2^2-0.1959X_3^2-0.608X_4^2+0.944X_1X_2+0.544X_1X_3-1.731X_1X_4+0.0656X_2X_3-0.0342X_2X_4+0.0396X_3X_4. \quad (2)$$

With $R^2$ =0.951

$X_1$, $X_2$, $X_3$, and $X_4$ represent the coded variables for pH, extraction temperature, sample weight, and extraction time, respectively.

The squared multiple correlation coefficient ($R^2$) is a key measure of the model's predictive accuracy, where $R^2$ = 100% indicates perfect predictability, and $R^2$ = 0% suggests no predictive capability. The quality of the developed model was assessed based on the $R^2$ value, which reflects the correlation between the observed experimental data and the values predicted by the model.

For equations (1) and (2), the $R^2$ values were 0.941 and 0.951, respectively, which are relatively high. This indicates a strong agreement between the experimental results and the predictions generated by the model. Additionally, the $R^2$ predicted values were 0.722 for equation (1) and 0.732 for equation (2), suggesting that the model would perform well in predicting new observations and can reliably generalize to unseen data. These values demonstrate that the proposed models can effectively capture the underlying relationships between the variables, making them suitable for guiding the optimization of the extraction process.

### 3.2.2. Contour plot analysis

A contour plot is a graphical depiction of a three-dimensional response surface, displayed as a function of two independent variables while keeping all other variables constant. These graphs can visually show the main effects and interaction effects of independent factors on the answer. The two-dimensional contour plots shown in Figures 5 and 6 helped examine how the factors interacted with the answers.

Figure 5 illustrates how the high concentration of sodium hydroxide and sample weight, together with the maint enance of the other parameters at their centre levels, led to the high colour yield recovery.

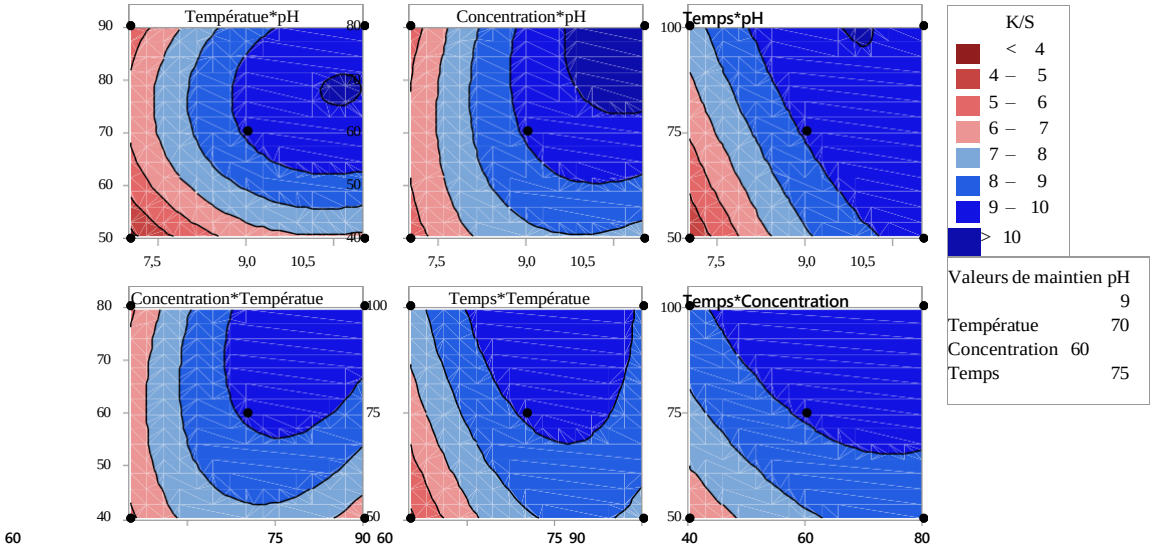


**Fig. 5** Contour plot analysis for the colour yield (K/S)

Figure 6 illustrates that although changes in time levels had no discernible impact on the reaction, high rates of t otal phenolic content can be attained with increases in weight, temperature, and pH.

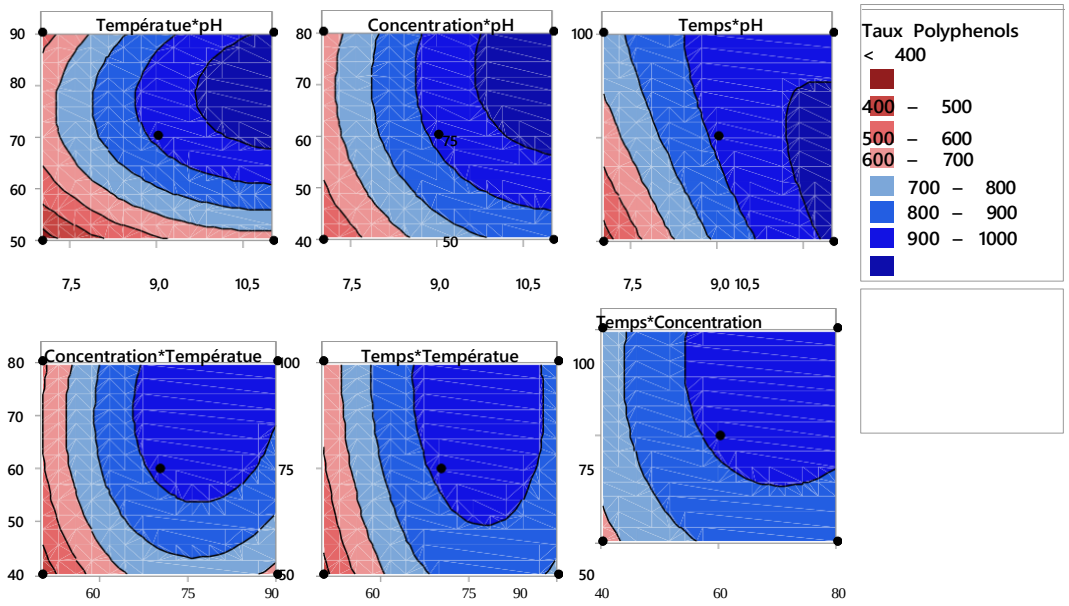


**Fig. 6** Contour plot analysis for the total phenolic content (TPC)

## 4. CONCLUSION

Spent coffee grounds have demonstrated potential for dyeing wool fibres, yielding notable colour values. The effects of key extraction parameters such as pH, sample weight, extraction time, and temperature were systematically evaluated using response surface methodology (RSM). The findings from this study provide valuable insights, serving as a predictive guide for optimizing natural dye extraction from spent coffee grounds under various experimental conditions.

## REFERENCES

1. Ridder, M.: Coffee Consumption Worldwide from 2012/13 to 2021/22 with a Forecast to 2022/23(in Million 60kg Bags).” https://www.statista.com/statistics/292595/global-coffee- consumption/(2023).
2. Deshmukh, A.: The World’s Top Coffee Producing Countries. https://www.visualcapitalist.com/worlds-top-coffee-producing-countries/(2021).
3. NAZAN.A. K.: Designing Textile Accessories from Coffee Ground. Ind.Textila.73,282-287(2022)
4. Mongkholrattanasit, R., Nakpathom, M., Vuthiganond,N.: Eco-Dyeing with Biocolorant from Spent Coffee Ground on Low Molecular Weight Chitosan Crosslinked Cotton. Sustain. Chem.Pharm. 20,100389 (2024)
5. Melaku,A., Demeke,G., Aschale,M., Alemayehu,F., Semegn, G.:Extraction and Characterization of Natural Dye Stuff from Spent Coffee Ground and Bio-Mordant from Mango Bark. J. Nat. Fibers. 20,2276725(2023)
6. Xiang,C., Nam, N.: Natural Dyeing Application of Used Coffee Grounds as a Potential resource. Int. J. Fash. Des. Technol. Educ.12, 335-345(2019)
7. Chungkrang,L., Bhuyan, S., Phukan,A.V.: Natural Dyes: Extraction and Applications. Int.J.Curr.Microbiol.App.Sci. 10, 1669-1677(2021)
8. Campos-Vega ,R., Loarca-Piña , G., Vergara-Castañeda,H. A., Oomah,B.D.:Spent coffee grounds: A review on current research and future prospects. Trends Food Sci.45,24-36(2015)
9. Xia,W., Li,Z., Tang,Y., Li,Q.: Sustainable Recycling of Café Waste as Natural BioResource and Its Value Adding Applications in Green and Effective Dyeing/Bio Finishing of Textile.Sep. Purif. Technol.309,123091(2023)
10. Low, J.H., Abdul Rahman,W.A.W., Jamarosliza, J.: The Influence of Extraction Parameters on Spent Coffee Grounds as a Renewable Tannin Resource.J.Clean. Prod. 101,222-228(2015)
11. Roychand,R., Kilmartin-Lynch, S., Saberian,M., Li,J., Zhang,G., Li, C.Q.: Transforming Spent Coffee Grounds into a Valuable Resource for the Enhancement of Concrete Strength. J.Clean. Prod. 419,138205(2023)
12. Mammen, D., Bhattacharya, S. D., Arun, A., Vinay M. R.: Natural Dyes: Scope and Challenges. Scientific Publishers (2006)
13. Ferreira,T., Shuler, J., Guimarães,R., Farah,A.: Introduction to Coffee Plant and Genetics. In: Farah, A.(eds.), pp.1-25. ECCC Environmental eBooks (2019)

# Valorization of office paper recycling processes

**Fatma Zahra Sahraoui, Imen Maatouk, Arwa Turki, Asma El Oudiani**
*Laboratory of Textile Engineering (LGTex), University of Monastir, Ksar-Hellal, 5070, Tunisia*
*E-mail :Fatmazahrasahraoui@gmail.com*

**ABSTRACT**
This study aimed mainly at recycling office paper waste to develop a new paper by exploiting different defibering methods, including the use of seawater to overcome the lack of tap water resources.The study results of the difference between recycled fibers defibered by seawater and tap water with a 2-sample test did not show significant differences in fiber dimensions. However, the results showed decreases in the physico-mechanical properties of papers made from FdM fibers compared with those made from FdR fibers, highlighting the need to mix these fibers, in order to save precious water resources and reduce costs. And paves the way for the need to strengthen these papers impacted by recycling and defibering

**KEYWORDS:** Recycling, waste office paper, regenerated fiber, FdM: fibers defibrated by sea water.

## 1. INTRODUCTION

The global consumption of paper and cardboard was more than 414 million tons in 2022 and which is increased by 60 MT consumed in the world from 2009 to 2021 where paper represented 3/4 of the tonnage of waste produced due to the increase in economic and administrative activities that generate a large amount of paper waste in offices. This presents an interesting source of raw material to be recycled thus reducing the environmental impact and promoting a circular economy. While, traditional paper recycling has limitations, including washing and chemical treatments require excessive water consumption, 130L for the manufacture of 500 sheets, compared to 51.1L for the production of the same quantity of sheets from wood . As well, the quality of recycled papers is often lower, due to their low strength, caused by the fibers cut into small pieces resulting in shortened fibers which do not make it possible to obtain a high-quality paper product. Lipkiewicz has observed a method to protect the quality of fibers and resulting papers by cutting the paper into pieces with a surface area greater than 25 mm² during the shredding process does not significantly affect the tensile properties of papers made from recycled fibers [1]. And for an eco-responsible approach aimed at minimizing the use of fresh water while sea water could pose additional challenges, notably in terms of its salinity, sea water contains 96.5% water and of 3.5% salt [2] These salts can affect the structure and strength of fibers, which could influence the quality of recycled paper as well as the sodium chloride content can form hydrochloric acid with cellulose which causes damage to the fibers [3]. On the other hand, sea salt is used in the paper industry for the production of bleached pulp. It is used to remove impurities from the pulp and to improve the quality of the paper [4].
This research explores the shredding method approved by Lipkiewicz with the use of seawater in the defibration of waste paper. However, characterization is then introduced, allowing the impact of defibration and shredding on pulp quality to be assessed.

## 2. MATERIELS ET METHODES

**Materials:** for our study, we used waste printed-papers (monochrome ink) collected from LGTex laboratory and sea water from Monastir touristic-area.

**Reducing the size of office paper waste:** the A4 paper was cut manually into pieces having a surface area between 25 mm² and 40 mm² according to the Lipkiewicz method. Then these pieces were soaked in sea-water then tap-water for 12 hrs, moving on to the grinding of these soaked pieces until total defibration at a pulp concentration of 12%, using a 3500rpm laboratory mixer, and finally the drying of the pulp according to ISO 287.

**Measurement of the dimensions of the recycled fibers**: using a Leica DM500 optical microscope with a magnification of 4x0.10 and 10x0.22, the measurement of the length and width of the 300 fibers according to ASTM D5103-07 (2018) was made.

**Evaluation:** the distribution of the lengths and widths of fibers defibrated by two types of water (sea water, tap water) was examined with the normal distribution curve and the difference between fibers with a 2-sample test, using the "Minitab" software.

## 3. RESULTS AND DISCUSSIONS

### 3.1. Impact of shredding on recycled fibers

**Fig.1** and **Fig.2** show a microscopic view at different magnifications for both fibers defibrated with sea water

"**FdM**" (**Fig 1.A** and **Fig 2.A**) and with tap water "**FdR**" (**Fig 1.B** and **Fig 2.B**)

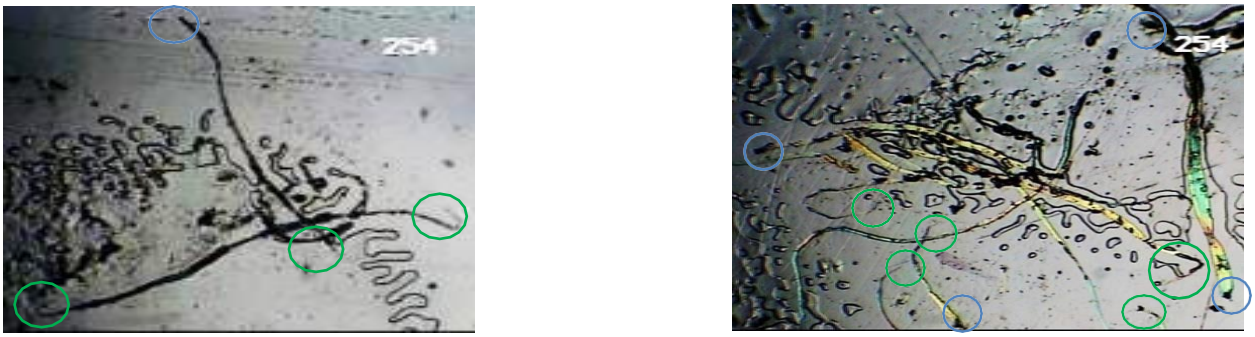

**A.** FdM **B.** FdR

**Fig.1** Microscopic view of fibers with 4x0.10 (**A)** FdM and (**B)** FdR

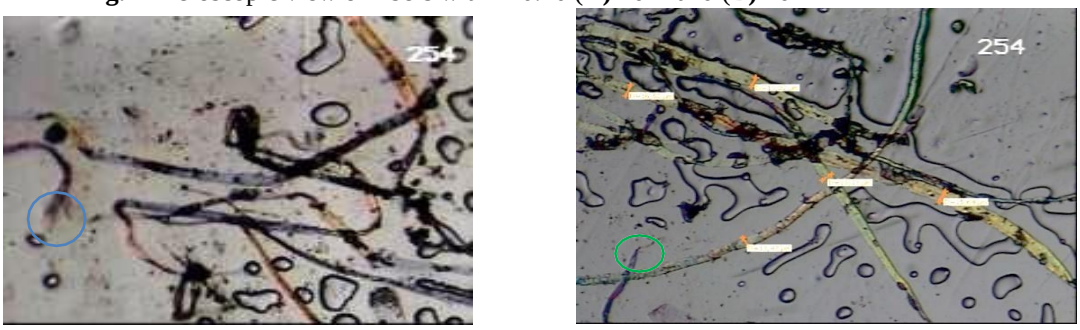

**A.** FdM **B.** FdR

**Fig.2** Microscopic view of fibers with 10x0.22 (**A)** FdM and (**B)** FdR

The microscopic observation (**Fig.1** and **Fig.2**) shows the presence of both intact fibers (green circle) and cut fibers (blue circle). The vast majority of fibers remain intact, this indicates that there is a slight shortening of the length of the FdM and FdR fibers defibrated by the two types of water (sea water, tap water), in accordance with the study results of Lipkiewicz, et al (2021) which postulates that the method cut into pieces with a surface area between 25 mm² and 40 mm2 it does not significantly influence the properties of waste paper pulp.
And to confirm the modification obtained between the structure of FdM and FdR fibers it would be necessary to measure the dimensions of the fibers by examining the distribution of their lengths and widths.

### 3.2. Evaluation of recycled fiber morphologies

**Fig.3** and **Fig.4** showing the dispersion of the length and width of both fibers (FdM in red and FdR in blue).

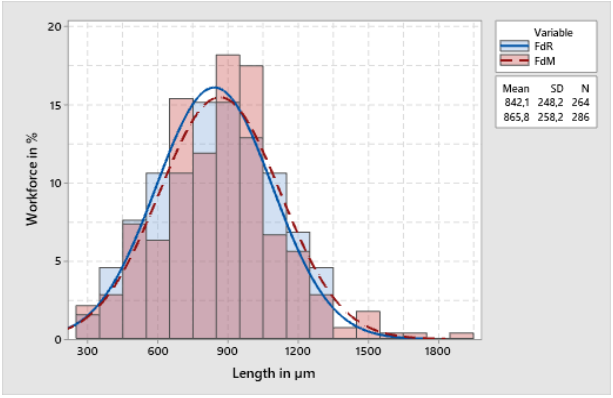


**Fig. 3** Recycled fiber length distribution

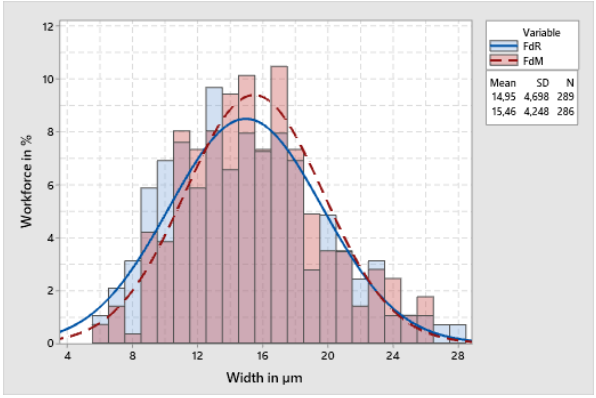


**Fig. 4** Recycled fiber width distribution

The FdR lengths (the blue histogram (**Fig.3**)), were centered between 0.6 and 1.1 mm and correspond well to the fitted distribution line with a mean of 0.8421 mm. While the lengths of FdM (the red histogram (**Fig.3**)), were more dispersed between 0.5 to 1.2 mm and they are slightly shifted compared to the fitted distribution with mean of 0.8658 µm Which translates into the fact that FdR fibers are more homogeneous than FdM. This result can be attributed to the influence of sea salts present in seawater. The widths of FdR (the blue histogram (**Fig.4**)), are more dispersed from 9 to 18 µm and which move away from the mean of 14.95 µm especially on the side where the fiber is thin with a peak of 13 µm for 9.8%. This indicates that the majority of FdR fibers lose their swellingcapacity. This was also explained by Lyne and Gallay.1950 who cocluded that bleached pulps, showed

a more marked tendency to lose their swelling capacity during drying, compared to unbleached pulps (**Fig.6**). It is also suggested by Stone and Scallan (1966) as well as Ruvo and Htun (1983) that the loss of swelling capacity is related to the closure of pores in the cell walls [5]. On the other hand, the widths of FdM (the red histogram (**Fig.4**)), occur at values between 9 and 21 µm with a peak extending from 14 to 17 µm of 10.5% and corresponds well to the adjusted distribution line of mean of 15.46 µm which indicates that the presence of sea salts causes swelling of the fibers and opening their pores. This leads to say that the presence of ions dissolved in seawater increases the swelling capacity and can cause the rupture of inter-fiber bonds which weaken the properties of the fibers and paper produced thereafter.

**Fig.6** and **Fig.7** represent a comparison of the mean lengths in mm and mean widths in µm of the different fibres; virgin fibers (blue), recycled fibers (green) and fibers from our study (orange).

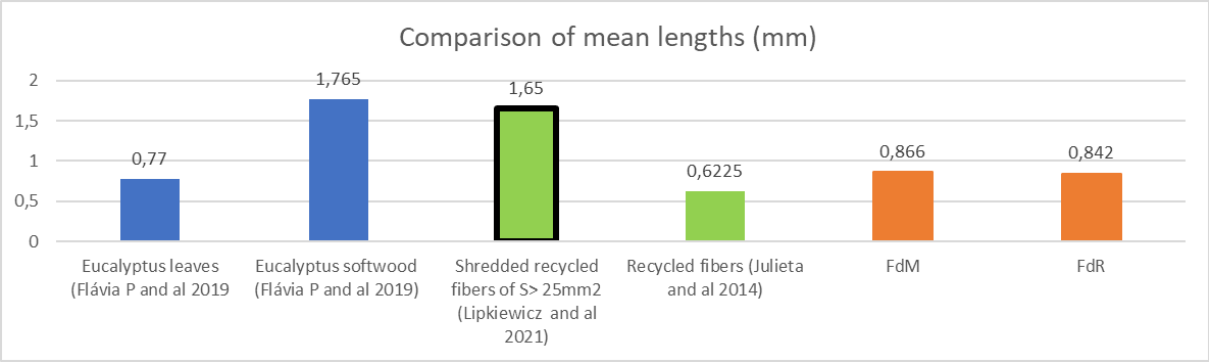


**Fig. 5** Histogram of average lengths of different fibers

The quality of regenerated fibres (**green**) is often inferior compared to virgin fibres (**blue**). The fibres examined in our study (**orange**) have length values of 0.8658mm and 0.8421mm for fibres defibrated by seawater (FdM) and defibrated by tap water (FdR) respectively. These length results are almost equal and which shows that the use of seawater has no clear influence on fibre length. However, Češek & Milichovský (2005) showed that increasing the degree of mixing of the pulp increases fibre shortening [6]. On the other hand, **Fig.5** shows that the method conducted by Lipkiewicz, et al (2021) minimises the decrease in fibre lengths compared to the length of fibres from conventional recycling approved by Julieta which were equal to 0.6225mm [7].

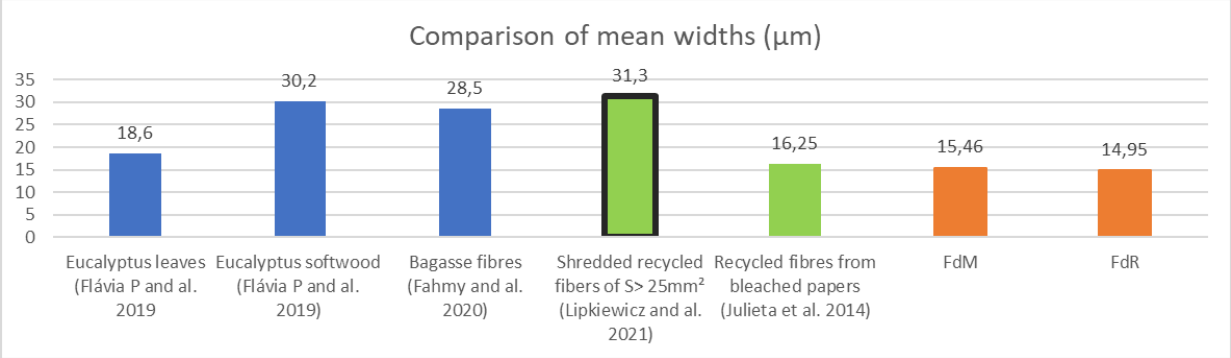


**Fig.6** Histogram of average widths of different fibers

Although the width distribution (**Fig.4**) is different but the average values (**Fig.6**) of two fibers are almost equal at 15.46 and 14.95 µm for FdM and FdR respectively. This is confirmed by the bleaching effect [9] where the width values of recycled bleached paper fibers range between 15.7 to 16.8 µm with an average of 16.25 µm (**Fig.6**).

### 3.3. Determination of the statistical significance of recycled fiber dimensions in our study

To comprehend whether the differences in length and width measurements among the two fibers are statistically significant (i.e., FdR ≠ FdM). a 2-sample test with 95% confidence interval CI was used.

**Table 1.** Estimation of fiber difference

| | **Mean length** | **Mean width** |
|---|---|---|
| **P value** | 0,273 | 0,171 |

In **Tab.1**, the difference of means in the evaluations of mean fiber length and width, the P value is less than 0.5 for length and width respectively with 0.273 and 0.171, so the null hypothesis where FdR = FdM is verified and there is no significant difference between defibration with seawater and tap water on fiber length and width. This result proves the possibility of replacing tap water with seawater to improve water resource management.

## 4. CONCLUSION

In our study, we focused on recycling office paper to create a new product while reducing recycled fiber quality using a specific cutting method and minimizing tap water consumption by substituting it with sea water. We examined how sea water affects the morphological modification of recycled fibers compared to tap water. The evaluated morphological parameters are the length and width of the fibers identified using optical microscope equipment. First, the microscopic view (**Fig.1** and **Fig.2**) indicates that most fibers remain intact, suggesting a slight shortening of FdM and FdR fibers treated with sea water and tap water using the approved cutting method. The length distribution (**Fig.3**) of FdR fibers appears normal, while FdM lengths are more dispersed. FdR fibers are more homogeneous in length than FdM fibers, which are affected by dissolved sea salts. And for the fiber width distribution (**Fig.4**) show that in FdM, sea salts cause fiber swelling and pore opening, unlike the FdR Dissolved seawater ions enhance swelling and can break inter-fiber bonds, weakening the fibers and resulting paper properties. Then a 2-sample test confirmed that there is no significant difference between fiber dimensions from defibering with seawater and tap water. This suggests that seawater can replace tap water in paper recycling, improving water resource management and reducing fresh water waste.

To achieve the best physical-mechanical properties of the final product, we can mix seawater with tap water to reduce mixing speed and reinforce the papers with bio-sourced minerals like calcium carbonate from eggshell waste (ECC).

## REFERENCES

1. Lipkiewicz,A., Małachowska,E., Dubowik,M., Przybysz,P.: Impact of shredding degree on papermaking potential of recycled waste. Scientific Reports, 11,17528 (2021)
2. GHAOUACI, S.: Cours Licence Aquaculture et Pisciculture Matière : CHIMIE MARINE https://www.univ-chlef.dz/fsnv/wp-content/uploads/Cours-chimie-marine-L3- Aquaculture.pdf
3.Pérez,S.: Structure and morphology of cellulose.https://www.researchgate.net/publication/281877184_Structure_et_morphologie_de_la_cellulose (2000).
4. TAPIN-LINGUA, S., MEYER,V., PETIT-CONIL,M.: Biotechnologies in the paper industry. Engineering technique. https://www.techniques-ingenieur.fr/base-documentaire/materiaux-th11/papiers-et-cartons- 42832210/biotechnologies-dans-l-industrie-papetiere-bio4200/(2008).
5. Čabalová,I.,Kačík,F., Geffert,A., Kačíková,D.: The Effects of Paper Recycling and its Environmental Impact. In Environmental Management in Practice from Environmental Management in Practice. In Broniewicz,E.(eds), (2011)
6. Benitez, J. B., Koga, M. E.T., Otero D'Almeida, M. L., Felissia, F. E., Park, S. W., Area, M. C.: OFFICE PAPER RECYCLABILITY: FIBROUS CHARACTERISTICS. 75, 48 - 53 (2014)
7. Hubbe, M., Venditti, R., J.Rojas, O.: What happens to cellulosic fibers during papermaking and recycling?. BioResources.2, 739-788(2007)

# Green Innovation in Indigo Dyeing: Advancing Sustainable Practices through Foam Dyeing Technology

**Oumaima Amara[a,b], Maha Abdellileh[a,b], Walid Hedrich[c], Nizar Meksi[a,b], Hatem Dhaouadi[a]**

*(a) Laboratory of the Environment Chemistry & Clean Processes, Faculty of Sciences of Monastir, University of Monastir, Monastir, Tunisia.*
*(b) Textile Engineering Department, National Engineering School of Monastir, University of Monastir, Monastir, Tunisia.*
*(c) Industrial Textile Company (SITEX), Ksar Hellal, Tunisia.*
*Email: amara1oumaima@gmail.com*

**ABSTRACT**

Indigo is considered as the preferred dye for denim fabrics. In this paper, the traditional indigo dyeing process is replaced by a cleaner alternative known as "foam dyeing". This method offers significant savings in water consumption, chemical dyes, and energy, by eliminating the conventional reduction step in the indigo dyeing process. The present work aims to develop an eco-friendly approach for dyeing cotton fabric with indigo through foam application. The influence of indigo dye and foam auxiliary products on foam bath quality was studied. The results reveal that an increase in the quantity of the foaming agent increases foam stability. Moreover, rheological analysis of foams containing indigo dye indicates both pseudo-plastic and thixotropic characteristics. Furthermore, after a residence time of 15 minutes, the foam starts to destabilize. Finally, the influence of indigo dye and foam auxiliary products on the dyeing quality was studied. The dyeing results showed greater coloristic yield with high color fastness.

**KEYWORDS:** Cotton fiber, Indigo dye, Foam application, Ecological process.

## 1. INTRODUCTION

Indigo stands as one of the most significant dyes within the indigoid class. This dye has been used from ancient times to the present day to produce a blue color. Nowadays, indigo reigns as the premier choice for dyeing denim fabrics. However, its insolubility complicates the dyeing process. Prior to application onto textiles, indigo must be converted into its soluble form through a reduction reaction with sodium dithionite to obtain the 'leucosoluble form' of indigo capable of penetrating the textile [1].

The use of this reducing agent has several technical and ecological problems, such as, storage problems and corrosiveness. Also, during the reducing process, large amounts of sulfate and sulfite ions derived from the oxidation of sodium dithionite was produced, which can cause an adverse effect in the environment due to their toxicity and corrosive nature [2].

Several researchers have proposed replacing this reducing agent with more environmentally friendly alternatives in order to solve these problems. Sodium dithionite was substituted by several eco-friendly reducing agents, such as borohydride and α-hydroxycarbonyls [2-3]. However, these alternatives typically exhibit lower dyeing performance compared to sodium dithionite. Indirect electrochemical reduction of indigo was extensively explored [4]. In this approach, a regenerable redox system was employed in the dye bath, and continuously restored by cathodic reduction

Foam dyeing method with low liquid supply, low energy consumption, and low emission has attracted great attention. Foam is defined as a dispersion of a large volume of gas in a small volume of liquid, requires the presence of surfactant molecules for its formation. While relatively recent in the textile industry, foam technology offers numerous advantages. It has been applied in various areas of textile wet processing, including sizing, printing, finishing, and dyeing. Foam technology is renowned for its significant water and energy savings. It can reduce water usage by up to 40%, energy consumption by up to 50%, and dye chemical usage by up to 20% compared to traditional processes [5]. Additionally, it involves low liquid feeding, low energy consumption, and generates less sewage, making it an environmentally preferable option.

The present study proposes an ecological indigo dyeing process using a foam system. This method enables the dyeing of cotton samples using insoluble indigo, thus avoiding the reduction step using the harmful sodium dithionite.

## 2. MATERIAL AND METHODS

### 2.1. Chemicals and Materials

A bleached 100% cotton fabric was dyed with indigo dye ($C_{16}H_4N_2O_2$, Bezema-Switzerland). Laviron NSO (Pulcra Chemicals, USA) was used as surfactant (foaming agent). Lurapret (THOR,France) was used as a binder. Albatex (Hunstman, USA) was used as a dispersing agent. Acid cellulase enzyme (Novo Nordisk, Danemark) and pumice stones were used in washing.

### 2.2. Foam preparation and dyeing process

The foam was obtained by mixing 6% of the foaming agent, 50% of the binding agent, 0.4% of the dispersing agent, 45% of the distilled water and 2% of indigo dye. The mixture was stirred using a mixer for 3 min at 1000 rpm to ensure homogeneity and foam formation. Then, it was applied to the cotton fabric, spreading the foam using a rotating aluminum squeegee. Following application, the textile was subjected to a heat treatment at 110° C for 5 min in order to improve the fixation onto the fabric.

### 2.3. Foam half time measurement

The foam was poured into a 1000 mL test tube, and the stop watch was initiated. The foam's half-life was measured once it had reached half of its initial volume (500 mL).

### 2.4. Apparent viscosity measurement

The apparent viscosity of the foam was measured using a Rheotec RC30 type rheometer (France). This rheometer is equipped with a CC14 DIN coaxial cylinder system.

### 2.5. Color evaluation

The color strength (K/S) of dyed samples was measured using a Datacolor spectrocolorimeter with data Master 2.3 software (Spectraflash SF 400, Datacolor International, USA) under illuminant D65. The color strength (K/S) values were calculated using the Kubelka–Munk equation [6]:

$$\frac{K}{S}\frac{(1-R)^2}{2R} - \frac{(1-R_0^2)}{2R_0^2} \quad \textbf{(1)}$$

### 2.6. Evaluation of dyeing fastness

The colorfastness to rubbing was evaluated according to the ISO 105-X 12 test methods using a crockmeter (James Heal, UK). The light fastness was measured following the ISO 105-B02 standard using a XEenotst (CTC, France). Additionally, the wash fastness was determined in accordance with the ISO 105-C06 standard using a pressure autoclave of the AHIBA type (Datacolor International, USA).

### 2.7. Measurement of mechanical properties

The mechanical properties, particularly the tensile strength (ISO 13934-2), of the dyed samples were measured using a dynamometer (LRX, USA) at a translation speed of 300 mm/min.

## 3.RESULTS AND DISCUSSIONS

### 3.1. Evaluation of foam bath quality

Each foam has a half-life, which determines its stability over time. The influence of the main components of the dyeing bath (foaming agent, dispersant agent, indigo dye, and binding agent) on the foam's stability was studied. Generally, an increase in the concentration of each foam component improves the quality of the foam bath, particularly the foaming agent. The half-life of the foam increases with higher quantities of foaming agent, resulting in more stable foam. The role of surfactants in foaming agents is to reduce the surface tension of the liquid and facilitate foam formation.

### 3.2. Study of the rheological behavior of foam

#### 3.2.1. Effect of the residence time of foams on its rheological properties

The foam was prepared, and then a portion of this solution was collected every 15 minutes. Subsequently, the apparent viscosity of the foam was measured at various shear rates. The results are depicted in Figure 1.

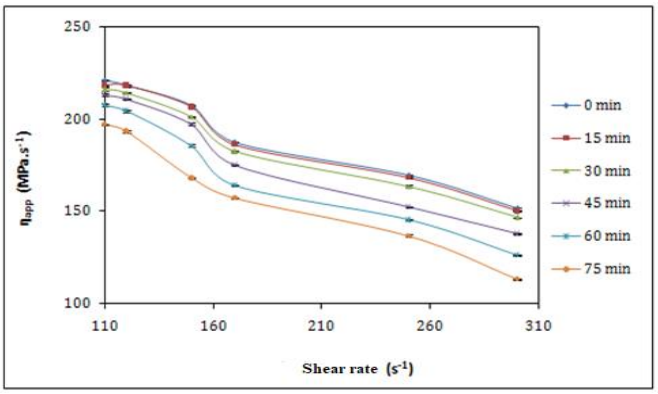


**Fig. 1:** Effect of shear rate on the evolution of apparent viscosity for different foam residence times

Based on this figure it can be noted that the apparent viscosity decreases with increasing the shear rate indication a pseudo-plastic behavior of the foam. Furthermore, within duration of less than 15 minutes, the shear rate exhibits no influence on the rheological properties of the foam. However, beyond this timeframe, there is a gradual decrease in apparent viscosity, indicating a decrease in foam stability.

#### 3.2.2.Thixotropic behavior of foam

To investigate the thixotropic behavior of the foam, a test involving both increasing and decreasing hear rates was conducted to observe hysteresis cycles. It was observed that the hysteresis loops obtained demonstrate thixotropic behavior (see Figure 2). Additionally, it was noted that the apparent viscosity decreases over time

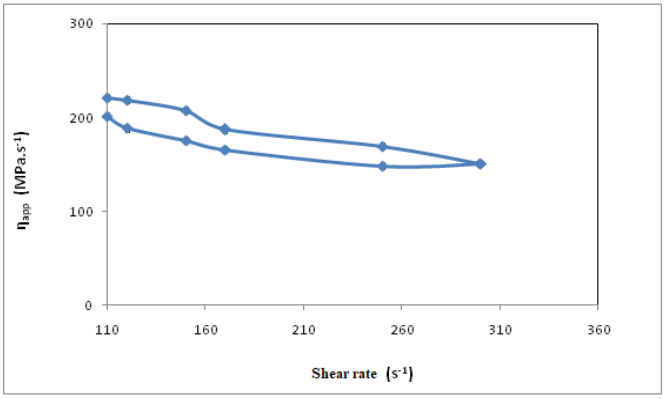


**Fig. 2:** Thixotropic behavior of foam

### 3.3. Evaluation of the dyeing quality

#### 3.3.1. Evaluation of color strength of the dyed sample

In this part, the effect of certain parameters (the dye concentration, the foaming agent concentration, the dispersing agent concentration, and the binding agent concentration) on the color strength of the dyed samples was studied. Figure 3 shows an increase in the color strength value with increasing the dye concentration.Additionally, an increase in the quantity of binding agent was found to enhance the color strength of dyed cotton samples.

After washing, the K/S values exhibit a slight decrease. The mechanical action of washing with pumice stones has a more pronounced effect compared to enzymatic action.

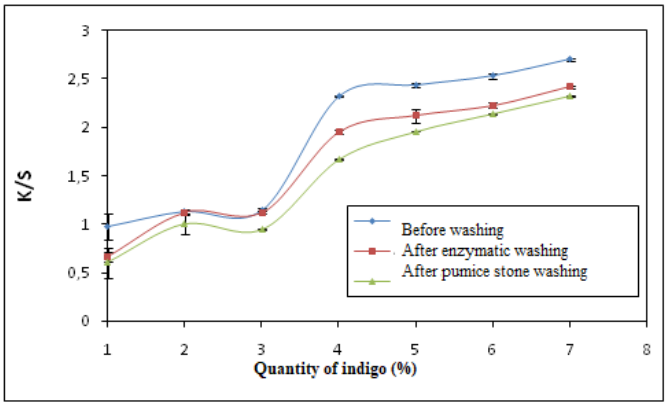


**Fig. 3:** Evolution of the color strength of the dyed samples depending on the indigo concentration

### 3.4. Evaluation of dyeing fastness

The results obtained demonstrate excellent rubbing fastness, ranging from 4/5 to 5, a light fastness rating of 7, and a wash fastness rating of 4/5 for the indigo-dyed samples studied. These results can be attributed to the effective dispersion of the dye, which facilitates its fixation. Additionally, the binding agent enhances the dye's fixation

### 3.5. Measurement of mechanical properties

The mechanical properties of cotton fabrics dyed by foam application were evaluated through tensile strength measurements. Preliminary results indicate a tensile strength of 54.5 N in the warp direction and 36.15 N in the weft direction prior to dyeing. After the dyeing process, a slight decrease in tensile strength was observed, with a reduction of 6% in the warp direction and 5% in the weft direction.

## 3. CONCLUSION

This research paper introduces an innovative approach to dyeing cotton fiber with indigo dye using foam application. This novel dyeing process offers ecological, technical, and economic advantages, including reduced water, dye, chemical, and energy consumption. The study evaluates foam quality, rheological behavior, and dyeing quality. It was observed that the half-life of the foam increases with an increase in the quantity of foaming agent. Additionally, rheological studies of the foams revealed that indigo dye exhibits both pseudo-plastic and thixotropic behavior. Furthermore, it was noted that beyond a residence time of 15 minutes, the foams begin to destabilize. Moreover, the influence of indigo dye on dyeing quality was investigated. It was found that the presence of indigo in the foam enhances color yield and improves colorfastness.

## REFERENCES

1. Meksi,N., Kechida,M., Mhenni, M.F.: Cotton dyeing by indigo with the borohydride process: Effect of some experimental conditions on indigo reduction and dyeing quality. Chem. Ing. J. 131, 187-193 (2007).
2. Meksi,N., Ben ticha,M., Kechida, M., Mhenni, M.F.: Using of ecofriendly α-hydroxycarbonyls as reducing agents to replace sodium dithionite in indigo dyeing processes. Clean. Prod.J, 24, 149-158 (2012).
3. Bozic,M., Kokol,V., Gubitz, G. M.: Indigo Dyeing of Polyamide Using Enzymes for Dye Reduction. Tex. Rea. J. 79(10), 895-907 (2009).
4. Bechtold,T., Burtscher,E., Kühnel,G., Bobleter,O.: Electrochemical reduction processes in indigo dyeing. J. Soc. Dye. Colour. 113, 135-144 (1997).
5. Zhu,D., Wan,Z., Zhao,X., Liao,S., Wang,Q., Liu,L., Yi, C.: Foaming indigo: An efficient technology for yarn dyeing. Dye & Pig. J. 197 (2022).
6. Kubelka,P.: New contributions to the optics of intensely light-scattering materials. Part I Opt. Soc. J. Am. 38 448-457 (1948).

# Comparative Analysis of Natural and Synthetic Resins for Eco-Friendly Hydrophobic Treatments in Textile Applications

**Wafa Ghedira[a,b], Marwa Souissi[a,c], Fernando Carrillo Navarrete[d], Chedly Boudokhane[a,e], Hatem Dhaouadi[a,b].**

*(a) Laboratory of Research Environmental Chemistry and clean processes, Faculty of Sciences of Monastir, University of Monastir, 5019 Monastir, Tunisia.*
*(b) Department of chemistry, Faculty of Sciences of Monastir, Tunisia.*
*(c) Higher Institute of Technological Studies (ISET) of Ksar-Hellal, 5070 Ksar-Hellal, Tunisia.*
*(d) Institut d'Investigació Tèxtil i Cooperació Industrial de Terrassa (INTEXTER), Universitat Politècnica de Catalunya, Colom 15, 08222 Terrassa, Spain*
*(e) Societé CHIMITEX PLUS, 4000 Sousse,Tunisia*

**ABSTRACT**

With growing concerns over the use of hazardous substances in waterproofing treatments for textiles, this study explores the comparison of natural and synthetic resins as safer alternatives to harmful fluorinated compounds that pose risks to human health. An eco-friendly process was employed to treat cotton fabric using various resin formulations. The chemical compositions of three distinct resins were analyzed through Fourier Transform Infrared Spectroscopy (FTIR). These resins were designed to enhance the hydrophobic properties of the textile, improving water resistance. To assess the effectiveness of the treatments, contact angles were measured, with results exceeding 100°, indicating excellent water repellency. In addition, mechanical properties (tensile strength and elongation) and morphological analysis of the treated fabrics were conducted to further evaluate the impact of the treatments. The findings suggest that the treated fabrics, demonstrating both water repellency and durability, have significant potential for various applications in textile product manufacturing.

**KEYWORDS** Natural Resins, Synthetic Resins, Contact angle, hydrophobic surfaces, eco-friendly treatment

## 1. INTRODUCTION

In recent years, increasing environmental awareness and regulatory pressures have significantly driven efforts to reduce or eliminate hazardous chemicals in textile waterproofing treatments. Fluorinated resins, traditionally favored for their superior water-repellent properties, have come under scrutiny due to their detrimental effects on human health and the environment. These perfluorinated compounds (PFCs) are persistent in nature, leading to bioaccumulation and widespread pollution, which pose long-term health risks, including endocrine disruption and carcinogenic effects[1].

Research indicates that PFCs can migrate from textiles into the environment, leading to soil and water contamination, which affects aquatic ecosystems and ultimately human health through the food chain. In response to these concerns, the textile industry is increasingly exploring sustainable alternatives that do not compromise functionality while prioritizing safety and environmental stewardship[2].

This research aims to address these pressing challenges by developing safer, eco-friendly waterproofing solutions for textile materials. Specifically, the study focuses on replacing fluorinated compounds with non-toxic, sustainable resins that offer comparable performance in terms of water repellency [3]. Recent advancements in bio-based and natural resins have shown promise in providing effective waterproofing without the harmful side effects associated with traditional fluorinated treatments[4]. To achieve this, an innovative and environmentally conscious finishing process will be applied to cotton fabric, leveraging the benefits of alternative resins to deliver effective waterproofing while ensuring safety and sustainability. This approach follows the principles of green chemistry and helps develop sustainable practices in the textile industry.

## 2. MATERIAL AND METHODS

### 2.1. Analysis of resins

The resins employed in the cotton treatment were analyzed using Fourier Transform Infrared (FTIR) spectroscopy with a PerkinElmer spectrophotometer. The spectral range covers from 400 to 4000 $cm^{-1}$, and the analysis was conducted under conditions of 16 scans at a resolution of 4 $cm^{-1}$.

### 2.2. Preparation and application of resins solutions on textile supports

The study examined a range of resin compositions: 100% natural resin, Foil T, and PU38, applied individually; combinations of two resins, including 50% natural resin with 50% Foil T and 50% natural resin with 50% PU38; and a three-resin blend consisting of 50% natural resin, 25% Foil T, and 25% PU38. These resins were suspended in a solution of alcohol and water, using a dispersing agent to ensure proper distribution. One liter of this suspension was prepared for immersion of the fabric mixture, which was then processed to remove excess liquid by passing it through the rollers of a padding machine. The impregnated fabric samples were dried at room temperature in a laboratory dryer (Rame ERNST BENZ AG textile machines, Rümlang-Zurich) and subsequently heat-treated to promote polymerization.

### 2.3. Characterizations of treated cotton

#### 2.3.1. Contact angle measurement

Contact angle measurements were conducted using the sessile drop method with a DSA 100 drop shape analysis instrument (Krüss GmbH, Hamburg). The contact angle (θ) is calculated using the equation:

$$q= 2 \times \text{Arctg} \quad \textbf{(1)}$$

Samples were secured on a measurement table, and a droplet of distilled water was placed on their surface, illuminated with an optical illuminator. A stereo microscope captured an image of the droplet, and three points corresponding to the droplet's extremities and apex were selected using a computer mouse. The surface is classified as hydrophilic if the contact angle is less than 90° and hydrophobic if it exceeds 90°[5].

#### 2.3.2. Mechanical properties

The tensile strength and elongation at break of the samples were measured using tensile testing machine type Zwick, Germany,in accordance with ISO 13934-1. Tests were conducted with a gauge length of 50 mm and a crosshead speed of 100 mm/min. The reported results represent the average of five measurements per sample.

#### 2.3.3. Morphological Analysis by SEM

The samples were characterized and analyzed using a Phenom scanning electron microscope (Phenom ProX Desktop SEM, Thermo Fisher Scientific, U.S.) to examine the morphology of the cotton fabric treated with various resins.

## 3. RESULTS AND DISCUSSIONS

### 3.1. FTIR analysis

The analysis of the IR spectra provides significant insights into the chemical composition of the three resins utilized in this study. **Fig. 1**, attributed to the natural resin, reveals three strong peaks corresponding to the hydrocarbon C-H bands at 2975, 2920, and 2850 $cm^{-1}$. Additional bands observed at approximately 730 $cm^{-1}$ and 1465 $cm^{-1}$ correspond to the bending vibrations of C-H in hydrocarbons. Furthermore, bands around 1730 $cm^{-1}$ are indicative of the bending vibrations of C=O in esters and free fatty acids, while bands at approximately 1240 $cm^{-1}$ are associated with the bending vibrations of C-O in esters. Collectively, these FTIR findings substantiate the chemical composition of the natural resin. **Fig. 2 and 3** present the FTIR spectra of the synthetic resins Foil T and PU 38, respectively. Both spectra exhibit a strong peak in the range of 3300-3500 $cm^{-1}$, attributed to the N-H band of amides, along with C=O absorption bands of urethane at 1700-1730 $cm^{-1}$ and C-O bands of ether in the range of 1000-1250 $cm^{-1}$. Together, these FTIR findings confirm the chemical composition of the two synthetic resins based on polyurethane.

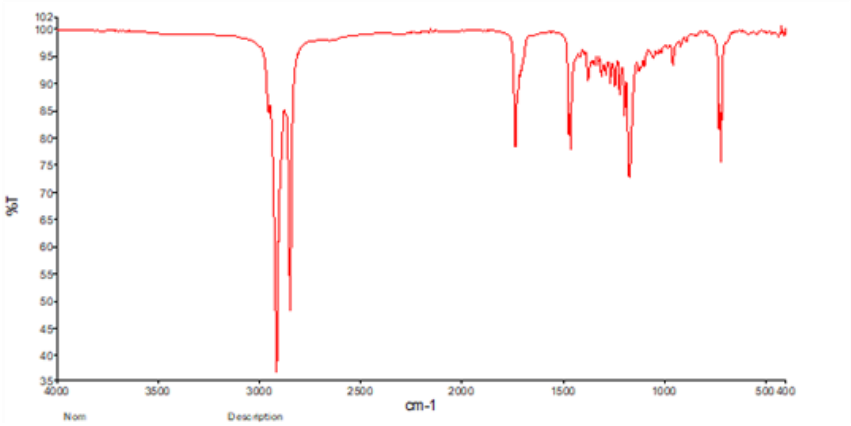


**Fig. 1** FTIR spectrum of natural resins

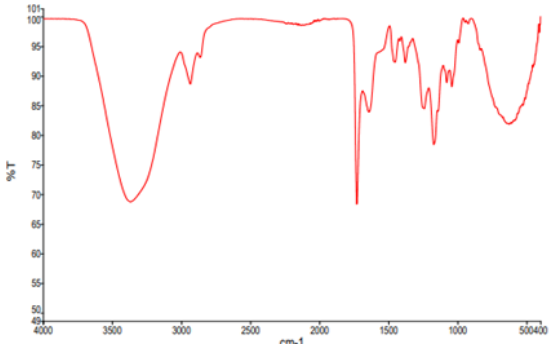


**Fig. 2** FTIR spectrum of Foil T

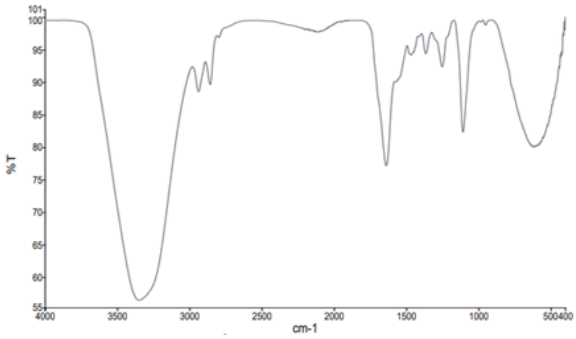


**Fig. 3** FTIR spectrum of PU38

### 3.2. Contact angle of coating process

The contact angle measurements reveal varying degrees of hydrophobicity across the resin compositions studied. As shown on **table 1**, the 100% natural resin exhibited a contact angle of 90.8°, indicating significant water repellency. In contrast, both 100% Foil T and 100% PU38 demonstrated complete hydrophilicity with a contact angle of 0°. The mixture of 50% natural resin and 50% PU38 achieved a moderate contact angle of 71°, while the combination of 50% natural resin and 50% Foil T showed a much higher angle of 95.2°, reflecting enhanced water resistance. Notably, the mixture of 50% natural resin, 25% Foil T, and 25% PU38 exhibited the highest contact angle of 105.5°, indicating excellent hydrophobic properties and making it particularly suitable for various applications.

**Table 1. Contact angle measurement**

| Treated samples | Contact angle (°) |
|---|---|
| 100% Natural Resin | 90,8 |
| 100% Foil T | 0 |
| 100% PU38 | 0 |
| 50% Natural Resin / 50% PU38 | 71,0 |
| 50% Natural Resin / 50% Foil T | 95,2 |
| 50% Natural Resin / 25% Foil T/25%PU38 | 105,5 |

### 3.3. Mechanical properties

The tensile strength and elongation results in table 2 reveal distinct effects of different treatments on cotton fabric. Untreated cotton exhibits the highest tensile strength (1448.74 N) and the lowest elasticity (13.96%). Treatments with natural resin and PU38 lead to noticeable reductions in tensile strength, with a decrease of up to 20.6%, yet significantly enhance the fabric's elongation at break, indicating improved elasticity. Among these, natural resin treatment alone reduces tensile strength the most (1231.18 N), but increases elongation to 19.48%.Combination treatments, such as natural resin with Foil T or PU38, further reduce tensile strength, indicating that multiple treatments may lead to cumulative weakening of the fabric. However, these combinations still improve elongation, highlighting the possibility of tailoring treatments to achieve a balance between strength and flexibility based on the specific performance requirements of the fabric.

**Table 2.** Tensile strength (Fmax) and elongation at break (ebr) of cotton before and after treatment.

| Samples | $F_{max}$ (N) | $\varepsilon_{br}$ (%) |
|---|---|---|
| Cotton | 1448,74 | 13.96 |
| Treated cotton with natural resin | 1231,18 | 19.48 |
| Treated cotton with Foil T | 1340,40 | 17.27 |
| Treated cotton with PU38 | 1373,53 | 19.00 |
| Treated cotton with natural resin / PU38 | 1150,19 | 18.83 |
| Treated cotton with natural resin/ Foil T | 1135,71 | 18.43 |
| Treated cotton with natural resin/ Foil T/PU38 | 1156,25 | 17.47 |

### 3.4. Morphological analysis

All SEM images reveal the morphological structure of cotton fiber surfaces following modification with the mixture of three resins (Fig. 4). Compared to untreated cotton (Fig. 5), notable differences are observed, indicating that the coating process has altered the morphological structure of the cotton fibers. This change suggests that the application of natural resin and polyurethane-based resin effectively modifies the surface characteristics of the cotton, potentially enhancing its hydrophobic properties and overall performance. The slight differences observed before and after treatment may be attributed to the deposition of the resin, which creates a protective layer over the fibers, thereby influencing their structural integrity and interaction with moisture.

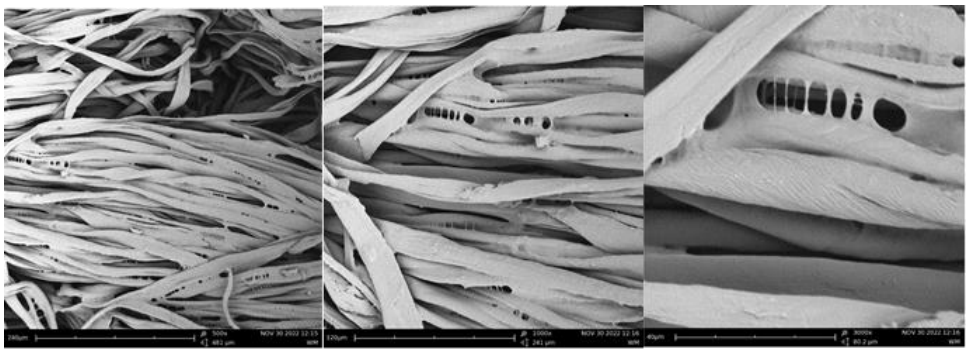

**(a)** **(b)** **(c)**

**Fig. 4** Scanning electron microscope (SEM) images of cotton fibers after modification with mixture resins ; (a)- magnification 445×; (b)- magnification 1000×; (c)-magnification 2000×.

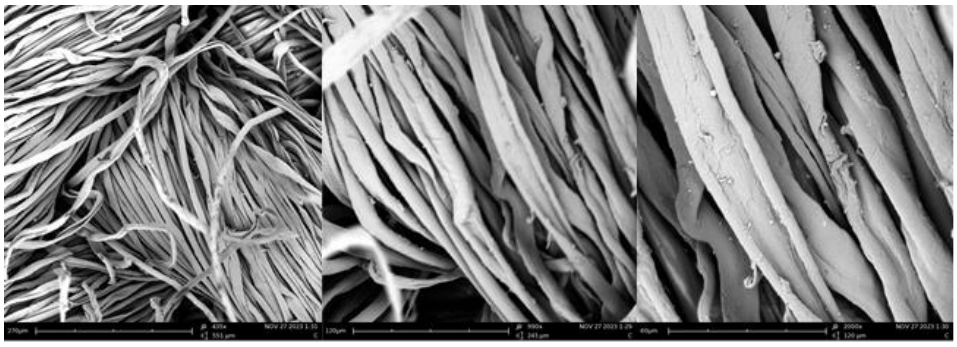

**(a)** **(b)** **(c)**

**Fig. 5** Scanning electron microscope (SEM) images of cotton fibers before modification with mixture resins; (a)- magnification 450×; (b)- magnification 1000×; (c)-magnification 2000×.

## 4. CONCLUSION

The study's results demonstrate that the cotton fabric treated with resin mixtures exhibited exceptional water repellency, as evidenced by a remarkable contact angle exceeding 100°. This elevated contact angle confirms the effectiveness of the eco-friendly treatment and highlights the superior hydrophobic properties conferred to the textile. Such properties significantly enhance the fabric's ability to repel water, making it particularly suitable for a variety of applications that require reliable moisture resistance, including outdoor apparel, protective clothing, and textile products designed for environments where water exposure is a concern. The treatment's effectiveness in creating a robust moisture barrier underscores its potential for commercial viability and practical use.

## REFERENCES

1. Chambers, W.S., Hopkins, J.G., Richards, S.M.: A review of per-and polyfluorinated alkyl substance impairment of reproduction. Front. toxicol., 3, 732436 (2021).

2. Zahid, M., Mazzon,G., Athanassiou,A., S.Bayer,I. : Environmentally benign non-wettable textile treatments: A review of recent state-of-the-art. Adv. Colloid Interface Sci. 270, 216-250(2019).

3. Periyasamy, A.P. :Microfiber emissions from functionalized textiles: potential threat for human health and environmental risks. Toxics. 11,406 (2023).

4. Szulc, J., Machnowski,W., Kowalaka,S., Jachowicz,A., Ruman,T., Steglinska,A., Gutarowska,B. : Beeswax-modified textiles: method of preparation and assessment of antimicrobial properties. Polymers. 12, 344 (2020).

5. Ponomar,M., Krasnyuk,E., Butylskii,D., Nikonenko,V., Wang,Y., Jiang,C., Xu,T., Pismenskaya,N. : Sessile Drop Method: Critical Analysis and Optimization for Measuring the Contact Angle of an Ion-Exchange Membrane Surface.Membranes. 12,765(2022)

# Biomaterials and Nanotechnology

# Study of the Compression Performance of Composite Materials Based on Waste Tire and Natural Fibers

**Mouna Boudagga[a], Faouzi Khedher[a], Boubaker Jaouachi[a]**

*(a) Textile Engineering Laboratory, University of Monastir, Tunisia*
*E-mail: mounaboudaga321@gmail.com*

**ABSTRACT**

Today, the enormous amount of tire waste generated by the tire industry poses serious environmental problems, thus their recovery has become essential. Currently, using tire residues in composite materials represents a promising avenue. Due to their ecological impact and contribution to sustainable development, biocomposites have been attracting increasing interest in recent years. These materials are generally made from biodegradable matrix or reinforcements. Furthermore, natural fiber-reinforced composite materials have properties that are comparable to those of synthetic fiber-reinforced composites, allowing them to be used in a wide range of industrial sectors. This article supports sustainable development strategies by exploiting waste tires and natural fibers to create bio-composites with essential properties. The matrix was made using two different rubber particle sizes. Waste fibers from flax, wool, and cotton were used as reinforcements. The mechanical behavior of composites is influenced by their structure, fiber type, and volume fractions. The compression tests have revealed that composites based on rubber powders reinforced with wool fibers have improved in their properties.

**KEYWORDS**: Composite materials, natural fibers, waste tires, compression test, mechanical behavior

## 1. INTRODUCTION

The rapid growth of the automotive industry in recent decades has caused major environmental and health issues associated with used tires. About 1.5 billion tires are produced annually worldwide, equivalent to about 17 million tons of used tires [1]. According to the National Waste Management Agency, Tunisia's estimated national deposit of pneumatic waste was 32,000 tons in 2015, but it will be over 2.5 million units by 2025 [2]. To protect the environment, and reduce storage and reuse costs, it has become essential to recover this waste. Additionally, the lifespan of this waste can be increased through the creation of new materials from recycled ones. Currently, there are several ways to recycle used tires, such as retreading, energy recovery, and recycling. Recycling is now more suitable for various industrial applications, such as road infrastructure, playground filling, civil engineering, and several other products. Tensile strength, impact resistance, weather resistance, elasticity, compressibility, durability, and thermal and acoustic insulation, are the most demanded in most applications.

At present, the use of pneumatic waste in composite materials is a highly promising method. Composite materials are a viable alternative due to their low density, ease of implementation, and shock-absorbing qualities. Frequently, these materials are constructed with a polymer matrix and fibrous reinforcement. Low cost, low density, biodegradability, availability, high specific modulus, and recycling capacity make natural fiber composites of great interest. It has been demonstrated by various studies that natural fibers are excellent fillers and can produce materials that are effective due to their high mechanical, physical, and thermal properties [3]. Furthermore, several studies have shown that incorporating these tire wastes into concrete is a sustainable solution [4].

John et al. gave an interesting explanation of their research on green composites that were made up of different plant fibers and different biodegradable matrix such as rubber, poly (lactic acid), poly (butylene succinate), poly(hydroxybutanoate), and soy-derived matrix. The mechanical properties of bio-composites that are made of natural fibers have been studied by several authors [5]. C. Gourier, examined the effect of adding flax fibers to poly-lactic acid (PLA). It was shown that the flexural stiffness of PLA increased from 3.4 to 8.4 GPa with the addition of 30% flax fiber. PLA/linen composite has a higher tensile strength than PP/linen composites, which are typically utilized in industrial applications like automotive industries [6].

## 2. MATERIAL AND METHODS

The fibers used as reinforcement are waste-combed flax fibers, carded wool, and frayed cotton. The matrix employed was derived from rubber, extracted from crushed tires, which are presented in two forms: powders and aggregates.

The thermo-compression technique was employed for the implementation of the sandwich composite in our study. The fiber quantity was distributed equally between the two layers of rubber. Previous research on the same material [7] [8] suggests that a reinforcement rate of 0.8% is necessary for a better outcome. We chose to experiment with three distinct reinforcement rates 0.3%, 0.5%, and 0.7%. To achieve a well-consolidated composite material, the consolidation time was 75 minutes and the temperature setting was 180°C.

To evaluate the impact of matrix particle size on the mechanical properties of the composite material, we experimented with three different types of matrix: a powder tire size that was less than 0.8mm, an aggregate size of 3.5mm, and a combination of both (with a percentage of 75% powder and 25% aggregate) were selected according to a preliminary study.

Knowing the mechanical properties of the composite material is necessary to understand its behavior while it is used. A compression test was conducted on the different combinations using an LLOYD-type dynamometer on specimens that were prepared following the ISO 14126 standard.

## 3. RESULTS AND DISCUSSIONS

Figure 1 illustrates the general appearance of the compressive behavior of composite materials that are made from tire waste and reinforced with natural fibers.

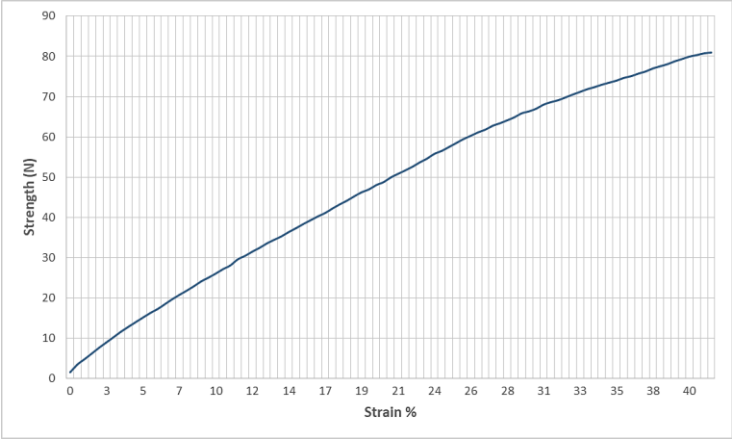


**Fig. 1.** Compression curve of a powder tire composite loaded with 0.5% flax fiber

**Table 1.** Compression test result

| **Type of reinforcement** | | **Flax** | | | **Wool** | | | **Cotton** | | | **-** |
|---|---|---|---|---|---|---|---|---|---|---|---|
| **Reinforcement rate** | | **0.3%** | **0.5%** | **0.7%** | **0.3%** | **0.5%** | **0.7%** | **0.3%** | **0.5%** | **0.7%** | **0%** |
| **Strength (N)** | **Powder** | 66.80 | 81.38 | 58.57 | 130.27 | 102.45 | 154.69 | 67.19 | 74.55 | 50.17 | 182.94 |
| | **Aggregate** | 54.50 | 114.49 | 44.18 | 90.84 | 73.64 | 56.20 | 55.46 | 46.04 | 29.78 | 77.45 |
| | **Mixture** | 44.57 | 47.02 | 35.59 | 115.3 | 100.51 | 128.36 | 48.85 | 70.96 | 34.84 | 163.50 |
| **Elongation** | **Powder** | 39.71 | 40.50 | 36.89 | 52.39 | 52.98 | 55.20 | 38.72 | 39.72 | 21.28 | 69.59 |

| | | | | | | | | | | | |
|---|---|---|---|---|---|---|---|---|---|---|---|
| **(%)** | **Aggregate** | 32.58 | 25.57 | 20.84 | 47.51 | 45.96 | 37.99 | 33.70 | 25.68 | 20.18 | 50.36 |
| | **Mixture** | 25.30 | 21.00 | 19.72 | 50.57 | 50.72 | 52.77 | 22.25 | 35.38 | 18.49 | 64.74 |

**1. Effect of matrix type**

The study of matrix types reveals that composites based on powder matrix have superior compressive strength and deformation capacity for the various reinforcements employed. In addition, composite materials made using tire powder and 0.5% wool fibers have a maximum strength of around 102N. The composite with the highest deformation percentage is the one made with tire powder and 0.7% wool fibers, which is approximately 55% deformable.

**2. Effect of reinforcement type**

**2.1. Flax fibers**

The findings reveal that the most robust material, which is constructed from an aggregate matrix and reinforced with 0.5% of the reinforcement rate, has a compressive force that is equal to 114.5N. While composites reinforced with 0.3% fiber provide the best deformation, it's important to note that the deformation percentage decreases with an increase in load rate. The material's deformability increases with fewer fibers due to linen fiber's rigidity and low extensibility.

**2.2. Wool fibers**

According to the results, using an aggregate matrix decreases the strength and deformation of composite materials compared to other matrix types. which in turn decreases by increasing the fiber content. On the other hand, an improvement in the properties of composite materials based on powder tires and mixtures can be observed when the reinforcement rate is increased. Composite materials that offer the best properties are those that have 0.7% reinforcement for powder and blend matrices.

**2.3. Cotton fibers**

Regardless of the matrix used, the results demonstrate that composite materials with a reinforcement rate of 0.5% have the best mechanical properties. Whereas, materials that use tire aggregates as their matrix have a maximum force and deformation value of 0.3% fibers.

**3. Effect of reinforcement rate**

The study's findings indicate that increasing the reinforcement rate results in a decrease in resistance and deformation of the materials. An overload of fiber material can lead to excess fibers, which can lead to fewer contact points between the different parts of the composite, which results in less cohesion between them.

## CONCLUSION

Recovering industrial waste is still a major trend and crucial for researchers. The applications of composite materials in different fields that require lightweight materials and recycling opportunities are interesting since they have minimal environmental impact and material cost reduction.

This study aims to evaluate the mechanical properties of composite materials that are made of rubber matrices and fibrous reinforcements. The properties of the composites obtained were compared by analyzing the rate and types of reinforcement, as well as the matrix used. Composites with a powder matrix achieved the best results.

The best mechanical properties are provided by waste wool composites, which are superior to 100% tire structures and increase with increasing reinforcement rate. Their low density, as well as their high compressibility, can promote their application in civil engineering as damping plates for playgrounds and sports halls, or as thermal and acoustic insulation panels.

## REFERENCES

1. Aouled Mhemed, H. : Energy and environmental recovery of used tire waste: improvement of liquid pyrolysis products by catalysis. PhD thesis. N° 2021IMTA0236 (2021)

2. Ajam,L., Belgaied, M., et Jomaa, S.: Mechanical and environmental study of the valorization of waste tires in bituminous concrete applied in Tunisia, Int. J. Pavement Res. Technol.. (2020). doi: 10.1007/s42947-020-0031-2
3. Vidil, L.: Study of 2D natural materials Potential for use as reinforcement for composite materials. PhD thesis. University of Antilles. (2019)
4. Roche, N.: Vibro-acoustic behavior of materials and structures based on recycled tire crumbs. PhD thesis. Lyon doctoral school. (2010)
5. Gourier, C.: Contribution to the study of bio-composite materials with a polyamide-11 thermoplastic matrix and reinforced with flax fibers. PhD thesis. University of Bretagne Loire. France. (2016)
6. John, M., J. et al: Cellulosic fiber-reinforced green composites, Composite Interfaces, vol. 14, nº 7-9, p. 733-751, VSP (2007)
7. Haddaji, K. : Contribution to the identification of an innovative product based on shredded tires and textile waste. Master's thesis. University of Monastir (2021)
8. Brahem, M., Jaouachi, B., Damien, S., Ben Marzoug, I. and Sakli, F.: Study of the tensile and compression performance of composite materials based on rubber particles and alpha fibers. Journal of Industrial Textiles. (2018). doi: 10.1177/1528083716682921

# Development of Bio-Functional Textiles Based on Colocynth Oil Microcapsules

**Abir Nour Maatallah, Fadhel Jaafar, Neji Ladhari**

*Higher Institut of Fashion of Monastir, Monestir5000, Tunisia*
*Textile engineering laboratory, University of Monastir, Iset of Ksar Hellal, Tunisia*
*E-mail : abirmaatallahnour@gmail.com*

## ABSTRACT

This study focuses on the development of microcapsules containing colocynth oil, a natural antimicrobial agent. The microcapsules were fabricated using ethylcellulose as a polymer and sodium lauryl sulfate as a surfactant. The encapsulation efficiency reached 92.16%, indicating successful encapsulation of the oil. Morphological analysis revealed a spherical shape with a size distribution that influences the release kinetics of the active ingredient.

The microcapsules were characterized for particle size, zeta potential, and thermal properties. The results suggest that the microcapsules are suitable for incorporation into textiles, offering a promising approach for the development of antimicrobial wound dressings and other medical applications.

**KEYWORDS:** Colocynth oil, Microencapsulation, Biotextile, Antibacterial dressings, Biocompatibility.

## 1. INTRODUCTION

Recent advances in medical textiles have led to increasing interest in the use of innovative materials in the manufacture of wound dressings and medical articles [1]. Wound dressings are crucial elements in the management of wounds, whether surgical, traumatic or chronic, as they provide a protective barrier while promoting an environment conducive to healing. Textiles used in the design of wound dressings must meet strict standards in terms of safety, biocompatibility, sterility and functionality in order to ensure optimal therapeutic results [2]. The properties of textiles intended for wound dressings, whether woven, knitted or non-woven, play an important role in their clinical efficacy. They must be designed with materials that guarantee the absence of toxicity, allergic reactions, as well as sterility and biocompatibility [3]. In addition, they must have good mechanical properties to ensure easy handling and adequate wound protection. Sterility is of paramount importance for dressings, requiring that the polymers used in their manufacture can withstand specific physical and chemical conditions.
The essential oil "colocynth", is particularly notable in Tunisia for its medicinal properties, including anti-inflammatory, antidiabetic, antibacterial and antifungal, antioxidant. In addition to its health benefits, it offers interesting prospects for the manufacture of antimicrobial textiles thanks to its antibacterial properties. Its traditional use in Tunisian medicine and its local availability promote the development of innovative textiles while supporting sustainable production practices [4]. In this study, we are focused on the development of microcapsules containing colocynth oil, a natural antimicrobial agent [5].

## 2. MATERIAL AND METHODS

**Raw materials:** Sodium lauryl sulfate as surfactant, ethylcellulose as polymer, ethyl acetate and cyclohexane as solvents (provided by Philadelphia, United Kingdom and France respectively), and colocynth essential oil (obtained from ALVIA parapharmacy).
**Preparation of microcapsules:** Colocynth oil microcapsules were prepared by dissolving ethylcellulose in ethyl acetate and forming an emulsion with sodium lauryl sulfate in water. The emulsion was poured into water to form the microcapsules, then separated by centrifugation, filtered, and dried [6].

**Characterization:**
- Particle size and zeta potential: measured with a MALVERN ZETASIZER.
- Percentage of encapsulated oil: determined by dissolving the microcapsules in cyclohexane.
- Encapsulation efficiency: calculated by relating the mass of encapsulated oil to the total mass of oil used.
- Morphological analysis: by ThermoFisher Scientific SEM.
- FTIR-ATR spectroscopy: to identify functional groups.
- DSC calorimetry: to analyze the thermal properties of the microcapsules.

## 3. RESULTS AND DISCUSSIONS

### 3.1. Quantitative analysis of the presence of colocynth oil in microcapsules

**Table 1**. Mass of oil contained in microcapsules

| | Average | CV(%) |
|---|---|---|
| Initial mass of microcapsules (mg) | 200,11 | 0,06 |
| Mass of dissolved ethylcellulose (mg) | 70,11 | 6,65 |
| Mass of oil obtained (mg) | 129,1 | 3,31 |
| Percentage of oil (%) | 64,96 | 3,59 |

Measurements of the amount of colocynth oil encapsulated in ethylcellulose microcapsules were carried out to confirm the presence and percentage of encapsulated oil. The results, summarized in **Table 1**, show an average mass of oil obtained of 129.1 mg, representing 64.96% of the mass of the microcapsules. The low standard deviation indicates good reproducibility of the process. Thus, the high percentage of encapsulated oil (65%) suggests that the microcapsules obtained are of the "reservoir" type.

### 3.2. Encapsulation efficiency

The encapsulation efficiency, calculated by subtracting the amount of unencapsulated oil from the initial amount of oil used, is 92.16%. This indicates efficient encapsulation of colocynth oil by ethylcellulose.

### 3.3. Morphological analysis by scanning electron microscopy (SEM)

Observation of the microcapsules under a scanning electron microscope reveals a generally spherical shape with a significant dispersion of sizes (**Fig.1 and Fig. 2**). This size variation impacts the kinetics of release of the active ingredient, with larger microcapsules tending to release colocynth oil more slowly compared to smaller ones.

**Table 2.** Measuring the distribution of the microcapsules obtained

| | Dh(nm) | PDI |
|---|---|---|
| Sample 1 | 173,17±4,7 9 | 0,147 ±0,01 |
| Sample 2 | 181,6 ±4,79 | 0,144 ±0,01 |
| Sample 3 | 186,3 ±4,79 | 0,133 ±0,01 |

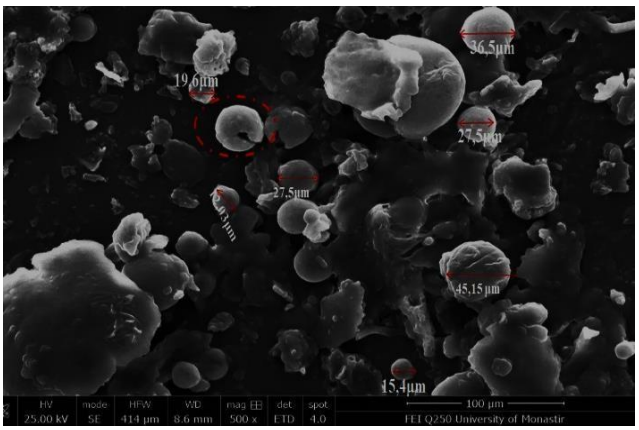


**Fig. 1** Microcapsules containing "colocynth" oil (500x magnification)

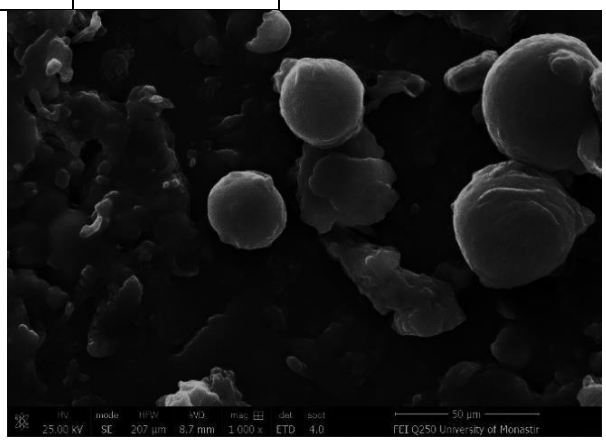

**Fig. 2** Microcapsules containing "colocynth" oi

### 3.4. Granulometric analysis by laser granulometer (MALVERN "ZETASIZER" NANO SERIES

A notable observation from the analysis of these data is that as successive dilutions are made, the microcapsules display specific characteristics, they become smaller and more evenly distributed in terms of size. This trend is accompanied by a decrease in the Poly Dispersity Index (PDI), indicating a more uniform distribution of particle sizes in the samples. These changes are observed over several successive dilution.

### 3.5. Fourier Transform Infrared Analysis (FTIR-ATR)

The FTIR-ATR spectrum of the microcapsules shows the presence of characteristic bands of ethylcellulose and colocynth oil (**Fig 3**). The observed vibrations indicate a conservation of the molecular characteristics of ethylcellulose and an interaction with colocynth oil, with specific bands associated with functional groups and characteristic bonds.

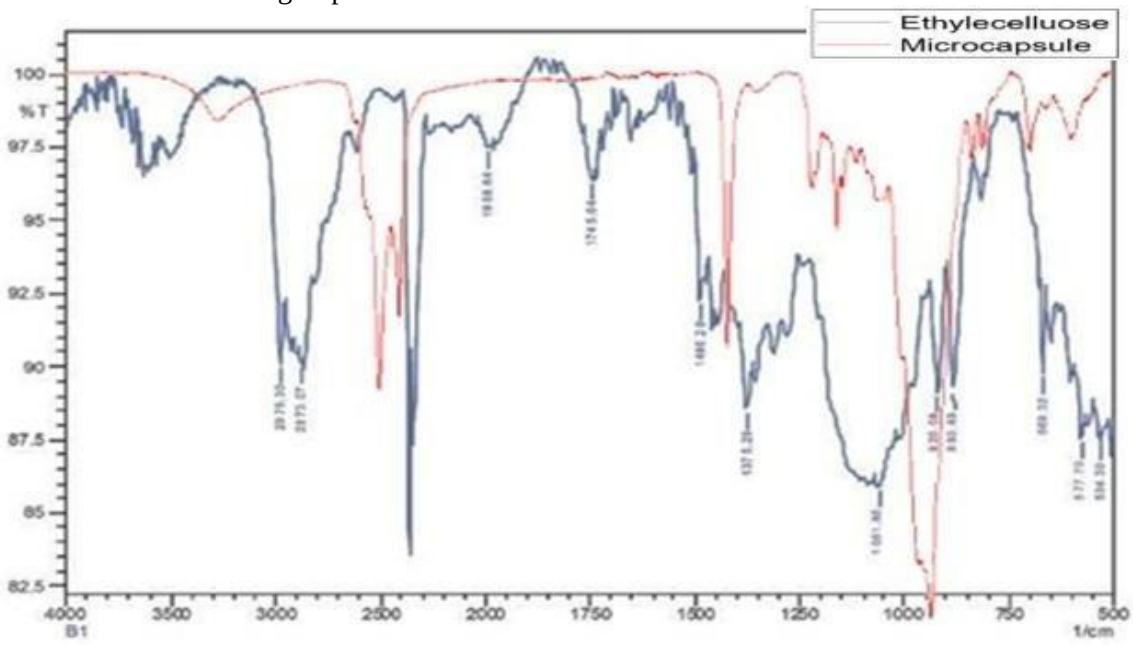


**Fig. 3** Fourier transform infrared spectra (FTIR-ATR) of ethylcellulose [7] and (FTIR-ATR) of colocynth oil

### 3.6. Differential scanning calorimetry (DSC) analysis

DSC thermograms of microcapsules show endothermic and exothermic peaks at different temperatures (**Fig 4**). The results indicate complex thermal reactions and a stabilization phase of microcapsules, with potential degradation of the active ingredient at high temperatures, which is relevant for the stability of microcapsules.

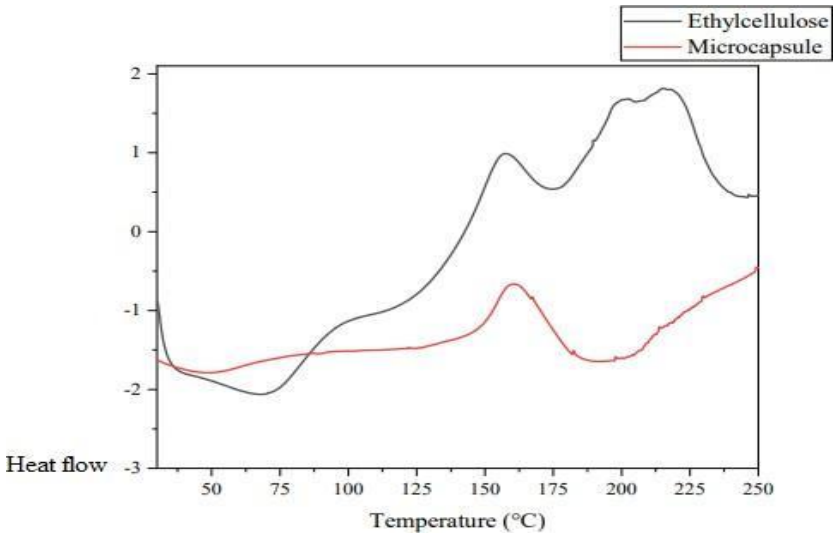


**Fig. 4** DSC thermograms of microcapsules and ethylcellulose at a heating rate of 10 °C/min

## 4. CONCLUSION

This study successfully developed microcapsules containing colocynth oil, a natural antimicrobial agent with potential applications in textile-based wound dressings. The microencapsulation process demonstrated high efficiency, resulting in a significant amount of encapsulated oil. The microcapsules exhibited a spherical morphology and a size distribution that can influence the controlled release of the active ingredient.

The characterization of the microcapsules revealed their suitability for incorporation into textile materials. The presence of colocynth oil within the microcapsules offers a promising avenue for the development of antimicrobial textiles with enhanced wound healing properties. The results also show that the microcapsules have a homogeneous particle size distribution and retain the bioactive properties of the essential oil, with a significant percentage of encapsulated oil (65%). These characteristics are essential to ensure a controlled and prolonged release of the active agents, thus increasing the effectiveness of the dressings. Further research is warranted to investigate the release kinetics of colocynth oil from the microcapsules under various conditions and to evaluate their efficacy in inhibiting microbial growth on textile substrates.

## REFERENCES

1. Qin, Y. (2016). An overview of medical textile products. Medical Textile Materials, 13–22.
2. Horžić, M., Marić, K., & Bunoza, D. (1995). The Temperature Dynamics During the Healing Processing of a Surgical Wound. Biomedizinische Technik, 40(4), 106–109.
3. Alejandra Mogrovejo, 2018, Conception et évaluation d'un pansement à libération de deux principes actifs pour le traitement des plaies chroniques. Diss. Université de Lille.
4. Marzouk, B., et al. "Antibacterial and antifungal activities of several populations of Tunisian Citrullus colocynthis Schrad. immature fruits and seeds." Journal de mycologie médicale 20.3 (2010): 179-184.
5. Le mode d'action des huiles essentielles sur les bactéries – Laboratoire DUMANI. (n.d.). Retrieved January 21, 2022, from https://laboratoiredumani.fr/le-mode-daction-des-huilesessentielles-sur-les-bacteries/.
6. Jaâfar, F, et al. 2012, Impregnation of ethylcellulose microcapsules containing jojoba oil onto compressive knits developed for high burns. Fibers and Polymers, 13: p. 346-351.
7. Preparation and in vitro & in vivo evaluation of cephalexin matrix tablets November 2018Brazilian Jornal of Pharmaceutical Sciences 54(3) Follow journal DOI:10.1590/s2175-97902018000317277.

# Lavender essential oil nanocapsules embedded in polyamide gauze dressing

**Asma Fraj** [a], **Fadhel Jaâfar** [a], **Luisa Coderch** [b], **Neji Ladhari** [a], **Meritxell Marti** [b]

[a] *Textile Engineering Laboratory of ISET Ksar Hillel, BP 68, Street Hadj Ali Soua, Ksar Hellal 5070, University of Monastir, Tunisia.*
[b] *Textiles and Cosmetic Innovations, Institute of Advanced Chemistry of Catalunya (IQAC-CSIC), c/ Jordi Girona 18-26 08034, Barcelona, Spain*

*E-mail: asma.fraj@enim.rnu.tn*

## ABSTRACT

For centuries, herbal medicinal products utilization has steadily increased due to their healing therapeutic potentials, their safe toxicological profiles, and their improved microbial safety. Recently, *Lavandula angustifolia* essential oil has shown tremendous potential in the field of nanotechnology to fend against microorganisms' wound ulcers. From this perspective, this study aims to develop and characterize lavender essential oil-loaded polycaprolactone nanocapsules embedded into polyamide gauze dressing. The polymeric nanocapsules showed a nano-scale size of 181.00 ± 0,40 nm, a monomodal size distribution of 0.12 ± 0.02, a negative zeta potential value of -33.00 ± 1.15 mV, and an encapsulation efficiency of 83.23 ± 0.02%. Morphology and physical properties of nanocapsules using several analytical techniques (ATR-FTIR, and TGA) were performed. Furthermore, the polyamide gauze dressing impregnation was assessed using bath exhaustion finishing, and the efficacy of impregnation was verified through SEM. Thermal properties revealed the thermal stability of the nanocapsules. Likewise, attenuated Total Reflectance Fourier Transform Infrared results indicated the successful incorporation of lavender into nanocapsules.

**KEYWORDS:** *Lavandula angustifolia* essential oil, nanoscale particles, thermal behavior, wound dressing

## 1. INTRODUCTION

*Lavandula angustifolia* essential oil has been used for centuries as a remedy to treat illnesses. It has been known to possess several therapeutic activities such as anti-inflammatory [1], anti-tumor [2], antifungal [3], antioxidant [4], and antimicrobial properties [5], which are attributed mainly to linalool and linalyl acetate [6]. Nowadays, nanoencapsulation of essential oils within biodegradable delivery systems has the potential to overcome their susceptibility, increase their aqueous solubility, and improve their pharmacological activity [7]. Polycaprolactone (PCL) is considered a better candidate for the design of nanoconstructs to deliver various natural therapeutic agents. PCL has been widely adopted as a suitable biomaterial due to its high thermal stability, relatively slow degradability, and good biocompatibility, which eases its use as a model polymer in biomedical applications [8,9]. Functional wound dressings, based on the combination of conventional textiles with advanced delivery systems, are described as promising systems for the delivery of active compounds. Therefore, functional wound dressings should be designed to control the infection, maintain a moist wound environment, and promote healing [10].

## 2. MATERIAL AND METHODS

### a. Materials

Polycaprolactone (PCL) (average molecular weight of 45 000), Tween® 80, and Span® 80 were obtained from Sigma–Aldrich Chemicals Private Ltd. (Madrid, Spain). Lavender essential oil (LEO)

was purchased from (Terpeniclabs, Barcelona Spain). Standard spun nylon 6.6 (PA) was purchased from Testfabrics, USA. All other reagents and solvents were of analytical grade.

### b. Methods

#### i. Preparation of nanocapsules by nanoprecipitation

The polymeric nanocapsules of LEO were prepared via a nanoprecipitation process adopted by Fessi et al. [11]. The organic phase was prepared by dissolving PCL in an acetone solution under stirring and by mild heating for 15 min. LEO and Span® 80 were, then, mixed into the resulting solution. Further, the organic phase was added dropwise into the aqueous phase and kept under moderate magnetic stirring for 10 min. Subsequently, acetone was removed through evaporation at 40 °C under reduced pressure.

### c. Characterization

#### i. Particle size, size distribution, Z-potential, and encapsulation efficiency analyses

The hydrodynamic size (PS) and polydispersity index (PDI) analyses were performed by dynamic light scattering (DLS) using a Nano ZS Zetasizer ZEN3600 (Malvern Instruments Ltd., Malvern, Worcestershire, UK). The zeta potential (ZP) was measured by electrophoretic mobility considering the water dielectric constant of 78.5. All samples were, initially, dispersed in Milli-Q water (1:100, v/v). Three replicates of each formulation were measured at a room temperature of 25 °C. The encapsulation efficiency (EE%) of lavender was determined by the ultrafiltration-centrifugation technique at 9000 rpm at 4 °C for 15 minutes. The pellet was extracted using methanol as an extracting solvent, vortexed vigorously, and centrifuged. The extracted oil was collected and quantified spectrophotometrically at 210 nm. All measurements were made in triplicate batches and presented as mean ± standard deviation.

### d. Thermal analyses

The thermal properties of the NCs and their compounds were analyzed by Thermogravimetric analysis (TGA) performed with a TGA instrument (Model TGA/SDTA 851e; Mettler Toledo), with STARe software (version SW 9.30). Approximately 5.00 ± 0.1 mg of each sample was weighted using a microbalance (XPR2, Mettler Toledo). They were packed into an aluminum pierced pan (100 µL) and heated under a nitrogen stream (50 mL/min) from 25 °C to 550 °C at a heating rate of 10 °C/min.

### e. ATR-FTIR assessment of the particles

The Attenuated Total Reflectance Fourier Transform Infrared (ATR-FTIR) spectroscopy was performed to investigate the functional groups present in the NCs. The samples were placed for spectra recording on a NICOLET AVATAR 360 FTIR Spectrophotometer (Nicolet Instruments, Inc., Madison, WI, USA) equipped with an attenuated total reflection (ATR) sampling accessory that used a diamond with an angle of incidence of 45° in a horizontal orientation. FT-IR Spectra were collected by reflectance at 4 $cm^{-1}$ resolution and coadded 32 scans in the 500 - 4000 $cm^{-1}$ wavenumber range.

### f. The nanocapsules' impregnation process on PA fabric

The NCs were applied onto PA fabric by the bath exhaustion process. Briefly, a piece of 3g of PA was immersed in 30 mL of NCs suspension and was agitated for 1 hour at 40 °C in a Bain Marie. The textile sample was, then, uniformly drained using a pad-dry-machine having a measured width of 30 cm (ERNEST-BENZ-AG-KLDHT and KTF/m250) with a padding pressure applied to obtain a 100% pick-up ratio. The treated samples were dried overnight and conditioned in standard laboratory conditions (20 ± 2 °C and 65 ± 5% relative humidity) for 24h. The sample was weighed again to calculate the pickup mass of NCs absorbed by the PA fibers.

### g. Scanning electron microscopy

The scanning electron microscope (SEM) type Hitachi instrument TM-1000 was used to study the surface observation of virgin and functionalized PA fabrics. PA samples were placed on a carbon adhesive disc, fixed on a standard sample holder, and then, were observed. All samples were, then, examined with suitable accelerating voltage and magnification, and a representative image was reported.

## 3.RESULTS AND DISCUSSIONS

### h. Characterization of nanocapsules

The colloidal NCs dispersions were obtained with a transparent to opalescent bluish aspect presenting a Tyndall effect. The nanoprecipitation is simple and versatile and allows the formation of stable and homogeneous NCs-loaded lavender essential oil. Dynamic light scattering measurements showed that the polymeric NCs exhibited a nano-scale size of 181.00 ± 0.40 nm and a monomodal size distribution of 0.12 ± 0.02. Furthermore, a negative zeta potential value of -33.00 ± 1.15 mV was obtained reflecting an electrostatic stabilization effect that contributes to avoiding aggregation of the fine particles in the colloidal system. Besides, a high encapsulation efficiency of 83.23 ± 2.40% was obtained.

### i. ATR-FTIR of the nanocapsules

The PCL spectrum **Fig. 1** presented a strong characteristic peak in 1723.25cm$^{-1}$ attributed to the carbonyl-stretching mode C=O. Two vibration bands were observed at 2943.02 cm$^{-1}$ and 2866.49 cm$^{-1}$ assigned to asymmetric and symmetric stretching of $CH_2$, respectively. Moreover, the peak at 1294 cm$^{-1}$ was assigned to the backbone C–C and CO– stretching modes in the crystalline phase of PCL, whereas the peaks at 1178 cm$^{-1}$ and 1163.8 cm$^{-1}$ are due to symmetric C–O–C stretching and C–O, C–C stretching in the amorphous phase, respectively [12]. LEO spectrum showed a strong absorption peak at 1723 cm$^{-1}$ characteristic of the C=O stretching band [13]. Moreover, no chemical reactions between the raw materials were verified since there was no formation of new peaks in the spectrum of the NCs.

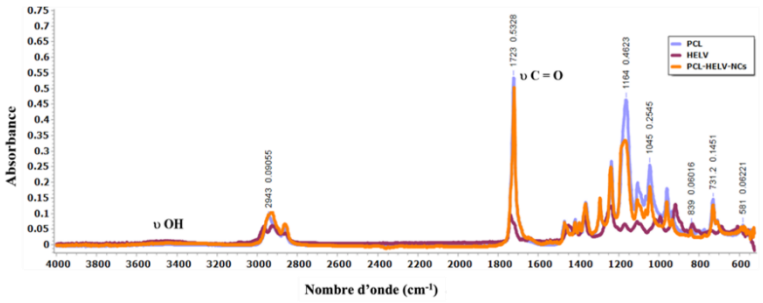


**Fig.1** ATR-FTIR of PCL, LEO, and PCL-LEO-NCs.

### j. Thermal analysis

The PCL started degrading slowly after 300 °C and reached the decomposition temperature at 414.87°C, which was due to the complete breakage of the C-C backbone of the PCL chains. **Fig. 2** showed that the mass loss of LEO of 95.04% was observed at 205.90 °C which is associated with the total evaporation of the oil. The degradation of NCs also occurred in a single step with a mass loss of 97.68% and a Tmax of 398.82 °C, associated with the total decomposition of the main chains of the polymer.

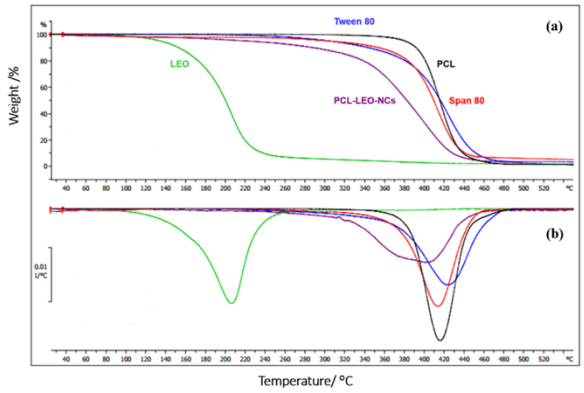


**Fig.2** Thermogravimetric curves of (A): (a) PCL, LEO, and PCL-LEO-NCs (b) the first derivatives (DTGA), and (b) the first derivatives (DTGA).

### k. Morphology and surface characteristics

The virgin and functionalized PA fibers were analyzed by SEM to verify the morphology of the PA samples before and after impregnation. The results reported in **Fig. 3** revealed a spherical shape of nanocapsules ranging between 180 and 200 nm. Micrographs observed at higher magnification (×1000) showed the nanocapsules distribution on the fibers where they were hosted outside and inside the dip of the PA fibers. They were visible and did not appear to be damaged by the mechanical and thermal treatments undergone.

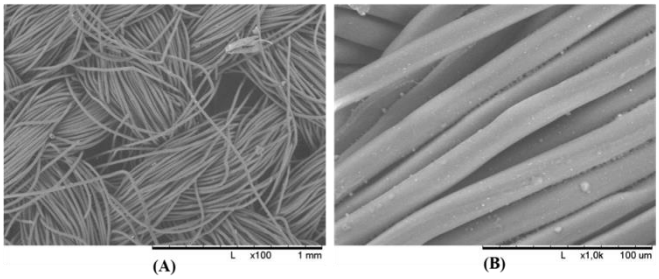


**Fig.3** Scanning electron micrographs of (A) virgin PA and (B) PCL-LEO-NCs impregnated in PA fibers

## CONCLUSION

This study provided interesting results of the successful preparation of lavender-based polycaprolactone nanocapsules through nanoprecipitation. Uniform spherical nanocapsules were prepared with good characteristics of particle size distribution PDI (< 0.2) and high encapsulation efficiency of 83.23 ± 0.02%. Bath exhaustion-assisted impregnation was applied to incorporate lavender
into PA fibers to be potentially applied as a wound dressing in future applications.

## REFERENCES

[1] da Silva, G.L., Luft, C., Lunardelli, A., Amaral, R.H., da Silva Melo, D.A., Donadio, M.V.F., Nunes, F.B., de Azambuja, M.S., Santana, J.C., Moraes, C.M.B., Mello, R.O., Cassel, E., Pereira, M.A. de A., de Oliveira, J.R.: Antioxidant, analgesic and anti-inflammatory effects of lavender essential oil. An. Acad. Bras. Cienc. 87, 1397–1408 (2015).

[2] Rejane, C., Bertoncini, A., Dermondes, G.T.: Clinics in Oncology Application of Lavender in Integrative Medicine: From Aromatherapy to Potential Anticancer Treatment OPEN ACCESS Lavender as a Multipurpose Plant, Remedy Publications LLC (2020).

[3] D'Auria, F.D., Tecca, M., Strippoli, V., Salvatore, G., Battinelli, L., Mazzanti, G.: Antifungal activity of Lavandula angustifolia essential oil against Candida albicans yeast and mycelial form. Med. Mycol. 43, 391–396 (2005).

[4] Soheili, M., Salami, M.: Lavandula angustifolia biological characteristics: An in vitro study (2019).

[5] Messaoudi Moussii, I., Nayme, K., Timinouni, M., Jamaleddine, J., Filali, H., Hakkou, F.: Synergistic antibacterial effects of Moroccan Artemisia herba alba, Lavandula angustifolia and Rosmarinus officinalis essential oils. Synergy 10, 100057 (2020)

[6] Caputo, L., Souza, L., Alloisio, S., Cornara, L., De Feo, V.: Coriandrum sativum and Lavandula angustifolia Essential Oils: Chemical Composition and Activity on Central Nervous System. Int. J. Mol. Sci. 17, 1999 (2016).

[7] de Matos, S.P., Teixeira, H.F., de Lima, Á.A.N., Veiga-Junior, V.F., Koester, L.S.: Essential oils and isolated terpenes in nanosystems designed for topical administration: a review. Biomolecules 9, 138 (2019).

[8] Cerkez, I., Sezer, A., Bhullar, S.K.: Fabrication and characterization of electrospun poly(e-caprolactone) fibrous membrane with antibacterial functionality. R. Soc. Open Sci. 4, 160911(2017).

[9] Malikmammadov, E., Tanir, T.E., Kiziltay, A., Hasirci, V., Hasirci, N.: PCL and PCL- based materials in biomedical applications. J. Biomater. Sci. Polym. Ed. 29, 863–893 (2018).

[10] Chermnykh, E.S., Kiseleva, E. V, Rogovaya, O.S., Rippa, A.L., Vasiliev, A. V, Vorotelyak, E.A.: Tissue-engineered biological dressing accelerates skin wound healing in mice via formation of provisional connective tissue. Histol. Histopathol. 33, 1189–1199 (2018).

[11] Fessi, H., Puisieux, F., Devissaguet, J. P., Ammoury, N., Benita, S.: Nanocapsule formation by interfacial polymer deposition following solvent displacement. International Journal of Pharmaceutics,

55(1), R1-R4 (1989).

[12] Elzein, T., Nasser-Eddine, M., Delaite, C., Bistac, S., Dumas, P.: FTIR study of polycaprolactone chain organization at interfaces. Journal of Colloid and Interface Science, 273(2), 381-387 (2004).

[13] Bayramzadeh, N., Mehrkhou, F., Pourmirza, A. A., Mahmoudian, M.: Fumigant Toxicity of Two Nano-Capsulated Essential Oils with Sublethal Rate of Phosphine against Three Stored-Product Pests. J. Agr. Sci. Tech, 21(4), 857-872 (2019).

# Synthesis, Characterization, X-ray Molecular Structure, Antioxidant, Antifungal, and Allelopathic Activity of a New Isonicotinate-Derived meso-Tetraarylporphyrin

**Nour Elhouda dardouri[a], Thierry Roisnel [b], Habib Nasri[a]**

(a) *University of Monastir, Laboratory of Physical chemistry of Materials, Faculty of Science of MonastIR (LR01ES19), Avenue of Environment, 5019 Monastir, Tunisia*
*(b) Institute of Chemical Sciences of Rennes, UMR 6226, University of Rennes 1, Beaulieu Campus, 35042 Rennes, France*
*E-mail : nourelhoudadardouri@gmail.com*

**ABSTRACT:**
The present paper describes the synthesis of an isonicotinate-derived meso-arylporphyrin, that has been fully characterized by spectroscopic methods (including fluorescence spectroscopy), as well as elemental analysis and HR-MS. The structure of an n-hexane monosolvate has been determined by single-crystal X-ray diffraction analysis. The radical scavenging activity of this new porphyrin against the 2,2-diphenyl-1-picrylhydrazyl (DPPH) radical has been measured. Its antifungal activity against three yeast strains (C. albicans ATCC 90028, C. glabrata ATCC 64677, and C. tropicalis ATCC 64677) has been tested using the disk diffusion and microdilution methods. Whereas the measured antioxidant activity was low, the porphyrin showed moderate but encouraging antifungal activity. Finally, a study of its effect on the germination of lentil seeds revealed interesting allelopathic properties.
**KEYWORD**: free base porphyrin, isonicotinic acid, antioxidant activity, antifungal activity, allelopathic activity.

## 1. INTRODUCTION

The presence of porphyrins in myriad biological systems, coupled with the ability to finely tune their chemical and physical properties, position both free base porphyrins and metalloporphyrins as adaptable materials and as crucial for scientific investigations. The deep-rooted biological importance of these tetrapyrrolic macrocycles and their ex-ceptional electronic and structural properties have spurred their widespread utilization, encompassing their use as photosensitizers in photodynamic therapy [1] and in functionalization reactions [2], as sensors [3], in solar cells [4], and more recently, as organocatalysts [5] and photoredox catalysts [6]. The availability of a large num-ber of porphyrins and metalloporphyrins in these applications is made possible mainly thanks to the work of Adler and Longo [7] and Lindsey [8], who uncovered simple methods for the preparation of free porphyrins with acceptable yields.

## 2. MATERIAL AND METHODS

Commercially available reagents, catalysts, and solvents were used as received. Dichloromethane for porphyrin synthesis was distilled from $CaH_2$, and THF was dried by distillation from $LiAlH_4$. Deuterated solvents were obtained from Merck Life Science. Thin-layer chromatography was performed on Merck 60 F254 silica gel plates, with visualization by UV light or chemical developers. Chromatographic purifications were conducted on silica gel columns using solvent mixtures (hexane, ethyl acetate, dichloromethane, and methanol). NMR spectra were recorded at 400 MHz with a Varian Mercury 400 spectrometer, and IR spectra were obtained using a Nicolet 6700 FTIR instrument. UV–vis spectra were measured on a Cary 500-scan spectrophotometer with quartz cuvettes, and porphyrin solutions were degassed before measurement.

## 3. RESULTS AND DISCUSSIONS

### 3.1. Synthesis and characterization of $H_2$TMIPP (1).

The free-base porphyrin $H_2$TMIPP (1) was synthesized in two steps from vanillin (2) and isonicotinic acid (3). First, vanillin was acylated with isonicotinic acid in dichloromethane using DCC as a coupling agent and DMAP as a catalyst, yielding formylisonicotinate 4 with 71% efficiency. The resulting aldehyde was then condensed with pyrrole using the Adler and Longo method (reflux in propionic acid), yielding free-base porphyrin (1) with a 29% yield.

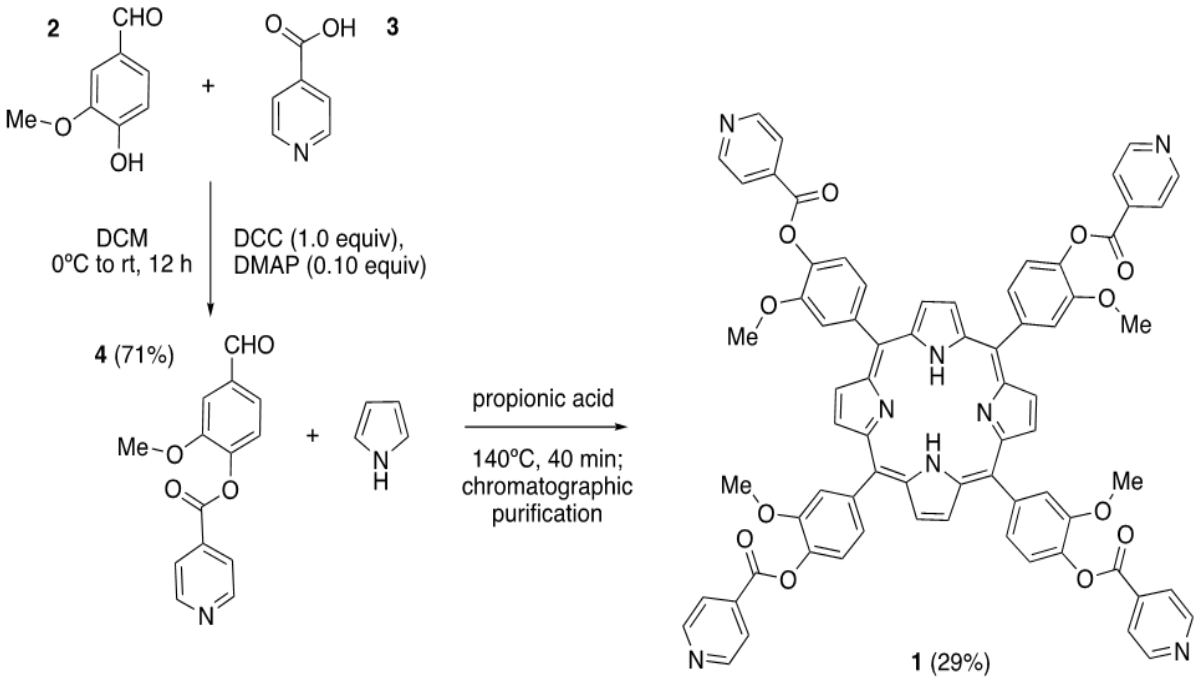


**Scheme 1.** Synthesis of $H_2$TMIP (1).

This compound was fully characterized by IR, $^1$H-NMR, and $^{13}$C-NMR spectroscopy, and by HRMS-ESI spectrometry. A detailed discussion of its spectroscopic properties can be found in the Supporting Information. Recrystallization of 1 from DCM/hexane (diffusion method) afforded a single crystal that was suitable for X-ray diffraction analysis. The molecular structure of 1 showed it had crystallized with a *n*-hexane solvent molecule, a point that was also confirmed by elemental analysis.

### 3.2. Biological properties of $H_2$TMIPP (1)

#### 3.2.1. Antioxidant activity

The antioxidant activity of $H_2$TMIPP (1) was evaluated using the DPPH radical assay. The DPPH radical, which is purple, turns yellow upon reaction with antioxidants. Results showed that $H_2$TMIPP's radical scavenging activity was weak, increasing only slightly from 19.07% to 27.89% as concentration rose, with an IC50 of 3.6412 ± 0.4256 mg/mL, compared to 0.01321 ± 0.0062 mg/mL for ascorbic acid. The weak antioxidant effect is likely due to electron-withdrawing carbonyl groups in $H_2$TMIPP, which reduce its ability to donate electrons despite the presence of electron-donating methoxy groups.

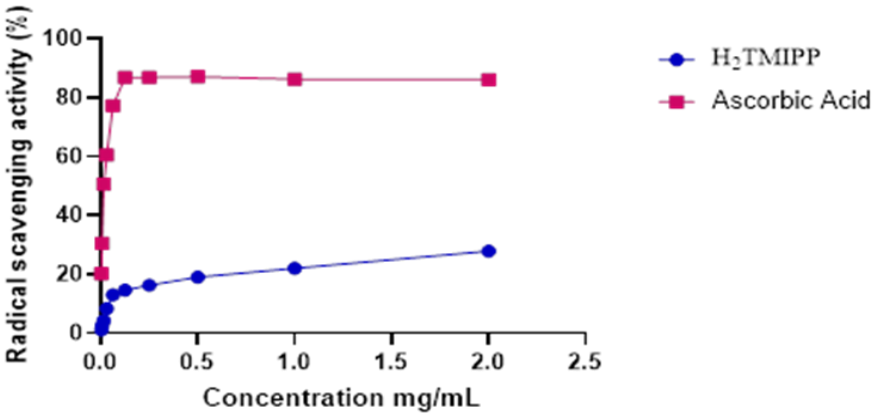


**Fig. 1** Radical scavenging activity of $H_2$TMIPP (1) and of ascorbic acid as a function of the concentration.

### 3.2.2. Antifungal activity

#### 3.2.2.1. The disk diffusion method

The antifungal activity of $H_2$TMIPP (1) was assessed using disk diffusion against *Candida albicans*, *Candida glabrata*, and *Candida tropicalis*. Inhibition zones were measured, with dimethyl sulfoxide (DMSO) as a negative control and Amphotericin B as a positive control. $H_2$TMIPP showed moderate antifungal effects, producing inhibition zones of 12 ± 0.5 mm for *C. albicans* and 12 ± 0.4 mm for *C. tropicalis*, compared to 20 ± 1 mm and 20 ± 0.6 mm for Amphotericin B. Against *C. glabrata*, $H_2$TMIPP showed lower activity with an inhibition zone of 8 ± 0.3 mm. These results indicate that $H_2$TMIPP moderately inhibits fungal growth.

**Table 1.** Antifungal susceptibility disk diffusion test: measured Inhibition Zone Diameters (mm).

| **Inhibition diameters (mm)** | | | |
|---|---|---|---|
| Inhibitor | *C.albicans* (ATCC 90028) | *C. glabrata* (ATCC 64677) | *C. tropicalis* (ATCC 66029) |
| $H_2$TMIPP (**1**) | 12 ± 0.5 | 8 ± 0.3 | 12 ± 0.4 |
| Amphotericin B (0.1 mg) | 20 ± 1 | 15 ± 0.5 | 20 ± 0.6 |

### 2.3.3. Allelopathic activity

Figure 4 demonstrates the effects of various concentrations of $H_2$TMIPP (1) on lentil seed germination, above-ground growth, root development, and hydration. Germination was unaffected at 0.625 mg/mL but showed progressive inhibition above 1.25 mg/mL, reaching 50% inhibition at 10 mg/mL. Aerial growth was significantly inhibited (37.94%) even at 0.625 mg/mL, with inhibition reaching 71.7% at 10 mg/mL. Root growth followed a similar trend, with inhibition reaching 74.13% at 10 mg/mL. Seedling hydration was reduced, ranging from 66.87% to 71.37%, indicating that H2TMIPP negatively affects lentil seedling growth and hydration.

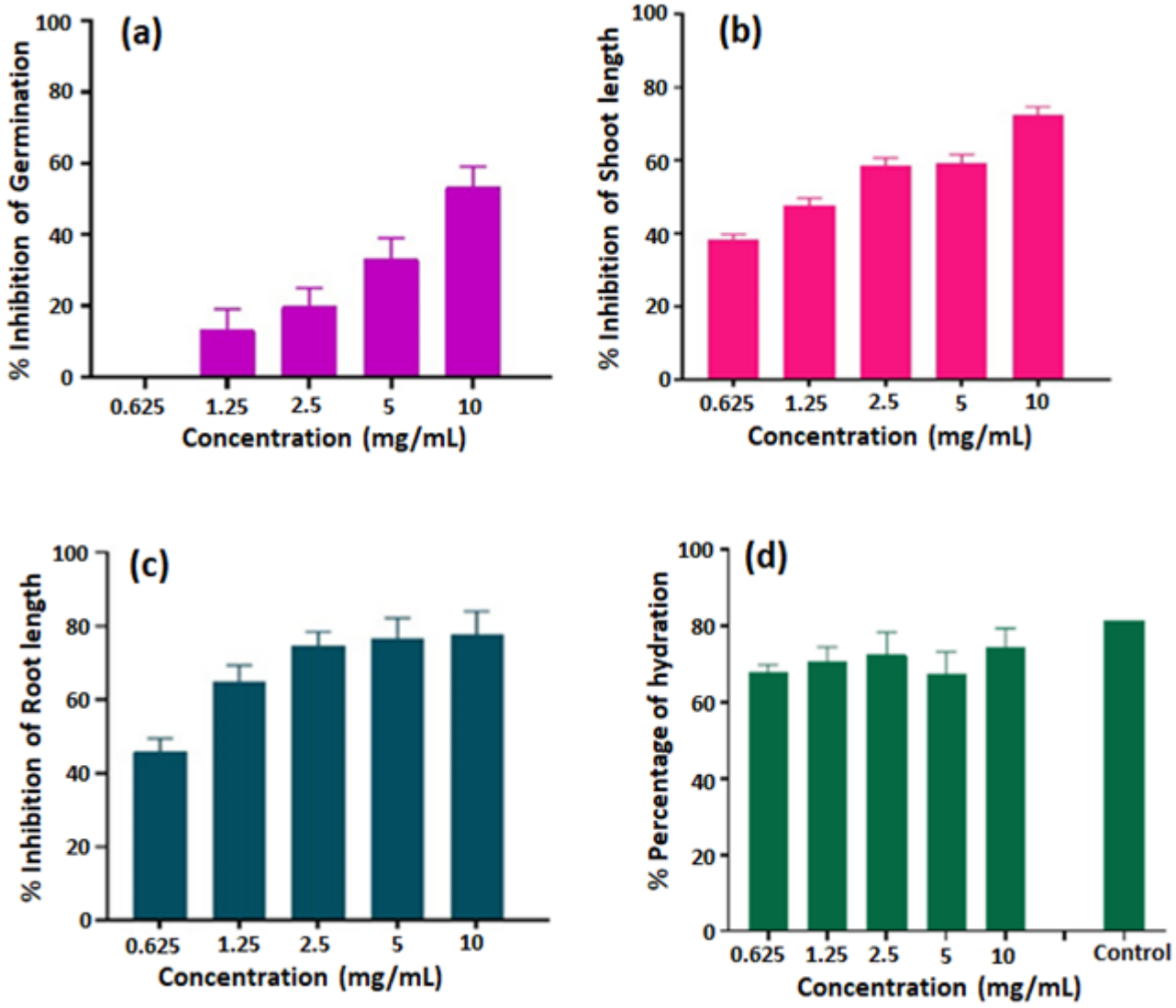


**Fig. 2** Allelopathic effects of porphyrin $H_2$TMIPP (1) on the germination (a), shoot length (b), root length (c), and hydration (d) of Lens culinaris Medik (lens). Significant difference, one-way ANOVA, $p < 0.05$.

## 1. CONCLUSION

In conclusion, a new meso-tetraarylporphyrin, $H_2$TMIPP (1), was successfully synthesized and characterized using NMR, IR, UV/Vis, fluorescence, high-resolution ESI mass spectrometry, and single-crystal X-ray diffraction. The antioxidant activity of $H_2$TMIPP was tested using the DPPH assay, showing weak scavenging properties compared to ascorbic acid. The compound demonstrated moderate antifungal activity against *C. albicans*, *C. glabrata*, and *C. tropicalis* using disk diffusion and microdilution methods, compared to Amphotericin B. Additionally, $H_2$TMIPP exhibited notable allelopathic effects on lentil seeds, including 50% inhibition of germination, 71.7% inhibition of aerial growth, 74.13% inhibition of root growth, and a hydration percentage between 66.87% and 74.13%, highlighting its potential allelopathic properties.

## REFERENCES

1. Chen, J.-J.; Hong, G.; Gao, L.-J.; Liu, T.-J.; Cao, W.-J. In vitro and in vivo antitumor activity of a novel porphyrin-based photosensitizer for photodynamic therapy, J. Cancer Res. Clin. Oncol. 2015, 141, 1553–1561. DOI: 10.1007/s00432-015-1918-1.

2. Campestrini, S.; Tonellato, U. Photoinitiated Olefin Epoxidation with Molecular Oxygen, Sensitized by Free Base Porphyrins and Promoted by Hexacarbonylmolybdenum in Homogeneous Solution. Eur. J. Org. Chem. 2002, 3827–3832. DOI: 10.1002/1099-0690(200211)2002:22<3827::AID-EJOC827>3.0.CO;2-Z.

3. Norvaiša, K.; Kielmann, M.; Senge, M.O. Porphyrins as Colorimetric and Photometric Biosensors in Modern Bioanalytical Systems. ChemBioChem 2020, 21, 1793–1807. DOI:10.1002/cbic.202000067.

4. Tang, F.; Wu, J.; Lin, Z.; Wu, H.; Peng, X. A free base porphyrin as an effective modifier of the cathode interlayer for organic solar cells. Appl. Surf. Sci. 2023, 635, 157720. DOI:10.1016/j.apsusc.2023.157720.

5. Roucan, M.; Kielmann, M.; Connon, S.J.; Bernhard, S.S.R.; Senge, M.O. Conformational control of nonplanar free base porphyrins: towards bifunctional catalysts of tunable basicity. Chem. Commun. 2018, 54, 26–29. DOI: 10.1039/C7CC08099A.

6. Torres, P.; Guillén, M.; Escribà, M.; Crusats, J.; Moyano, A. Synthesis of New Amino-Functionalized Porphyrins: Preliminary Study of Their Organophotocatalytic Activity. Molecules 2023, 28, 1997. DOI: 10.3390/molecules28041997.

7. Adler, A.D.; Longo, F.R.; Finarelli, J.D.; Goldmacher, J.; Assour, J.; Korsakoff, L. A simplified synthesis for meso-tetraphenylporphine. J. Org. Chem. 1967, 32, 476–476. DOI: 10.1021/jo01288a053.

8. Wagner, R.W.; Lawrence, D.S.; Lindsey, J.S. An improved synthesis of tetramesitylporphyrin. Tetrahedron Lett. 1987, 28, 3069–3070. DOI: 10.1016/S0040-4039(00)96287-7.

# Pepper seeds polysaccharide: Extraction, structural characterization, and biological assesment

**Zeineb Mzoughi [a], Manel Sfar [a], Houda Lazreg [b], Didier Le Cerf [c], Hatem Majdoub [a]**

(a) *University of Monastir, Laboratory of Interfaces and Advanced Materials, Faculty of Sciences of Monastir, Monastir 5000, Tunisia*
(b) *University of Monastir, Laboratory of Genetics, Biodiversity and Bioresource Valorization, Higher Institute of Biotechnology of Monastir, 5000, Monastir, Tunisia*
(c) *Normandie Univ, UNIROUEN, INSA Rouen, CNRS, PBS, UMR 6270 & FR 3038, 76000 Rouen, France*
*E-mail: mzoughizeineb.lima@gmail.com; zeineb.mzoughi@fsm.rnu.tn*

## ABSTRACT

Currently, the high added-value compounds contained in plant by-products and wastes offer a wide spectrum of opportunities for their reuse and valorization, contributing to the circular economy. These biowastes contain a great level of marketable bio-products extracted for added-value products such polysaccharides. Current study deals with polysaccharide extraction from chili pepper (Capsicum annuum) seeds waste (CAP) using ultrasonic extraction technique. The extracted polysaccharide was characterized using Fourier Transform Infrared Spectroscopy (FTIR) analysis, UV_vis, Size Exclusion Chromatography (SEC/MALS/DRI), GC-MS after hydrolysis and NMR. Polysaccharide from Capsicum annuum (CAP) seeds was composed of galactose, glucose arabinose, rhamnose, xylose, mannose and fructose in molar percentage of 64.5 %, 7.0 %, 4.7%, 2.9 %, 2.6 %, 7.2 % and 11.1 %, respectively with a weight average molecular weight of 480 kDa and a large dispersity. Finally, results showed that Capsicum annuum seeds polysaccharide presents strong antioxidant activities and an interesting antiglycation and α-amylase inhibitory properties.

**KEYWORDS:** pepper seeds, by-products valorization, polysaccharides, ultrasonic-assisted extraction, protein glycation, α-amylase.

## 1. Introduction

Red chili pepper (*Capsicum annuum* L.) is one of the most widely grown, cultivated and consumed fruit vegetable in the world mainly as spice. In Tunisia, pepper (*capsicum annuum* L.) is an economically important crop coming right after tomato and potato in terms of cropped vegetable areas, of about 20 000 ha, and with an average production of about 346 000 tons during the last five years [1]. It is widely grown in all Tunisian regions both in the field and under greenhouses and occupies the 4$^{th}$ largest area planted by gardening [2].These crops ensure a continuous supply of pepper market and Tunisia ranking as one of the major of pepper producers and exporters in Africa [3]. The red pepper variety (*Capsicum annum* L.) is highly demanded by the global food industry. After processing, a by-product is produced, which amounts to approximately 65% in weight of raw material. It is currently disposed of as municipal solid waste [4]. Pepper seed is a by-product from the processing of pepper products such as pepper power, pepper paste, chopper pepper, and chili pepper, among others [5-8]. Substantial quantities of pepper seeds are generated annually account for 450-500 g kg$^{-1}$ of the total pepper weight and often are ignored [9], and these by-products are usually disposed and regarded as solid waste [5, 7, 10], which created a major problem and aggravated the industry's burden on the treatment of waste concurrently leading to the environment pollution . It is expensive to handle, transport and dispose this waste, to date, these solid wastes pepper seed resources have not been fully utilized. Nevertheless, similar to pepper fruits, pepper seeds are also a promising source of nutritional constitutes and bioactive compounds such as phenolics and capsaicinoids, which can be used for its nutritional properties and biological potential [7, 10].

Polysaccharides are natural carbohydrate used in the field of food, cosmetics and medicines due to their therapeutic effect, biodegradability and low toxicity [11]. Likewise, polysaccharides have been reported to play an important biological activities in relation with their structural features such as free radical scavengers [12] and antidiabetic proprieties [13].

Diabetes mellitus (DM), a chronic metabolic disease, can induce many types of diabetic complications such as atherosclerosis, a variety of neuropathies, blindness and end-stage renal failure [14]. DM usually manifests as the persistent elevation in both fasting and postprandial glucose levels, which results in disturbances of carbohydrate, lipid and protein metabolism [15]. Alpha-amylase is an enzyme that hydrolyses the polysaccharides to oligosaccharides. Thus, the inhibitors of α-amylase can delay glucose absorption and prevent postprandial blood glucose level elevation [16, 17]. In fact, several studies showed that polysaccharides have a confirmed α-amylase inhibitory activity [18-20]. Likewise, this activity is strongly influenced by the monosaccharide composition and molecular weight distribution. In addition, several studies revealed that polysaccharide with high molecular weight and high glucose content exhibited enhanced inhibitory activity against amylase [21, 22]. Therefore, identifying a novel inhibitor of α-amylase activity with good antioxidant properties would constitute a good therapeutic and preventive target for human health.

Conventional techniques to obtain polysaccharides, such as heating, boiling, or refluxing, usually require long extraction time and high extraction temperature, but the extraction efficiency was low [23]. Recently, the use of ultrasonic-assisted extraction of constituents from different materials has been shown to have tremendous research potential. Compared with traditional methods, this extraction approach has many advantages, such as shorter extraction time, use of less solvent and higher extraction rate [24, 25]. So far, it has been widely employed to extract polysaccharides from different materials with great extraction efficiency [26]. This great extraction efficiency by ultrasonic treatment is mainly attributed to its mechanical effects, which greatly facilitate mass transfer between immiscible phases through a super agitation [27].

To the best of our knowledge, there has been no information regards the optimization of ultrasonic-assisted extraction of polysaccharides from *capsicum annum* L. seeds by RSM. In this study, the ultrasonic-assisted extraction parameters (ratio of liquid to solid, extraction temperature and time) of polysaccharides from *capsicum annum* L. seeds was firstly investigated and optimized using a three-level, three-variable Box–Behnken design (BBD). NMR, GCMS, SEC, UV and FTIR analysis were performed to characterize the extracted pepper polysaccharide structure. Antioxidant, antiglycation and α-amylase inhibitory effect of polysaccharide was also determined

## 2. Materials and methods

### 2.1. Plant materials

Tunisian variety of *Capsicum annum* L. (*Solanaceae* family) were purchased in June 2020, from the region of Korba in the northeast of Tunisia; latitude 36340 38.22″(N); longitude 10510 29.63″(E) and the altitude is 637 m. Plant identification was carried by a botanist. After that, seeds were collected from pepper fruit, milled to obtain a thin powder, defatted with petroleum ether (20% (w/v)) for 4 h and then left to dry at 40°C for 48h to obtain the defatted pepper seeds flour.

### 2.2. Polysaccharides ultrasonic-extraction process

The powder of *Capsicum annum* seeds was firstly extracted with 80% ethanol for 24 hours to remove interference components such as monosaccharide, disaccharide, oligosaccharide and polyphenols in the samples. Extraction of polysaccharides was performed by the method of Xie, Shen, Nie, Li and Xie (2011) with some modifications. The polysaccharide was extracted with aqueous solution processed according to a Box-Behnken design (BBD) with 3 variables and the ultrasonic treatment (KQ2200E, Kunshan Ultrasonic Instrument Co.,Jiangsu, China) was performed with an ultrasonic

power (80–160 W), extraction temperature (30–70 ◦C), extraction time (20–100 min) and water-to-raw material ratio (5–25 mL/g).

The sonicated mixture was centrifuged at 4000 rpm for 15 min, and the supernatant was collected, deproteinized by Sevag method, dialyzed and freeze-dried to obtain CAP. The polysaccharides extraction yield (%) is calculated as follows:

Extraction yield (%) = $(W_0/W) \times 100$ (1)

where Wo (g) is the dried CAP weight and W (g) is the dried powder of pepper seeds weight.

## 3. Results and discussion

### 3.1. Procedure optimization

#### 3.1.1. Statistical analysis and model fitting

The main purpose of this part is to evaluate the impact of the selected variables on the isolation yield of CAP polysaccharide, with the objective of determining the optimal conditions. The process variables for the extraction yield at different conditions: ultrasonic power ($X_1$), liquid–solid ratio ($X_2$), extraction time ($X_3$), and the experimental and predicted data are presented in **Table 1**. The results of quadratic model fitting within the data are summarized in **Table 2**. ANOVA for lack of fit test was insignificant ($p>0.05$), suggesting that the model fitted, adequately, the experimental data. Additionally, the $R^2$ value (0.9839) of the extraction yield proved that there is a significant correlation degree between response and variables.

**Table. 1.** Process variables and their ranges

| **Factors** | **Symbol** | **Levels** | | |
|---|---|---|---|---|
| | | -1 | 0 | 1 |
| **Power (W)** | $X_1$ | 50 | 100 | 150 |
| **Temperature (°C)** | $X_2$ | 40 | 65 | 90 |
| **Extraction Time (min)** | $X_3$ | 5 | 20 | 35 |

**Table.2.** Box -Behnken design with independent variables for the extraction yield of pepper seeds polysaccharide

| **Experiments** | **Independent variables** | **Responses** |
|---|---|---|

| | Power (W), $X_1$ | Temperature (°C), $X_2$ | Time (min), $X_3$ | Y (%) | |
|---|---|---|---|---|---|
| | | | | Experimental yield | Predicted yield |
| **1** | 50(-1) | 40(-1) | 20(0) | 08.01 | 10.23 |
| **2** | 150(1) | 40(-1) | 20(0) | 08.82 | 12.78 |
| **3** | 50(-1) | 90(1) | 20(0) | 08.47 | 09.46 |
| **4** | 150(1) | 90(1) | 20(0) | 10.59 | 11.41 |
| **5** | 50(-1) | 65(0) | 5(-1) | 10.16 | 08.85 |
| **6** | 150(1) | 65(0) | 5(-1) | 11.41 | 11.91 |
| **7** | 50(-1) | 65(0) | 35(1) | 10.23 | 12.78 |
| **8** | 150(1) | 65(0) | 35(1) | 11.90 | 10.23 |
| **9** | 100(0) | 40(-1) | 5(-1) | 08.72 | 10.04 |
| **10** | 100(0) | 90(1) | 5(-1) | 10.20 | 08.44 |
| **11** | 100(0) | 40(-1) | 35(1) | 09.49 | 12.78 |
| **12** | 100(0) | 90(1) | 35(1) | 10.02 | 08.04 |
| **13** | 100(0) | 65(0) | 20(0) | 12.81 | 08.70 |
| **14** | 100(0) | 65(0) | 20(0) | 12.88 | 12.78 |
| **15** | 100(0) | 65(0) | 20(0) | 12.70 | 10.16 |
| **16** | 100(0) | 65(0) | 20(0) | 12.80 | 12.78 |
| **17** | 100(0) | 65(0) | 20(0) | 12.73 | 10.56 |

### 3.1.2. Response surface investigation

The expression of the correlation model between the theoretical response and operational conditions in term of coded variable was expressed by the flowing second -order polynomial equation:

$$Y\ (\%) = 21.91 + 5.42\ X_1 + 1.53\ X_2 - 1.27\ X_3 + 2.08\ X_1\ X_2 - 2.44\ X_1\ X_3 + 0.2375\ X_2\ X_3 - 6.67\ X_1^2 - 0.3025\ X_2^2 + 1.55\ X_3^2$$

Statistically, the F-test and p-value were used to evaluate the significance of regression model. As indicated in Table 2, low p-value (0.001) and the value of predicted $R^2$ testify the validity of the model [29]. Moreover, the low value of variation coefficient (C.V.%) and the relatively high value of Adeq precision revealed a more efficient precision of the trial values and a high reliability degree [30]. Contour plot 3D and graphic surface were plotted for the polysaccharide extraction yield from *Capsicum annum* seeds (**Fig. 1**).

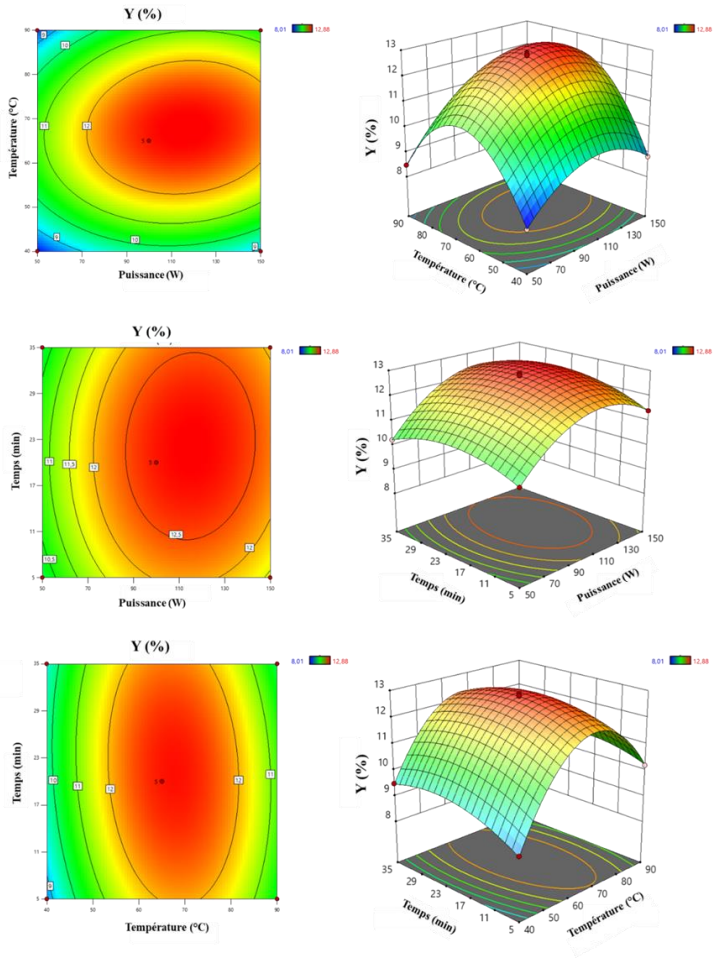


**Fig.1.** Response surface plots 2D (right) and contour plots 3D (left) representing the effect of process variables on extraction polysaccharide yield from pepper seeds ($Y_{CAP}$, %)

### 3.1.3. Determination of the optimal extraction conditions

This method aims to determine the level of trial parameters which potentially allow s reaching the highest extraction yield of polysaccharides. Therefore, the optimal parameters were as follows: ultrasonic power was 686.57 W, liquid–solid ratio was 43.33 mL/g and extraction time was 1.27 min. Under these conditions, the experimental extraction yield was 26.51%, in accordance with the predicted value (25.91%).

## 4. Conclusion

In this research, polysaccharides were effectively isolated, through ultrasonic assisted extraction, from Tunisian pepper seeds. Furthermore, the characterization via FTIR, NMR and UV-vis revealed that CAP was a polysaccharide containing arabinose, galactose, mannose, rhamnose, glucose and xylose. CAP exhibit a flexible chain conformation and has a weight average molecular mass of 480 000 g/mol with a dispersity of 14.8 due to presence of aggregates. Moreover, CAP has an evident antioxidant, anti-glycation and α-amylase inhibitory effects. Thus, CAP might be a novel source of natural antioxidant with potential value for health food and for therapeutics.

## REFERENCES

[1] S. Mannai, H. Jabnoun-Khiareddine, B. Nasraoui, M. Daami-Remadi, Biocontrol of Pythium Damping-Off on Pepper (Capsicum Annuum) with Selected Fungal and Rhizobacterial Agents, International Journal of Phytopathology 9(1) (2020) 29-42.
[2] Z. Kaouther, B.F. Mariem, M. Fardaous, H. Cherif, Impact of salt stress (NaCl) on growth, chlorophyll content and fluorescence of Tunisian cultivars of chili pepper (Capsicum frutescens L.), Journal of Stress Physiology & Biochemistry 8(4) (2012).
[3] F. Stat, Food and Agriculture organization statistics, Tunisia, 2013.
[4] A. Romo-Hualde, A. Yetano-Cunchillos, C. González-Ferrero, M. Sáiz-Abajo, C. González-Navarro, Supercritical fluid extraction and microencapsulation of bioactive compounds from red pepper (Capsicum annum L.) by-products, Food Chemistry 133(3) (2012) 1045-1049.
[5] M. Li, X. Wen, Y. Peng, Y. Wang, K. Wang, Y. Ni, Functional properties of protein isolates from bell pepper (Capsicum annuum L. var. annuum) seeds, LWT 97 (2018) 802-810.
[6] E. Firatligil-Durmus, O. Evranuz, Response surface methodology for protein extraction optimization of red pepper seed (Capsicum frutescens), LWT-Food Science and Technology 43(2) (2010) 226-231.
[7] J. Sung, M.-H. Bang, J. Lee, Bioassay-guided isolation of anti-adipogenic compounds from defatted pepper (Capsicum annuum L.) seeds, journal of functional foods 14 (2015) 670-675.
[8] G. Jeon, Y. Choi, S.M. LEE, Y. Kim, M. Oh, H.S. JEONG, J. Lee, Antioxidant and antiproliferative properties of hot pepper (Capsicum annuum L.) seeds, Journal of Food Biochemistry 36(5) (2012) 595-603.
[9] W. Jinyan, W. Yuqi, L. ZHENG, N. Shifeng, F. Zhaoyun, Y. Ruiqing, C. Kaixun, Kinetic study on extraction of red pepper seed oil with supercritical CO2, Chinese Journal of Chemical Engineering 22(1) (2014) 44-50.
[10] Y. Zou, K. Ma, M. Tian, Chemical composition and nutritive value of hot pepper seed (Capsicum annuum) grown in Northeast Region of China, Food science and technology 35 (2015) 659-663.
[11] K. Alba, A.P. Laws, V. Kontogiorgos, Isolation and characterization of acetylated LM-pectins extracted from okra pods, Food Hydrocolloids 43 (2015) 726-735.
[12] M.A. Chaouch, J. Hafsa, C. Rihouey, D. Le Cerf, H. Majdoub, Effect of pH during extraction on the antioxidant and antiglycated activities of polysaccharides from opuntia ficus indica, Journal of Food Biochemistry 40(3) (2016) 316-325.
[13] H. Jiang, Y. Xu, C. Sun, M. Adu-Frimpong, J. Yu, W. Deng, X. Xu, Physicochemical properties and antidiabetic effects of a polysaccharide obtained from Polygonatum odoratum, International Journal of Food Science & Technology 53(12) (2018) 2810-2822.
[14] R. Simpson, G.A. Morris, The anti-diabetic potential of polysaccharides extracted from members of the cucurbit family: A review, Bioactive Carbohydrates and Dietary Fibre 3(2) (2014) 106-114.
[15] T. Chen, M. Zhang, J. Li, M.M. Surhio, B. Li, M. Ye, Structural characterization and hypoglycemic activity of Trichosanthes peel polysaccharide, LWT 70 (2016) 55-62.
[16] K.-T. Kim, L.-E. Rioux, S.L. Turgeon, Alpha-amylase and alpha-glucosidase inhibition is differentially modulated by fucoidan obtained from Fucus vesiculosus and Ascophyllum nodosum, Phytochemistry 98 (2014) 27-33.
[17] B.T. Trinh, D. Staerk, A.K. Jäger, Screening for potential α-glucosidase and α-amylase inhibitory constituents from selected Vietnamese plants used to treat type 2 diabetes, Journal of ethnopharmacology 186 (2016) 189-195.
[18] C. Wang, R.K. Santhanam, X. Gao, Z. Chen, Y. Chen, C. Wang, L. Xu, H. Chen, Preparation, characterization of polysaccharides fractions from Inonotus obliquus and their effects on α-amylase, α-glucosidase activity and H2O2-induced oxidative damage in hepatic L02 cells, Journal of Functional Foods 48 (2018) 179-189.
[19] S. Wu, M. Lai, J. Luo, J. Pan, L.-M. Zhang, L. Yang, Interactions between α-amylase and an acidic branched polysaccharide from green tea, International journal of biological macromolecules 94 (2017) 669-678.

[20] S. Amamou, H. Lazreg, J. Hafsa, H. Majdoub, C. Rihouey, D. Le Cerf, L. Achour, Effect of extraction condition on the antioxidant, antiglycation and α-amylase inhibitory activities of Opuntia macrorhiza fruit peels polysaccharides, Lwt 127 (2020) 109411.
[21] H.-F. Tan, C.-Y. Gan, Polysaccharide with antioxidant, α-amylase inhibitory and ACE inhibitory activities from Momordica charantia, International journal of biological macromolecules 85 (2016) 487-496.
[22] Y. Xu, Y. Guo, Y. Gao, X. Niu, L. Wang, X. Li, H. Chen, Z. Yu, Y. Yang, Seperation, characterization and inhibition on α-glucosidase, α-amylase and glycation of a polysaccharide from blackcurrant fruits, Lwt 93 (2018) 16-23.
[23] N. Tsochatzidis, P. Guiraud, A. Wilhelm, H. Delmas, Determination of velocity, size and concentration of ultrasonic cavitation bubbles by the phase-Doppler technique, Chemical engineering science 56(5) (2001) 1831-1840.
[24] X. Chen, W. Wang, S. Li, J. Xue, L. Fan, Z. Sheng, Y. Chen, Optimization of ultrasound-assisted extraction of Lingzhi polysaccharides using response surface methodology and its inhibitory effect on cervical cancer cells, Carbohydrate Polymers 80(3) (2010) 944-948.
[25] X.-q. Chen, Y. Zhang, Ultrasonic-associated extraction of water soluble polysaccharides from defatted Korean pine kernel, Journal of Forestry Research 18(2) (2007) 133-135.
[26] J.-H. Xie, M.-Y. Shen, M.-Y. Xie, S.-P. Nie, Y. Chen, C. Li, D.-F. Huang, Y.-X. Wang, Ultrasonic-assisted extraction, antimicrobial and antioxidant activities of Cyclocarya paliurus (Batal.) Iljinskaja polysaccharides, Carbohydrate polymers 89(1) (2012) 177-184.
[27] K. Zhong, Q. Wang, Optimization of ultrasonic extraction of polysaccharides from dried longan pulp using response surface methodology, Carbohydrate polymers 80(1) (2010) 19-25.
[28] S. Adisakwattana, Cinnamic acid and its derivatives: mechanisms for prevention and management of diabetes and its complications, Nutrients 9(2) (2017) 163.
[29] J.P. Maran, V. Sivakumar, R. Sridhar, V.P. Immanuel, Development of model for mechanical properties of tapioca starch based edible films, Industrial Crops and Products 42 (2013) 159-168.
[30] Z. Mzoughi, A. Abdelhamid, C. Rihouey, D. Le Cerf, A. Bouraoui, H. Majdoub, Optimized extraction of pectin-like polysaccharide from Suaeda fruticosa leaves: Characterization, antioxidant, anti-inflammatory and analgesic activities, Carbohydrate polymers 185 (2018) 127-137.

# E-poster Presentations

# Environment and Climate Changes

# Climate change effects on stucture and diversity of benthic fauna associated with *Zostera noltei* meadows in the Gulf of Gabès

**Nawfel Mosbahi[a], Lassad Neifar[a], Jean-Claude Dauvin[b]**

*(a) Laboratoire de Biodiversité Marine et Environnement, Faculté des Sciences de Sfax, Université de Sfax, BP 1171, 3038 Sfax, Tunisie*
*(b) Université de Caen Normandie, UNICAEN, Laboratoire Morphodynamique Continentale et Côtière, CNRS, UMR 6143 M2C, 24*
*(c) Rue des Tilleuls, 14000 Caen, France*

*Email: nawfel.mosbahi.etud@fss.usf.tn*

**ABSTRACT**

Marine macrophytes are the most productive and diverse coastal marine ecosystems on the planet. These ecosystems provide nursery grounds and food for fish and invertebrates, coastline protection from erosion, carbon sequestration, and nutrient fixation. For marine macrophytes, temperature is generally the most important range limiting factor, and ocean warming is considered the most severe threat among global climate change factors. To assess the effects of climate change on *Zostera noltei* meadows in the Gulf of Gabès, the present work study the structure, the spatial and temporal variation of the macrobenthic communities associated with intertidal *Z.noltei* seagrass beds. Samples were collected on 8 stations during twelve years (2012 to 2024) during the spring periods. A total of 204 macrobenthos taxa associated with intertidal *Zostera noltei* beds are identified from the 8 stations during the all sampling campaigns, with a taxonomic dominance of crustaceans (38%), molluscs (23%) and annelids (25%). Abundance varies from 2244 to 16,844 ind·m$^{-2}$ with a mean value of 6,142 ind·m$^{-2}$. Analysis of the trophic structure shows that the majority of stations are strongly represented by carnivores (40%), followed by the non-selective deposit feeders (18%). The benthic diversity indices indicated notable annual variations, characterized by an increase in species diversity alongside a low individual density. The multivariate analysis (ANOSIM and BIOENV) further revealed a significant presence of alien species over the past three years, which positively correlated with fluctuations in environmental conditions, such as temperature changes in the Gulf of Gabès. These results highlight the significant impacts of climate change on benthic fauna in the Gulf of Gabès. This is further evidenced by the decline of *Z. noltei* habitat and the increasing dominance of the Lessepsian seagrass *Halophila stipulacea* in the intertidal zones of the Gulf of Gabès.

**KEYWORDS:** Climate change, *Zostera noltei*, Macrobenthic fauna, Gulf of Gabès.

# Impact of operating conditions, membrane properties and plant design on the energetic performance of vacuum membrane distillation desalination

**Rihab MILADI[a], Nader FRIKHA[a], Slimane GABSI[a]**

*(a) Laboratory Energy, Water, Environment and Process, (University of Gabes, National Engineering School of Gabes, Street Omar Ibn ElKhattab, 6029 Gabes, Tunisia)*
*E-mail: rihab.miladi@outlook.com*

## ABSTRACT

Membrane distillation (MD) is an emerging technology desalinating highly concentrated solutions. This technology has many advantages over other desalination processes. Indeed, MD can be coupled with solar energy, allowing for the production of clean water in a sustainable way. However, its energy efficiency is relatively low compared to other desalination processes that have reached industrial scale. In this study, we aim to quantify how membrane properties, process conditions, and plant design affect the energetic performance of vacuum membrane distillation. The results show that specific energy consumption decreases significantly with the increase of the vacuum level and feed temperature. In addition, it has been proven that the optimal rejection rate is between 5 and 10% for more efficient energy use in the installation. Furthermore, the distillation of waste streams has considerably improved the performance of the system, leading to an increase in productivity of 32%, a reduction in specific average energy consumption from 610 kWh/$m^3$ to 463 kWh/$m^3$, and a decrease in the specific cost of water production from 17.9 \$/$m^3$ to 15.9 \$/$m^3$. Additionally, multi-stage technology has proved highly effective in reducing specific energy consumption by up to 200 kWh/$m^3$ for systems with more than five stages.

**KEYWORDS :** Vacuum membrane distillation , Energetic performance, Optimization, Seawater,.

# Preparation and characterization of activated carbons derived from Prickly Pear Seeds through chemical activation using $H_3PO_4$.

**Maryi Teieb [a], Hatem Dhaouadi [a], Sonia Dridi-Dhaouadi [a, b]**

*(a) Research Laboratory of Environmental Chemistry and Clean Processes Faculty of Sciences, University of Monastir, Monastir, Tunisia*
*(b) Preparatory Institute for Engineering Studies, University of Monastir, Tunisia;*
*E-mail:meryiteyeib@gmail.com*

## ABSTRACT

Essential oils are important in the cosmetic industry because of their wide range of aromatic and healing properties. These natural extracts are commonly included in perfumes, lotions, and creams, offering pleasant scents as well as skin-enhancing and wellness-promoting benefits. The Prickly Pear seed oil is highly intriguing due to its classification as an edible oil, possessing a significant level of unsaturation along with antioxidant, antimicrobial, and biological properties. Nevertheless, after extracting essential oils, prickly pear seeds have the potential to be converted into cost-effective adsorbents with high adsorption performances for the removal of different pollutants. To accomplish this goal, the conversion of biomass to activated carbon is essential to enhance its adsorption efficiency. SC-PPSAC was prepared by chemical activation with 3M orthophosphoric acid ($H_3PO_4$). The chemical activation process was carried out using two impregnation ratios (1 and 2) and final carbonization temperatures (300–500 °C). An examination was conducted on the effects of carbonization temperature and impregnation ratio on the iodine number, methylene blue (MB) value, and yield of the activated carbon. The optimal conditions were established to be: an activation temperature of 400 °C and an impregnation ratio was 2. Then, SC-PPSAC was synthesized with a carbonization temperature of 400 °C, at a carbonization time of 1h, and an impregnation ratio of 2/1 (w/w). Under ideal circumstances, the iodine number was 1111.25 mg/g, the MB value was 17.5 mg/g and the yield was 53.55%.

**KEYWORDS:** Prickly Pear seed, Chemical activation, Orthophosphoric acid, Activated Carbon.

# Enhancing Thermal Performance of Parabolic Trough Solar Collector by Internal Inserted Fins and External Metallic Layer

**Anissa GHOMRASSI[a], Hatem MHIRI[a], Philippe BOURNOT[b]**

*(a) Thermal and Thermodynamics Laboratory in Industrial Processes, National Engineering School of Monastir, Tunisia*
*(b) IUSTI, UMR CNRS 6595, Château-Gombert technopole, 5 Enrico Fermi street, Marseille 13013, France*
*E-mail: ghomrassi.anissa@hotmail.com*

## ABSTRACT

In this paper, the impact of inserts with various shapes on the thermal performance of a cylindro-parabolic collector is studied numerically.

To conduct this study in-depth, the adopted method consists of two major steps. In the first step, the concentrated solar heat flux densities in a focal area are calculated using the SOLTRACE software. In the second step, CFD simulations are carried out to analyze and optimize the thermal performance of the receiver tube. The heat flux densities calculated by SOLTRACE are used as thermal boundary conditions for the receiver tube. A series of numerical simulations was performed for four absorber tubes.

The results show that the Nusselt number increases for tubes with inserts compared to smooth tubes. This is due to enhanced heat transfer resulting from vortex generation, rapid exchange, and improved mixing within the flow. All modified models exhibit a more uniform temperature distribution than the smooth absorber tube, where the inserted fins ensure proper mixing of heat flux between the heated wall (receiving concentrated solar power) and the cold fluid region (upper wall exposed to direct solar flux).

**KEYWORDS :** Parabolic trough collector, inserted fins, CFD, performance enhancement.

# New Ventilation Technique to Prevent Sewer Blockages

**Hella ADOUNI[a], Yoldoss CHOUARI[a], Hervé BOURNOT[b], Wassim KRIAA[a], Hatem MHIRI[a]**

*(a) LTTPI, National Engineering School of Monastir, University of Monastir, Tunisia*
*(b) Aix Marseille University, CNRS, IUSTI, Marseille, France*
*E-mail: hella.adouni2@gmail.com*

## ABSTRACT

Blockages in sewer systems are a significant issue, leading to flooding and posing risks to both public safety and the environment. Existing obstructions, such as tree roots intruding into pipes, can make these situations worse. This article suggests a new method to prevent blockages in confined sewer channels, particularly those with blocks attached to the ceiling. The proposed solution uses a ventilation technique involving inclined jets of air injected along the channel walls.

To understand how this technique works, numerical simulations were carried out using the Volume of Fluid (VOF) model, a multiphase flow model that can simulate the movement of different fluids, such as air and water, within a system. The study focused on air-water flow in horizontal channels that have a block on the ceiling, which can cause blockages. The research introduced a lateral ventilation method using two parietal (wall-mounted) jets, which partially alleviated the blockage problem by preventing the formation of the first slug at the channel's entrance. By extending this method with additional jets placed side-by-side along the entire length of the channel, the blockage phenomenon was completely eliminated. This finding is particularly important for preventing floods and overflows in sewer systems.

In conclusion, the study shows that the new ventilation technique with inclined parietal jets is an effective strategy for dealing with blockages in sewer channels, especially those with ceiling blocks. By strategically positioning these jets along the channel, it is possible to prevent or completely eliminate blockages, thereby enhancing the efficiency of sewer systems and reducing the risk of flooding and environmental damage.

**KEYWORDS:** Blockage phenomenon, Ceiling blocks, Lateral Ventilation, Confined flow.

# Retrospective study of clinical and immunohistochemical parameters of lung cancer in the Gafsa mining basin

**Raoudha Sadraoui[a], Monia Saidi[a], Imen Kallel[b]**

*(a) Laboratory of Biotechnology and Bio-monitoring of the Environment and Oasis Ecosystems - Department of Life Sciences - Faculty of Sciences of Gafsa, City Zarroug 2112-Gafsa-Tunisia. .*
*(b) Research Laboratory of Environmental ToxicologyMicrobiology and Health (LR17ES06), Faculty of Sciences, University of Sfax,3038 Sfax, Tunisia*
*sadraouiraoudha@yahoo.fr*

## ABSTRACT

The present study is based on a retrospective study of lung cancer in the Gafsa mining basin region. This epidemiological study affected 110 patients (97 men and 13 women) whose average age was 59 ±10 years. The largest age groups for both women and men were 60-70 and 50-60 respectively. Geographically, patients are concentrated in mining centers (Mdhila (23.64%) and Métlaoui (20.91)). Over 79% of patients smoke and 20% are alcoholics.

The histological study highlights that non-small cell lung cancer (NSCLC) was the most represented (94.85%) and its two subtypes, namely adenocarcinoma (52.58%) and squamous cell carcinoma (39). 17%). Small cell lung cancer (SCLC) presented only 5.15% of patients and large cell carcinoma represented only 3.1%. The TNM classification of patients showed that more than 64% had a tumor of size T4, 42.6% had metastasized nodules (N2). While 63% presented metastatic extension.

The therapeutic modalities were mainly chemotherapy (21%) and radiotherapy (32.1%) with a combination of chemotherapy and radiotherapy of 18.51%. The correlations between the parameters (markers and metastasis; tumor types: metastasis, smoking status, alcoholic status) are statistically not significant. Five different groups of patients were distinguished using a multidimensional analysis that was based on 13 main variables and the PCA and the HAC.

**KEYWORDS:** Broncho-pulmonary cancer, TNM, Histological type, Multidimensional analysis

# Clean Processes and Renewable Energy

# Investigation of the corrosion inhibition efficiency of eutectic solvents as a function of concentration and their impact on sustainable chemistry

**Aya GUELLOUT [a], Ilhem KAABI[b], Meriem GUELLOUT[c] , Yacine BENGUERBA[d]**

[a] *Department of Process Engineering, Faculty of Technology, Ferhat Abbas University of Setif, Setif, 19000,* ***Algeria***
[b] *Laboratory of Microbiology, El Manar Tunis University,* ***Tunisia***
[c] *Electrochemistry of Molecular Materials and Complexes Laboratory (LEMMC), University Ferhat Abbas Setif-1, Setif,* ***Algeria****.*
[d] *Biopharmacy And Pharmacotechnics Laboratory (LPBT), Ferhat Abbas Setif 1 University, 19000, Setif,* ***Algeria***
*Email of the corresponding author (ayaguellout93@gmail.com)*

## ABSTRACT

This study introduces an innovative approach to corrosion mitigation by investigating the use of eutectic solvents (ES) as eco-friendly corrosion inhibitors. These solvents, celebrated for their environmentally benign nature and tunable physicochemical properties, offer a sustainable alternative to conventional inhibitors. The research focuses on understanding the impact of ES concentration on their inhibition efficiency in acidic environments. Electrochemical techniques, including Electrochemical Impedance Spectroscopy (EIS) and potentiodynamic polarization, alongside surface characterization methods, were employed to evaluate performance.

The findings reveal a concentration-dependent inhibition efficiency, with optimal concentrations forming a robust and uniform protective layer on the metal surface through synergistic adsorption mechanisms. Conversely, suboptimal concentrations result in diminished protective stability, leading to reduced corrosion resistance. This study underscores the potential of eutectic solvents in advancing sustainable anticorrosion strategies while aligning with green chemistry principles. Future investigations are encouraged to delve into the interaction mechanisms and assess long-term performance in industrial settings.

**KEYWORDS:** Eutectic Solvents, Corrosion Inhibition, Eco-Friendly Chemistry, Electrochemical Analysis, Green Corrosion Strategies

.

# Mathematical modeling of thin-layer draining solar drying of sewage sludge

**Azza MASMOUDI[a], Ahlem BEN SIK ALI[a], Hatem DHAOUADI[b], Hatem MHIRI[a]**

*(a) Laboratory of Thermal and Thermodynamic of industrial processes, National Engineering School of Monastir, Avenue Ibn El Jazzar - 5019 Monastir, Tunisia*

*(b) Laboratory of Environmental Chemistry and Clean Processes, Faculty of Sciences of Monastir, Environment Avenue 5019 Monastir, Tunisia*

*E-mail: azza.masmoudi@gmail.com*

## ABSTRACT

Drying kinetics of sewage sludge in a thin-layer procedure was investigated during the summer season. The experiments were conducted in a lab-scale draining greenhouse by changing the airflow rate. The first one is without ventilation. The other experiments were carried out with increasing the air velocity. The final moisture content was 0.12 kg water /kg DS. The drying time of the sludge layer of 2 cm thickness varied from 3 to 6 days. Then, the drying time decreased by increasing the air velocity. Five established mathematical models were explored to characterize the drying behavior of sewage sludge in thin-layer inside the draining greenhouse. The coefficient of determination $R^2$ and the chi-square parameter $\chi 2$ are two criteria for selecting the appropriate model to the description of the shape of sludge drying kinetics. The Midilli and Kucuk model seems to be the most appropriate to describe the drying curves of sludge with the highest value of determination coefficient and the lowest chi-square parameter.

**KEYWORDS:** Sewage sludge, Draining solar drying, Drying kinetics, Thin-layer, Airflow rate.

# Experimental Study and Evaluation of Single Slope Solar Still Combined With external reflector and sponges

**Jamel Madiouli[a,b], Souhir Mankai[a,b], Fatma Ouled Saad[a,b], Jalila Sghaier[a]**

*(a) Laboratoire de Recherche Thermique et Thermodynamique des Procédés Industriels (LRTTPI), National Engineering School of Monastir, Monastir, Tunisia*

*(b) Higher Institute of Applied Sciences and Technology of Kairouan, Tunisia*

*E-mail: jamel_mad@yahoo.fr*

## ABSTRACT

Freshwater productivity by solar desalination offers promising approach for obtaining clean water from brackish water. However, this technique requires energy improvement to bridge the gap between water demand and water supply. In this work, experimental, energy and economic analysis of single-slope solar stills using external reflector and sponges as wick material was undertaken. For the analysis, three cases were considered, namely Case I: Conventional Solar Still CSS, Case II: Modified Solar Still with sponges and Case III: Modified Solar Still with sponges and external reflector. The results showed that the total accumulated productivity in Case II and Case III improved by 13 % and 34%, respectively, as compared to Case I.

The energy efficiency was found highest for the solar still with sponges and external reflector (Case III). Based on the cost per liter of potable water generated, it can be concluded that the usage of solar still using the sponge material and the mirror as a reflector is a cost-effective option.

**KEYWORDS:** Solar still, Productivity, External reflector, wick material.

# Performance enhancement of the basin type solar still using turbulence system

**Fatma Ouled Saad[a,b], Souhir Mankai[a,b] , Jamel Madiouli[a,b], Jalila Sghaier[a]**

*(a) Laboratoire de Recherche Thermique et Thermodynamique des Procédés Industriels (LRTTPI), National Engineering School of Monastir, Monastir, Tunisia*
*(b) Higher Institute of Applied Sciences and Technology of Kairouan, Tunisia*
*E-mail: ouledsaad_fatma@yahoo.fr*

## ABSTRACT

In order to overcome the low productivity of solar desalination systems, modified solar stills with revolving metallic discs were introduced as a novel distillation mechanism. To improve the system water's evaporative surface and solar radiation exposure, six revolving discs attached on two vertical shafts were placed in the basin. To enhance the turbulence effect and break the water surface tension, metallic rods were fixed on the discs. The system was powered by a DC-motor using a photovoltaic system.

The effect of different discs' rotational velocities (0.025, 0.15, 0.2, 0.5, 1.0, 1.5, 2.0, 2.5, and 4 rpm) on the productivity of the modified solar stills (MSSRDR) were investigated. The best production, with an increase of 94.82%, was obtained by the spinning discs with rods system at 0.5 rpm.

The MSSRDR has a maximum thermal efficiency, which is 29.8%, at 0.5rpm while the efficiency of conventional solar still was only 15%. An economic analysis was carried out to confirm the profitability of the MSSRDR system. The cost of distilled water using the conventional system (CSS) was 0.057 $/L, whereas for the modified system it was 0.054 $/L.

**KEYWORDS:** Solar still efficiency, Thermal solar energy, Water desalination, Productivity enhancement, Rotating Discs with Rods.

# Numerical Study on the Optimization of Wind Capture Efficiency: A Focus on Divergent-Convergent Angles

**Marwa Ezzine[a, c], Hiba cherif [a, c] Zied Guidara[b ,c], Jalila Sghaier[a]**

*(a) Laboratory of Thermal research and Thermodynamics of Industrial Processes (LTTPI), National School of Engineers of Monastir (ENIM), University of Monastir,Road ibn El Jazzar 5019 Monastir, TUNISIA*

*(b) Laboratory of Electro-Mechanic Systems (LASEM), National School of Engineers of Sfax (ENIS), University of Sfax , B.P. 1173, Road Soukra km 3.5, 3038 Sfax, TUNISIA*

*(c) Department of Mechanical Engineering, ISSAT, University of Kairouan, Tunisia*
*Email: marwaezzine26@gmail.com*

## ABSTRACT

Wind energy, a renewable resource, harnesses natural airflows to generate electricity. This paper presents a numerical study focused on optimizing the efficiency of wind capture systems, with particular attention to the divergent-convergent section. The primary goal is to investigate how the angles of the divergent and convergent parts influence system performance, especially in maximizing wind velocity within the cylindrical section. We begin by simulating various configurations, each with different angles, to assess their impact on the system's wind capture capacity. Subsequently, we establish the relationship between this capacity and the amplification coefficient, which measures the increase in wind speed throughout the system. By comparing these results, we identify the optimal angle that enhances both wind capture efficiency and wind speed amplification relative to a reference system. This study paves the way for optimizing system design to achieve superior performance under diverse wind conditions, contributing to more efficient and cost-effective wind energy solutions.

**KEYWORDS:** Wind energy, numerical study, wind capture system, wind catcher, performance optimization.

# Empirical correlation derived by CFD simulation on Mixing in a Rapidly Mixed Tubular Burner

**Yoldoss Chouari[a], Hella Adouni[a], Herve Bournot [b], Wassim Kriaa[a], Hatem Mhiri[a]**

*(a) LTTPI, National Engineering School of Monastir (ENIM), Av. Ibn El Jazzar, 5019 Monastir, Tunisia*
*(b) IUSTI, UMRCNRS 6595, 5 rue Enrico Fermi, Technopôle de Château-Gombert, 13013 Marseille, France*
*Corresponding author: E-mail address: yoldoss.chouari@yahoo.fr*

## ABSTRACT

A series of numerical investigations are performed to study the mixing process of fuel and oxidizer in a rapidly mixed Tubular Flame Burner (RTFB) using the Fluent 16.2 CFD code, which is based on the finite volume approach. The mixing layer thickness is identified via the Lagrangian Discrete Phase Model (DPM). Two closure turbulence models are examined; the first order realizable k-ε model and the second order Reynolds Stress Model (RSM) are confronted to experimental data. Predicted results elaborated by the RSM model prove to be the most suitable turbulence model.

The effects of several important parameters such as the geometric parameters characterizing the RTFB (Slit width W, Slit length L, Slits number N ), the Velocity ratio (α) and nature of fuel/oxidizer (Hydrogen/air, methane/air, propane/air) were numerically studied. The current work presents a mathematical correlation between the mixing coefficient and the different parameters characterizing the RTFB is established. The detailed results presented in this paper provide a direct calculating method for the mixing time for the three nature of fuel/oxidizer (Hydrogen/air, methane/air, propane/air) and for any rapidly mixed tubular flame burner design.

**KEYWORDS :** Numerical Correlation, CFD, Rapidly mixed Tubular flame burner, fuel/oxidizer, Mixing coefficient.

# Numerical Analysis of Solar Receiver Configurations with Integrated Heat Exchanger

**Hiba Cherif, Jalila Sghaier, and Hatem Mhiri**

*Unit of thermal and Thermodynamics in Industrial Processes, National Engineering School of Monastir Monastir 5000, Tunisia*

hiba.cherif@yahoo.fr

## ABSTRACT

The solar receiver is an essential element to optimize the efficiency, reliability and profitability of solar thermal energy production. It absorbs concentrated solar radiation from mirrors or lenses and converts it into heat. This heat is then used to drive a turbine or generate electricity through a thermal cycle like a Rankine cycle. It provides a clean and renewable energy source without the emissions associated with fossil fuel power generation. The importance of the receiver of the parabolic solar concentrator is studied numerically using commercial CFD Ansys Fluent in this paper. Different configurations of solar receiver are studied: the cylindrical solar receiver and the cylindrical receiver with heat exchanger. Various geometric parameters of the heat exchanger are analyzed in depth to identify the most optimal configuration. This includes examining the effects of different shapes, sizes, and structural arrangements on heat transfer efficiency, pressure drop, and overall performance. By studying these parameters, the goal is to find the design that maximizes thermal efficiency while minimizing energy losses and operational costs. The investigation helps to determine the ideal balance between performance and practicality, ensuring the heat exchanger operates effectively in a wide range of conditions. The results of the numerical simulations indicate that the optimal configuration of the heat exchanger receiver significantly improves both the heat transfer rate and the outlet fluid temperature. This improvement is achieved through a careful adjustment of geometric parameters such as fin shapes, surface area, and flow channel arrangements, which allow for more efficient absorption and distribution of thermal energy.
This study presents the first in-depth investigation of a cylindrical receiver integrated with a heat exchanger, marking a novel contribution to the field of concentrating solar power (CSP) systems.

**KEYWORDS:** Parabolic dish, Solar receiver, Cylinder, CFD, Solar energy

# Photodegradation of a cationic dye in the presence of natural iron oxide

**Abdessalem Omri[a,b], Mourad Benzina[a]**

*(a) Laboratory of Water-Energy-Environment (LR3E), code: AD-10-02, National School of Engineers of Sfax, University of Sfax, BP W, 3038 Sfax, Tunisia.*
*(b) Faculty of Sciences of Gafsa, University of Gafsa, 2112 Gafsa, Tunisia.*
*Email: omri.abdesslem.taieb@gmail.com*

## ABSTRACT

The natural material "siderite" was used to oxidize the Rhodamine B dye by the heterogeneous photo-Fenton reaction. Physicochemical analysis of natural siderite has confirmed that this material is characterized by an iron oxide content equal to 57%, specific surface area of 35,75 $m^2/g$ and a porosity of 28%. The results of the oxidation study show that the siderite catalyst is efficient. A degradation percentage of 90% was obtained under the following operating conditions: reaction time t = 45 min, pH = 3, initial concentration of ($H_2O_2$) = 0.2 mol/L and mass of catalyst = 0.3 g. Monitoring of the COD reveals that the rate of mineralization of RhB by this process is very feasible.

**KEYWORDS:** Rhodamine B, oxidation, siderite, Fenton hétérogène.

# A Trombe Wall Optimised for Mediterranean Climate: an Architectural Strategy for Energy Efficiency

***Marwa Ammar*, Nahed Soussi, Ameni Mokni, Hatem Mhiri**

*Laboratory of Thermal and Thermodynamic of Industrial Processes, National School of Engineers of Monastir, road of Ouardanine, 5000 Monastir, Tunisia*

*ammarmriwa@gmail.com*

**ABSTRACT**

The flow within a solar system using the Trombe wall technique has been investigated in this paper. An innovative Trombe wall façade comprising transparent walls and transparent slats was investigated to improve the profitability of the conventional Trombe wall. Both the type of slats and the environmental conditions in the simulation were selected based on the winter solstice day for a Mediterranean climate.
Heat loss from the glass due to radiation and convection was taken into account in the modelling. A verification test was carried out not only for the modelling of the classic Trombe wall but also for the modelling of the innovative Trombe wall. By applying this innovative configuration, we found the lowest convection losses through the transparent cover and simultaneously the highest solar radiation gain. The innovative transparent Trombe wall with inclined slats increases the room heating hours from 9 to 11 hours. The minimum heat loss from the walls and the highest thermal efficiency of 50% can be obtained.
The envisaged reconception of the Trombe wall should be applicable to residential or tertiary buildings throughout the winter because of its high level of efficiency during the evening hours. This new design should be an architectural strategy for greater energy efficiency with a very low carbon impact.

**KEYWORDS:** Trombe Wall, Mediterranean climate, CFD, Thermal Efficiency

# Effect of Trombe wall design on building energy consumption and thermal comfort: A case study in the Mediterranean climate of Monastir

**Nahed Soussi, Marwa Ammar, Ameni Mokni, Hatem Mhiri**

*Laboratory of Thermal and Thermodynamic of Industrial Processes,*
*National Engineering School of Monastir, road of Ouardanine, 5000 Monastir, Tunisia*
nahed.soussi@yahoo.fr
ammarmriwa@gmail.com
ameni26@yahoo.fr

## ABSTRACT

This paper evaluates the efficiency of a Trombe wall as a passive solar design on building energy consumption and indoor temperature in the Mediterranean climate of Monastir. The study focused on the indoor temperature as well as heating and cooling demands for two building configurations: with and without TW. Four different winter days were selected (22 November, 22 December, 22 January and 22 February) to evaluate the Trombe wall performance under the coldest conditions. In addition, the annual energy demands for heating and cooling were estimated for the two configurations. The results demonstrate that, on the selected winter days, Trombe wall configuration enhances the indoor temperature. Even on December 22, the winter solstice, which is the day with the least favorable climate, thermal comfort has been improved. This led to a significant reduction in heating demand. Shading devices such overhangs and adjustable louvers were proposed to moderate the negative effects of summertime overheating while maintaining the passive heating benefits in winter. The investigation conducted is relevant because it offers a cost-effective, environmentally friendly heating option that enhances home thermal comfort throughout the coldest months of the year.

**KEYWORDS:** Trombe wall, Indoor temperature, Passive heating, Energy simulation, Mediterranean climate.

# Experimental Study and Evaluation of Single Slope Solar Still Combined With external reflector and Packed Bed

**Souhir Mankai[a,b], Fatma Ouled Saad[a,b], Jamel Madiouli[a,b], Jalila Sghaier[a]**

*(a) Laboratoire de Recherche Thermique et Thermodynamique des Procédés Industriels (LRTTPI), National Engineering School of Monastir, Monastir, Tunisia*
*(b) Higher Institute of Applied Sciences and Technology of Kairouan, Tunisia*
*E-mail: souhirmankai@yahoo.fr*

## ABSTRACT

In this study, the influence of coupling external reflector and bundled glass ball layer (PLGB) as Sensible thermal energy on the water productivity of Single Slope Solar Still is studied. The experiments were conducted in Kairouan city, Tunisia in March 2023. Four single slope solar stills with similar dimensions are used. The first tested still is the conventional one (CSS), the second one is the Modified Solar Still with external reflector (MSS-external reflector), the third one is Modified Solar Still with PLGB (MSS-PLGB) and the fourth one is Modified Solar Still with external reflector and PLGB (MSS-external reflector+PLGB). Each single solar still is made with mild steel sheets and an area of 0.64 $m^2$. A distillate collection through having the "V" form towards the inside of the front wall. Transparent glass of 5 mm thickness is employed as cover and plays the role of a condensing surface. The glass has an inclination of 35° with the horizontal, which is the latitude of the experimental site. Both solar stills were evaluated considering water depth of 3 cm, and the required parameters were measured and tabulated during one working day. For the MSS-PLGB, PLGB is positioned at the basin of solar still. This layer acts as a sensible thermal storage medium. For the MSS-external reflector, the mirror can track manually the sun beams along the zenith axis to capture the maximum possible solar energy.

The experimental results revealed that the daily productivity of solar still with external reflector, with PLGB and with both external reflector and PLGB were, respectively, 16.07%, 29.41% and 55.38% higher than that of conventional solar still. An economic analysis was carried out. One liter of distilled water generated with MSS with mirror, MSS-PLGB and MSS Mirror+PLGB costs \$0.1, \$0.05 and \$0.08 respectively instead of \$0.067 with a CSS.

**KEYWORDS:** Desalination, Solar still, Productivity, External reflector, Sensible thermal energy storage.

# Sustainable Textiles and Circular Economy

# Ecological Dyeing of Cotton Fiber with Indigo Carmine Dye: Development of Foam Dyeing Technology

**Oumaima Amara[a,b], Maha Abdellileh[a,b], Walid Hedrich[c], Nizar Meksi[a,b], Hatem Dhaouadi[a]**

*(a) Laboratory of the Environment Chemistry & Clean Processes, Faculty of Sciences of Monastir, University of Monastir, Monastir, Tunisia.*
*(b) Textile Engineering Department, National Engineering School of Monastir, University of Monastir, Monastir, Tunisia.*
*(c) Industrial Textile Company (SITEX), Ksar Hellal, Tunisia.*
*Email: amara1oumaima@gmail.com*

## ABSTRACT

In the textile industry, traditional indigo dyeing stands out for its heavy consumption of water and energy, presenting significant ecological challenges primarily because of the conventional reduction step necessary for applying indigo dye. As a cleaner alternative, foam dyeing has been proposed, promising savings in water, chemicals, and energy. To further mitigate environmental impact, indigo carmine, an eco-friendlier dye, has been selected for this method. However, it often yield slower dyeing quality compared to the traditional indigo process. Therefore, before dyeing, the cotton samples were treated with the cationic agent Croscolor DRT to improve the fiber's affinity for the dye and thus optimize the dyeing quality. A study was conducted on the effect of different concentrations of Croscolor DRT to determine the optimal concentration capable of enhancing dyeing performance. The impact of indigo carmine and foam auxiliary products on foam quality was evaluated. It was observed that increasing the quantity of foaming agent enhances foam stability. Additionally, indigo carmine contributes to foam stability owing to its solubility, facilitating better dispersion within the foam. Also, the influence of indigo carmine dye and auxiliary products on dyeing quality was investigated. The use of Croscolor DRT notably enhanced the dyeing quality of indigo carmine dyed samples. Pre-treated samples exhibited superior dye uptake and brighter shades compared to untreated samples. Moreover, unlike traditional indigo, which yields dull shades, dyed cotton samples with indigo carmine yields bright and vibrant colors. Finally, a comparative study was conducted between foam dyeing using indigo carmine and traditional indigo dyeing, in terms of water and energy consumption. The results showed that the foam dyeing method allowed for an approximately 80% reduction in energy consumption and a 50 to 60% decrease in water consumption compared to the traditional method.

**KEYWORDS:** Clean process, Foam dyeing, Indigo carmine, Modified cotton.

# Enhanced Biological Activities and Efficiency of Textile Fibers Dyed with Various Extracts from *Hypericum Triquetrifolium* Turra

**Wided Fersi [a,b], Noureddine Baaka[a,c], Hatem Dhaouadi[a], Sonia Dridi-Dhaouadi[a,d]**

*(a) University of Monastir, Faculty of Sciences of Monastir, Research laboratory - Environmental Chemistry and Clean Processes (LR21ES04), 5000 Monastir, Tunisia*
*(b) Department of Chemical, Biological, Pharmaceutical and Environmental Sciences, University of Messina, Italy.*
*(c) Higher Institute of Fashion Trades of Monastir, Monastir, Tunisia.*
*(d) Preparatory Institute for Engineering Studies of Monastir, 5019 Monastir, Tunisia.*

## ABSTRACT

This study examines the antioxidant, antibacterial and antibiofilm properties of extracts from the aerial parts of *Hypericum Triquetrifolium* Turra, using various extraction methods. Selected extracts, known for their high polyphenol content and antioxidant activity, were tested against *Staphylococcus aureus* and *Escherichia coli*.

The methanol extract demonstrated the highest antibacterial efficacy, with minimum inhibitory and bactericidal concentrations. Antibiofilm activity was significant for both the maceration and soxhlet extracts. Safety assessments via the *Artemia salina* lethality bioassay showed no toxicity for extracts and dyed fibres remained non-toxic at 10 mg/mL.

These results highlight the potential of *Hypericum Triquetrifolium* extracts as effective antioxidant, antibacterial and antibiofilm agents, and the safety of the dyed fibres for biological textile applications. The enhanced biological activities and efficacy of the dyed fibers demonstrate their promising prospects in the textile industry.

**KEYWORDS:** Polyphenols, flavonoids, antioxidant, antibacterial, antibiofilm, *Staphylococcus aureus*.

# Eco-friendly microwave-assisted dyeing of wool with natural colorant extracted from date palm fiber fibrilium

**Rawdha Znegui[a,b], Noureddine Baaka[a,b], Nizar Meksi[a,c], Hatem Dhaouadi[a]**

*(a) Laboratory of Environmental Chemistry and Clean Process (LCE2P-LR21ES04), Faculty of Sciences of Monastir, University of Monastir, Monastir 5019, Tunisia*
*(b) Department of Textile and Fashion Management, Higher Institute of Fashion of Monastir, Monastir 5000, Tunisia*
*(c) Department of Textile, National Engineering School of Monastir, University of Monastir, 5000 Monastir, Tunisia*

## ABSTRACT

With the growing global interest in plant-based dyes and eco-friendly products, driven by their unique biological and Ayurvedic properties, this study investigates the potential of date palm fiber fibrilium as a natural dye source for wool fibers. Microwave energy was employed to optimize the dyeing process, providing an efficient and sustainable alternative to conventional heating methods.

Key dyeing parameters, including microwave power, dyeing time, and pH of the dye bath, were carefully analyzed to assess their influence on dye uptake and the overall dyeing efficiency of wool fabrics. To ensure durable color fastness, two natural mordants (tannic acid and kermes oak) were applied in the pre-mordanting phase. Additionally, we evaluated the impact of two commonly used metal mordants, alum and ferrous sulfate, on dye absorption and color intensity.

The study reveals the richness of palm oil fibrillium plants in terms of polyphenols, flavonoids, tannins, and saponines. High concentrations of these compounds lead to higher powers, longer durations, and an intermediate pH. The most influential parameters for colorant K/S in micro-onde-aided tanning are pressure, temperature, and pH. Kermes is the best mordant type. The results show that fabrics dyed with palm oil fibrillium extract have average solidities at lavage, light, and freezing, indicating that this tanning method can produce colored textiles with acceptable durability standards.

This study highlights the potential of natural mordants and innovative dyeing methods like microwave-assisted dyeing to create sustainable, eco-friendly textiles.

**KEYWORDS:** date palm fiber fibrillium, microwave, dyeing, wool.

# Biomaterials and Nanotechnology

# Synthesis and characterizations of carbon xerogels from pyrogallol and formaldehyde for the electrical applications

**Belguesmi Aymen** [a], **Souilah Amal** [a], **ELaloui Elimame** [a], **Fattoum Arbi** [a,b]

*(a) Laboratory for the Applications of Materials to the Environment, Water and Energy. Science Faculty of Gafsa, Sidi Ahmed Zaroug University Campus 2112-Gafsa, Tunisia*
*(b) IPEI Gafsa 2112, University of Gafsa , Tunisia*

*Email: Aymenbelguesmi258@gmail.com / limemealoui@gmail.com*

## ABSTRACT

The sol-gel method consists in obtaining very pure products from selected precursors containing only carbon and oxygen as heteroatoms to form a polymeric resin. The proposed synthesis reaction is a polycondensation of pyrogallol with formaldehyde in water in the presence of two catalysts (HCl and $HClO_4$) with the addition of doping elements (K and Ca) at ambient temperature. By varying the parameters, an optimization is carried out by the factorial design method (2k): by following three characteristics of the prepared nano xerogels: density, gel time and physical characterization (electrical impedance): this method consists in determining the dielectric properties such as permittivity, conductivity and impedance. The results obtained show the different applications of carbon nano xerogel in energy storage and as a conductor.

**KEYWORDS:** Sol-Gel, pyrogallol, formaldehyde, activated carbon, conductors.

# A comparative study of MXenes' properties in previous researches for energy storage and conversion

**Chaima Gharbi, Mohsen Mhadhbi, Lamia Khedhiri**

*Laboratory of Useful Materials, National Institute of Research and Pysicochemical Analysis, SidiThabet, Ariana 2020, Tunisia*
*Email: chaimag754@gmail.com*

**ABSTRACT:**

MXenes have emerged as promising nano-materials in many applications. Recently, they are used as electrodesfor developing efficient energy storage and conversion systems in virtue of the metallic conductivity, high Li storage capacity, high theoretical capacitance, low diffusion barrier and hydrophilic surfaces. According to previous researches, MXenes have various properties depending on the composition, structure, and processing conditions. For instance, the 2D MXenes with binairy metalsoffer even better flexibility in tuning of properties than single metal carbides. In the present study, we provide evidence of the effects of transition metal on the MXenes'electronic properties and electrochemical performance for energy sectors.

**KEYWORDS:** MXene; electronic properties; binary metals transition; energy storage.

# Spectroscopic, Structural Characterization of a New Cadmium(II) Acetato Meso-Arylporphyrin: Analysis of Electrical Conductance and Dielectric Properties

**Nour Elhouda Dardouri[a], Thierry Roisnel[b], Habib Nasri[a]**

*(a) University of Monastir, Laboratory of Physical chemistry of Materials, Faculty of Science of MonastIR (LR01ES19), Avenue of Environment, 5019 Monastir, Tunisia*
*(b) Institute of Chemical Sciences of Rennes, UMR 6226, University of Rennes 1, Beaulieu Campus, 35042 Rennes, France*
*E-mail : nourelhoudadardouri@gmail.com*

**ABSTRACT:**

The presents paper a combined experimental and computational investigation of the cadmium(II) (acetato)-*meso*-tetra(*para*-methoxyphenyl)porphyrin ion complex[Cd(TMPP)(OAc)]$^-$ , which was prepared by the reaction of [Cd(TMPP)] with an excess of NaOAc and crysptand-222 in chloroform. This new Cd(II) *meso*-arylporphyrin was characterized by elementary analysis and UV–Vis, IR, and $^1$H NMR spectroscopic techniques along with single crystal X-ray diffraction. This later study shows that the $Cd^{2+}$center ion adopts a distorted square pyramidal geometry and is coordinated by the four nitrogens of the TMPP porphyrinate and the oxygen atom of the acetato axial ligand. The intermolecular interactions in the crystal lattice of [Cd(TMPP)(OAc)]$^-$, determined using the PLATON program, are of types O–H…O, C–H…H, C–H…Cl, C–H…Cg and C–Cl…Cg (Cg is the centroid of a phenyl or a pyrrole ring) involving the [Cd(TMPP)(OAc)]$^-$ ion complex, the [Na(crypt-222)]$^+$ counterion, and the chloroform and water molecules found in the crystal lattice of complex . Furthermore, experimental tests have been carried out concerning the impedance and dielectric spectroscopy of the InGa/[Cd(TMPP)(OAc)]/InGa device.

**KEYWORDS:** Cadmium(II)porphyrincomplex, X-raymolecularstructure, UV–Visspectroscopy, Electrical conductance and dielectricpropertie.

# Green Chemistry and Natural Substances

# Biotechnological valorization of *Cucumis melo* L. seeds for food industries: Storage conditions and functional features

**Sana Mallek-Ayadi and Neila Bahloul**

*Research Group of Agri-Food Processing Engineering, Laboratory of Applied Fluid Mechanics, Process Engineering and Environment, National School of Engineers of Sfax, Tunisia*
*E-mail : sana.mallek@yahoo.fr*

## ABSTRACT

In botanical terms, the muskmelon or *Cucumis melo* L. belongs to the Cucurbitaceae family and is extensively cultivated in various tropical and temperate regions across the globe. Melon seeds are regarded as the main by-products which can be utilized as a source of nutrients for food and pharmaceutical purposes. In this context, the aim of this work is to determine the thermodynamic characteristics of melon seeds associated with moisture adsorption isotherms and to investigate the functional properties of these by-products. Moisture sorption isotherms are valuable tools for prediction of the stability and shelf-life of agricultural products in order to optimize the best storage conditions. Moisture adsorption isotherms of melon seeds were determined at water activities and temperatures ranging from 0.11 to 0.97 and from 30 to 60 °C, respectively, using the standard static-gravimetric method. The shape of the adsorption isotherms was of type II typical of high sugar fruits according to the Brunauer–Emmett–Teller (BET) classification. Furthermore, at constant temperature the equilibrium moisture content increases with increasing water activity. Both temperature and water activity have significant effects on experimental equilibrium moisture content values. Moreover, equilibrium moisture contents data were correlated by different mathematical models usually applied to fruits. The Peleg model showed satisfactory fits to the experimental data. As for determination of the functional properties (water and oil retention capacities) and color, the results show that melon seeds have characteristics that may be useful in industrial applications.

**KEYWORDS:** *Cucumis melo* L. seeds, water activities, adsorption isotherms, Peleg model, functional properties.

# Supercritical $CO_2$ Extraction and Physicochemical Characterization of Polysaccharides from Orange Peels: Sustainable Ingredients for Cosmetic Formulations

**Zeineb Mzoughi [a], Lobna Dems [a], Didier Le Cerf [b], Hatem Dhaouadi [c], Hatem Majdoub [a]**

*(a) University of Monastir, Laboratory of Interfaces and Advanced Materials, Faculty of Sciences of Monastir, Monastir 5000, Tunisia*
*(b) Normandie Univ, UNIROUEN, INSA Rouen, CNRS, PBS, UMR 6270 & FR 3038, 76000 Rouen, France*
*(c) University of Monastir, Faculty of Sciences of Monastir, Laboratory of Environmental Chemistry and Clean Process (LCE2P-LR21ES04), 5019 Monastir, Tunisia*

*E-mail: mzoughizeineb.lima@gmail.com; zeineb.mzoughi@fsm.rnu.tn*

## ABSTRACT

This study investigates the use of supercritical $CO_2$ extraction to obtain polysaccharides from orange peels, aiming to explore sustainable ingredients for cosmetic formulations. The extraction process was optimized to achieve a yield of 4.5% while preserving the physicochemical integrity of the polysaccharides. Characterization through techniques such as FTIR, NMR, and rheological analysis revealed that the extracted polysaccharides exhibited excellent water retention properties, with a viscosity of 1800 cP at 25°C, suggesting strong moisturizing potential. Molecular weight analysis indicated an average molecular weight of $3.2 \times 10^6$ g/mol, suitable for use in skin care formulations. In addition, stability studies demonstrated that these polysaccharides maintained their functional properties under varying pH and temperature conditions, indicating their potential for enhancing formulation stability. These results highlight the polysaccharides' potential as natural, eco-friendly alternatives for cosmetic products, offering benefits like hydration, skin protection, and improved product performance. This work contributes to the development of sustainable ingredients derived from agricultural waste, supporting the growing demand for green cosmetics.

**KEYWORDS:** Polysaccharides from orange peels, extraction techniques, supercritical fluid extraction (SFE), physicochemical properties, cosmetic formulations.